LBL-35533
CONF-9310290
UC-413

Lawrence Berkeley Laboratory
UNIVERSITY OF CALIFORNIA

Accelerator & Fusion
Research Division

Proceedings of the Workshop on Post-Accelerator Issues
at the IsoSpin Laboratory, Berkeley, CA, October 27–29, 1993,
and to be published in Particle Accelerators

Post-Accelerator Issues at the IsoSpin Laboratory

Technical Editors: S. Chattopadhyay, Center for Beam Physics
J.M. Nitschke, IsoSpin Laboratory Studies Group

May 1994

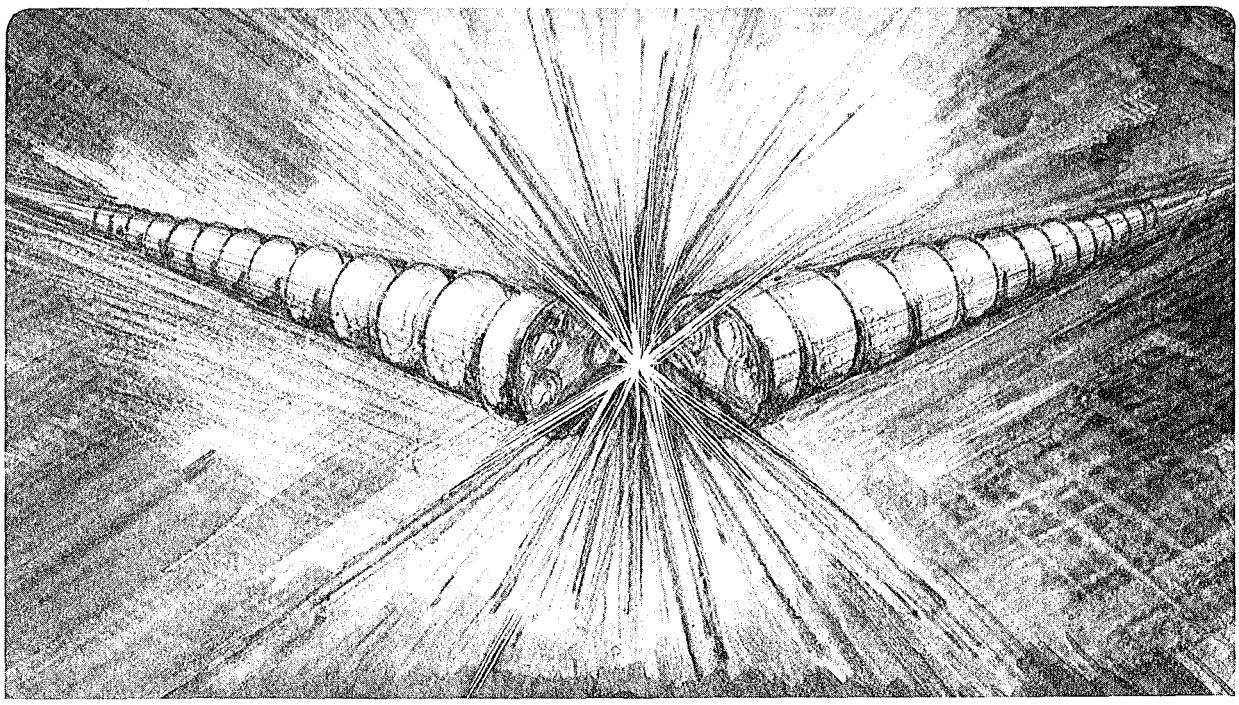

Prepared for the U.S. Department of Energy under Contract Number DE-AC03-76SF00098

LBL-35533
CONF-93-10290
UC-413
CBP Note-075

POST-ACCELERATOR ISSUES AT THE ISOSPIN LABORATORY

October 27-29, 1993

Sponsored by

Center for Beam Physics
Accelerator and Fusion Research Division

and

ISL Studies Group
Nuclear Science Division

Lawrence Berkeley Laboratory
Berkeley, CA 94720

* This work was supported by the Director, Office of Energy Research, Office of High Energy and Nuclear Physics, High Energy Physics Division, of the U.S. Department of Energy under Contract No. DE-AC03-76SF00098.

Table of Contents

FOREWORD

The workshop on "Post-Accelerator Issues at the Isospin Laboratory" was held at the Lawrence Berkeley Laboratory from October 27-29, 1993. It was sponsored by the Center for Beam Physics in the Accelerator and Fusion Research Division and the ISL Studies Group in the Nuclear Science Division. About forty scientists from around the world participated vigorously in this two and a half day workshop, (c.f. Agenda, Appendix D). Following various invited review talks from leading practitioners in the field on the first day, the workshop focussed around two working groups: (1) the Ion Source and Separators working group and (2) the Radio Frequency Quadrupoles and Linacs working group. The workshop closed with the two working groups summarizing and outlining the tasks for the future.

This report documents the proceedings of the workshop and includes the invited review talks, the two summary talks from the working groups and individual contributions from the participants. It is a complete assemblage of state-of-the-art thinking on ion sources, low-β, low-(q/A) accelerating structures, e.g. linacs and RFQs, isobar separators, phase-space matching, cyclotrons, etc., as relevant to radioactive beam facilities and the IsoSpin Laboratory. We regret to say that while the fascinating topic of superconducting low-velocity accelerator structure was covered by Dr. K. Shepard during the workshop, we can only reproduce the copies of the transparencies of his talk in the Appendix, since no written manuscript was available at the time of publication of this report.

We thank all the participants and contributors for a stimulating workshop. We hope that these proceedings will be a positive contribution to the realization of a future ISL.

S. Chattopadhyay
Center for Beam Physics

J. M. Nitschke
Isospin Studies Group

PHYSICS MOTIVATION AND CONCEPTS FOR THE ISOSPIN LABORATORY*

J. Michael Nitschke

ISL Studies Group
Nuclear Science Division
Lawrence Berkeley Laboratory
University of California
Berkeley, California 94720

1. INTRODUCTION

Nuclear physics and the development of particle accelerators have gone hand-in-hand since the early part of this century. The first nuclear reaction was carried out in 1930 by Cockcroft and Walton using protons accelerated to 300keV in the reaction ^{7}Li(p,2α). Subsequent developments progressed in two directions, heavier masses and higher energies. While heavier projectiles opened new vistas in the synthesis of new elements, the study of high spin phenomena, and the exploration of the nucleon drip lines, to mention only a few, higher energies allowed the study of nuclei at higher temperatures, the equation of state of nuclear matter, and ultimately collective phenomena resulting from the melting of the hadronic phase that may give rise to a plasma consisting of quarks and gluons.

A comparison between the chart of nuclides and nuclear model calculations shows that we know of the existence of only ~1/3 of all bound nuclei. Detailed nuclear structure information is limited to a narrow band of nuclei near the line of β-stability. One of the reasons for this is that, thus far, we have been limited experimentally to projectiles and targets of stable nuclei, due, in the past, to the technical difficulties of producing radioactive nuclear beams (RNB) with intensities sufficient for meaningful experiments.

Developments in the last two or so decades have changed this situation drastically. For the ISOL (Isotope Separator On-Line) method of producing RNBs high energy proton accelerators are now able to deliver primary beam intensities that are higher than can be handled with existing target technology.

Sources with high efficiencies and selectivity for singly and multiply charged ions have been developed, magnetic spectrometers with high resolution and transmission can now be built, and post-accelerators with excellent beam quality, duty factor, and transmission are in routine operation. Conversely, high-energy, high-current heavy ion accelerators can provide secondary RNBs with sufficient intensity via projectile fragmentation. In addition, experimental equipment has improved in efficiency, resolution, and acceptable data rates by several orders of magnitude.

In 1989 this author proposed the construction of a dedicated, flexible, radioactive nuclear beams facility that would provide intense beams of nearly all elements for a program of scientific studies in nuclear structure, nuclear reaction dynamics, astrophysics, high-spin physics, nuclei far from stability, material- and surface science, and atomic- and hyperfine-interaction physics. The initial name proposed for the new facility was "IsoSpin Factory" to underscore the key feature of this new physics tool; it was later changed to "IsoSpin Laboratory" (ISL). The ISL is now supported by a broad base of nuclear scientists and has been identified in the 1989 US Long Range Plan on Nuclear Science as one of the new potential construction projects for the second part of this decade. Since 1989 a number of conferences and workshops has been held in which the scientific and technical case for RNB facilities has been made.[1-6] An overview of existing and planned RNB facilities world-wide has been presented in ref. [7]. The purpose of this workshop is to focus on the North American plan for the ISL, which was initially summarized in a "White Paper"[8] but has since evolved in its scientific and technical scope.

2. SCIENTIFIC SCOPE

The ISL is based on the coupling of two accelerators: the first to deliver a high current light ion beam to a thick, hot spallation- or fission target and the second to accelerate the emanating radioactive species to energies in the range from a few keV to ~25MeV/u with excellent beam qualities, typical of modern heavy ion accelerators. These beams will facilitate a large panoply of experiments in nuclear- and astrophysics and in the applied sciences.

2.1 Nuclear Structure

One of the striking features of radioactive beam science is that the large number of stable and radioactive beam- and target combinations allows the systematic study of nuclear properties over long isotopic- and isotonic chains. It will be possible to create nuclei with exotic matter distributions and follow the evolution of nuclear shapes and nuclear structure from closed shell to closed shell and beyond, as in the case of $^{\sim 100}$Sn to $^{>132}$Sn.

The topics in nuclear structure are too numerous to discuss here in detail; a partial list includes:

study of shell model states near singly and doubly magic nuclei through single particle transfer reactions;

nuclear structure near N=Z, including neutron–proton pairing correlations, nuclear shapes, Coulomb energy effects, mirror nuclei, superallowed β–decay, and tests of shell–model predictions near ^{100}Sn and other closed–shell nuclei;

Coulomb excitation of unstable nuclei, giant resonances;

new collective modes, octupole–, oblate– , and triaxial deformations;

synthesis of new neutron–rich nuclei in the trans–uranium region, and new attempts at the synthesis of super–heavy elements;

nuclear structure near the drip lines;

high–spin physics, new regions of extreme nuclear deformation and configurations;

ground–state properties of exotic nuclei: masses, spins, moments, radii, skins and halos; and

charged–particle– and cluster radioactivity, including β–delayed radioactivities.

An overview of nuclear physics with radioactive beams is given by Warner in ref. [4].

2.2 Nuclear Reactions

Radioactive projectiles remove the restraint to the natural N/Z ratios of stable beams in nuclear reactions. The extended wave functions of loosely bound nuclei near the drip lines (skins and halos) may result in entirely new reaction processes such as the free flow of neutrons in sub-barrier fusion reactions ("neck formation") or "molecular bonding" mediated by the valence neutrons. Conversely, the same processes will yield information about nuclear wave functions, and the diffuseness and thickness of the outer nuclear optical potential. By combining exotic projectiles and/or targets, large reaction Q-values can be achieved that may lead to enhanced cross sections and the possibility of multiple (sequential) neutron transfers. Similarly, large probabilities for pair transfer will allow the study of collective effects resulting from the nuclear pairing field. One could, perhaps, hope to find a nuclear analogue to the Josephson effect.

Mapping of the fission-energy vs. deformation surface could be attempted by studying the fusion ("inverse fission") of two nuclei with special nuclear structure, i.e., near the doubly magic ^{132}Sn, leading to isotopes of Fm. Elucidating this process could point to reactions conducive to the formation of super-heavy elements. Other experiments directed towards an understanding of the fission process in heavy nuclei would involve the formation of currently not reachable nuclei with heavy RNBs on light stable targets in inverse kinematics, i.e., d(^{209}Th,p). The experiments require only modest beam intensities since the fission exit channels have high cross sections and are easily detectable with high efficiency. A unique feature of the ISL will be the production of *isomeric* beams and targets allowing reaction studies based on high spin states such as in ^{178}Hf^{16+}.

Classical elastic scattering experiments are ideally suited for low beam intensities. When carried out with a series of RNB isotopes they would reveal the spin- and isospin dependent nature of the nuclear potential. Large impact parameter scattering between mirror nuclei could be used to search for the pion content of nuclei without interferences due to non-zero Q-values in ordinary nuclei.[11] An example of a possible reaction is ^{18}Ne + ^{18}O.

It is obvious that, because of the low beam intensities, many nuclear reaction studies with RNBs will be carried out in inverse kinematics, which will ensure

high detection efficiencies. However, sufficient energy is needed to study highly asymmetric systems like d(^{132}Sn, p)^{133}Sn.

2.3 Astrophysics

The importance of RNBs for astrophysics stems mainly from the fact that in hot stellar environments many of the interacting nuclei are radioactive and that reactions with radioactive beams and targets could previously be studied in the laboratory only with difficulty. Such studies are, however, essential for the understanding of several stellar phenomena such as the hot CNO cycle, the rp–, s–, r–, and p–processes, and primordial nucleosynthesis, the big bang, as well as the energy balances of stars. Required are measurements of cross sections, reaction rates, masses, half–lives, β–strength functions, and decay properties. For the r–process the crucial experiments involve nuclei near the n–drip line, for the rp–process near the p–drip line, and for the s–process near β–stability. Spectroscopic measurements are also needed to interpret data from γ–ray observational astronomy.

Astrophysical RNB experiments face special challenges. Measurements of nuclear reaction rates far below the Coulomb barrier can have cross sections in the nanobarn or picobarn range, the width of important resonances may be very small (~meV or less), the n–drip line can only be reached for the lighter nuclei, and for many neutron–rich nuclei even basic ground–state properties like masses and half–lives are not known. For these and other reasons astrophysical experiments may pose the highest demands on the performance of the ISL, for example, maximum beam energies of 15–25MeV/u for inverse kinematics, small energy spread, beam purities $\leqq 10^{-5}$, and absolute energy calibrations to a few keV/u.

2.4 Atomic Physics and Material Science

Intense, pure beams of radioactive ions of many elements, with variable energies and of isotopes with different half–lives can become of great importance in materials research. This is based on the observation that a radioactive nucleus implanted in a host material will sense its electromagnetic environment via the hyperfine interaction and may reveal the characteristics of this environment in its decay features. Precise three–dimensional localization of implanted ions in a large variety of matrixes – including insulators – can be obtained.

Concentrations can be varied over many orders of magnitude and solubility limits can be exceeded. The usual alloying rules and limitations, in general, do not apply to implantation processes and metastable systems and exotic alloys may be formed. Radiation damage may change the properties of the target in ways that can not be achieved by other means, creating new phases and materials. These processes can be studied through a number of research techniques:

on-line nuclear orientation
NMR spectroscopy
Mössbauer spectroscopy
perturbed angular correlations
channeling of charged particles
high-resolution conversion electron spectroscopy
positron analysis
nuclear reaction analysis
use of radio tracers.

For some of these techniques polarized RNBs are desirable. An overview of the potential of radioactive ion beams in material science is given by Sawicki in ref. [2].

3. EXPERIMENTS

Compared to conventional stable-heavy-ion accelerators the beam intensities at the ISL will be several orders of magnitude lower for beams that are far from β-stability. This has to be taken into account in the planning and execution of experiments. It will require close interaction between the accelerator operation and the experimenter to decide on the best trade-off between "exoticness" and intensity. Certain elements will be easier to produce as RNBs than others. During the start-up phase of the ISL, for example, alkalis, noble gases, and halogens will be easier to obtain with good intensities than refractory elements like Os, W, Hf, etc. Taking this into account in the choice of the beam/target combination can make a difference of many orders of magnitude in the event rate of an experiment.

Figure 1 shows an attempt at a rough correlation between several types of nuclear physics experiments - shown over a range of cross sections - and the RNB intensities needed for a given detector sensitivity, assuming a typical target thickness for heavy ion experiments of 10^{18} cm^{-2}. For example, if the detector is

sensitive to a few counts per hour, brake-up reactions could be carried out with beams as low as $10^3 s^{-1}$, while rare multi-nucleon transfer reactions may require intensities of $10^9 s^{-1}$ or more. It is in the nature of the nuclear phenomena involved that, in general, the most interesting beams - the ones that are furthest from stability - have the lowest intensities. This is illustrated on the right side of fig. 1, which shows the correlation between the distance from stability [expressed in positive or negative neutron numbers, $\Delta n(Z)$] and the expected beam intensities at the ISL (uncorrected for radioactive decays in the target and ion source). Because of the strong decline of the intensity with neutron number it is advisable that the ISL be designed for the highest RNB currents that are technologically feasible.

It is clearly impossible to discuss even a representative sample of all the experiments that will be carried out at the ISL. A more manageable approach is to look at some of the instrumentation that may be necessary or desirable to deal with the idiosyncrasies of RNB experiments.

As a general requirement, detector systems, spectrometers, and beam lines have to be protected from deposits of long-lived beams or beams with long-lived daughters. Typical collimator/target arrangements will have to be modified. A collimator or target holder that intercepts, for example, only 10^4 ions/s (= 10^{-3}% of a typical radioactive beam of 10^9 ions/s) of a short-lived β^+-emitter will radiate, after a few half-lives, 2×10^4 511keV-photons/s into 4π. If the detection system is sensitive to this radiation the singles rates may become too high and/or useless data may be collected. In this connection, the micro structure of the RNB becomes important not only for time-of-flight measurements but also for background reduction. One of the requirements for protecting experimental equipment from the primary RNB is excellent beam quality from the post-accelerator, including the absence of halos.

Several specific instruments for the ISL are under discussion.[5] The cost of initial instrumentation will be a significant fraction of the total cost of the facility.

Highly desirable is a 4π array for γ rays and charged particles, equipped with Si-microstrip detectors and, perhaps, a time projection chamber. This could be combined with a "neutron-wall."

Another important instrument is an E×B separator for fusion reactions, with large acceptance (~20msr), higher order corrections, and ray-tracing capability.

One can also imagine experiments where the 4π array, the neutron wall, and the spectrometer are combined.

For reactions carried out in inverse kinematics a high resolution ($R \sim 10^4$) magnetic spectrograph with large solid angle (~20msr) is needed. It should have large momentum acceptance ($\Delta p/p \approx 10\%$) and ray tracing capability.

To achieve large solid angles (500msr - 4π) for the collection of reaction products coaxial devices, like superconducting solenoids, are useful. They are very effective in separating the beam from weak reaction channels, their resolution, however, is poor.

Penning and Paul traps have become powerful devices for measuring nuclear and atomic properties even of single ions.[12] Conversely, large volume traps may in the future be able to store large numbers of ions, which would have many uses at RNB facilities (Moore in ref. [5]).

Ultimately it may be desirable to couple the ISL with a storage ring. This requires an effective bunching mechanism for injection to conserve the average RNB intensity. The ring could be used for internal target experiments to increase the luminosity over single pass experiments and to cool the circulating radioactive ions, as well as to accelerate them to higher energies. Electron cooling would improve beam quality by several orders of magnitude and would allow collinear experiments to study interactions between radioactive-, laser-, and electron beams. A storage ring would add considerably to the cost of the facility and may be considered a future option.

Astrophysicists need to measure (n,γ) cross sections for many neutron-rich isotopes. At the ISL several of these isotopes would be collected on-line as radioactive targets [probably on a moving tape collector to avoid build-up of long-lived daughter products, using the BRAMA concept (c.f. separate contribution to this workshop)] and irradiated by a small neutron generator that could generate a "stellar" neutron spectrum ($kT \approx 25$keV) from the reaction $^7Li(p,n)^7Be$. At a proton energy of 1912keV and a proton current of 150 μA a kinematically collimated beam of 10^9 n/s can be obtained.

It is anticipated that at the low-energy front end of the ISL ($E_{RNB} \leq 100$keV) much of the type of instrumentation that is presently installed or being developed at ISOLDE/CERN will be used.

4. CONCLUSION

The advent of RNBs in this decade may rival in importance the development of heavy ion beams in the 1960s. The possibility of vastly expanding the exploration of the isospin degree of freedom will create exciting new vistas for nuclear- and astrophysics. The ISL will allow the investigation of new features in nuclear reactions, give access to special nuclear regions and states, create nuclei with new modes of excitations and deformations, explore exotic matter distributions at extreme N/Z ratios, and create new nuclei at the limits of stability of nuclear matter. In astrophysics it will be possible to simulate in the laboratory conditions under which stellar processes like supernovae, nucleosynthesis, and different burning scenarios proceed. RNBs may even help to shed light on the early history of the universe. For material science the flexible nature of RNBs is attractive because it is possible to choose freely for a given element the half-life, nuclear decay properties, spatial distributions, and densities.

However, as in many scientific endeavors, the most exciting discoveries will be those that cannot be foreseen.

5. REFERENCES

[1] *First International Conference on Radioactive Nuclear Beams,* Berkeley, 1989, edited by W. D. Meyer, J. M. Nitschke, and E. B. Norman (World Scientific, Singapore, 1990).

[2] *Workshop on the Science of Intense Radioactive Ion Beams,* Los Alamos, NM, 1990, edited by J. B. McClelland and D. J. Vieira, LA-11964-C.

[3] *Intl. Workshop on the Physics and Techniques of Secondary Nuclear Beams,* Dourdan, France, 1992, edited by J. F. Bruandet, B. Fernandez, and M. Bex (Edition Frontiers, Gif-sur-Ivette, France, 1992).

[4] *Second International Conference on Radioactive Nuclear Beams,* Louvain-la-Neuve, 1991, edited by T. Delbar (Adam Hilger, Bristol, 1991).

[5] *Workshop on the Production and Use of Intense Radioactive Beams at the IsoSpin Laboratory,* Oak Ridge, TN, 1992, edited by J. G. Garrett (ORNL), to be published.

[6] *Third International Conference on Radioactive Nuclear Beams,* MSU, Michigan, 1993, edited by D.J. Morrissey (Edition Frontieres, Gif–sur–Yvette, 1993).

[7] J. M. Nitschke, in *XIII Intl. Conf. on Cyclotrons and their Applications,* Vancouver, Canada, 1992, edited by G. Dutto and M. K. Craddock (World Scientific), pp. 713–720.

[8] *The IsoSpin Laboratory,* LALP 91–51 (1991).

[9] P. H. Stelson, Phys. Lett. **205B**, 190 (1988).

[10] W. v. Oertzen, in *Intl. Workshop on the Physics and Techniques of Secondary Nuclear Beams,* Dourdan, France, 1992, edited by J. F. Bruandet and B. Fernandez (Edition Frontiers, Gif–sur–Ivette, France, 1992), pp. 142–153.

[11] J. P. Vary and M. A. Nagarajan, in *Prospects for Research with Radioactive Beams,* Washington, 1984, edited by J. M. Nitschke (LBL–18187), pp. 113–122.

[12] Proceedings of the workshop on *Traps for Antimatter and Radioactive Nuclei,* edited by J.M. D'Auria, D.R. Gill and A.I. Yavin, Hyperfine Interactions **81** (1993).

*Condensed from a talk given at the International School–Seminar on Heavy Ion Physics, Dubna, Russia, 10–15 May, 1993.

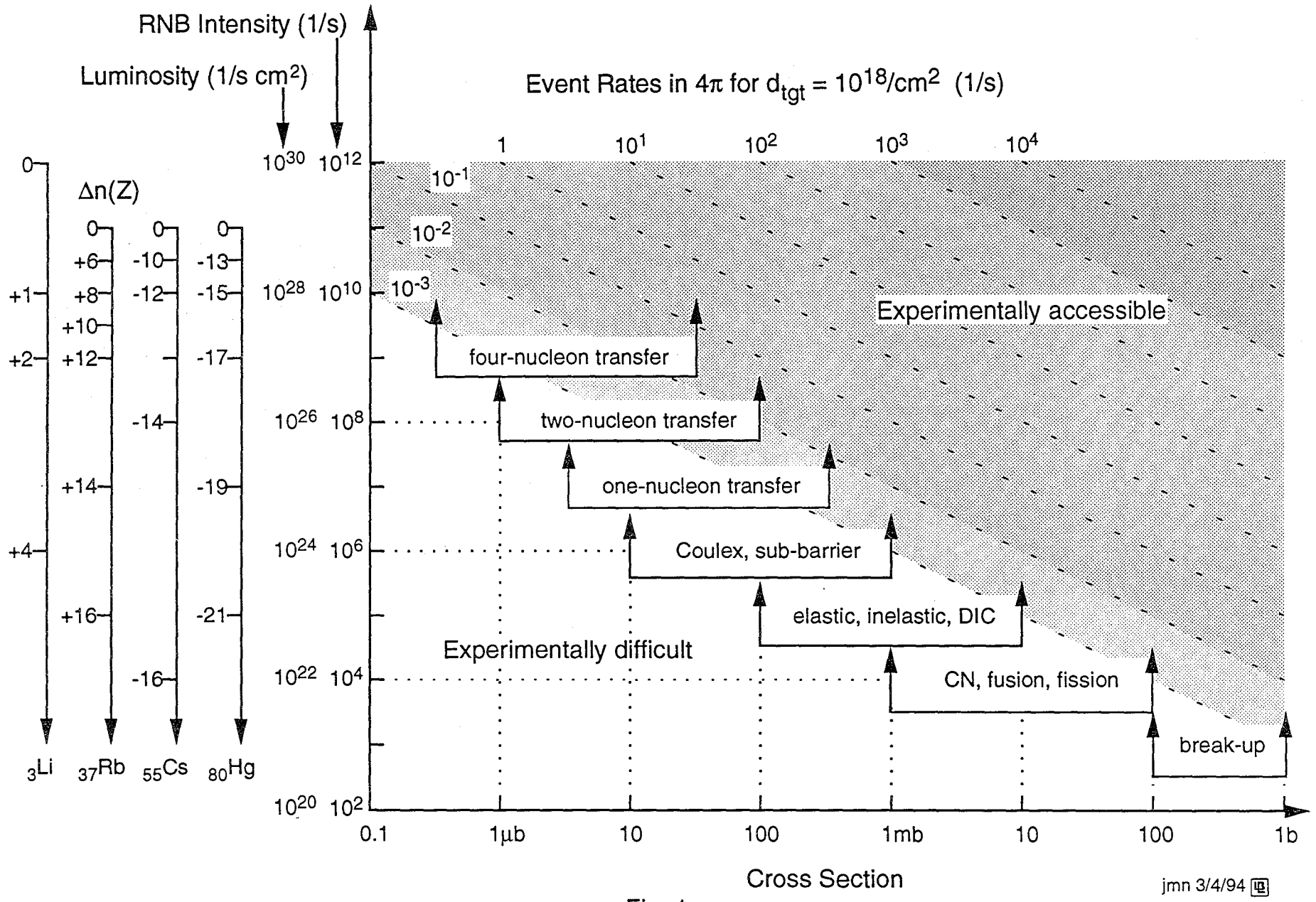
RNB Intensity (1/s)
Luminosity (1/s cm²)
Event Rates in 4π for d_tgt = 10^18/cm² (1/s)
Δn(Z)
0
+1
+2
+4
0
+6
+8
+10
+12
+14
+16
0
-10
-12
-14
-16
0
-13
-15
-17
-19
-21
3Li
37Rb
55Cs
80Hg
10^30
10^28
10^26
10^24
10^22
10^20
10^12
10^10
10^8
10^6
10^4
10^2
10^-1
10^-2
10^-3
1
10^1
10^2
10^3
10^4
Experimentally accessible
four-nucleon transfer
two-nucleon transfer
one-nucleon transfer
Coulex, sub-barrier
elastic, inelastic, DIC
CN, fusion, fission
break-up
Experimentally difficult
0.1
1μb
10
100
1mb
10
100
1b
Cross Section
jmn 3/4/94

Fig. 1

ACCELERATOR ISSUES AND CHALLENGES AT THE ISOSPIN LABORATORY

S. Chattopadhyay

Center for Beam Physics
Accelerator and Fusion Research Division
Lawrence Berkeley Laboratory
University of California
Berkeley, California

1. INTRODUCTION

The layout of an IsoSpin Laboratory as conceived presently and its current parametric specifications are shown in Figure 1 and Table 1 respectively. The generic features of such a facility are: large dynamic range (in energy, intensity, ion species (q/A), etc.), high intensity, high duty factor, required low beam emittances, high beam purity, operation under high radiation background (e.g. 60 kRad/hour @ 1 meter from target) and almost zero tolerance for beam loss (required transmission efficiency of ~100%). This last feature demands almost perfect matching of beam phase space from the ion source into the post accelerator and from the post accelerator into the high energy linac, etc. The goals of the ISL are unquestionably ambitious and challenging, leaving aside the demanding issues of targetry and radiation shielding, which were not in the scope of this workshop. Nevertheless, through dedicated R&D effort and focussed workshops in the past including the present one, reasonably feasible technical solutions seem to be emerging so that we are beginning to share an increasingly optimistic outlook on the realizability of the ISL in near future.

The major natural divisions of the post-accelerator complex are:

(a) High Energy Post-Accelerator or Secondary Beam Accelerator ($\gtrsim$ 100 keV/u).

(b) Low Energy Post-Accelerator or Secondary Beam Injector (< 100 keV/u),

(c) Isobar Separator and Matching Sections, and

(d) Ion Source.

In what follows, we discuss these four areas and raise the issues and questions in each area that this workshop was charged to address. Many of these questions were addressed at the ORNL workshop as well.

2. HIGH ENERGY POST ACCELERATOR

This part of the accelerator complex will be defined by $E > 100$ keV/u after the first stripping section and will also be referred to as the secondary beam accelerator. This is probably the "least speculative" portion of the post-accelerator complex with many available options:

(a) Low frequency "Heavy Ion Superconducting Linac" e.g. the ATLAS type;

(b) Specially designed room temperature, normal conducting linacs; and

(c) Storage rings.

Let us discuss these options briefly in the following.

2.1 **Superconducting Linac**

Superconducting linacs have high shunt impedances and allow cost-effective CW operation. Previous experience with such linacs and the possibility of advanced design promise exceptional beam quality and operational flexibility from such a linac. Since losses are low, the cavity shape is not important. This allows large apertures thus guaranteeing exceptional transverse acceptance and transmission. Usually, it is also possible to gain a high degree of control of longitudinal phase space leading to beams of high quality. In general one has a broad velocity acceptance and control over the linac velocity profile.

A typical prototypical technology is exemplified by the ATLAS linac at the Argonne National Laboratory, where one accelerates ions with $q/A \lesssim 1/10$, from 35 keV/u to $\gtrsim 6$ MeV/u with a longitudinal emittance of $\varepsilon_z \sim 10 - 20\pi$ keV · nsec.

Operation of a superconducting low temperature structure in the presence of radioactive decays and activation-induced quenches are believed to be of some concern, although not in any major way.

2.2 Normal Conducting Linac

Various low β, low (q/A) structures (including interdigital H-type accelerating structures) have been developed for linacs with applications to radioactive beams in mind. These are very high shunt impedance structures, with CW operation and good transverse acceptance. These structures are probably optimal, cost-wise, for very low-β ions ($\lesssim$ 250 keV/u). However, the longitudinal emittance expected from these structures is rather high ($\varepsilon_z \sim 400\ \pi$ keV $\cdot$ nsec) and flexibility in changing output energy, effect on beam emittance, etc. need to be explored further.

2.3 Storage Rings

Although the option of storage rings for radioactive nuclear beams was not in the scope of the workshop, we will comment on it because of its importance.

The advantages of the storage ring scenario are: (a) large luminosities can be obtained for relatively low primary beam intensities; (b) for beam particle currents $\lesssim 10^6$/s, internal target experiments will give higher luminosities than single-pass experiments because of multiple target traversals.

The ring can also be operated at transition energy for mass measurements. However, these scenarios require installation of an internal cold-cluster gas target in the ring and utilization of particle and gamma-ray detector arrays around the target.

Yet another significant factor to be considered is the fact that large background from the beam radioactive decay products are spread over a large area lending to significant reduction of gamma background relative to achievable levels in a fixed target experiment with same luminosity.

Storage ring scenarios thus deserve serious attention.

2.4 Outstanding Issues

The following questions on the secondary beam accelerator need to be addressed as quantitatively as possible:

(1) Is beam quality in the longitudinal phase space (e.g. longitudinal emittance) important?

(2) If so, what is the ultimate beam quality and control required for the farthest physics reach of the facility, experimentally?

(3) A superconducting linac option presents promise in good beam quality, energy stability, variability and flexibility. Is radioactivity in a cryogenic environment a serious concern?

(4) If beam quality is of no concern, room temperature structures offer optimal systems for very low-β at a reduced cost. How much lower cost?

(5) Beam intensities swing from 10^2 to 10^{13} pps in an ISL. Tuning and beam loading are expected to be tractable due to low current, but need to be looked at in detail.

(6) What is the optimum stripping scheme and optimum stripping energy? What are the relative merits or otherwise of gas vs. foil stripping?

(7) Finally, what is the ultimate accelerator configuration for accelerating low-β, low (q/A) ions (E ~ 100 keV, $\beta \geq 0.0015$, $q/A \geq 0.004$) to energies of ~ 10 MeV/u?

3. LOW ENERGY POST ACCELERATOR

This part of the accelerator complex will be defined by $E \lesssim 100$ keV/u and will also be referred to as the secondary beam injector. This is probably one of the "most difficult" portions of the post-accelerator complex. The difficulty is in designing an injector (RFQ, for example) that simultaneously satisfies the demands of CW operation, low input velocity, low q/A and reasonable acceptance. The beam specifications are: (q/A) ~ 1/240, normalized emittance of $\varepsilon_N \lesssim 1\ \pi$ mm–mrad and energy spread of $(\delta E/E) \sim 10^{-3}$. The possible options are: (a) room temperature RFQs; (b) superconducting RFQs and (c) cyclotrons.

3.1 **Radio Frequency Quadrupoles**

It is difficult to achieve large acceptance for low ion velocities and low (q/A) due to stringent RFQ focussing requirements for stability against transverse space charge, etc. The focussing coefficient, k, is proportional to $(q/A)\ (V/f^2)$ and hence for low (q/A), one needs low

frequencies (f) and high gradients (V). For example, beams of $^{238}U^{1+}$ at 1 keV/u cannot be focussed with present technologies unless we consider frequencies as low as 10 MHz or so. This seems to be a major technological problem.

In the domain of normal conducting RFQs, there exist, at present, designs and operating prototypes from various laboratories in Japan, Germany, USA, etc. As an example, prototype split coaxial RFQs with (q/A) ranging from 1/30 to 1/60, duty factor of 10% and state-of-the-art CW field level at 2.2 times the Kilpatrick limit already exist and reported at this workshop by Tokuda. There have been difficulties with CW operation (heating and power level) and high gradients. However, with proper design, there seem to be no fundamental barrier in reaching close to the (q/A) ~ 1/240 and CW (100% duty factor) regime, as reported by A. Schempp in this workshop.

In the domain of superconducting RFQs, while it has been possible to produce high gradients in short structures, difficulties are presented in sustaining high field levels in long structures. Moreover, the requirement of large transverse acceptance favors large beam tube aperture, hence low rf frequency which implies rather large rf structures. At present, studies have been restricted to a frequency of 50 MHz and beyond. This issues of structural rigidity and associated problem of 'microphonics' for such large structures lead to difficulties in good rf phase control. Superconducting RFQs have been discussed by K. Shepard at this workshop.

In order to simplify the RFQ tasks, the following two directions need to be explored in detail:

a) To decouple the "bunching" function from the "focussing and accelerating" function, by adding a separate prebuncher injecting into an efficient RFQ (see report by J. Staples at this workshop);

(b) To accommodate multiple requirements and the large dynamic range, different front ends may be needed for different mass ranges, allowing trade-off between transverse acceptance and initial charge state.

3.2 Cyclotrons

Cyclotrons can combine the functions of mass separation and acceleration and thus could be considered as potential substitutes for the RFQs and the high-resolution spectrometer. It has been claimed that if ECR sources with high metal efficiency ($^{238}U^{30+}$) could be developed, a cyclotron with K= 600, with no stripping, producing 10 MeV/u U^{30+} or 50 MeV/u O^{5+} and single-turn extraction (for good beam quality) would be an attractive option. Although cyclotrons were outside the detailed scope of this workshop, they should be seriously looked into. A review is presented by D. Clark at this workshop.

3.3 Outstanding Issues

The following questions regarding RFQs need to be addressed as quantitatively as possible:

(a) What is the ultimate reach of normal conducting RFQs in "q/A" and "Duty Factor", given our present understanding of the fundamental technological limitations due to high gradient, heating, etc.?

(b) Are there foreseeable technological innovations that push these limits further? How far?

(c) Is 50 MHz the lowest achievable frequency for a practical Superconducting RFQ structure with necessary stability?

(d) What are the relative difficulties of technological solutions, if any, for normal conducting vis-a-vis superconducting RFQs?

(e) Is there a multiple front-end injector solution, at least on paper, that look reasonable?

4. ISOBAR SEPARATOR AND MATCHING

For maximal transmission (i.e. minimal loss), phase-space matching throughout the post-accelerator is crucial. This requires sophisticated nonlinear design, possibly including space charge at lower energy for high ion currents.

'Purity' of the beam is of utmost importance as well. One has to do the very best in isobaric separation.

The following outstanding issues need to be addressed:

(a) Do we really need an isobar separator for all beams? What is the required power supply stability? What is the required beam energy spread and emittance?

(b) What are the consequences for the emittances, the necessary extraction potential and the design of the separator, should the current from the Ion Source be so high that we would require a medium-current isotope separator with full space-charge compensation?

(c) Problems of cross-contamination, high separation efficiency and high transmission simultaneously.

(d) Is multi-stage separation unavoidable?

5. ION SOURCES

Ion source characteristics (q/A, etc.) have a profound effect on the post-accelerator design. So far, ECR sources have been looked into in detail as the only contender for efficient production of highly charged ions. However, ECR sources presumably have large emittances (e.g. 400 π mm–mrad), which are clearly not acceptable. Potential alternatives e.g. laser-ion sources, etc. should be looked at.

Issues in ion sources that need to be addressed are:

(a) What are the advantages/disadvantages of starting the post-acceleration process with charge states $q > 1$ in the ion source compared to $q=1$?

(b) What are the promising new ion sources and their developments that could become relevant for the ISL? How important are Laser Ion Sources?

(c) What is the highest practical voltage we can really use for the extraction voltage in radiation environment?

(d) List beam characteristics of standard ISOL sources (emittance, $\delta E/E$, etc.). Can one develope an universal ion source?

(e) What is the maximum current expected from the Ion Source?

(f) Importance of atom/ion storage systems e.g. Paul traps, Penning traps, the GSI (Kirchner) scheme, etc.

6. OUTLOOK

The detailed technical contributions during the workshop are reproduced in these proceedings. These together with the two working group summary reports address most of the questions raised here and point the way to future work.

IsoSpin Laboratory Concept

(revised Nov. 1993)

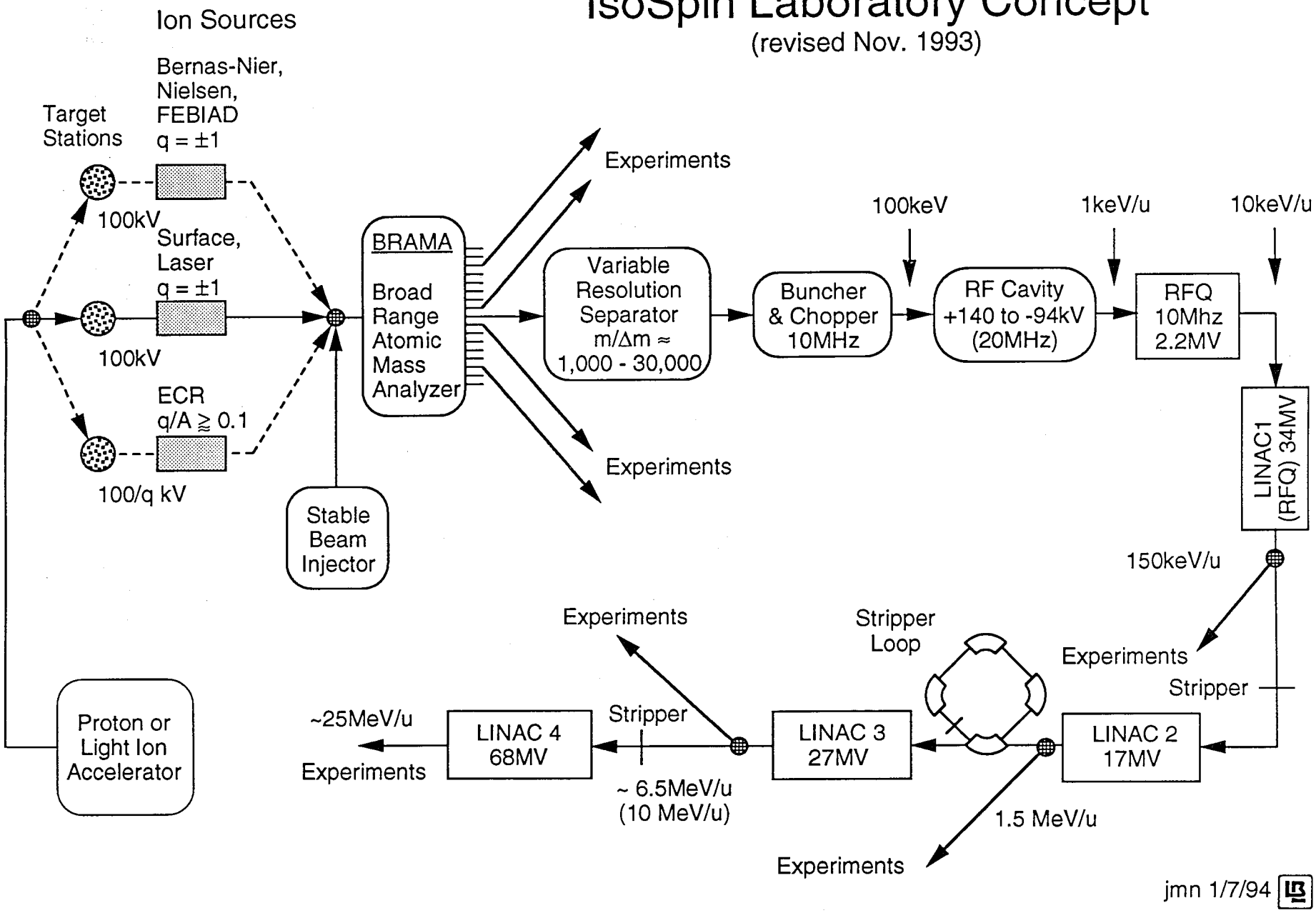

IsoSpin Laboratory

Revised Specifications (Nov. 1993)

Primary Beam Accelerator:

Particles:	p, (d, ^{3}He)
Energy:	0.5 - 1 GeV
Intensity:	100 - 200 μA (protons)
Beam structure:	CW (or pulsed ≥ 1% D.F.)

Target:

Matrix:	solid or liquid
Thickness:	~1 mol/cm^2
Power:	≤ 40 kW
Luminosity:	(4 - 8)×10^{38} s^{-1}·cm^{-2}

RNB Accelerator:

Energy Range:	0.2 - ~25 MeV/u
Intensity:	10^2 - 10^{11} pps
Mass Range:	1 - 240 u
Z Range:	1 - 93
Beam Purity:	<10^{-4} (<10^{-5} nucl. astrophys.)
Macro Beam Structure:	DC (or pulsed ≥ 25% D.F.)
Micro Beam Structure:	~ 100 ns (for TOF)
Energy Resolution:	0.1 - 1%
Emittance $\varepsilon_{x,y}$:	≲ 0.2 π mm·mrad (norm.)
Emittance ε_z:	~ 20 - 50 keV ns
Transmission:	≥ 90 % (excl. stripper losses)

ION SOURCES FOR RADIOACTIVE BEAMS

R. Kirchner

GSI Darmstadt, Postfach 110552, D-64220 Darmstadt, Germany

Abstract

The ion sources reviewed here, most of them developed for isotope separation on-line (ISOL), are classified according to their ionizing mechanism, utilizing electrons, heat, light, and penetration of matter. Emphasis is put on the beam-optical characteristics ion current density, energy spread, and emittance and on the ISOL-essentials "efficient, fast, and selective", both for the ion source and the complete target/ionsource-system.

Introduction

Ion sources for radioactive beam facilities have essentially the same task as the ones [1,2] developed for isotope separation on-line (ISOL). On a meeting of accelerator specialists it is close at hand to emphazise the demands to an ISOL-source by comparison with the demands to the more familiar accelerator ion sources. Common is the demand for reliabibility, universality, stability, long lifetime, low emittance and low energy spread. The difference lies in the fact that accelerator sources have to convert (usually unlimited and well-defined) charge materials into intense ion currents, whilst ISOL-sources have to convert the limited number of particles produced in nuclear reactions as ***efficiently*** as possible into ions, the corresponding ion current hardly ever reaching the μA-range. Since the "charge material" of ISOL-sources is radioactive, i.e. often of very limited lifetime, and composed of many elements, the conversion should proceed in a ***fast*** and ***selective***, i.e. element-specific way - requirements, generally without meaning for an accelerator source. A further difference may be that these three main requirements do not only apply to the ion source proper, but to the system of ion source and its production target.

Of the possible mechanisms leading to ionization, i.e. ***electron-bombardment, heat, interaction with light, penetration of matter,*** and ***high electric fields***, all except the last one have been utilized for ISOL-sources and serve for the subsequent classification.

1. Electron-impact Ion sources

Since electron-impact ionization cross-sections do not differ too strongly among neighbouring elements, the sources of this chapter are in principle universal and unselective. Limits of universality und thus a certain degree of selectivity may, however, arise from the fact some elements are not sufficiently volatile at the operation temperature of the ion source and are lost due to surface adsorption or diffusion into the bulk of the source enclosure.

1.1 Low pressure arc discharge ion sources

These sources typically are composed of a cylindrical anode, sealed by two end-plates (the cathode plate with the filament and the anti-cathode) to a hot and gastight enclosure for the gaseous discharge. Ions are created by fast (30-100 eV) glow electrons from the filament. At and avove a threshold pressure of 10^{-3} to 10^{-2}mbar, the primary electron current rises strongly to its saturation value due to formation of the cathode double-layer. This is the drop of practically the full discharge voltage within short distance of the filament, while the rest of the enclosure fills with the the practically neutral low pressure arc plasma. The resulting high flux of ionizing particles, often amplified by an external solenoidal field which additionally increases the ion-confining forces of the plasma, makes this class of sources quite efficient (typically 30% for Ar, Kr, or Xe). Depending on whether ion emission is performed axially through a hole in the cathode- oranti-cathode-plate, or radially through a slit in the anode, the design is a *Hollow-cathode* [3] , *Nielsen* [4] *or Bernas-Nier* [5-7] ion source. They all have both low emittance (emittance values given in this review refer to 90-95% of the beam intensity and 30 kV acceleration voltage) and energy spread ($\lesssim 20\pi$ mm mrad [6], few eV). Due to the pressure threshold (close to which the discharge tends strongly to instabilities) the output current density is quite high ($j_i > 10$ mA/cm^2). The high ion currents, especially for the Bernas-Nier source, are advantageous, if the ion source is coupled to targets emanating great amounts of material [7], exclude, however, the simple and economic low-intensity mass separator concept due to space charge problems.

1.2. *Space-charge compensated electron-bombardment sources*

Similar in design to the low pressure arc sources and like those suited for all elements of sufficient volatility at the temperature of the enclosure (up to 2500K), this class of sources avoids the arc threshold pressure and the associated instabilities by extracting the primary electrons by a grid. The main types, especially developed for ISOL applications, are the *FEBIAD*-source [8] with an axial cathode-grid geometry and the radial-geometry *EBGP*-source [9]. The advantage of the former is its rugged design, the advantage of the latter the non-necessity of a source magnet, its easy conversion into a high-temperature-cavity ionizer (chapter 2.2) and its high ultimate temperature by avoiding electrical insulators within the hot enclosure. Typical for these sources are high and widely pressure-independent ionization efficiencies

(20-70% for elements above neon). Similar in emittance and energy spread to the low pressure arc sources, they have substantially lower output current densities ($j_i < 1$ mA/cm^2) thus being easily compatible with any mass separator concept.

1.3. Electron-cyclotron resonance ion sources

Primarily intended as high-charge-state accelerator source, the *ECR*-source has now also found considerable appreciation as 1^+-ionsource in ISOL. Reason is the very high efficiency for gases [10-12], and especially its capability of dissociating and ionizing efficiently molecular gases of C, N, O, chemical reactivity preventing their handling in high temperature enclosures. Its principle is microwave-driven electron-bombardment ionization, the low-density discharge plasma being confined by a magnetic field configuration of axial mirror plus radial hexapole field. Typical are ion current densities of around 1 mA/cm^2 out of orifices from 3 to 10 mm diameter, however, with quite high emittances of 70 to 150π mm mrad [13,14]. A great advantage is the long lifetime and stable running conditions for gases due to the absence of wearing parts; disadvantageous is the strong decrease of efficiency with increasing pressure. Due to the cold enclosure ECR's can hardly compete in efficiency for less-volatile elements with high-temperature sources. If, however, high ionic charge states from the source are required by certain post-accelerator concepts, even efficiencies of around 1% as reached e.g. for high charge states of Ca are of unrivalled importance, although considerably lower than the 25% reached for Ar^{8+} [14].

2. Thermionic Ion sources

The ionization efficiency of thermo-ionizers is strongly dependent on the ionization potential (electron affinity) of the element considered. Differences in these quantities for neighbouring elements may make the ionization process intrincally selective.

2.1. Postive and negative surface ionization sources

Surface ionization occurs when a valence electron of an adsorbed atom has a sufficiently high chance to tunnel into the Fermi-sea represented by the adsorbing material. The ionization probability is given by the Saha-Langmuir equation, i.e. it is high and almost temperature-independent for $W_i < \varphi$ (W_i ionization potential of adsorbed atom, φ work function of surface), and strongly dependent on temperature and $(W_i-\varphi)$ for $W_i > \varphi$. Efficient ionization is thus restricted to elements with $W_i < 5.5$ eV, e.g. alkalines and alkaline earths, desorbing from *high*-workfunction surfaces such as W, Re, and Pt.

Analogously efficient negative surface ionization is possible for elements with electron affinities $E_A > \varphi$, e.g. the halogenes. It requires *low*-workfunction surfaces such as LaB_6 or BaO. Since these materials are limited in operation temperature, an ISOL-design should minimize the number of surface collisions [15], to avoid excessively long hold-up times.

2.2. High-temperature cavity ion sources

These sources are a special class of positive surface ionizers [16] , where the ionization takes place inside a closed (except for the outlet hole) volume [17] with the effect that atoms have a multifold chance of being surface-ionized. At high temperatures and low plasma densities the ionization efficiency may exceed the Saha-Langmuir values by orders of magnitude. For high neutral densities the amplification factor may be as high as the mean number of wall collisions [18]. This makes the coupling of relatively volatile targets unproblematic, as long as the vapour is not surface-ionized or only to low degree. In the opposite case, i.e. for high plasma densities, the efficiency may drop drastically, even below the values given by the Saha-Langmuir-equation. Its high temperature (up to >3000K) gives access to refractory elements; efficient ionization is, however, restricted to elements with $W_i < 7$ eV, e.g. the lanthanides. Ion currents may be as low as 1 $\mu A/cm^2$, energy spread and emittance are very low (<1eV, <2π mm mrad).

3. Laser ion sources

Multistep photo-ionization using intense laser light of 2 or 3 (eventually even of only 1 [19]) wavelength is of increasing importance both in trace analysis and ISOL [20-23]. Resonant excitation at least in the first step with subsequent transition(s) into the continuum or to auto-ionizing- or Rydberg-states, quarantees intrinsic selectivity of the ionization process which may, however, be limited due to surface ionization of neighbouring elements. Ionization efficiencies of the order of 10% are achieved for favourable excitation schemes, even using low duty-cycle pulsed lasers. Only these have usually sufficient power (either directly or for driving tunable dye-lasers) to saturate the transitions. To overcome the low duty-cycle, the photo-ions have to be effectively prevented from recombination, e.g. by confinement in the potential trough of a hot cavity [21] or in a gas cell [19], eventually combined with fast ejection geometries. The consequently bunched structure of the ion beam (typically 10 kHz, 10-30 μs) allows for enhanced selectivity by gated detection and may be useful for post-acceleration. Emittance and current density are low (comparable to hot cavity ionizers); the energy spread, however, may be some 10 eV, i.e. corresponding to the electrostatic potentials applied for fast ejection of the ion pulses.

4. Ion guides

The ion quide technique, developed in Jyväskylä [24] and adopted succesfully also by many other ISOL-groups [25], utilizes the fact that radioactive nuclei, when recoiling from their production target are highly charged and may be efficiently discharged to charge state 1^+ in a stopping gas as e.g. pure helium. It is thus a universal (but consequently unselective) and very fast "ion source", since there are no delays due to solid state diffusion and surface adsorption. Restrictions of the technique to light-ion induced reactions and to very thin

targets, as well as ion losses due to charge exchange with impurities, wall collisions , or three-body-recombination, however, limit the rates of separated isoptopes to values typically below 10^5/s and thus the applicability for RIB-projects.

5. The target/ion-source system

So far only the contribution of the ion source to the essentials ***efficient, fast,*** and ***selective*** of the target/ionsource-system was considered. The system adds to the losses by incomplete ionization the halflife-dependent losses due to the finite processing time between creation of a reaction product and its release from the system as an ion beam. On the other hand it may enable selectivity in cases, where this is not possible by the ionizing mechanism. Established techniques are "chemical evaporation", i.e. the on-line-formation of compounds [26], enabling often both improved separation of wanted elements and suppression of unwanted. A particularly favourable case is the formation of fluorides of Sr and Ba by adding CF_4 permitting practically 100%-efficient and completely exclusive separation as SrF^+ (BaF^+) ions [27,28].

Other techniques utilize the delays caused by solid-state diffusion in the target material or by surface adsorption at the walls of the system, most effectively by the latter [26,29]. The associated problems and perspectives are best exemplified by looking at the propagation of reaction products through two somewhat idealized ISOLDE-systems [26,30]. Both are supposed to be operated at 2500K and to use thick Ta targets consisting of 100 µm Ta-foils, and of 10 µm Ta-powder, respectively, thus minimizing the surface/volume-ratio of the target material and vice versa. Considered are reaction products of Xe, Yb, and Dy, which have practically the same solid-state diffusion speed in tantalum ($D \approx 5 \times 10^{-9} cm^2/s$) but very different mean sticking times on tantalum surfaces ($\tau_a \approx$ 0, 50µs, and 500µs, respectively). Xenon, though not a typical reaction product of Ta targets, is included to illustrate, how volatile elements, not suffering from sizeable wall sticking times, are still delayed in the gaseous phase by molecular flow. Calculations based on refs. [29-31] show in qualitative agreement with experiment [32] that for the foil target the main losses arise from solid state diffusion, and that the halflife-dependence of the release efficiency differs relatively little for the three elements (no selectivity), allowing even for the separation of shortlived Dy-isotopes. The "much faster" powder target, on the other hand, gives considerably better yields for the volatile Xe, while Dy (and most other lathanides) are strongly discriminated, thus opening for the most volatile lanthanide element Yb a wide halflife-window for reasonably efficient and selective separation.

References

[1] H.L. Ravn, Nucl. Instr. Meth. B70 (1992) 107
[2] P. Van Duppen et al, Rev. Sci. Instr. 63 (1992) 2381
[3] G. Sidenius, Radiation Effects 44 (1979), 145
[4] O. Almen and K.O. Nielsen, Nucl. Instr. Meth. 1 (1957), 302
[5] V.T. Koslowsky et al. Nucl. Instr. Meth B70 (1992) 245
[6] J.C. Puteaux et al, Nucl. Instr. Meth B26 (1987) 213
[7] J.C. Puteaux et al, Nucl. Instr. Meth. 186 (1981) 321
[8] R. Kirchner et al, Nucl. Instr. Meth. 133 (1976) 187 and B70 (1992) 56
[9] J.M. Nitschke, Nucl. Instr. Meth. A239 (1985) 1
[10] V. Bechtold et al, Proc. Workshop ECRIS, Jülich 1986, 248
[11] P. Decrock et al, Nucl. Instr. Meth. B58 (1992) 252
[12] L. Buchmann et al, Nucl. Instr. Meth B63 (1992) 521
[13] M. Huyse (Leuven), H. Schulte (GSI), private communication
[14] P. Sortais (GANIL), priv. comm.
[15] B. Vosicki et al, Nucl. Instr. Meth. 186 (1981 307
[16] G.J. Beyer et al, Nucl. Instr. Meth. 96 (1971) 347
[17] A. Latuszynski et al, Nucl. Instr. Meth. 125 (1975) 61
[18] R. Kirchner, Nucl. Instr. Meth. A292 (1990) 203
[19] Z.N. Quamhieh, Nucl. Instr. Meth B70 (1992) 131 and M. Huyse, private communication
[20] H.J. Kluge et al, Proc. Accelerated RIB Workshop, TRIUMF Rep. 85-1, 119
[21] G.D. Alkhazov et al, Nucl. Instr. Meth. A280 (1989) 141
[22] V.I. Mishin et al, Nucl. Instr. Meth B73 (1993) 550
[23] V.N. Fedoseyev et al, Annual Rep. 1992, Inst. Nucl. Chem., University Mainz (1993)
[24] J. Ärje et al, Phys. Rev. Lett. 54 (1985) 99
[25] Section II and IV in Nucl. Instr. Meth. B70 (1992) 50 and 213ff
[26] E. Hagebo et al, Nucl. Instr. Meth B70 (1992) 165
[27] R. Eder et al, Nucl. Instr. Meth B62 (1992) 535
[28] Y. Kawase et al, Nucl. Instr. Meth. B70 (1992) 146
[29] R. Kirchner et al, Nucl. Instr. Meth B70 (1992) 56 and 186
[30] L.C. Carraz et al, Nucl. Instr. Meth. 148 (1978) 217
[31] G. Rudstam, CERN-Report 70-3 (1970) 125
[32] T. Bjornstad et al, Phys. Scripta 34 (1986) 578

ION SOURCES FOR INITIAL USE AT THE HOLIFIELD RADIOACTIVE ION BEAM FACILITY

G. D. Alton
Oak Ridge National Laboratory*
P. O. Box 2008
Oak Ridge, Tennessee 37831-6368

The Holifield Radioactive Ion Beam Facility (HRIBF) now under construction at the Oak Ridge National Laboratory will use the 25-MV tandem accelerator for the acceleration of radioactive ion beams to energies appropriate for research in nuclear physics; negative ion beams are, therefore, required for injection into the tandem accelerator. Because charge exchange is an efficient means for converting initially positive ion beams to negative ion beams, both positive and negative ion sources are viable options for use at the facility; the choice of the type of ion source will depend on the overall efficiency for generating the radioactive species of interest. A high-temperature version of the CERN-ISOLDE positive ion source has been selected and a modified version of the source designed and fabricated for initial use at the HRIBF because of its low emittance, relatively high ionization efficiencies and species versatility, and because it has been engineered for remote installation, removal and servicing as required for safe handling in a high-radiation-level ISOL facility. Prototype plasma-sputter negative ion sources and negative surface-ionization sources are also under design consideration for generating negative radioactive ion beams from high-electron-affinity elements. The design features of these sources and expected efficiencies and beam qualities (emittances) will be described in this report.

* Managed by Martin Marietta Energy Systems, Inc., under contract No. DE-AC05-84OR21400 with the U.S. Department of Energy.

1.0 INTRODUCTION

Many of the nuclear reactions important for the understanding of nuclear structure and astrophysical phenomena are inaccessible to study using stable projectile/stable target combinations; they, therefore, can only be studied with accelerated radioactive ion beams (RIBs). As a consequence of these unique research opportunities, a number of RIB facilities have been proposed throughout the world [1], including the Holifield Radioactive Ion Beam Facility (HRIBF) [2,3] now under construction at the Oak Ridge National Laboratory.

The HRIBF has as its objective the production and acceleration of short-lived, proton-rich nuclei for the study of nuclear structure physics and astrophysics. In the HRIBF concept, intense light ion beams from the Oak Ridge Isochronous Cyclotron (ORIC) will be used to produce radioactive atoms in a thick-target, ISOL-type ion source mounted on a high-voltage platform which will serve as a second injector for the 25-MV tandem accelerator. Since the tandem accelerator requires negative ion beams, positive ion beams must be converted to negative ion beams through charge exchange prior to their injection into the tandem accelerator. Among the proposed initial species are radioactive beams of C, O, F, Na, Si, P, S, Cl, K, Cu, Ga, Ge, As, Se, Br, and Rb. An important capability of the HRIBF will be the ability to accelerate all of these beams to energies of at least 5 MeV/amu.

The success of this project will be critically dependent on the choice, design, and performance of the target/ion sources. For radioactive ion beam generation, these sources must operate stably for extended periods at elevated temperatures (>2000°C) and be designed to facilitate expedient and remote (if necessary) installation, removal,

and servicing, as required for safe handling of high-level, radioactively contaminated sources, source components, and ancillary equipment. The selection of a particular target/ion source or sources is critically important since their respective performances determine the intensity, beam quality, and the number of radioactive beams that can be provided for experimental use. High-ionization-efficiency sources are clearly desirable because of the low production rates of the radioactive species of interest, release losses which may be incurred through trapping within the target, and surface chemical reactions during transport from the target and through the source. The ISOL technique is complicated by high-temperature physics, chemistry, metallurgy, diffusion, and surface adsorption processes which take place in the target-ion source; all of these processes add to the delay times which result in losses of the short-lived radioactive species of interest.

For RIB generation, the source should ideally exhibit the following properties: high efficiency; high temperature operation in order to minimize the diffusion times from the target and residence times on surfaces; low energy spreads; chemical selectivity; flexibility for adaptation to different temperature ranges and modes of operation; target temperature control; long lifetime; and stable electrical and mechanical properties. While there are no sources which simultaneously meet all of these criteria, a number of sources have been developed at ISOL facilities which meet some of the requirements noted above. We have selected and designed an electron-beam plasma-type source patterned after the CERN-ISOLDE source [4] for initial use at the HRIBF. The HRIBF source is also described in Ref. 5. This source was chosen because of a number of reasons, including the following: 1) it is competitively efficient; 2) it has a wide range of species capabilities; 3) it has demonstrated reliability over many years of operation at the CERN-ISOLDE facility; 4) the target temperature can be controlled independently of the discharge parameters of the source; 5) the basic

geometry can be readily adapted to other types of sources; 6) it has been engineered for safe removal and installation in the high-radiation-level fields present at ISOL facilities; 7) the source has a low emittance (~2 π mm.mrad $MeV^{1/2}$).

High-efficiency negative-ion sources are obviously preferred for applications involving the postacceleration of RIBs with tandem accelerators such as at the HRIBF. We have designed a plasma-sputter negative-ion source specifically for generation of ion beams from high-electron-affinity elements, e.g., the group IV-A, V-A, VI-A, and VII-A elements. The source will be housed in the vacuum envelope of the HRIBF source. The design aspects and expected performance of this source type for a selected number of elements will also be presented. A complementary negative-surface-ionization source has also been designed for alternate use with the plasma-sputter negative ion source in generating RIBs from certain members of the group VI-A and VII-A elements; this source will also be briefly described.

2.0 THE HRIBF POSITIVE ION SOURCE

The CERN-ISOLDE on-line source [4] is in the class of electron beam plasma ion sources and, therefore, similar, in principle, to the forced-electron-beam-induced-arc-discharge (FEBIAD) source developed at GSI [6-8]. Sources of this type differ from conventional plasma discharge sources in that they do not require a minimum pressure for stable operation (commonly referred to as the Langmuir criterion for stable discharge). The source operates at pressures of more than one order of magnitude lower than the Nielsen plasma-discharge source [9] as reported in Ref. 10. The CERN-ISOLDE source is well suited for ISOL applications because, unlike the FEBIAD ion source, the target temperature can be independently controlled. Both

types of sources operate stably and efficiently over a pressure range of ~1 x 10^{-5} to ~2 x 10^{-4} Torr at elevated temperatures [10].

2.1 Ionization Efficiencies

The ionization efficiencies of the CERN-ISOLDE and FEBIAD ion sources are quite high for slow moving heavy ions; for low mass, fast moving atoms with high ionization potentials, the efficiencies are not as impressive. This effect can be readily observed by comparing the ionization efficiencies of the noble gas elements using the FEBIAD ion source [11]; the efficiencies for these elements were measured to be: Ne: 1.5%; Ar: 18%; Kr: 36%; and Xe: 54%. The ionization efficiencies for the noble gas elements, using the CERN-ISOLDE source, are close to those measured for the FEBIAD source. For example, the maximum efficiency recorded for the CERN-ISOLDE source with Xe is 56% [12].

The following empirical equation has been found to be useful in approximating ionization efficiencies η for noble gases in sources of this type:

$$\eta_{calc} = \frac{4\langle\ell\rangle D_o N_e}{A_o}\left(\frac{\pi M_i}{8kT_i}\right)^{1/2} \exp\{-Ip/\langle kT_e\rangle\}/[1 + \frac{4\langle\ell\rangle D_o N_e}{A_o}\left(\frac{\pi M_i}{8kT_i}\right)^{1/2} \exp\{-I_p/\langle kT_e\rangle\}]. \quad (1)$$

In Eq. 1, $\langle\ell\rangle$ = average path length for a particle in the plasma; D_o = constant (cm^2/s); A_o = emission area of the source; k = Boltzmann's constant; T_i = ion temperature; T_e = electron temperature; I_p = ionization potential; N_e = number of electrons in the valence shell of the atom with a given I_p; and M_i = mass of species. The following values are used for terms in Eq. 1 when estimating ionization efficiencies for the FEBIAD ion source: $\langle kT_e\rangle$ = 3.029 eV; T_i = 2273K; and $4\langle\ell\rangle D_o / A_o$ = 5.39 x 10^5 cm/s. Table 1

compares the efficiencies for a number of elements as calculated from Eq. 1, with those measured by using the FEBIAD, CERN-ISOLDE, and the electron-beam-generated plasma (EBGP) source [13].

2.2 Source Design Features

In designing the HRIBF target/ion source, particular emphasis was placed on the materials of construction, the thermal transport properties, the size and geometry of the target, and the number of species that the source can be used to process. Equal attention was given to design features which facilitate assembly and disassembly of contaminated source components to avoid potential radiation hazards to personnel during maintenance periods.

The target/ion source assembly, shown schematically in Figs. 1-3, incorporates many of the engineering features utilized in the CERN ISOLDE design [4]. The source assembly has been engineered to enable remote installation and removal in high-radiation fields and the transport of contaminated sources and components to and from remote servicing and storage areas. To install the source assembly, for example, the assembly is lowered by means of a remotely controlled overhead hoist mechanism onto locator pins associated with a linear motion carriage. The carriage is then pushed forward and clamped against the vacuum interface flange by a remotely controlled pneumatic actuator mechanism. The source assembly plugs into the interface flange, during which all electrical, gas feed, coolant, vacuum, and temperature monitoring connections are mated together. A schematic illustration of the source in the operational position is shown in Figure 1. Following this operation, the vacuum seal between the beam entrance port on the source vacuum chamber and beam line from the ORIC is also made by remote actuation of a similar pneumatic

clamping device. The vacuum chambers can then be pumped down or vented by remote control of the pumps and valves associated with the source and ORIC beam lines. To remove the source, the procedure is reversed. For servicing and storage, the source is simply lifted from the linear-motion carriage by means of an electrically driven chain hoist and transported to a separated shielded work or storage area.

The high-temperature target and ionization chamber of the source are shown schematically in Figs. 2 and 3. Following vacuum pump down, the source is outgassed by incrementally adding power to both the target reservoir and to the cathode until the source achieves a steady-state vacuum level at the anticipated operational temperature. Collimated ^{1}H, ^{2}D, ^{3}He, and ^{4}He ion beams from the ORIC will pass through a thin Re window where they will interact with the refractory target material chosen for the production of the desired radioactive beam. The Ta target material reservoir is lined with Ir or Re metal as are beam transport tubing and internal surfaces of the source to reduce the residence times of chemically active elements during adsorption. The thickness of the target is chosen so that the projectile has an energy spread within the target medium which approximates that required for optimum radioactive species production. The unreacted beam exits the target through a second Re window, then strikes a cooled C beam stop. This technique reduces the power deposited in the target and thereby simplifies temperature control problems.

The target reservoir is positioned within the inner diameter of a series-connected, resistively heated, triaxial Ta tube. The reservoir can be heated to temperatures exceeding 2000°C by passing a current through the tubular structure. The power required to heat the assembly to 2000°C is measured to be ~2.25 kW (4.5 V at 500 A). Temperature control will be maintained within ± 5°C by use of feedback circuitry driven by a two-color pyrometer to adjust the current through the heater.

The electron emitter cathode is also made of Ta and is resistively heated to thermionic emission temperatures, ≥ 2125°C. The electron beam, typically ≥ 250 mA, is accelerated through a potential difference of 200-300 V to the perforated anode plate where it passes into the cylindrical cavity of the anode structure and ionizes the gaseous material. Collimation of the electron beam is effected by adjusting the coaxially directed solenoidal magnetic fields so as to optimize the ionization efficiency of the species of interest. The cathode power required to achieve thermionic emission temperature will be ~ 2 kW (400 A at 5 V). The total power required to heat the target and cathode to the temperatures listed above and to ionize the vaporous material transported from the target to the ionization chamber of the source will be of the order of 4.5 kW.

The ion extraction electrode system for the source was iteratively designed by use of the computer code described in Ref. 14, which includes space charge and plasma optical effects. The extraction gap can be varied in order to optimally transport ion beams over a wide energy range as required for optimally converting positive ion beams to negative ion beams through charge exchange.

3.0 THE PLASMA-SPUTTER NEGATIVE ION SOURCE

The adsorption of less than a monolayer of a highly electropositive adsorbate material on the surface of a sample undergoing particle bombardment greatly enhances the probability for secondary negative ion formation [15].

In the prescription of Nørskov and Lundqvist [16], the probability for negative ion formation during sputtering can be represented by the following simple energy-dependent relation:

$$\eta_i = \frac{2}{\pi}\exp\left[-\beta\sqrt{M_2}\{\phi(\sigma) - E_A + V_i\}/\sqrt{2E_2}\cos\theta\right] \quad (2)$$

In Eq. 2, ϕ is the work function of the surface which is a function of the relative adsorbate coverage σ, E_A is the electron affinity of the ejected particle of mass M_2 and energy E_2, V_i is the image potential induced in the surface by the escaping ion, θ is the polar angle of the sputtered ion with respect to the surface normal and β is a constant. In Eq. 2, $\sqrt{2E_2/M_2}\cos\theta = v_\perp$ is the component of the velocity of the escaping particle perpendicular to the metal surface.

The technique of sputtering a surface covered with a fractional layer of a highly electropositive adsorbate material such as cesium has proved to be a universal method for generating atomic and molecular negative ion beams from most chemically active elements. In addition to being versatile in terms of species, sources based on this concept are simple in design, easy to operate, and generally have long lifetimes. Because of these factors, such sources are used extensively in most tandem electrostatic accelerator heavy ion physics research laboratories, as well as for use in a growing number of other applications, including high-energy ion implantation and tandem accelerator mass spectrometry. Positive ion beams, usually formed by either direct-surface ionization of a group IA element or in a heavy noble gas (Ar, Kr, or Xe) plasma discharge seeded with alkali metal vapor, are accelerated to energies between a few hundred eV and several keV where they sputter a sample containing the element of interest. The presence of a fractional layer of a highly electropositive adsorbate material is critically important to the enhancement of negative ion formation

during the sputtering process. A fraction of the sputter-ejected particles leave the adsorbate-covered surface as negative ions and are accelerated through an extraction aperture in the source. Several sources predicated on this principle have been developed, some of which are described in Ref. 17. Sources based on this principle are particularly appealing for applications involving the postacceleration of RIBs with tandem accelerators such as at the HRIBF. In particular, sources which use a plasma to sputter the sample [18,19] are especially attractive because this technique assures uniform sputtering and, consequently, good overlap of the bombarding species and the material containing the radioactive ion beam.

Figure 4 displays a schematic representation of a plasma sputter source now under design for potential use at the HRIBF. The source will be housed in the same vacuum envelope as the HRIBF source. Radioactive species from the target will be transported at high temperatures through the vapor transport tube into the plasma-discharge chamber where the vapor will be condensed on the cold cathode surface. A xenon plasma, seeded with cesium from an external oven, will be ignited either by a filament or an RF antenna. The final choice of the two means of igniting the plasma will be determined during off-line testing of the source. The radioactive ion beam will be formed by sputter ejection of atoms or molecules from the negatively biased spherical-geometry sputter probe covered with a partial layer of cesium adsorbate material. The double sheath surrounding the negatively biased sputter probe (spherical radius 30 mm and diameter ϕ = 12.5 mm), which is maintained at a variable voltage (0–1000 V) relative to housing, serves as the acceleration gap and lens for focusing the negative-ion beam through the exit aperture (diameter ϕ = 3 mm). At this point, the ion beam is further accelerated to energies up to 50 keV prior to mass analysis. The efficiencies of several negative ion species, estimated by Tsuji and Ishikawa [19], are shown in Table 2. The measured emittance of a similar geometry source is quite

good (~6π mm.mrad $MeV^{1/2}$) [20] even at mA intensity levels of Cu^-. This emittance is lower than the acceptance of the HRIBF 25-MV tandem accelerator [21].

4.0 NEGATIVE-SURFACE-IONIZATION SOURCE

For atoms or molecules leaving a heated surface, the probability of negative ion formation η_i arriving at a position far from the metal in a given state depends on the magnitude of the difference between the electron affinity E_A and the surface work function ϕ of the atom or molecule, i.e., $(E_A - \phi)$. For thermodynamic equilibrium processes, the ratio of ions to neutrals which leave an ideal surface can be predicted from Langmuir-Saha surface-ionization theory appropriate for negative ion formation. The form of the Langmuir-Saha equation for the probability of negative ion formation for neutral particles of electron affinity E_A interacting with a hot metal surface at temperature T and constant work function ϕ is given by

$$\eta_i = \frac{\omega_-}{\omega_0}\left(\frac{1-r_-}{1-r_0}\right)\exp\left(\frac{E_A-\phi}{kT}\right)x\left[1+\frac{\omega_-}{\omega_0}\left(\frac{1-r_-}{1-r_-}\right)\exp\left(\frac{E_A-\phi}{kT}\right)\right]^{-1}, \quad (3)$$

where r_-/r_0 are the reflection coefficients of the negative/neutral particles at the surface and ω_- and ω_0 are statistical weighting factors for the negative ion and neutral atom, respectively. ω_- and ω_0 are related to the total spin of the respective species given by $\omega = 2\sum_i s_i + 1$, where s_i is the spin of the electron. In principle, the halogen group of elements can be ionized with unit efficiency on a clean LaB_6 surface maintained at 1373 K. From Eq. 3, it is evident that negative ion yields could be enhanced by lowering the work function ϕ or increasing the surface temperature T for elements where $E_A \leq \phi$. The former can be effected by surface adsorption of minute amounts of low-work-function materials such as the group I-A and II-A elements. Analogously,

the adsorption of minute amounts of highly electronegative atoms or molecules such as oxygen or the halogens can deleteriously effect the negative surface ionization efficiency by raising the work function.

The negative form of surface ionization is also highly chemically selective and, therefore, can be used to great advantage for the generation of high-electron-affinity elements such as the group VII-A (halogens). Unfortunately, there is limited availability of a wide variety of stable, low-work-function materials. LaB_6 is the most frequently used low-work-function surface ionizer, having a work function ϕ = ~2.7 eV for polycrystalline and $\phi \simeq 2.36$ eV for single-crystalline material.

An on-line form of the negative-surface-ionization source has been developed at CERN-ISOLDE, which is equipped with a LaB_6 surface ionizer [22]. The positive/negative-surface-ionization source described in Ref. 23 has also been used to generate beams of UF_6^-. The HRIBF source can easily be retrofitted with a LaB_6 ionizer and used to efficiently ionize high-electron-affinity elements as clearly evidenced by the successful application described in Ref. 22. Figure 5 displays a negative-surface-ionization source which will be used as a complement to the HRIBF source. The vapor transport tube will be Ir coated tantalum and heated resistively to ~1100°C to again minimize the residence times on surfaces of chemically active materials. This source will serve as a backup source to the plasma-sputter-negative-ion source described in Section 3 for the generation of RIBs from the group VIIA elements.

5.0 DISCUSSION

The most difficult challenge related to the efficient generation of RIBs using the ISOL technique is associated with target and surface adsorption issues and not the ion source itself. The challenge is to select a target material which will withstand the high temperatures required to efficiently and promptly release the short-lived species of interest while preserving the physical integrity of the target material and the vacuum requirements of the ion source. The speed at which the element is released from the target is directly related to the diffusion properties of the species/target material combination [24]. As pointed out by Ravn [25], in general, each element must be considered separately, often requiring dedicated efforts to solve specific problems in order to generate useful RIBs of the element. Much work remains to be done in the area of target material selection and the development of techniques to enhance the release of elements from a properly chosen target material.

ISOL ion source development continues to be driven by needs for sources with improved chemical selectivity, high duty factors, and more universal species capabilities. Despite the fact that electron beam plasma ion sources have poor chemical selectivity characteristics, they have a decided advantage in that they are closer to being universal than other ISOL sources that have been developed to date. Of the electron beam sources, a modified version of the CERN-ISOLDE source has been chosen for use at the HRIBF because of the following: 1) it is competitively efficient; 2) it has demonstrated reliability over many years of operation at CERN-ISOLDE; 3) the target temperature can be controlled independently of the discharge parameters of the source; 4) it can be readily adapted for a wide range of operational temperatures and for other modes of operation; 5) it is readily adaptable to other types

of ion sources; and 6) it has been engineered for safe removal and installation in the high level radiation fields present at an ISOL facility.

Plasma or cesium sputter ion sources offer another possibility for the efficient formation of negative ion beams from high-electron-affinity elements. Sources based on this well-developed technology are not as sensitive to poisoning effects as are direct-negative-surface-ionization sources and, therefore, are very appealing for use at tandem-accelerator-based RIB facilities such as the HRIBF.

Surface ionization sources have reached a certain degree of maturity in their development, but still play important roles for the efficient generation of ion beams from specific elements. They offer a high degree of chemical selectivity and are usually simple and easy to operate. However, the ionizers in negative-surface-ionization sources may be easily poisoned and, therefore, may pose challenges for use at tandem-accelerator-based RIB facilities such as the HRIBF.

6.0 ACKNOWLEDGMENTS

The author would like to express his appreciation to all members of the HRIBF ion source group for contributions to this article. The author is also indebted to Ms. Jeanette McBride for typing the manuscript.

7.0 REFERENCES

[1] D. K. Olsen, Nucl. Instr. and Meth. A328, 303 (1993).

[2] The ORNL Radioactive Ion Beam Project, D. K. Olsen, G. D. Alton, R. L. Auble, C. Baktash, H. Blosser, H. K. Carter, J. Dellwo, D. T. Dowling, J. D. Garrett, D. L. Haynes, C. M. Jones, R. C. Juras, J. Kormicki, S. N. Lane, L. Lee, P. Mantica, F. Marti, M. J. Meigs, G. D. Mills, S. W. Mosko, L. Rayburn, C. A. Reed, R. L. Robinson, B. A. Tatum, and H. Wollnik, in Proceedings of the Workshop on the Production and Use of Intense Radioactive Ion Beams at the Isospin Laboratory, ORNL Conference Proceedings: CONF-9210121, p. 375.

[3] J. D. Garrett, G. D. Alton, C. Baktash, D. K. Olsen, and K. S. Toth, Nuclear Physics A557, 701C (1993).

[4] S. Sundell and H. L. Ravn, Nucl. Instr. and Meth. B70, 160 (1992).

[5] G. D. Alton, D. L. Haynes, G. D. Mills, and D. K. Olsen, Nucl. Instr. and Meth. A328, 325 (1993).

[6] R. Kirchner, D. Marx, O. Klepper, V. T. Koslowsky, T. Kühl, P. O. Larsson, E. Roeckl, K. Rykaczewski, D. Schandt, J. Eberz, G. Huber, H. Loehmann, R. Menges, and G. Ulm, Nucl. Instr. and Meth. A234, 224 (1985).

[7] R. Kirchner, K. Burkhard, W. Hüller, and O. Klepper, Nucl. Instr. and Meth. 186, 295 (1981).

[8] R. Kirchner, K. Burkhard, and O. Klepper, Nucl. Instr. and Meth. B70, 56 (1992).

[9] O. Almen and K. O. Nielsen, Nucl. Instr. and Meth. 1, 302 (1957).

[10] R. Kirchner and E. Roeckl, Nucl. Instr. and Meth. 133, 187 (1976).

[11] R. Kirchner, Nucl. Instr. and Meth. B70, 186 (1992).

[12] G. D. Alton and S. Sundell, unpublished.

[13] J. M. Nitschke, Nucl. Instr. and Meth. A236, 1 (1985).

[14] PBGUNS, Thunderbird Simulations, 626 Bradfield, Garland, Texas 75042-6005.

[15] G. D. Alton, Surf. Sci. 175, 226 (1986).

[16] J. K. Nørskov and B. I. Lundqvist, Phys. Rev. B19, 5661 (1979).

[17] G. D. Alton, Nucl. Instr. and Meth. B73, 221 (1993).

[18] G. D. Alton, Y. Mori, A. Takagi, A. Ueno, and S. Fukumoto, Nucl. Instr. and Meth. A270, 194 (1988).

[19] H. Tsuji and J. Ishikawa, Rev. Sci. Instr. 63, 2488 (1992).

[20] Y. Mori, Nucl. Instr. and Meth. A328, 146 (1993).

[21] J. D. Larson and C. M. Jones, Nucl. Instr. and Meth. 140, 489 (1977).

[22] B. Vosicki, T. Björnstad, L. C. Carraz, J. Heinemeier, and H. L. Ravn, Nucl. Instr. and Meth. 186, 307 (1981).

[23] G. D. Alton, M. T. Johnson, and G. D. Mills, Nucl. Instr. and Meth. A328, 154 (1993).

[24] G. D. Alton, H. K. Carter, I. Y. Lee, C. M. Jones, J. Kormicki, and D. K. Olsen, Nucl. Instr. and Meth. B66, 492 (1992).

[25] H. L. Ravn, Nucl. Instr. and Meth. B70, 107 (1992).

FIGURE CAPTIONS

Fig. 1. ORNL DWG 93-9581. Side cross-sectional view of the HRIBF target/ion source assembly in the operational position.

Fig. 2. ORNL DWG 93-9582. Cross-sectional side view of the HRIBF high-temperature target/ion source showing the target, vapor-transport tube, and ionization chamber of the source.

Fig. 3. ORNL DWG 93-9583. Cross-sectional top view of the HRIBF high-temperature target/ion source showing the target, vapor-transport tube, and ionization chamber of the source.

Fig. 4. ORNL DWG 93-9587. Schematic drawing of a plasma-sputter negative-ion source equipped with a RF plasma igniter which is now under design for potential use in the HRIBF. The source will be complementary to the HRIBF electron-beam-plasma source displayed in Figs. 1-3.

Fig. 5. ORNL DWG 93-9585. A negative-surface-ionizaton source design now under consideration for use in generating RIBs at the HRIBF from elements with high electron affinities such as the group VI-A and VII-A elements.

Table 1. Comparisons of calculated η_{calc} and experimentally measured η_{exp} ionization efficiencies for electron beam plasma ion sources. Estimated ionization efficiencies were calculated by using Eq. 1.

Z	Element	I_p(eV)	N_e	η_{calc}(%)	η_{exp}(%)	Ref.
10	^{20}Ne	21.56	8	2.2	1.6	8
18	^{40}Ar	15.76	8	17.8	19	8
24	^{54}Cr	6.77	1	38.0	>20	8
26	^{57}Fe	7.90	2	46.4	30	8
32	^{76}Ge	7.90	4	66.7	41	8
36	^{84}Kr	14.00	8	36.0	35	8
36	^{84}Kr	14.00	8	36.0	36	13
46	^{100}Pd	8.33	18	90.0	>25	8
47	^{107}Ag	7.58	1	39.8	47	8
47	^{109}Ag	7.58	1	40.2	50	8
50	^{116}Sn	7.34	4	74.8	53	8
50	^{124}Sn	7.34	4	77.4	54	8
54	^{129}Xe	12.13	8	56.0	52	8
54	^{132}Xe	12.13	8	56.6	53	8
54	^{132}Xe	12.13	8	56.6	56	12
79	^{197}Au	9.23	1	34.2	50	8
82	^{208}Pd	7.42	4	79.5	52.8	8
83	^{209}Bi	7.29	5	83.5	68.3	8

Table 2. Estimates of the probability for negative ion formation by xenon sputtering at optimum cesium coverage (Ref. 19)

Negative Ion	C–	Si–	Cu–	Ge–	Mo–	Ta–	W–
Probability (%)	18.3	15.6	12.1	13.6	(0.52)	(1.59)	8.07

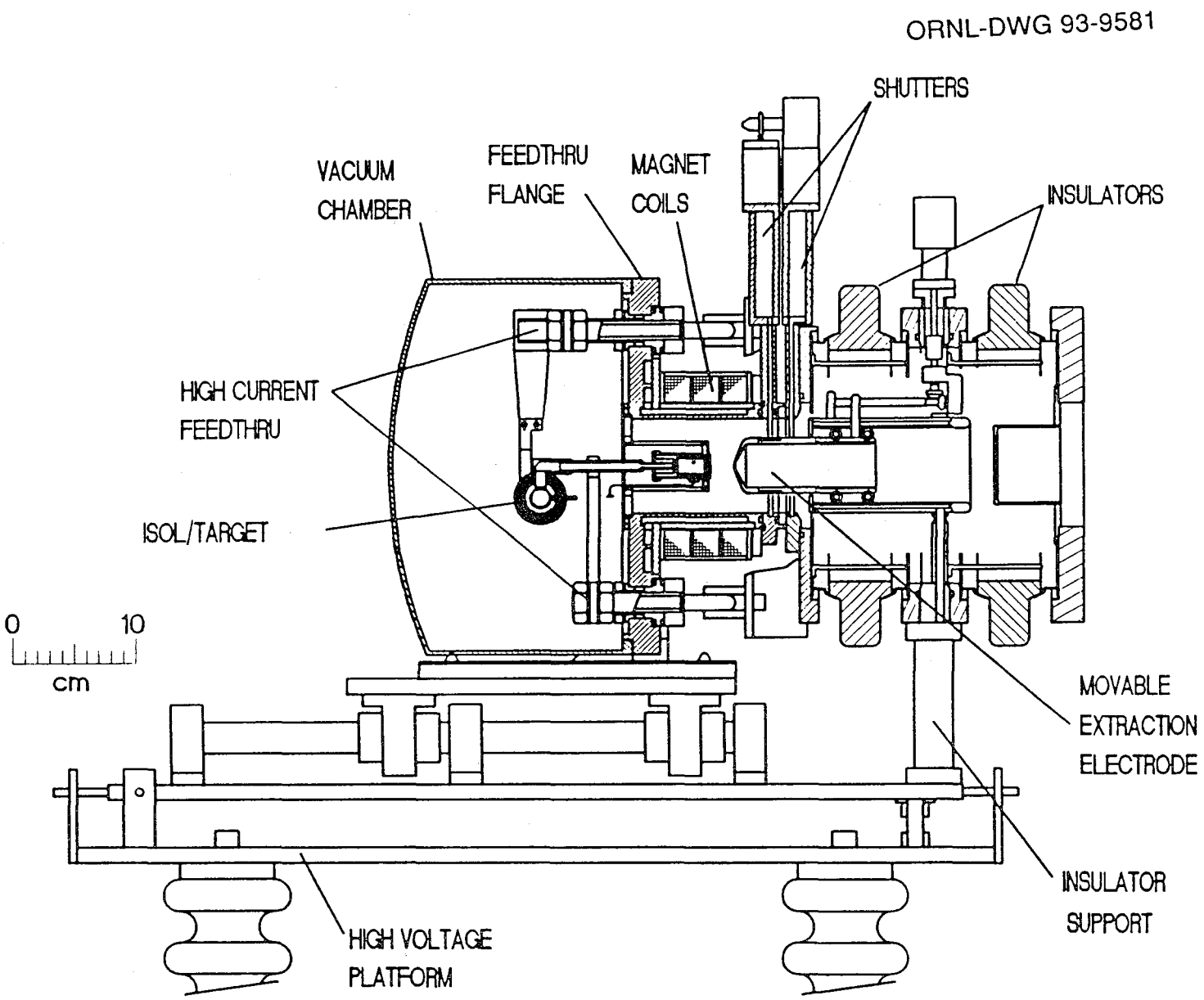
ORNL-DWG 93-9581
SHUTTERS
VACUUM CHAMBER
FEEDTHRU FLANGE
MAGNET COILS
INSULATORS
HIGH CURRENT FEEDTHRU
ISOL/TARGET
0
10
cm
MOVABLE EXTRACTION ELECTRODE
INSULATOR SUPPORT
HIGH VOLTAGE PLATFORM

Figure 1

ORNL-DWG 93-9582

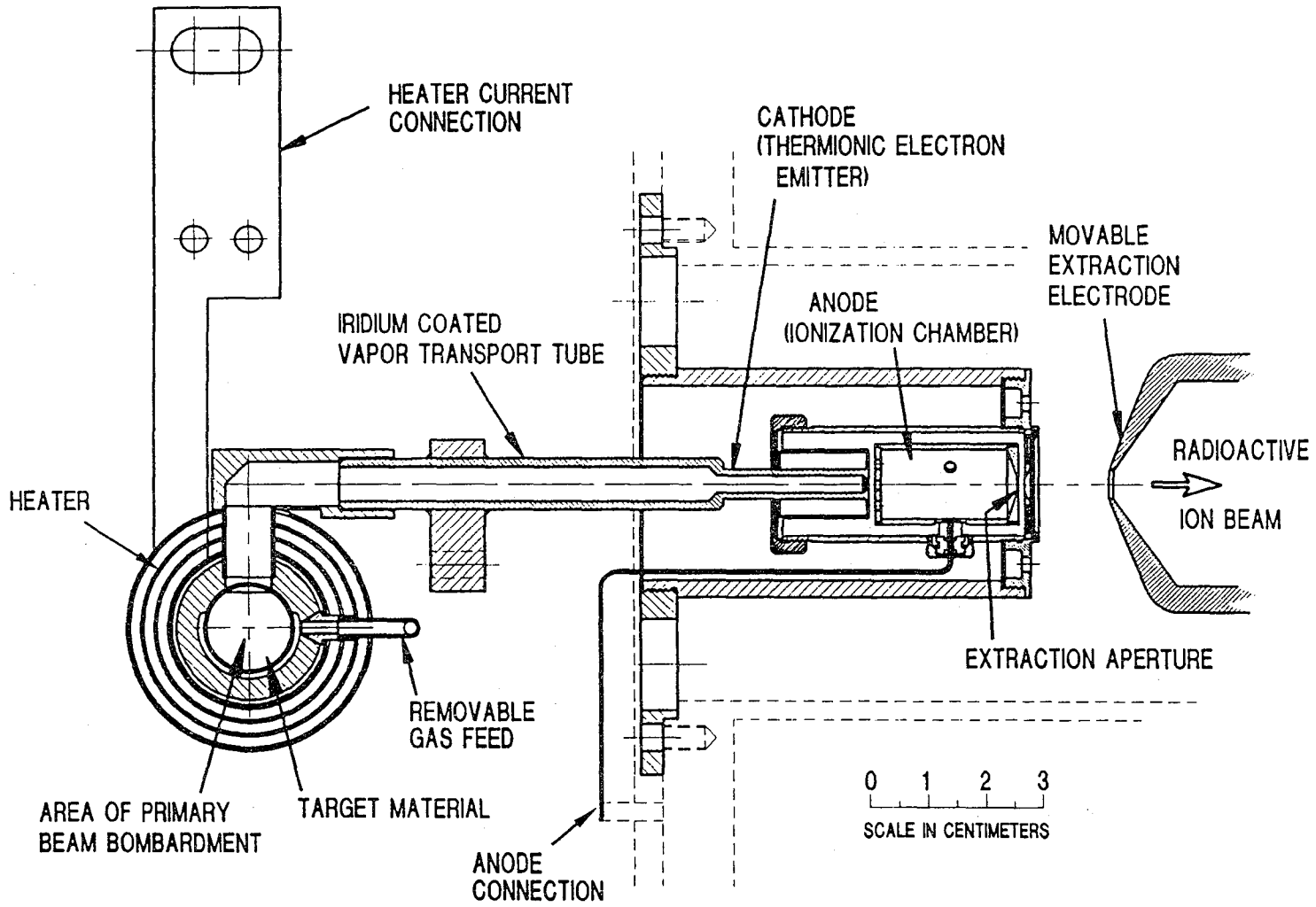

Figure 2

ORNL-DWG 93-9583

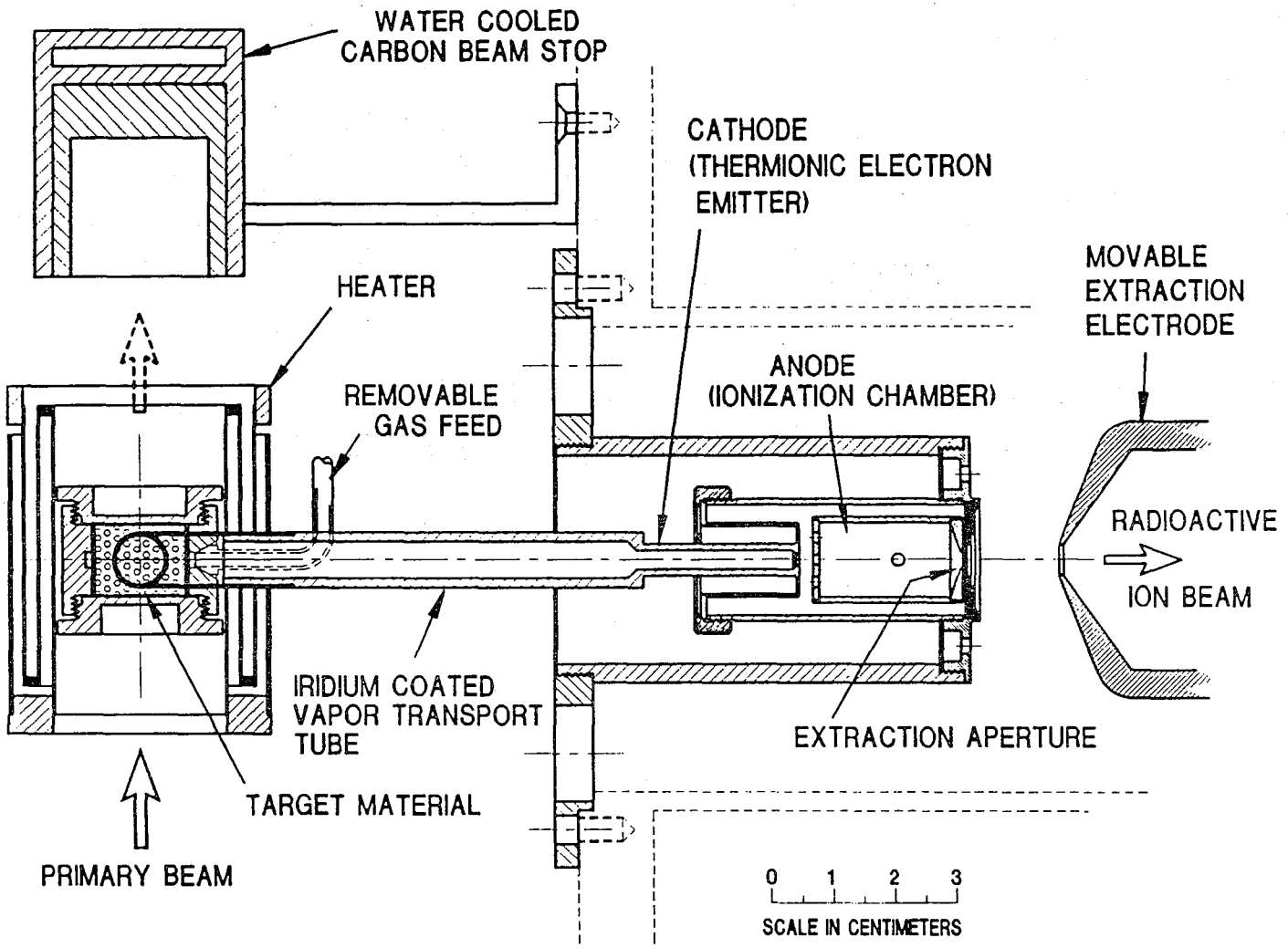

Figure 3

ORNL-DWG 93-9587

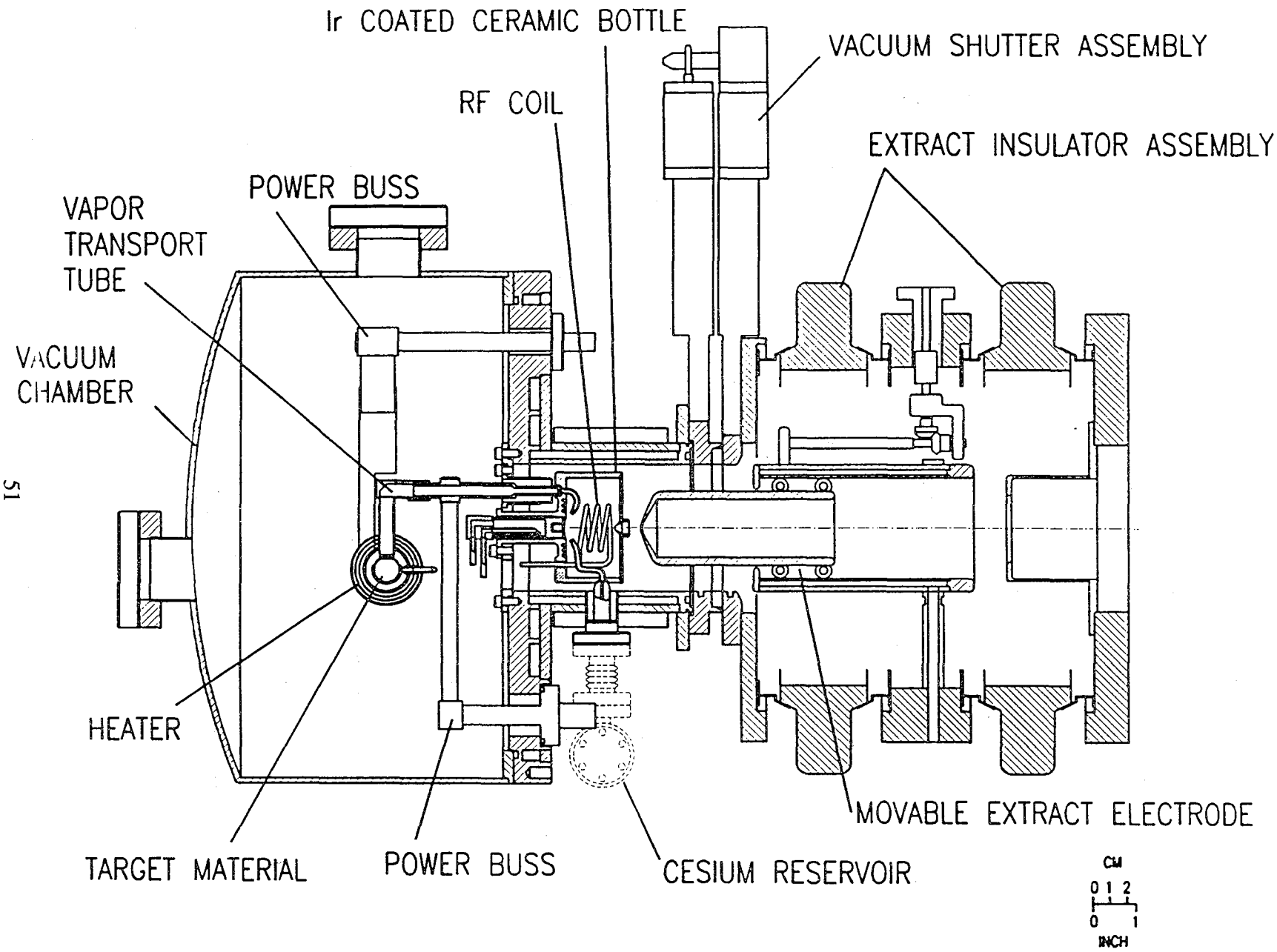

Figure 4

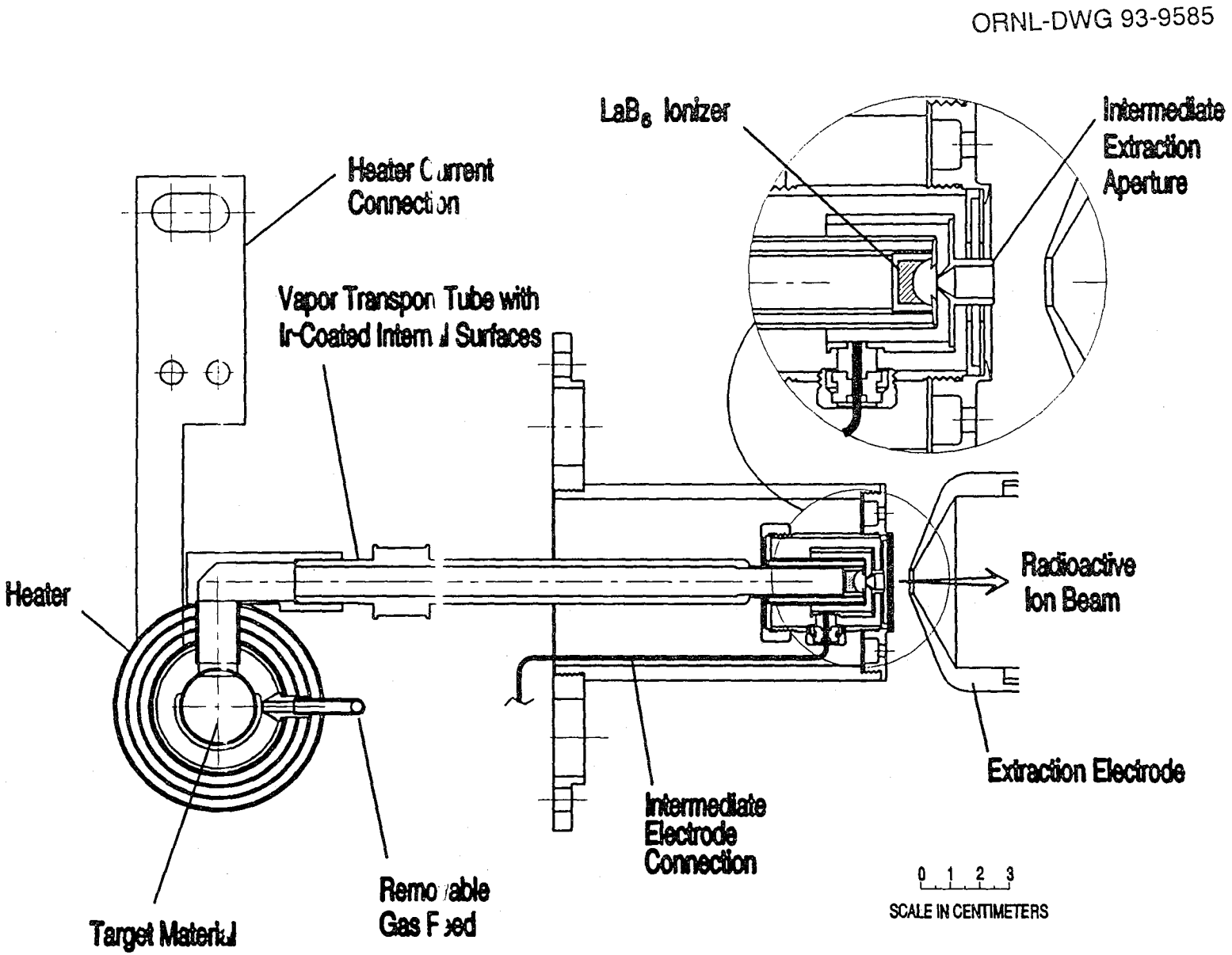
ORNL-DWG 93-9585
LaB_6 Ionizer
Intermediate Extraction Aperture
Heater Current Connection
Vapor Transport Tube with Ir-Coated Internal Surfaces
Heater
Radioactive Ion Beam
Extraction Electrode
Intermediate Electrode Connection
Target Material
Removable Gas Feed
0 1 2 3
SCALE IN CENTIMETERS

Figure 5

Separation and Matching of Ion Beams between Sources and Accelerators

H. Wollnik[1]
Oak Ridge National Laboratory, Oak Ridge, TN 37830

1. Introduction

For radioactive ion beam (RIB) facilities that provide accelerated ions of short lived nuclei it is essential that the produced short–lived nuclei of interest are ionized and delivered most efficiently to the postaccelerator. Equally important is, however, that isotopes of neighboring isobars and of neighboring elements within the same isobar are eliminated as effectively as possible. This is difficult to achieve, especially if the nuclei of interest are produced by spallation or by fission reactions since those reactions are not very specific and usually produce neighboring isobars and elements at intensities that often exceed considerably the produced intensities of the nuclei of interest.

For this reason very efficient separation techniques are required. Such techniques make use of differences in chemical properties and ionization probabilities of the atoms in question in the target ion source [1]. Most importantly, however, such ions of different mass–to–charge ratios are accelerated by the same potential difference (perhaps 60 kV) and passed through large magnetic dipole fields that deflect ions differently if they have different momentum–to–charge ratios.

2. Electromagnetic Isotope Separators

Since for the ions of interest in most cases a high ionization efficiency is mandatory, the target ion source usually is only able to achieve a modest attenuation of the undesired species except if laser ionization by specific

[1]permanent adress: 2. Physikalisches Institut, Universität Giessen, 35439 Giessen, Germany

light wave lengths can be used [2] or surface ionization. The main attenuation thus must be obtained by deflecting ions of different mass–to–charge ratios m/q differently by one or by several magnetic sector fields [3,4,5,6]. Note here that because of the desired high ionization efficiencies in most any case only singly–charged positive or singly–charged negative ions are used with q=$\pm$1.

Though such separation methods by magnetic sector fields are quite effective, there are limits [4] to how well ions of an undesired mass m_1 can be separated from the desired ions of mass m_0 after both had been accelerated to energies K_0 of perhaps K_0=60kV.

1. in a magnetic separator of a few meters path length several percent of the ions are scattered at residual gas atoms if the vacuum in that system is $\approx 10^{-7}$mbar. Some of the ions of the undesired mass m_1 here are scattered such that they pass through the separator exit slit that was positioned such as to transmit only ions of mass m_0. If the separator is designed to have a mass resolving power $R = M/\Delta M$ of about 2000, this contamination by ions of mass m_1 amounts to a few ppm of the overall intensity of the ions of mass m_1.[2]

   This contamination reduces if the masses m_1 and m_0 differ more and more. However, this drop off is usually not as rapid as one would hope, so that contamination levels of a few ppm persist also if m_1 and m_0 differ by several percent. A much more drastic reduction in contamination levels is achieved, however, if two separator stages are placed in series since in this case the attenuation factors of the first and of the second stage multiply so that usually less than 10^{-9} of the ions of mass m_1 are scattered into the beam of ions of mass m_0 [4,5,6].

2. In most any ion source the gas pressure is relatively high which causes also a reasonable high gas pressure in the acceleration region, perhaps 10^{-4}mbar. After some of the abundantly available ions of mass m_1 had been accelerated to perhaps $\overline{K} \approx$100eV they may thus collide with residual gas atoms of mass m_1 and transfer their charges. The newly formed ions of mass m_1 then are accelerated by the left over

[2]Note here that the intensity of ions of mass m_1 may exceed the intensity of ions of mass m_0 by many orders of magnitude.

part of the acceleration voltage. Besides the common 60keV ions of mass m_1 there thus will be some ions of mass m_1 accelerated to $K_0 - \overline{K} \approx 59.9$ keV. Since this charge exchange can take place at any potential $\overline{K}q$ in the acceleration region, the ions of mass m_1 can have quite different energies $K_0 - \overline{K}$ and thus also that of $K_0 - \overline{K} = K_0 m_0/m_1$. This energy would make the momentum of an ion of mass m_1 equal to the momentum $m_0 K_0$ of an ion of interest of mass m_0, which two momenta can not be distinguished by magnetic field arrangements [4,5].

Also this contamination of the ions of mass m_0 is about a few ppm of the intensity of the ions of mass m_1. It can be reduced only by using some electrostatic fields that can distinguish ions of different energies K_0 and $K_0 - \overline{K}$. In a radioactive ion beam facility such a separation is advantageously achieved by placing the two magnetic separator stages (postulated above in point 1) on two different electrostatic potentials [6]. This procedure, however, requires that the energy spread of the ions under consideration is very small as compared to the energy of the ions. An energy analysis by electrostatic sector fields, however, would be feasible as well and if combined with the momentum analysing capabilities of the discussed sector magnets could even allow for an energy focusing [7,8] so that ion sources with large energy spreads would not have to be excluded.

3. For ions of different elements that belong to the same isobaric chain the differences in their masses, i.e. the Q_β–values, are so small that only isotope separators of mass resolving power $R \geq 10^4$ can separate them from each other. Such isotope separators can be built [5], but they require a careful correction of their image aberrations [6,7,9].

3. The Layout of an Isotope Separator

Isotope separators are usually considered to be inseparable from their ion sources. Thus, only if the combined systems are optimized, one can expect a high performance isotope separation. This finding is mainly due to the fact that small changes in the gas pressure or the potential distribution in the ion source or even the temperature of the source change the optical properties of the extracted ion beam.

In order to at least relieve this close tie, one can place a focusing device between the ion source and the entrance slit of the actual isotope separator [3,5,6,8,9]. If in this arrangement the ion source properties change a little – the reason for which may only become obvious later – one may restore the deteriorated beam properties to what they had been before by slightly changing the optical properties of the focusing device. In doing so one has effectively decoupled the beam forming properties of the ion source from its properties to generate ions.

This prefocusing device can be an electrostatic round lens, however, it is much more advantageous to use an astigmatic device[3] instead. In this case namely it is possible to match the ion beam optimally to the optics of the sector magnet that performs the momentum analysis. A very good way to do this is [9] to make the sector magnet point–to–point focusing not only in the plane of deflection, i.e. the x–direction, but also in the perpendicular direction, i.e. the y–direction, for instance by using a homogeneous sector magnet with inclined pole–face boundaries. As a second step one then may adjust the astigmatic prefocusing device so that the beam has an x–image at the entrance slit but not a y–image. At this position the beam should rather be more or less parallel as far as the y–direction is concerned. Automatically then there is an x–image at the separator exit slit and the beam is again more or less parallel as far as the y–direction is concerned. As a consequence of this, the ion beam (see Fig.1) is rather wide in x–direction – perhaps ±100mm – but rather narrow in y–direction – perhaps ±5mm – in the middle of the sector magnet whose optic axis may be a circle of perhaps ρ_0=2000mm radius.

Such a design of an isotope separator equipped with a prefocusing device [9] has several advantages as compared to a separator in which the ion source sends the beam directly into the sector magnet:

1. The position of the x–image of the ion source can be adjusted to be exactly at the position of the entrance slit by changing the lens

[3]Such an astigmatic prefocusing device could consist of for instance 3 or better 4 electrostatic or magnetic quadrupole lenses. In the latter case then a variation of only the strengths of the 4 quadrupoles would allow to adjust all important four first–order elements of the transfer matrix in question to desired values, i.e. (X,X), (X,A), (Y,Y), (Y,B).

strengths of the prefocusing device. Thus small changes of the optics of the ion source can be counterbalanced without a deterioration of the separator performance.

2. A sector magnet can be used that has only a small magnet air gap, perhaps $\pm G_0 = \pm 25$mm for a sector field of radius ρ_0=2000mm. This fact can be rather important since the costs for a sector magnet usually increase more than linearly with an increase in $\pm G_0$.

3. A good correction of image aberrations of second order can usually be achieved already by a slight curvature of one or two of the field boundaries. This is so since the largest aberrations of a sector magnet are in most any case the aperture aberrations (X,AA)a_0^2+(X,BB)b_0^2 with $a_0 \approx dx/dz$ and $b_0 \approx dy/dz$ [7] and since in our case we have $a_0 \approx 20mrad$ and $b_0 \approx 2mrad$. Thus we really need to correct only (X,AA) by curving one or two field boundaries without worrying to much about the magnitude of (X,BB) which inevitably will increase by achieving (X,AA)=0 because (X,AA) +(X,BB) =const for a stigmatic focusing separator stage, as it was postulated above.

4. If the space charge of the initial ion beam should not be negligible the proposed design is quite favourable since it ensures that until into the sector magnet the ion beam cross section at no position is very small. Thus space charge forces are kept within limits everywhere.

4. Bunched Beams

In principle there is no need to require the ion beams in a RIB facility to be bunched in order to achieve a good mass separation. However, there are advantages in postulating the beam to be bunched at different positions in the system

1. Part or all of the ion beam transport system can be used as a time–of–flight mass analyzer [10] whose separating power provides an additional means of purifying the beam of ions of mass m_0. Such a purification would be especially effective since it would differentiate not between ions of slightly different momenta as does any one of the assumed sector magnets, but of ions of slightly different velocities.

2. Providing a bunched beam to the postaccelerator allows for an easier coupling of the ion beam to any RF-device and thus in most cases for a more efficient beam capture and smaller emittance growth.

3. Though accelerators for stable ion beams are built to provide DC beams whenever possible, so that coincidence experiments become easier, there are advantages for accelerators for unstable ion beams if they are built to provide ions only during short periods. The reason is that very often there are only a few ions available to be accelerated. Thus, very often the question is not how many ions are accelerated in one bunch but rather whether in one accelerator bunch there is one ion or none. In this case the signal to noise ratio for an experiment increases if it does not have to wait for an event to happen at an arbitrary time, but if it can expect this event to happen only during short time windows.

The bunching for the first two points should be done before the beam is entered into the postaccelerator either by an in–line or an orthogonal–acceleration bunching device as shown in Fig.2. The bunching for the third point should be done after or in the postaccelerator.

Since any bunching device induces beam losses for an incoming DC beam, it is quite advantageous that it seems possible [12] to extract a pulsed beam from a good ion source with little or no intensity losses as compared to a DC extraction[4].

5. Matching an Ion Beam to the Acceptance of an Accelerator

To enter an ion beam into an accelerator structure one must preaccelerate the ions properly. In case of an electrostatic accelerator the ion energy should always be the same while the ion velocity should always be the same in an RF accelerator. In the second case thus the ion energy must

[4]As compared to a DC beam it was possible in the case of ref. [11] to extract more than 5 times higher currents during each pulse if only during 20% of the time ions were extracted. The overall extracted beam current thus was greater or equal than the initial DC beam.

linearly increase with the ion mass. Consequently the isotope separator system should feature several potentials:

1. V_0 the ion source potential.
2. V_1 the potential of the first stage of the isotope separator, with $V_0 - V_1 \approx 60\text{kV}$.
3. V_2 the potential of the second stage separator with $V_1 - V_2 \leq 100\text{kV}$.
4. V_3 the potential of the entrance to the ion postaccelerator, with $V_3 - V_0 = K_r(m_0/m_r)$ where K_r is the energy that makes an ion of mass m_r move with the correct velocity into the postaccelerator

Obviously there is only one potential arbitrary and one should choose it such that the overall sum of technical difficulties becomes smallest [6]. In most cases this leads to making V_2=0. This would allow to keep the rather large second stage separator at ground potential and at the same time all parasitic experiments that may want to use a well mass analyzed beam of short lived nuclei. This would require, however, the accelerator entrance to be not at ground potential.

Additional to this requirement of a proper ion velocity at the entrance of the accelerator one needs to postulate that the ion beam does not exceed the acceptance phase space of the accelerator, i.e the lateral phase space in x,a and y,b but also in the longitudinal phase space in δ_t, δ_K with δ_t=T/T_0-1 and δ_K=K/K_0-1 describing relative time and energy deviations.

6. Conclusion

To mass separate and match beams of ions of short lived nuclei to a postaccelerator seems very well possible. The isotope separator in question, however, becomes rather elaborate consisting of at least two large magnetic separator stages that and transport the ion beam to the postaccelerator. As an additional means of purification one may employ a time–of–flight mass analyzer after the ion beam has been bunched to very short pulses. Since the accelerator requires all entering ions of mass m_1 to have a certain velocity $v_0 \propto \sqrt{K_0/m_0}$ the potential difference K/q between the ion source

and the accelerator must attain a certain value $K = K_0 m_0/m_1$. Thus different parts of the system must be at considerably different electrostatic potentials.

References

1. S.Sundell and H.L.Ravn, Nucl. Instr. and Methods **B70**(1987)160
2. V.I.Mishin et al., Nucl. Instr. and Methods in print
3. H.Wollnik, "Proc. Int. Conf. El. Isotope Sep.", eds. H.Wagner and W.Walcher, BMBW Forsch. Ber. K 70-28 (1970)282
4. H.Wollnik, Int. J. Mass Spectr. and Ion Phys. **30**(1979)137
5. C.Geisse et al., Nucl. Instr. and Methods **B26**(1987)120
6. H.Wollnik, "Proc. ORNL RIB workshop", ed J.Garrett, ORNL, Conf 9210121 (1992)213
7. H. Wollnik, "Optics of Charged Particles", 1987 Acad. Press, Orlando
8. K.Sunaoshi et al., Nucl. Instr. and Methods **B70**(1992)421
9. H.Wollnik, Nucl. Instr. and Methods **B56/57**(1991)1096
10. H.Wollnik, Mass Spectr. Rev., in print
11. Y.Shirakabe, Nucl. Instr. and Methods in print
12. J.H.Dawson and M.Guilhaus, Rapid Comm. in Mass Spectr. **3**(1989)155

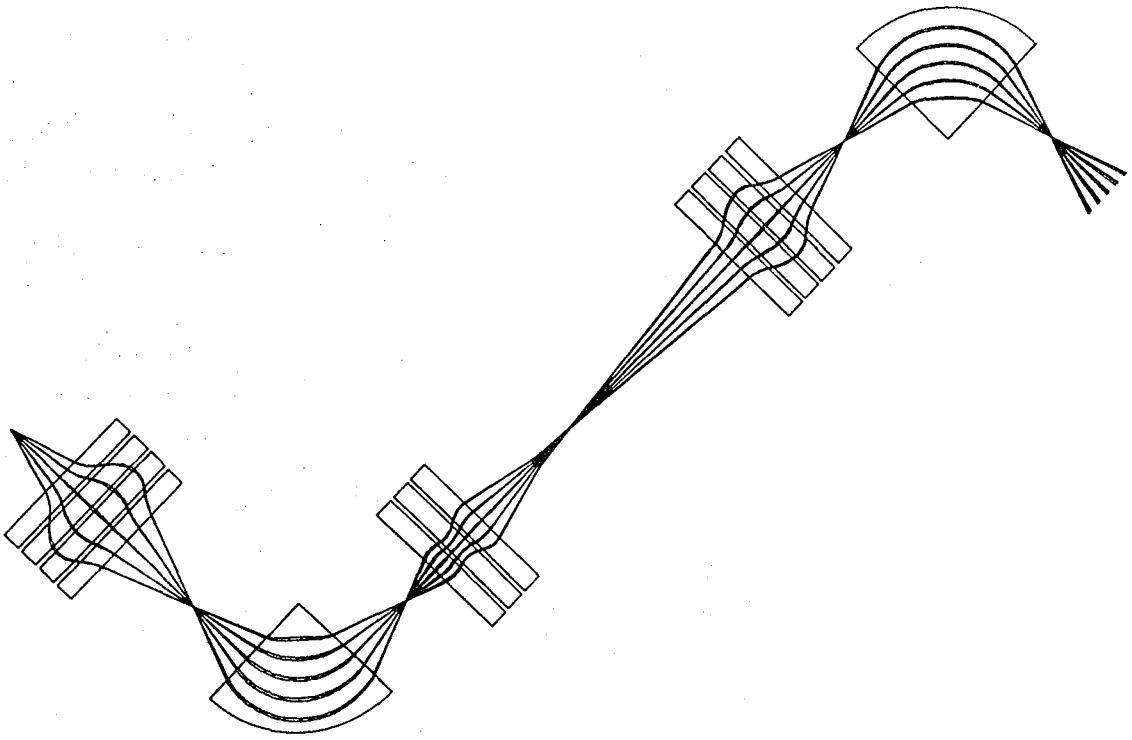

Fig.1 A two–stage sector magnet separator that separates charged particles according to their momentum–to–charge ratios mv/q. Note that the two separator stages are at different electrostatic potentials so that in the second stage the ions have been accelerated by perhaps 250 kV relative to the first stage. Note also that each sector magnet is preceded by an astigmatic focusing device that ensures that the beam is focused to the respective entrance slits but is more or less parallel in the perpendicular direction.

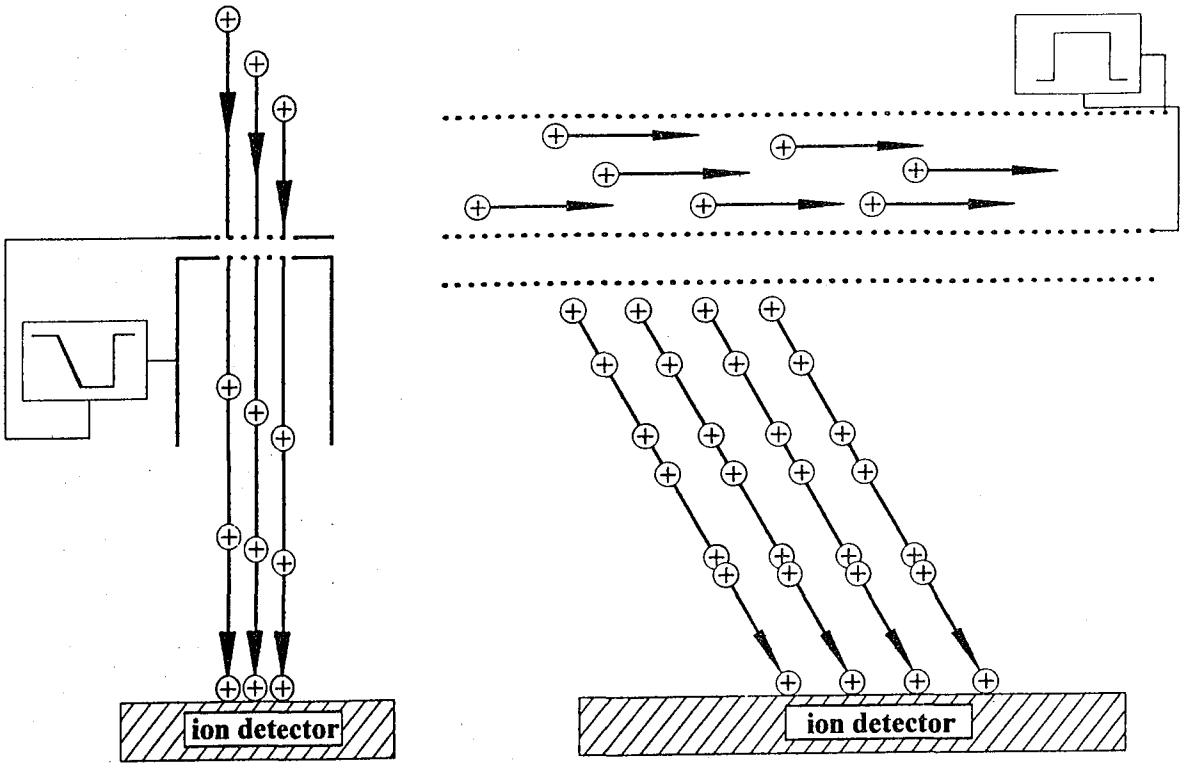

Fig.2 Two designs of ion bunchers are indicated. The first buncher decelerates the first of a group of ions and accelerates the last so that after some time they arrive simultaneously at some plane. The corresponding acceleration gap must be powered by some sawtooth generator which ususally is approximated by some sinusoidally varying voltage. The second buncher accelerates the ions by a field perpendicularly to the initial direction of the ions. This buncher requires the ions to have rather low initial energies, for instance 10 eV. Here the ions that have a longer distance to go get a higher energy so that after some specified flight distance they all can catch up with each other. In this buncher the main accelerating field is a DC field with only its first portion being pulsed. The pulsed field requires only a simple square pulse with rather modest rise times. For this device it is very useful to make the incoming ion beam as parallel as possible by some lens, so that the ions have only a very small energy spread in the final direction of the ions [12].

Proceedings of the Workshop on Post-Accelerator Issues at the Iso-Spin Laboratory
October 27-29, 1993, Berkeley CA

BRAMA, a Broad Range Atomic Mass Analyzer for the ISL

J. Michael Nitschke
Lawrence Berkeley Laboratory
1 Cyclotron Road, Berkeley CA 94720

Abstract

An alternative to conventional on-line isotope separators for use in radioactive beam facilities is described. It consists of an analyzer with a static magnetic field that is capable of separating a wide mixture of (radioactive) ions into mass bins ranging from 6 to 240u. If incorporated into the ISL, BRAMA would make several low-energy radioactive beams available for experiments *simultaneously*, in addition to the beam that is being delivered to the post-accelerator. A preliminary ion-optical geometry is discussed.

1. Introduction

A key component of the IsoSpin Laboratory (ISL) concept is the on-line isotope separator that connects the ion source to the post-accelerator. On-line isotope separation has become a well established tool in nuclear physics, astrophysics and material science since the mid 1960's. Also, during this time the use of radioactive targets and projectiles was mentioned for the first time.[1] Most on-line isotope separators analyze ions from ion sources or He-jet systems with a combination of electric and magnetic fields that are adjusted to the desired isobaric mass chain. In the focal plane of the analyzer a range of ±10 - 15% of the center mass is typically available and some on-line isotope separator facilities make use of these side beams for additional experiments. An example is the beam switch yard at ISOLDE/CERN.[2] However, the range of usable masses that is available from a conventional isotope separator is often much smaller than the range of radioactive products that is being produced, in particular when high-energy-spallation- and fragmentation reactions or fission are being used. The out-of-range isotopes typically are implanted in the walls of the vacuum chamber of the separator where they may cause unwanted scattering and long-term contamination. This a particularly serious problem in the important case of uranium targets. If, for instance, ^{238}U is used to produce light neutron-rich isotopes between He and Ca many of the fission fragments are lost inside the vacuum chamber.

In its original incarnation and in later versions like the Bench Mark Facility[3] and variations thereof [4] the ISL had an ISOLDE-type isotope separator as its front-end. The most disturbing fact about using this type of isotope separator in conjunction with the ISL is that most of the radioactive isotopes, which are very expensive and cumbersome to produce, are wasted because the narrow range of the separator is poorly matched to the broad-range production mechanisms.

Another point is that many isotopes, particularly near stability, are produced almost independently of the target material, albeit with varying intensities and subject to the mass and charge limitations given by the target and the projectile. This is illustrated in Table 1 for the case of positive surface ionization where it is shown that a large number of light isotopes can be produced with a wide variety of targets. (This example should not detract from the fact that for a given element and isotope there may only be one *optimal* target.) Conversely, Table 1 also illustrates that heavy targets are quite universal in producing a wide variety of elements. These considerations have led to a reevaluation of the method of on-line isotope separation at the ISL, as first reported in [5].

2. The Broad Range Atomic Mass Analyzer (BRAMA)

It is proposed that the conventional tunable isotope separator be replaced by a Broad Range Atomic Mass Analyzer (BRAMA) with a *fixed* magnetic field that sorts the incoming ion mixture into mass bins in the range of $A \approx 6 - 240$. (The magnetic field should be reversible to allow the analysis of negative ions.) The mass range was chosen to accommodate the lightest RNB of interest (^{6}He) and to permit the mass separation of simple molecules of the heavier elements that may be advantageous for reasons of beam purity.

A design of a broad-range spectrometer was published by Morgan et al.[6] for electrons with momenta of 1 - 25 MeV/c. Ion optical work on a 1-100 MeV proton spectrometer was reported by Enge.[7] Following this lead, we carried out preliminary calculations of a broad range spectrometer based on a design first published by Borggreen et al. [8]

Preliminary choice of basic parameters for BRAMA:

Ion Energy: 100 keV
Maximum Magnetic Rigidity: 0.705Tm
Mass Range: 6 - 240u
$(B\rho)_{max}/(B\rho)_{min}$: 6.3
Mass Resolution: $m/\Delta m \gtrapprox 1000$
Dispersion at Mass 240: ~1cm
Sector Angle: 108.7^0
Entrance Angle: 35^0

A minimum ionic radius of 0.4m for A=6 was chosen, which results in a field of 0.28T and a maximum radius of 2.52m for A=240. The dispersion along the focal plane $\delta s/\delta A$ is calculated to be $0.18A^{-1/2}$ and varies from 7.4 to 1.2 cm for mass 6 to 240, respectively. The ion-optical geometry of BRAMA is shown in Fig. 1, and the mass positions and dispersions in Fig. 2. The approximate length of the focal plane is 4.7m. The focal plane angle with respect to the field boundary is $\sim 19^0$.

An important design feature is the beam switch-yard that directs different masses to experiments and the post-accelerator. Fig. 1 shows an example of three masses that are selected with *movable* slits in the focal plane. The slits are mechanically attached to electrostatic deflectors that deflect the beams parallel to the focal plane towards the

electrostatic distribution deflectors shown to the left. From there the mass-selected beams enter beam lines that lead to the experiments or the post-accelerator. By moving the first deflectors along the focal plane each beam line can be supplied with any mass chain in the range from A=6 to 240u. (Of course, any given mass position can be used only once.) Moving the deflectors parallel to the focal plane does not affect the position of the central rays. It will, however, affect the focusing, which can be corrected with electrostatic focusing elements as shown.

3. Operational Considerations

Substituting BRAMA for the conventional on-line isotope separator will significantly enhance the operation of the ISL. This can best be demonstrated by referring to Fig. 3, which shows a schematic functional diagram of the ISL front-end. The input to BRAMA can be selected from several target/ion source stations. (These stations may be equipped with specialized targets and/or sources that emphasize certain half-life ranges or selectively ionize certain groups of elements.) The mass channels of BRAMA can be considered "spigots" from which all available isotopes can be tapped *simultaneously*. A few examples are shown in the figure.

- The tap with the highest priority is the beam that will be post-accelerated.
- A light-ion beam is made available for astrophysics. (A small dedicated post-accelerator could be added here in the future.)
- Another beam goes to a high voltage platform for condensed matter physics with polarized beams.
- An isotope of the ion-source-support gas could be used to monitor ion source performance.
- A new class of experiments can be carried out where an on-line target is collected and bombarded by an accelerated radioactive (or stable) beam; for example the "cold fusion" reaction $^{130}Sn(^{132}Sn,\gamma)^{262}Fm$ would lead to a new nucleus at the N=162 neutron deformed shell. Or multi-neutron transfer reactions with light neutron-rich beams on radioactive targets could be studied.
- All mass positions not needed for on-line experiments are available to collect isotopes for use as off-line targets or in bio-medical experiments. Long-lived isotopes could be collected for extended periods of time, even from different production targets. They could be chemically purified to remove isobaric contaminants.
- A moving-tape collector could be installed for short-lived activities.
- Very few radioactive ions would strike the wall of the vacuum chamber; mainly tritium and molecules with A>240. (A special "tritium trap" could be installed since the mass-3 beam will always appear at the same position.) Most "waste" isotopes will be collected in the focal plane.

Fig. 3 shows "clean-up" stages in front of most experiments since BRAMA will, in general, have insufficient mass resolution ($m/\Delta m \approx 1000$) to resolve isobars. These stages can take different forms, from additional magnetic and electric fields, as in case of the post-accelerator branch, to implantation and re-ionization, and laser techniques. In many cases beam purification may be simplified by a judicious choice of ion sources. If, for example, a uranium target is used together with a negative (LaB_6) ion source mainly halogens will be ionized and radioactive isotopes of different halogens do not

overlap in mass and thus, don't cause cross contamination. A particularly favorable situation occurs when laser ionization is used since the "cocktail" of laser wave lengths can be chosen such that only a limited number of isotopes is ionized.

This work was supported by the Director, Office of Energy Research Division of Nuclear Physics of the Office of High Energy and Nuclear Physics of the U.S. Department of Energy under Contract DE-AC03-76SF00098.

4. References

[1] J. P. Bondorf, in *Nuclides far off the Stability Line,* Lysekil, Sweden, 1966, edited by W. Fosterling, C.J. Herrlander, and H. Ryde (Almquist & Wiksell, Stockholm), p. 681.

[2] H. L. Ravn et al., in *Nuclei far from Stability/Atomic Masses and Fundamental Constants 1992,* Bernkastel-Kues, 1992, edited by R. Neugart and A. Wöhr (Institute of Physics Publishing, Bristol and Philadelphia), p. 919.

[3] ISL Steering Committee, The *IsoSpin Laboratory, Research Opportunities with Radioactive Nuclear Beams*, LALP 91-51 (1991).

[4] *Workshop on the Production and Use of Intense Radioactive Beams,* Oak Ridge, TN, 1992, edited by J. G. Garrett (ORNL).

[5] J. M. Nitschke, *206th American Chemical Society Meeting, Division of Nuclear Chemistry and Technology,* Chicago, August 22-27, 1993.

[6] G. L. Morgan et al., Nuclear Instruments and Methods in Physics Research **A306**, 544 (1991).

[7] H. A. Enge, Private communication (1993).

[8] J. Borggreen, B. Elbek, and L. P. Nielsen, Nuclear Instruments and Methods **24**, 1 (1963).

Target Isotope	CaO	^{93}Nb	^{139}La	^{181}Ta	^{238}UC
^{8}Li	10^{11}	10^{11}	10^{11}	10^{11}	10^{11}
^{11}Li	10^{7}	10^{7}	10^{8}	10^{8}	10^{8}
^{20}Na	10^{9}	10^{8}	108	108	10^{9}
^{30}Na	10^{4}	10^{5}	10^{5}	10^{5}	10^{9}
^{50}K	0	10^{4}	10^{4}	10^{5}	10^{9}
^{97}Rb	0	0	10^{2}	10^{3}	10^{8}
^{111}In	0	0	10^{10}	10^{9}	10^{9}
^{121}Cs	0	0	10^{10}	10^{9}	10^{8}
^{144}Cs	0	0	0	0	10^{9}

Table 1. Orders of magnitude of radioactive beam intensities (lower estimates) in ions/s of selected isotopes for different target materials obtained from a hypothetical RNB facility as described in Ref. [3] Target thicknesses are 1mole/cm^2 and the primary beam is 1-GeV 100μA protons, *no radioactive decay corrections have been applied*, positive surface ionization is assumed, and acceleration- and stripping efficiencies have been included. For further details see [3].

BRAMA

(Broad Range Atomic Mass Analyser)

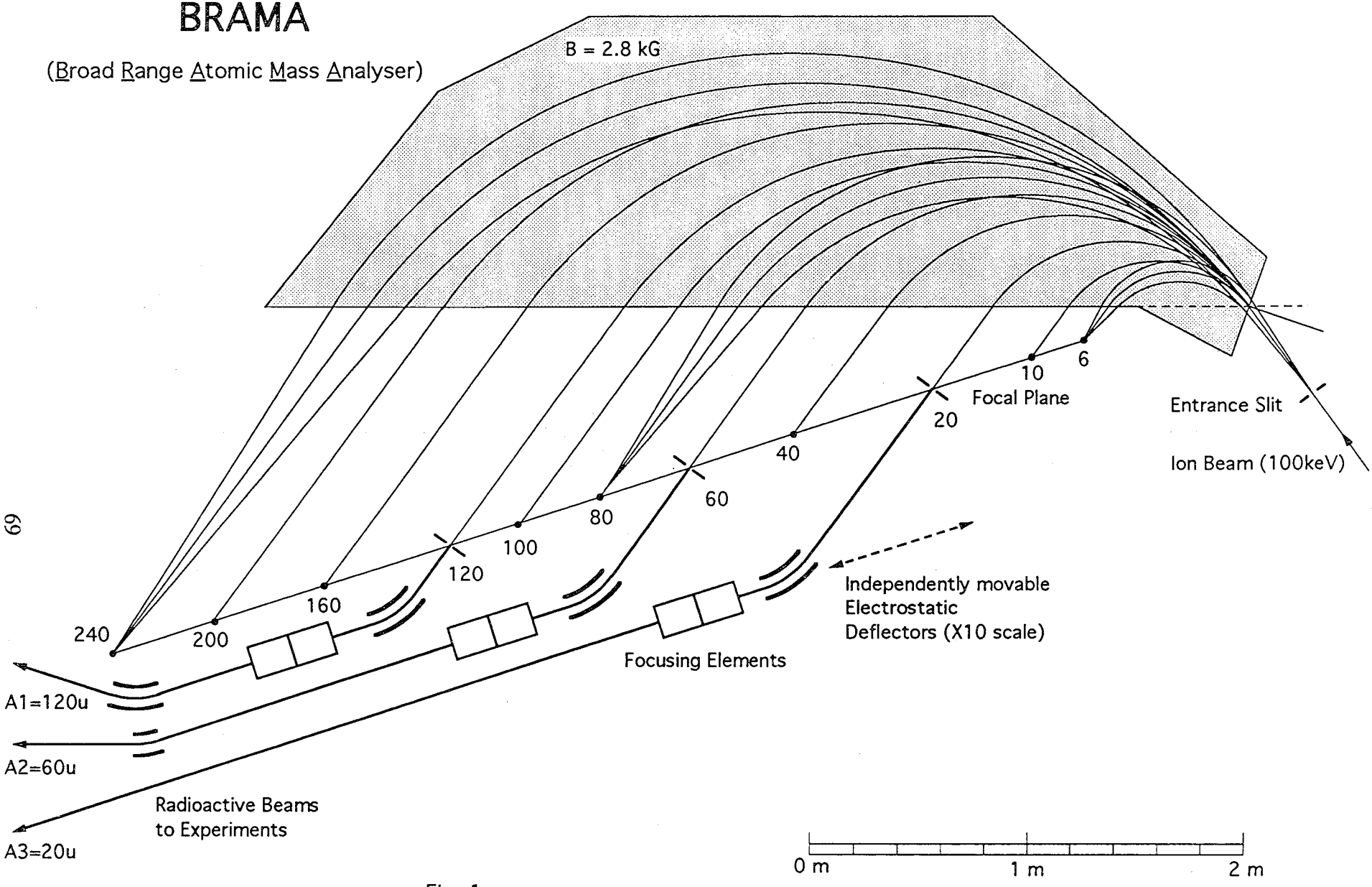

Fig. 1

jmn 11/10/93

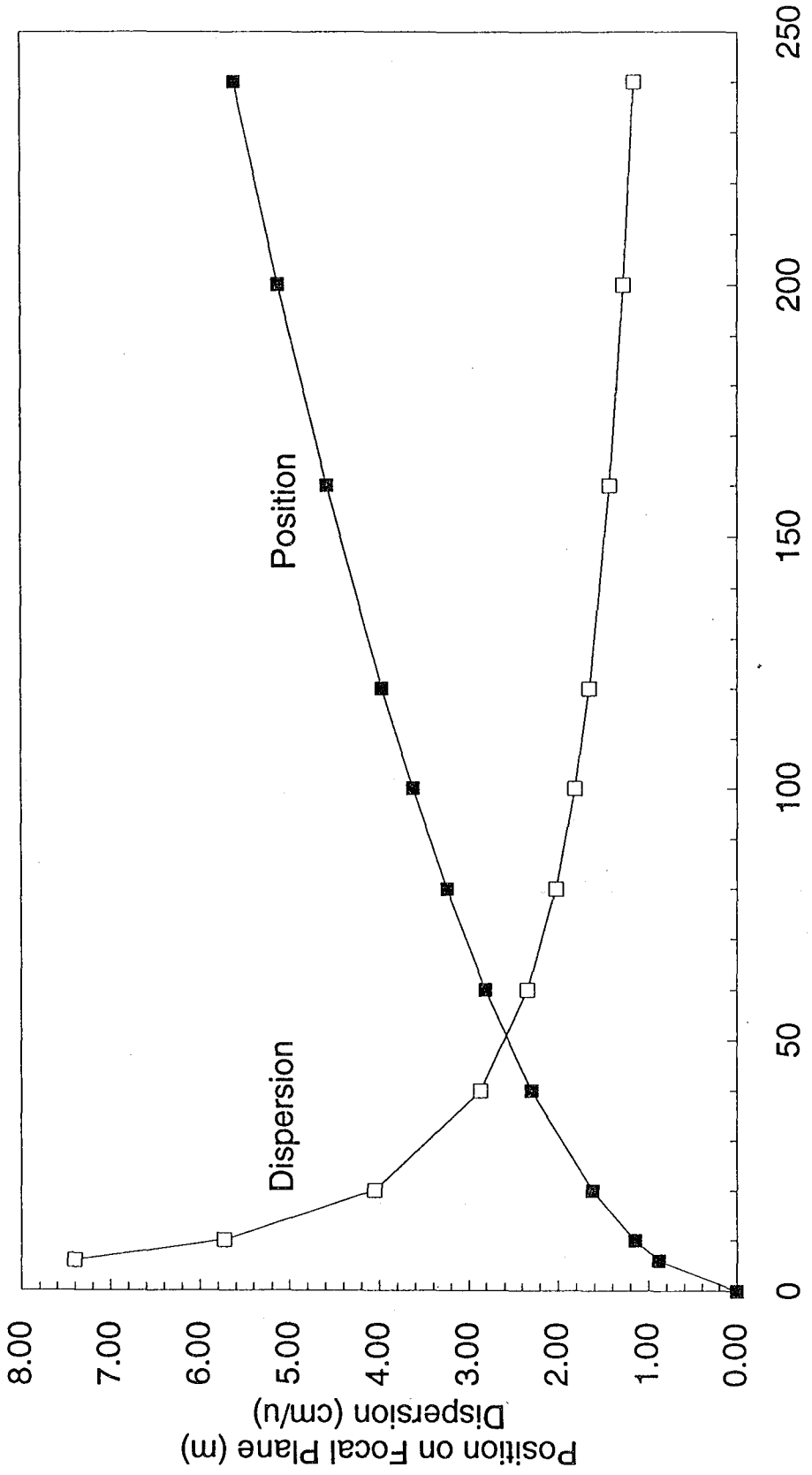
Position on Focal Plane (m)
Dispersion (cm/u)
8.00
7.00
6.00
5.00
4.00
3.00
2.00
1.00
0.00
0
50
100
150
200
250
Mass (u)
Position
Dispersion

Fig. 2

Modified ISL Front End

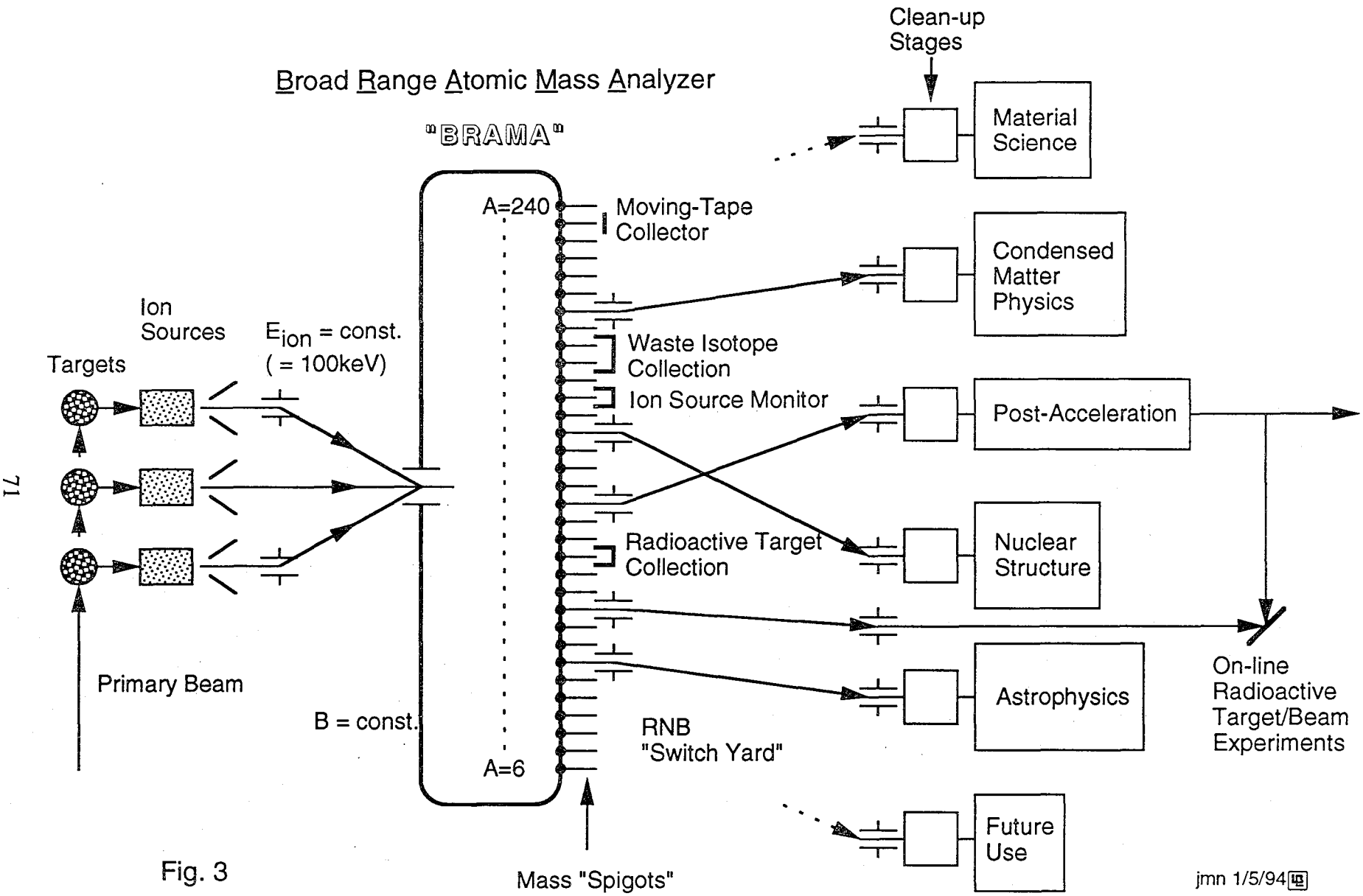

Fig. 3

PROGRESS IN NORMAL CONDUCTING RFQs IN FRANKFURT*

A. Schempp
Institut für Angewandte Physik
Johann Wolfgang Goethe-Universität
D-60054 Frankfurt/Main, FRG

Summary

Two Heavy Ion RFQs [1,2,3] have been built for the UNILAC at GSI, a new high charge state injector (HLI) and a prototype of a new high current injector (HSI). Both can be seen as branches of actual RFQ development. The HLI-RFQ accelerates U^{28+} ions from an ECR-ion source from 2.5keV/u to 300keV/u with a high duty cycle of now 25% at an operating frequency of 108.5MHz. The Spiral-RFQ for the HSI accelerator accepts low energy (2.2keV/u), high current (25 mA) beams with low charge states (U^{2+},Xe^{+}) at an operating frequency of 27 MHz. Results of structure development and beam experiments for both structures are discussed which can be seen as model for the first crucial part of a RFQ for low charged radioactive beams concerning low frequency operation, high duty factor and beam dynamics properties.

Introduction

The GSI accelerator system [4,5] consists of the new 18 Tm heavy ion synchrotron SIS and the experimental storage ring ESR, both fed by the old UNILAC.
With these new rings and the UNILAC injector it is possible to accelerate all elements up to Uranium to energies above 1 GeV/u. The SIS and the ESR are now working for more than two years.

Two new injectors HSI (**H**ochstrom**i**njektor) and HLI (**H**ochladungs**i**njektor) have been planned to fill the SIS ring with short bursts of high current heavy ion beams and to continue providing low current, high duty factor beams for the nuclear physics research program at the UNILAC [6] .

The high charge state injector HLI [7] consists of a combination of an ECR ion source, a 4-Rod-RFQ and an IH-structure, both operating at a frequency of 108.5 MHz. The HLI enables direct injection of U^{28+} into the Alvarez part of the UNILAC at an energy of 1.4MeV/u without stripping. This injector is designed for a beam current of 5μA for the heaviest ions. The HLI is succesfully working and delivering beams for experiments since June 92.

The high current injector HSI is designed to fill the SIS up to its space charge limit and will accept e.g. U^{2+} or Xe^{+} beams with currents as high as 25mA at low initial particle energies of 2.2 keV/u. The Spiral-RFQ-accelerator is working at the (UNILAC)-Wideroe frequency of 27 MHz, which allows a beam transfer without frequency jump. Presently a gas stripper at 216 keV/u is planned which will produce a reasonable fraction of the necessary charge state of U^{10+} for acceleration in the second Wideroe part of the UNILAC. The second gas stripper at 1.4 MeV/u provides the U^{28+} beam for postacceleration in the Alvarez-part of the UNILAC and injection into the SIS. Fig. 1 shows a layout of the GSI accelerator system with the HLI and the planned HSI injector.

* Supported by the BMFT under contract 060F351I

The Spiral-RFQ-Prototype

A prototype of the Spiral-RFQ [8,9,10] has been built for both, rf and beam test purposes. The structure length is 4 meters but nevertheless the electrodes consist of the first 231 RFQ-cells, one third of the HSI's total cell number. These 231 cells cover the crucial low-energy part of the HSI-RFQ, where the dc-beam is converted into a bunched beam. Therefore the 4 m prototype can give relevant information on beam properties e.g. on emittance growth. A survey over the main parameters of the RFQ-Prototype is given in table 1.

Table 1
Main Parameters of the Spiral-RFQ

f	27.1 [MHz]	length	3.95 [m]
cells	231	Rp	520 [kΩm]
T_{in}	2.2 [keV/u]	T_{out}	17.6 [keV/u]
ϕ_s	39 (°)	a	6.0 [mm]
m	1.458	a_N	0.9 [π mm*mrad]
U_{el}	1.51 A/q [kV]	I	0.23 A/q[mA]

A rectangular vacuum chamber made of Aluminium has been chosen for the Spiral RFQ. Eight large lids give easy access and simplify the mounting and adjustment of the RFQ electrodes. The structure has been aligned with an opto-mechanical system. The rod-electrodes are fixed on electrode carriers, each about 100 mm long and with precisely milled washers to the spiral supports which allow an alignment with a precision of approx. 0.1mm, less than 3% of the aperture radius. Fig. 2 shows a scheme of a spiral-RFQ resonator cell

The field distribution along the beam axis has a maximum deviation of less than 2%. With the existing equipment rf-tests have been performed up to 35 kW pulsed input power (67 kV) and 7.2 kW in cw operation. No mechanical and cooling problems could be observed despite the design was for a duty factor of less than 1% (average power of 2 kW). From beam- and rf-measurements an Rp-value of 520 kΩm could be determined,which has been checked with x-ray spectroscopy at higher field levels.

These first beam experiments have been done at the Institut für Angewandte Physik. Due to the limited rf-power and extraction voltage light ions (He^+) have been used for the experiments. The corresponding electrode voltage and beam current are 6 kV and 0.8 mA, respectively. Fig. 3 shows a scheme of the experimental setup.

The beam from a duoplasmatron source was matched into the RFQ by two electrostatic einzellenses. For beam analysis an emittance-measurement-device, a fast Faraday-cup and an analyzing magnet had been installed. The maximum transmitted beam current was 980 μA, but due to the input emittance with the typical aberrations of einzellenses the transmission at design voltage has been less than 40%. PARMTEQ calculations with this input emittance delivered transmission curves which are in good agreement with the measurements. Fig. 5 shows the calculated transmission curves vs. electrode voltage for the design input emittance (ε_{norm} =0.3 π mm mrad, α_X=0.8, β_X=0.1 mm/mrad), the emittance with the aberrations of the einzellenses (ε_{norm}=0.5 πmm mrad, α_X=-0.8, β_X=0.04 mm/mrad) and the measured transmission. N^+ in the beam, caused by a leaky valve in front of the ion source, is responsible for the tail of the measured transmission curve. The calculated transport of N^+ is shown in Fig. 4 too.

In Fig. 5 the measured energy spectrum is plotted for the design voltage. Calculations give a much smaller energy spread (ε_{design}), but the results of the measurements can be reproduced with good accuracy, if the measured emittance is used as input for the calculations.
The He^+ experiments have been finished successfully. In a next step the RFQ has been installed at the high current injector test stand at GSI where it will be tested with heavy ions, a high current source and a magnetic injection system to check the full specifications.
Presently the RFQ is mounted at GSI and vacuum- and rf-plumbing is completed.

The HLI-RFQ

The new "High Charge State Injector (HLI)" for the UNILAC has been built to provide 2 to 20 MeV/u beams for the low energy program of GSI. It consists of an ECR-source which accelerates from 2.5keV/u t0 300keV/u for injection into the following IH-structure that further accelerates the beam to 1.4 MeV/u which is the proper energy for the injection into the first Alvarez part of the UNILAC [5,6], as schematically shown in fig. 6.

The resonator consists of four rods arranged as a quadrupole. Diagonally opposite rods are connected by spirally shaped stems or in case of higher frequency with straight stems that are positioned on a common base plate. The quadrupole field between the electrodes is achieved by a $\lambda/2$-resonance which results from the electrodes acting as capacitance and the stems acting as inductivity. When the structure frequency and electrode voltage have been chosen to give good focusing properties, the length has to be optimized with respect e.g. to the beam emittance, the power consumption and the beam transmission.

The mechanical design of this type of accelerator structure allows cooling of all components. The stems, the electrodes, and the tuning blocks are mounted into the tank by screws to be able to change components in case of problems with high duty factor operation, which is required for the HLI-RFQ. Fig. 7 shows the final particle design parameters along the RFQ structure, table 2 summarizes characteristic parameters. The slow increase of the ion energy T as function of RFQ cell number N is demonstrating the fact that a significant part of the structure is required for bunching. After the RFQ had been assembled, aligned and tuned the field flatness was examined and optimized under low power conditions. The field variation along the axis was less than 5%.

Table 2
Main Parameters of the HLI-RFQ

f	108.5 [MHz]	length	2.95 [m]
cells	287	Rp	175 [kΩm]
T_{in}	2.5 [keV/u]	T_{out}	300 [keV/u]
fs	18 [°]	a	3.0 [mm]
m	2.1	a_N	0.5 [π mm*mrad]
U_{el}	9.4 A/q [kV]	transmission	>90%

The first beam tests showed encouraging results. [11,12], . The output beam had the proper bunch structure and ion energy. The width of the bunch, measured by time of flight measurents with two probes, was less than 1 nsec. The energy of the ion beam and the radial emittance was in good agreement with the theory as shown in fig. 8. A closer inspection of the output beam showed a lower transmission of only 40-50%. Experiments with reduced input emittance and with Helium at increased electrode voltage resulted in the required

transmissions values of 90%. A first realignment of the electrodes improved the tranmission. For an emittance of $\varepsilon = 115\ \pi$ mm mrad (design value) the transmission now was 94%. For the experiment the emittance was changed by an aperture in the injection beam line. Also rf-operation revealed some problems: rf-operation was stable, with very little multipacting at low levels and a quick thermal equilibrium at power levels up to 130 kW (25% d.f.) with small frequency shifts. At high power levels an rf modulation caused by ponderomotoric forces was observed, which was qualitatively similar to the effects studied at spiral loaded cavities [13]. This effect was characterized as mechanical oscillations of the electrode ends, which were excited at the pulse repetition frequency. Its resonance is at 178 Hz at which it shows strong amplitude resp. forward power modulation, if the tank amplitude is kept constant during the pulse by the control system. Even the pertubation could be controlled at 50 Hz repetition rate and design field value, this effect makes it difficult to achieve 50% df without additional mechanical stabilisation of the electrodes. An improved feedback system would solve this problem as well, but it would be not ideal for routine operation.

With an improved cooling tube for the electrodes, which gives a stiffer system at the same time, and a better alignment the operational properties have been improved. Fig. 9 shows the improved transmission curve. The temperature of the rods is now raised by 6 degrees only at full field level and the mechanical oscillations are supressed. The maximum power load of the RFQ has been raised to 175 kW / 25% df and several U^{28+} user beam times have been successful, at least from the accelerator point of view. [14].

RFQs for the Acceleration of Radioactive Beams

General features of the proposed accelerators for radioactive beams at ISL are a final energy of 10MeV/u for all ions up to mass 240u starting with singly charged ions from a complex target-ion source - high resolution mass separator system with gives a starting energy of 100 keV for all ions. The optimum postaccelerator should be able to accelerate all these ions with 100% transmission without emittance growth. It would work with 100% duty cycle (DC or CW mode) and have a microstructure with 10 MHz beam bunch repetition rate.

To put the problems of the low energy part into a proper perspective a comparison with the HILAC or UNILAC parameters shows the step ahead in expected performance. Aside the duty factor problem which will dominate all the linac engineering the low specific charge q/A of the ions to be accelerated is the most difficult input parameter for the beam dynamics design While the UNILAC starts with charge state q=10 for the heaviest ion (q=28 at the new HLI injector), the ISL machine will start with singly charged ions, which means all focusing and accelerating gradients should be increased by a factor of ten (A/q) to give the same beam dynamics. Such parameters are not assumed even in the most optimistic designs therefore restrictions in the mass range and/or duty factor are made in most cases.

ISL will make use of the full mass range. The design of the prestripper part of the linac which accelerates the single charged ions $q/A \geq 1/240$ from 100 keV to 100 keV/u for which a sufficient stripping effiency is assumed to increase the charge state to $q/A > 1/20$ is shown in fig. 10a. To match the beam from the mass separator to the input of the first rf-linac structure with its inherent velocity profile, the first RFQ is being installed at a HV-platform. Lowering the injection energy of the RFQ to 1keV/u the platform voltage could be reduced to 140kV max. A short rf-cavity than has to match the energy of the beam from the platform to the input of the second RFQ. Its total "voltage gain" of 22 MV shows the scale of the machine, which can be compared to the "high current injector" planned at GSI for the pulsed injection into the SIS.

The HV-platform poses some problems concerning the radial and axial matching into the first and second RFQ. It could be omitted like shown in Fig. 10b. if a special energy matching cavity is put in front of the RFQ1. Another simplification is the skipping of adiabatic bunching part in the first RFQ which has been done for the cluster-RFQ and the cyclotron injector at HMI [15,16]. For low current application this option can be used but would need a HV-platform for the ion source or a 140 kV cavity and a drift of appr. 3 m in case of the 100 keV beam of ISL. Using an external (harmonic) buncher results in a compact solution for RFQ1 which should operate at 10MHz to provide the beam mictrostructure and the strong focusing at low energy.

The matching into the first RFQ is somewhat complicated because the energy matching cavity will change the bunching and the radial matching for RFQ1, which is an interesting optimization problem. The structure for the 10 MHz-RFQ could be a modification of the Spiral-RFQ built for GSI or a twin-line 4-rod structure like the one being built for heavy clusters (operating frequency 5 MHz) [17]. The RFQ1 would be 4.5 m long and need about 50 kW rf-power.

In the reference design worked out at the Oak Ridge and LBL workshops the second RFQ would work at 50MHz which would enable the application e.g. of superconducting RFQs, which would be saving power consumption. But unfortunately the jump from 10 to 50 MHz for such low specific charges is not possible at these low energies.

Applying the adiabatic damping in classical accelerators, the frequency can be doubled, if the energy has been increased by a factor of $T_f/T_i = 6.5$. In our designs at least a factor of $T_f/T_i=10$ would be applied, because of the paramter variations in the RFQ. A factor of 5 in frequency would require a factor of appr. $T_f/T_i=70$ in energy to ensure proper phase width acceptance. In addition the focusing strength of the "high frequency" (50 MHz) RFQ is limited. A electrode voltage e.g. of U= 400kV would be be needed to give the same phase advance per cell as in RFQ1. The maximum field strengthes are 90 MV/m (8.5 U_K) which comes close to the best values obtained in short prototype tests, but are unreasonable for longer structures like RFQ2, which would be approximately 5.5m long.

It would be more realistic to switch to 20 MHz for RFQ2, with still a modest power of 20kW/m but a length of 24m for a final energy of 100keV/u. Going to 30MHz would not reduce the length, but nearly double the power load and increase the peak fields by 50%. At 50 MHz the phase advance per cell would be to small ($\sigma<5^o$)and the power losss rather large (P=60kW/m).

These design considerations for the prestripper part will have to be modified by the optimization of the complete system. It is likely that the dominant role of the losses and the emittance growth caused by the strippers will make discussions about some percentage savings not useful, even it is a multiplying factor in the overall transmission.

Less universal but more effective in terms of acceleration would be to start with a higher charge state as with an ECR source. The broad charge state spectrum and the large emittance of these sources is an disadvantage but the accelerator design would be straightforward either following the GSI-HLI injector or the ANL-ATLAS designs.

An alternative solution especially suited for lighter radioactive ions is discussed at MPI Heidelberg and MSI Stockholm. As demonstrated for "normal" ions the EBIS ion source can be operated in a special mode where ions are collected successivly ionized and extracted in a pseudo cw mode [18].. Measurments at MSI have demonstated an efficiency of 14% [19]., that means that the amount of input ions to ions in a single charge state is as high as for the passage of a single stripper. The limits for heavier masses have to be evaluated but the accelerator part is rather simple, e.g. standard postaccellerator systems like MPI, ANL and pulsed operation with e.g. 25% d.f. is also matched to the ion source program.

The prestripper part of the ISL accelerator would indeed be another class of machine, and the restriction to lighter masses (A/q≤60) e.g. at TRIUMPF [20] leeds to more classical solutions too.

The basic design parameters for singly charged radioactive heavy ions (m=240u) dicussed obove result in a large, long accelerator but the parameters for a injector with good beam emittance and high transmission like the focusing strength, the field gradients, and the ratio of power/length are feasable.

Acknowledgements

The work on the HSI and HLI structures naturally is the work of a group of people, from which I want especially mention the contributions of J. Klabunde, H. Deitinghoff, A. Kipper, J. Madlung and J. Friedrich.

References

[1] I. M. Kapchinskiy, V. Teplyakov, Prib.Tekh.Eksp.119, No.2(1970) p.17,19
[2] R. H. Stokes, T. P. Wangler, Ann, Rev. Nucl. Part. Instr. 38 (1989) p.97
[3] A. Schempp, Habilitationsschrift, Univ. Frankfurt 1990
[4] D. Böhne, K. Blasche, B. Franczak, B. Franzke, H. Prange, R. Steiner, "The Performance of the SIS and Developments at GSI", EPAC II, World Sci. (1990)p.18
[5] N. Angert, L. Dahl, J. Glatz, J. Klabunde, M. Müller, B. Wolf, "The UNILAC Modifications for an Improved Synchrotron Performance", EPAC 90, Ed. Front.(1990)p.503
[6] J. Klabunde, "The UNILAC Upgrade Project", LINAC88, CEBAF-Rep. 89-001 (1989) p. 243
[7] A. Schempp, PAC89, "4-Rod-RFQ Injectors for the GSI Linac" PAC89, IEEE89CH2669 (1989) p.1093
[8] A. Schempp, H. Deitinghoff, A. Kipper "Development of a 27 MHz Heavy-Ion-Spiral RFQ", NIM A278 (1989) p.169
[9] A. Schempp, A. Kipper, H. Deitinghoff, J. Madlung, "The GSI High Current RFQ Prototype",NIM B79 (1993) p. 714
[10] A. Kipper, A. Schempp, H. Deitinghoff, J. Madlung, O. Engels, A. Firjahn- Andersch, H. Vormann, "The High Current Spiral-RFQ Prototype" LINAC 92, AECL Rep.-10728 (1992) p. 416
[11] J. Klabunde, "The High Charge State Injector for GSI" LINAC 92, AECL Rep.-10728 (1992) p. 570
[12] J. Friedrich, A. Schempp, H. Deitinghoff, J. Madlung, O. Engels, A. Firjahn-Andersch, H. Vormann, "The High Current Spiral-RFQ Prototype" LINAC 92, AECL Rep.-10728 (1992) p. 416
[13] A. Schempp, W. Rohrbach, H. Klein, "Measurements on Spiral Resonators at high Field Levels", NIM 140 (1977) p.1
[14] J. Klabunde, private communication
[15] A. Schempp, H. Deitinghoff, J. Madlung, U. Bessler, J. Friedrich, J. Dehem, R.Veith, H.O.Moser, G. Hadinger, M.J. Gaillard, R. Genre, J. Martin "Development of a Variable Energy RFQ for Cluster Acceleration" EPAC 90, Ed. Front.(1990) p.40
[16] A. Schempp, "ISL-Beschleuniger" Univ. Frankfurt, IAP Int. Rep. 93-8
[17] A. Schempp, "A Varaible Energy RFQ for the Acceleration of Heavy Clusters" Proc. of "Polyatomic Ion Impact on Solids" StMalo, France 1993
[18] R. Becker, M. Kleinod, E.Donets, A. Pikin, "Accu EBIS: Collection and Ionisation of Radioactive Products" EPAC 90, Ed. Front.(1990) p.981
[19] D. Habs, L. Lilleby, private communication
[20] H. Schneider, ISL-Worshop, LBL, Oct. 27-29, 1993

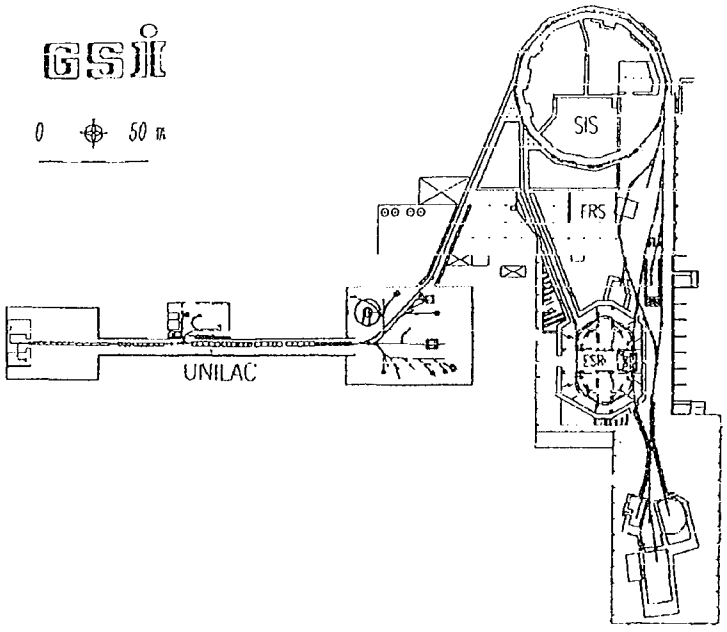

Fig 1 Plan view of the GSI accelerator facility

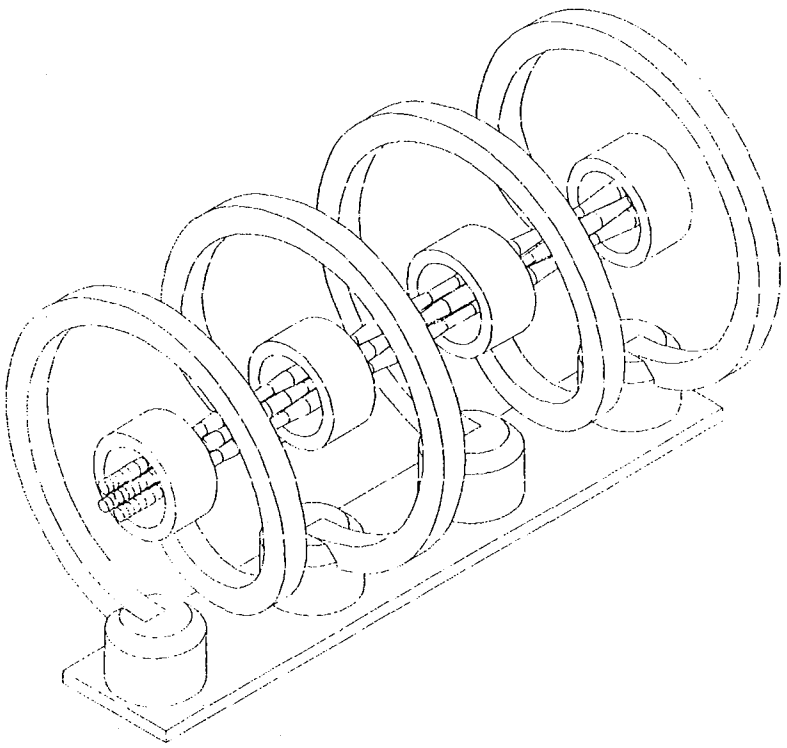

Fig 2 Scheme of the Spiral-RFQ structure

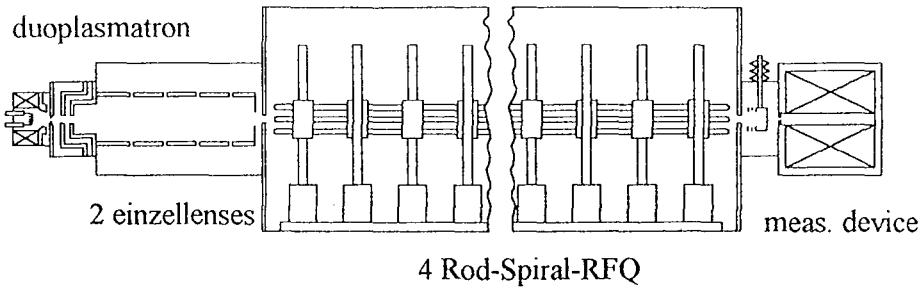

Fig 3 Scheme of the experimental set up for beam tests

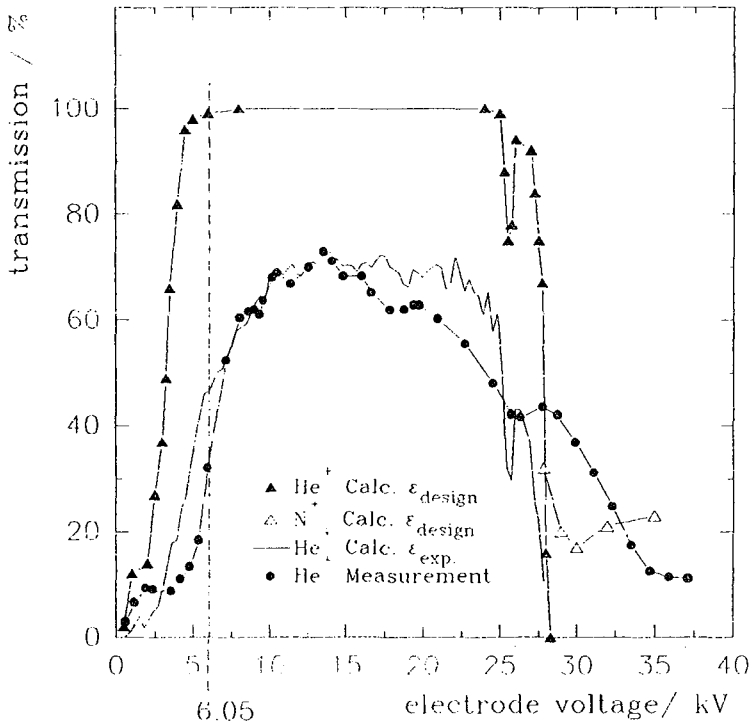

Fig. 4 Calculated and measured transmission curves

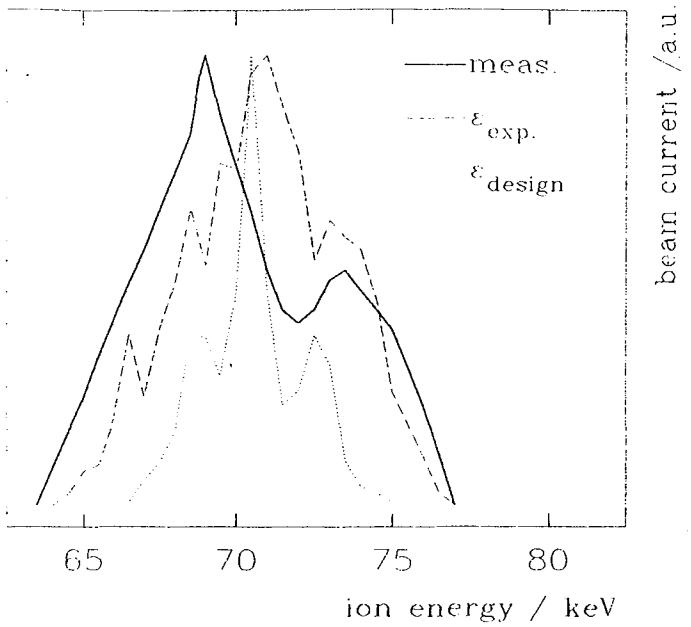

Fig. 5 Measured and calculated energy spread

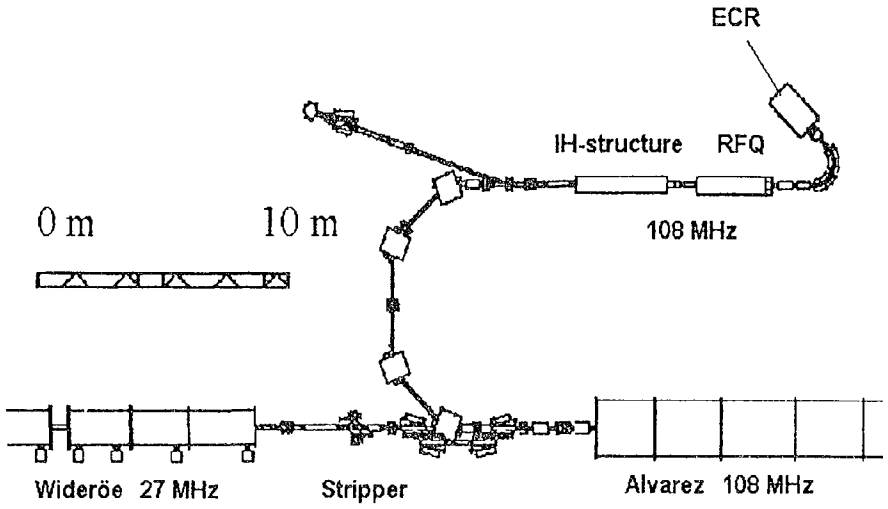

Fig.6 Layout of the HLI-injector of GSI

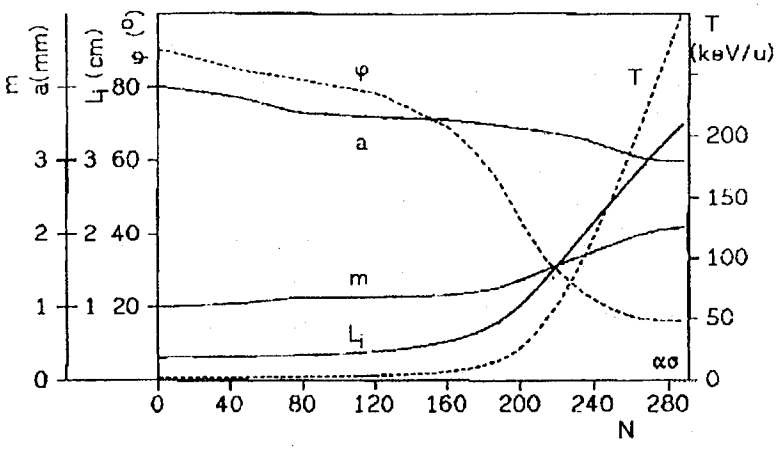

Fig 7 Beam dynamics layout of the HSI-prototype-RFQ

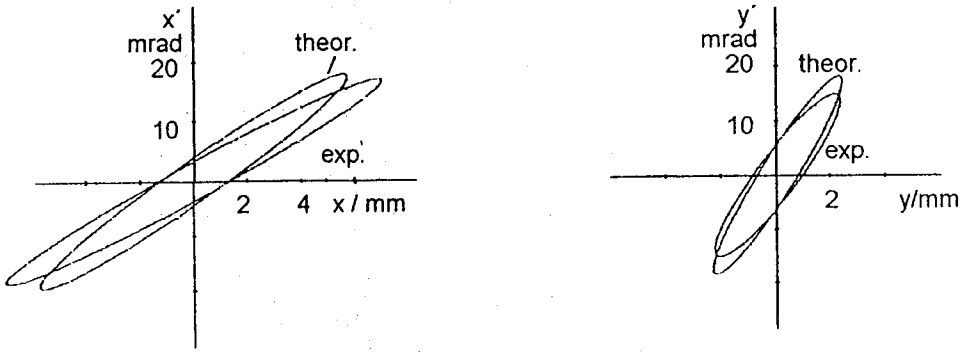

Fig. 8 Measured and calculated beam emittances at the HLI-RFQ

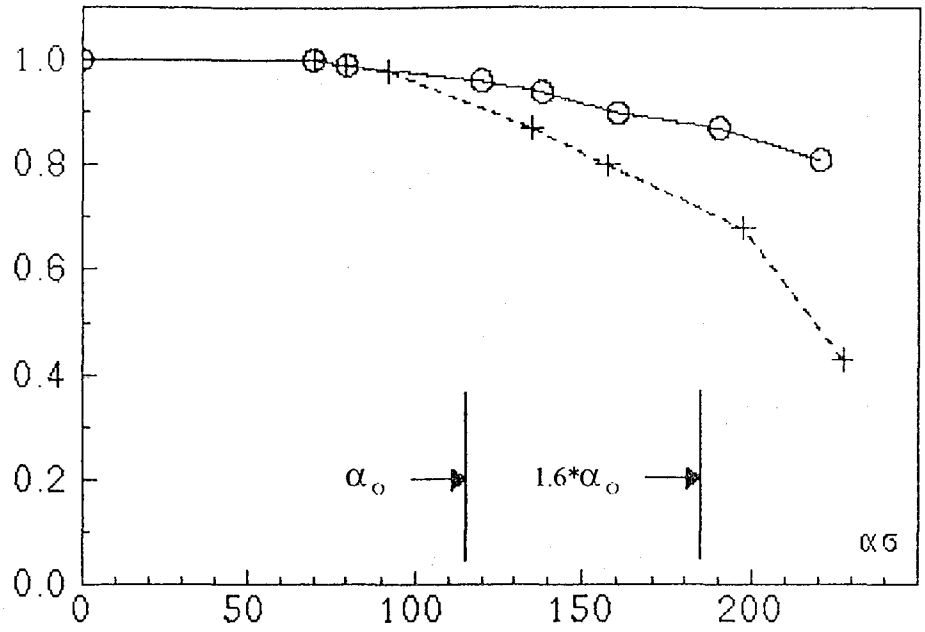

Fig.9 Transmission curves for the HLI-RFQ

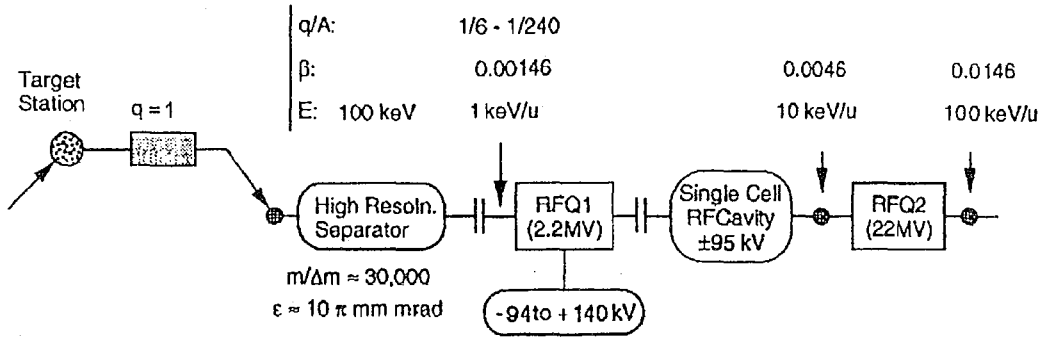

a.)

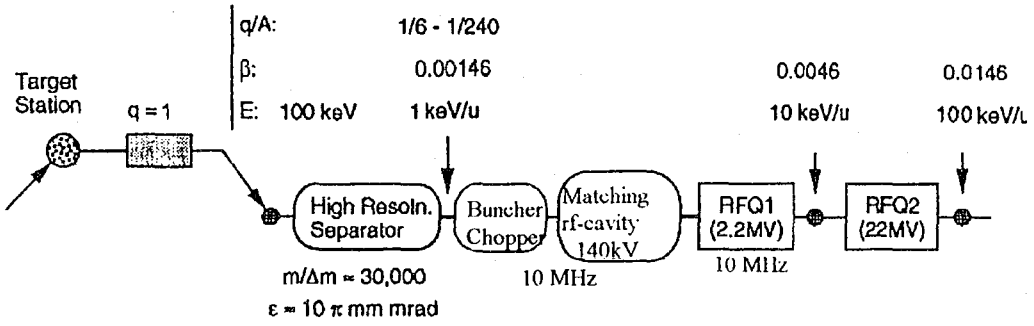

b.)

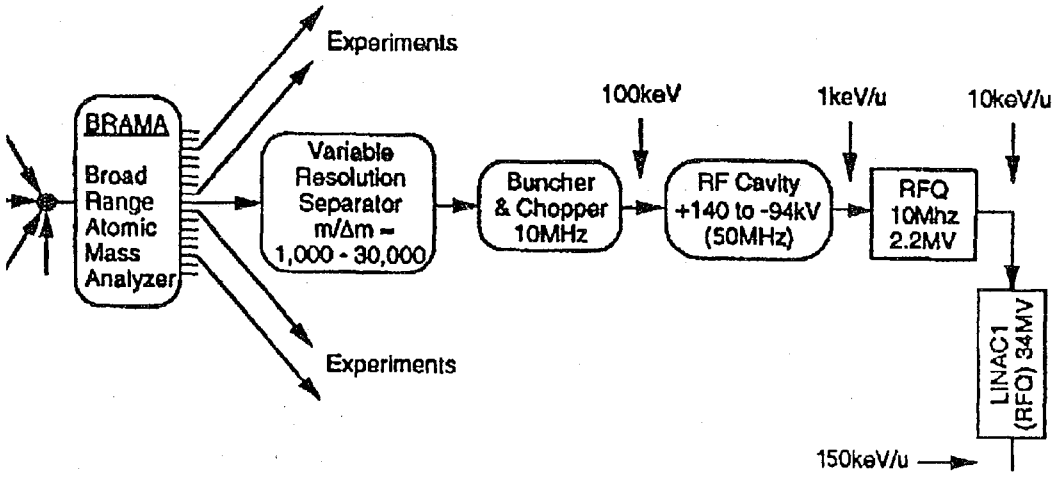

c.)

Fig. 10 Layouts of the injector for heavy radioactive beams

Progress in Low β, Low q/A RFQ's at INS

N. Tokuda
Institute for Nuclear Study, University of Tokyo,
Tanashi, Tokyo 188, Japan

Abstract

Two split coaxial RFQ's (SCRFQ's) are presented. Both operate at 25.5 MHz and accelerate ions with a charge-to-mass ratio q/A greater than 1/30. One SCRFQ is a prototype (0.9 m diameter, 2.1 m length, 45 keV/u output energy), and the other is its extended version (0.9 m, 8.6 m, 172 keV/u). The prototype was constructed in 1989 and underwent rf and acceleration tests for two years. Through experience obtained with the prototype SCRFQ, we are now constructing the longer machine. The cavity construction is to be finished in the spring of 1994. The new SCRFQ will be used as the front-end linac in the E-Arena Test Facility, now under construction in INS. In the facility radioactive nuclei will be accelerated by the SCRFQ and an interdigital-H linac (the output energy is variable in a range of 172 through 1046 keV/u) and delivered to nuclear physics experiments.

1. Introduction

Split coaxial RFQ's (SCRFQ's) have been developed at INS since 1984. In this paper two SCRFQ's, which operate at 25.5 MHz and accelerate ions with a charge-to-mass ratio q/A greater than 1/30, are presented. One SCRFQ is a prototype (the length is 2.1 m, and the output energy is 45 keV/u) [1], and the other is its extended version (8.6 m, 172 keV/u).

Our SCRFQ structure is featured by modulated vanes, same as the ones used in the four-vane RFQ, and a multi-module structure [2]. This structure was devised so that we could diminish the defect of the split coaxial resonator: the inner electrodes are cantilevers, and therefore the electrodes are not firm. In the multi-module structure, however, each electrode is supported at a few points. At the prototype SCRFQ, for instance, the whole cavity (2.1 m long) comprises three module cavities (0.7 m long each), but the vanes are bars with the whole length of 2.1 m. Each vane is fixed at two points: one vane end is fixed to a cavtiy end wall, and at a point 1.4 m apart from it, the vane is supported by a stem. Since the length of the cantilever part is only 0.7 m, the electrodes are mechanically stable. Moreover, owing to the vanes with the whole length, it is easier to align the vanes precisely.

The prototype SCRFQ was constructed in 1989. Through rf and beam tests for two years, we gained confidence in our SCRFQ structure, and decided to build a longer machine. The long SCRFQ, in which the prototype is included, is now under construction, to be completed in the spring of 1994. The new SCRFQ is to be used as the front-end linac in the E-Arena Test Facility. In this facility, radioactive nuclei will be accelerated by the SCRFQ and an interdigital-H linac [3 $\sim$ 7]. The output beam, whose energy is fully variable in a range of 172 $\sim$ 1046 keV/u, is used for nuclear physics experiments.

This paper describes the experience obtained with the prototype SCRFQ and the design of the long SCRFQ.

2. Prototype SCRFQ

2.1. Summary of Obtained Results

Main parameters of the prototype SCRFQ are listed in Table 1. Through the construction and operation of the prototype SCRFQ, we obtained the following results. Concerning cavity and rf aspects, (1) the vane alignment was accurate within ± 40 μm; (2) the quadrant field balance was better than $\pm 0.7\%$ at any axial position; (3) the intervane voltage was flat over the vane length; (4) an intervane voltage of 118 kV, or a field strength of 190 kV/cm, was achieved; and (5) a 20% duty factor was possible with a peak power of 80 kW generating an intervane voltage of 109 kV. As for beam dynamics, (6) the vane-tip geometry is such that the transverse radius of curvature ρ_T is equal to r_0; for $\rho_T = r_0$ vanes, it is indispensable to correct the aperture radius a and modulation index m so that the corrected A_{10} coefficient might be equal to the A coefficient of the two-term potential function; and (7) the longitudinal beam dynamics in the radial matching section is not yet clear, and hence we must figure out the field distribution by using a three-dimensional field solver. Detailed descriptions on these results are presented below.

2.2. Cavity Structure

The structure of the prototype SCRFQ is shown in Fig. 1, and the conceptual diagram of the resonator in Fig. 2. The whole cavity comprises three module cavities, each of which is 0.9 m in inner diameter and 0.7 m in length. The modulated vanes, which are one-body bars of 2.1 m long, are fixed to back plates.

Table 1
Main parameters of the prototype SCRFQ.

Frequency (f)	25.5 MHz	$\lambda = 11.76$ m
Charge-to-mass ratio (q/A)	$\geq 1/30$	
Input energy (T_{in})	1 keV/u	$\beta = 0.00146$
Output energy (T_{out})	45.4 keV/u	$\beta = 0.00984$
Normalized emittance (ϵ_n)	0.06 π cm·mrad	$\epsilon = 41.1\,\pi$ cm·mrad (input)
Vane length (L_v)	213.5 cm	
Number of cells (N_c)	136	34 cells in radial matcher
Intervane voltage (V_{vv})	109.3 kV	$q/A = 1/30$ ions
Maximum surface electric field (E_s)	176.2 kV/cm	2.47 Kilpatrick ($\kappa_{max} = 1.525$)
Mean bore radius (r_0)	0.9458 cm	
Minimum bore radius (a_{min})	0.5214 cm	
Margin of bore radius (a_{min}/a_{beam})	1.2	zero-current beam
Maximum modulation index (m_{max})	2.50	
Final synchronous phase (ϕ_f)	$-30°$	
Focusing strength (B)	6.0	
Maximum defocusing strength (Δ_b)	-0.20	

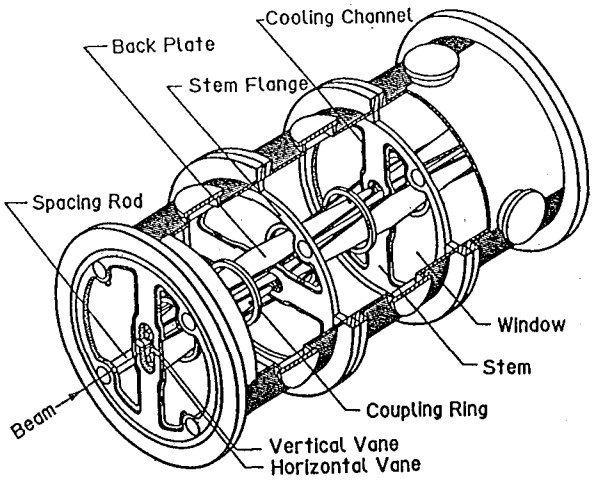

Fig. 1. Structure of the prototype SCRFQ (25.5 MHz, 0.9 m in diameter, 2.1 m in length, three module-cavities).

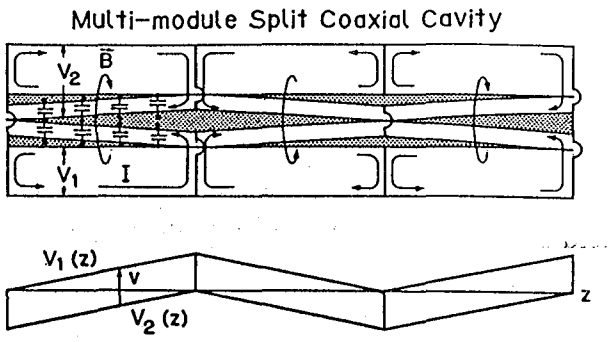

Fig. 2. Conceptual diagram of a three-module split coaxial resonator.

The materials for the cavtiy parts are as follows: (1) mild steel with 100-μm-thick copper plating for the cavity cylinder and end walls, (2) oxygen-free copper for the back plates and the stem flanges, (3) copper-plated stainless steel for the spacing rods, and (4) chromium-copper alloy (1% Cr + 99% Cu) for the vanes. Three different types of rf contanctors are used: (1) silver-plated stainless tubes (3.28 mm in diameter) between tank cylinders, (2) copper strips (1 mm $\times$ 26 mm cross section) between a stem flange and a tank cylinder, (3) shield spirals between a stem flange and a spacing rod. No contactor is inserted between a vane and a back plate.

The inner structure of the cavity was assembled outside the tank and built into the tank. The parts are bolted together. First, the stem flanges and the spacing rods were connected together into a frame, then the back-plates and the vanes were attached. For inspection of vane alignment, the interior assembly was set on a table; by the use of a dial gauge, vane positions were measured from a horizontal reference plane and a vertical one. The vane-alignment errors were less than ± 40 μm, as shown in Fig. 3.

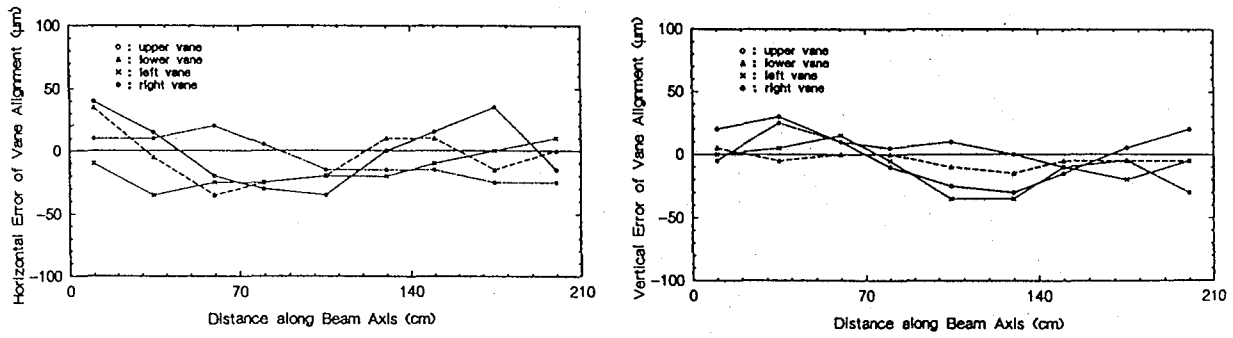

Fig. 3. Vane-alignment errors in the horizontal and the vertical directions (left and right figures, respectively) measured before the inner electrode was built in the tank.

2.3 Low-power tests

The resonant frequency of the cavity was first tuned roughly to 25.45 MHz by adjusting the window areas of the stem flanges (see Fig. 1), *i.e.*, we controlled the inductances associated with the magnetic fluxes around the stems [8]. Initially the windows were closed with plates with a half-moon shape; the resonant frequency measured 28.88 MHz. Then the plates were removed one by one. At every removal, the frequency decreased by 1.1 MHz, and finally reached 24.68 MHz. This meant the windows should be almost open for the frequency of 25.45 MHz. Hence we bolted copper strips along the stems; the stem width of 12 cm was thereby increased to 21 cm. For further fine tuning to 25.5 MHz, we used three inductive tuners, one tuner per module cavity. The tuners are copper cylinders, driven by stepping motors. The adjustable frequency range was about 50 kHz. The unloaded Q-value measured at 25.5 MHz is 6400, about 84% of a calculated value.

The azimuthal field balance was tested by pulling a cylindrical teflon bead (20 mm diameter, 10 mm length) down each quadrant [9]. The bead was set between neighboring vanes so that it touched them. Figure 4 shows the obtained phase shifts, approximately proportional to the square of the field amplitude. Four curves corresponding to the quadrants are drawn. The field strengths in the quadrants are balanced so well that the four curves are overlapped. We obtained $|\delta_i(z)| \leq 0.67\%$ at any axial position z, defining alignment error as $\delta_i(z) \equiv E_i(z)/\overline{E}(z) - 1$, where $E_i(z)$ is the field amplitude in the i-th quadrant, and $\overline{E}(z) = \frac{1}{4}\sum E_i(z))$.

The curves in Fig. 4 are almost flat, except for three small dips at ends of the modules. The dips are due to stems, enhancing the field strength at the bead position. Such dips were not observed in another measurement by setting a bead (teflon cylinder, 0.95 cm diameter, 0.75 cm length) on the beam axis and pulling it down. The thick line in Fig. 5 indicates the experimental result [9]. The thin line was obtained by a calculation under assumptions that the electric field is same as the one derived from the two-term potential function (Eq. 1, Sec. 2.4.2), and that the intervane voltage is constant over the vane length. From this result and the flat curves in Fig. 4, we conclude the distribution of the intervane voltage is flat.

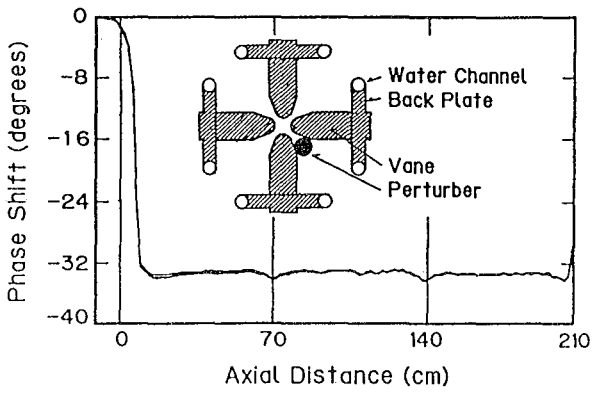

Fig. 4. Measured field strengths (approximately $\propto$ |phase shift|$^{1/2}$) between neighboring vanes. Four curves for the quadrants are plotted.

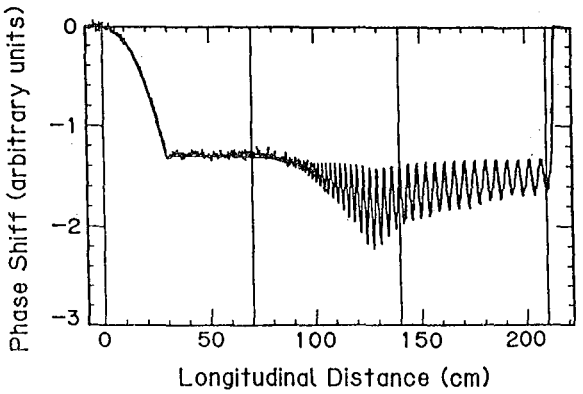

Fig. 5. Field strengths in the beam aperture; the thick line indicates a measured strength, and the thin line a calculated one.

2.2. High-power tests

The driving rf power is fed to the cavity through a loop coupler (9 cm × 20 cm). The loop is rotatable for the impedance matching to 50 Ω; a VSWR of 1.01 was obtained by rotating the loop by 19° to the magnetic flux. The power source with an Eimac 4CW30000A tube has a peak power of 100 kW at maximum. The maximum duty factor at this power is 20%. The rf power is transmitted to the loop coupler through a 5.9-m-long WX-120D coaxial line.

The intervane voltage is derived from the signal from a monitor loop [9]. The calibration constant was obtained as follows. We applied directly voltage between neighboring vanes by connecting them to a signal generator with a cable, and measured the output voltage from the monitor loop. The resulting monitor loop voltage against an intervane voltage of 1 V was 0.1225 mV.

During the initial conditioning of the cavity, we increased the input power step by step with duty factors of 0.6 ~ 3%. Figure 6 shows the progress in the attained intervane voltage. After an aging time (operation time × duty factor) of 2.5 hours, we obtained 110 kV [9]. Further aging put the cavity into stable operation at higher intervane voltages and duty factors. Figure 7 shows a process that the sparking frequency decreased with time during a conditioning with an intervane voltage of 114 kV and a duty factor of 2% [10]. At a higher duty factor of 9%, we attained an intervane voltage of 118 kV. Using a field enhancement factor of 1.525 given by Crandall [11], we estimate the highest surface field to be 190 kV/cm (2.7 Kilpatrick).

The shift of the resonant frequency was measured as a function of the average input power; the duty factor was 10% and the repetition rate was 100 Hz [12]. The result is indicated with dots in Fig. 8. The resonant frequency, 25.480 MHz initially, increased to 25.608 MHz (Δf = 128 kHz) at a power of 8.5 kW and an intervane voltage of 112.7 kV. The observed frequency shift was unexpectedly large; this was due to the coupling rings. As shown in Fig. 9, they are fixed to diametrically opposed back plates. Since the rings are not cooled by water, they expanded under the high-power operation and pulled apart the vanes. As a result the intervane capacitance decreased, and the resonant frequency increased.

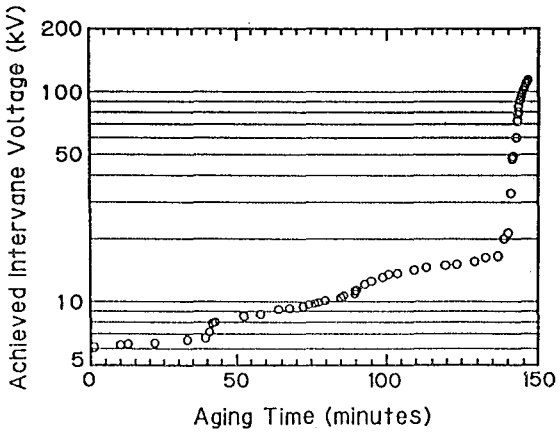

Fig. 6. Attained intervane voltage as a function of the aging time (operation time × duty factor) during the initial rf contidioning.

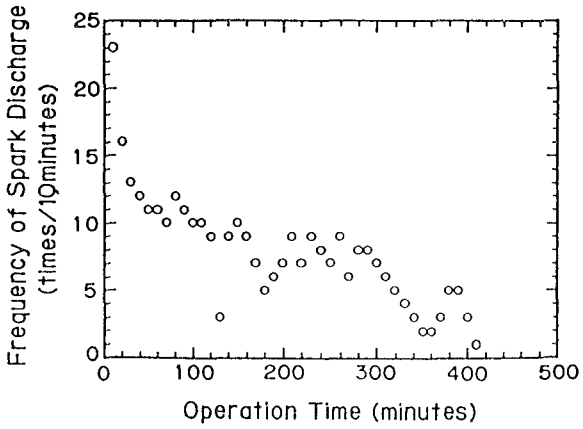

Fig. 7. Reduction of spark discharge frequency during an rf conditioning with an intervane voltage of 114 kV and a duty factor of 2%.

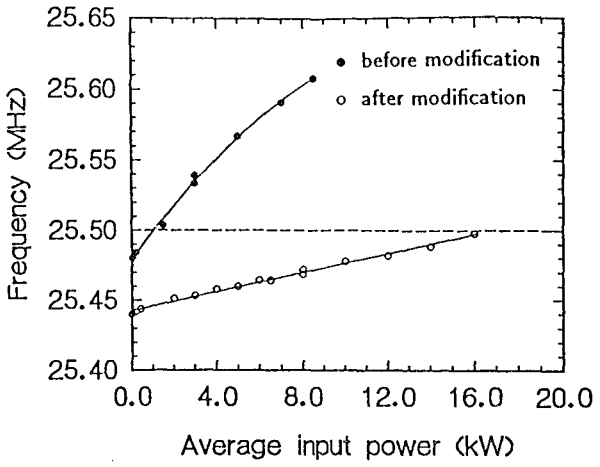

Fig. 8. Shifts of resonant frequency *vs.* average input power, before and after the modification of the coupling rings.

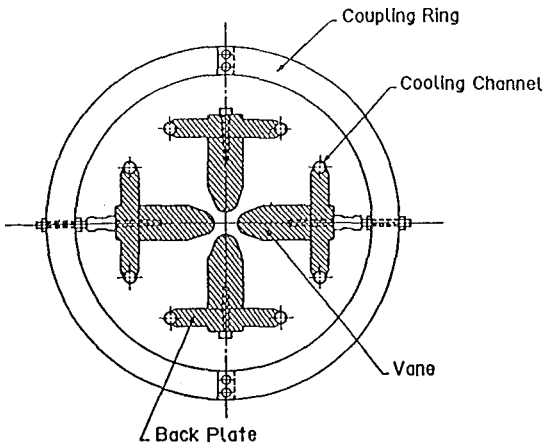

Fig. 9. Coupling ring, fixed to back plates. The ring comprises two arcs bolted together.

In order to reduce the frequecy shift, we modified the coupling rings and re-measured the frequency shift. A coupling ring is composed of two arcs bolted together at places 90° apart from the rods connecting the arcs to the back plates. We removed the bolts and turned the arcs on the rods in opposite directions. The vanes became thereby free of the force from the coupling rings. In the frequecny-shift measurement, the cavity was operated at a 10% duty (100 Hz) for average powers lower than 8 kW; for higher powers, the peak power was kept at 80 kW (intervane voltage = 109.3 kV), and the repetition rate was increased up to a duty factor of 20%. The open circles in Fig. 8 are the frequency shifts after the ring modification; the frequency shift were suppressed appreciably. The initial frequency was 25.44 MHz, lower by 40 kHz than that before the ring modification. This frequency decrease is due to the increase of the capacitance between the back plates and the turned arcs. The resonant frequency was 25.47 MHz (Δf = 29 kHz) at an average power of 8 kW, and at 16 kW, 25.50 MHz (Δf = 56 kHz).

The resonant frequency is stabilized by using the three inductive tuners, which are driven by stepping motors. In the feedback loop the stepping motors receive the phase difference between the driving rf and the picked-up signal from the monitor loop. A frequency stabilization within ±200 Hz has been obtained under an operation with an average power of 12 kW (60 kW × 20%).

From the frequency-shift measurements, we found that the coupling rings are harmful. From this experience and the observations described below, we consider that the coupling rings should be removed.[1] The purpose of the rings was to gain a better vane alignment. During the inspection of the vane alignment, however, we found that the coupling rings received no force from the back plates; this means that the vanes could have been aligned well enough without the coupling rings. Moreover, we conducted beam tests with the disconnected coupling rings and verified that good beam performances were obtained. The test issues were as follows: (1) transverse emittance profiles of the output beam at various intervane voltages (N^+ beam, maximum P_{ave} = 5.9 kW), (2) transmission efficiencies as a

[1]No coupling ring is used in the long SCRFQ under construction.

function of the intervane voltage (N^+ beam, maximum $P_{ave} = 7.0$ kW), and (3) transmission efficiencies as a function of the duty factor (N^+ and N_2^+ beams, maximum $P_{ave} = 16.0$ kW), The tests Nos. 1 and 2 yielded results almost same as those with the original connected coupling rings. At the test No. 3, the transmission efficiencies were independent of the duty factor.

2.4. Acceleration Tests

2.4.1. Introductory remarks

Figure 10 shows the layout of the acceleration test stand. The ions used in acceleration tests are N_2^+, N^+, and Ne^+, which are produced in an ECR ion source. We conducted experiments on the following issues: transverse emittance and energy profiles of the output beam at various intervane voltages, transmission efficiency as a function of the intervane voltage, transmission efficiency as a function of the input energy [12 $\sim$ 14]. The results showed that there was no problem in the transverse beam dynamics. As for the longitudinal beam dynamics, however, we have two subjects to discuss: one is the A_{10} coefficient for the $\rho_T = r_0$ vane, and the other is the beam motion in the radial matching section.

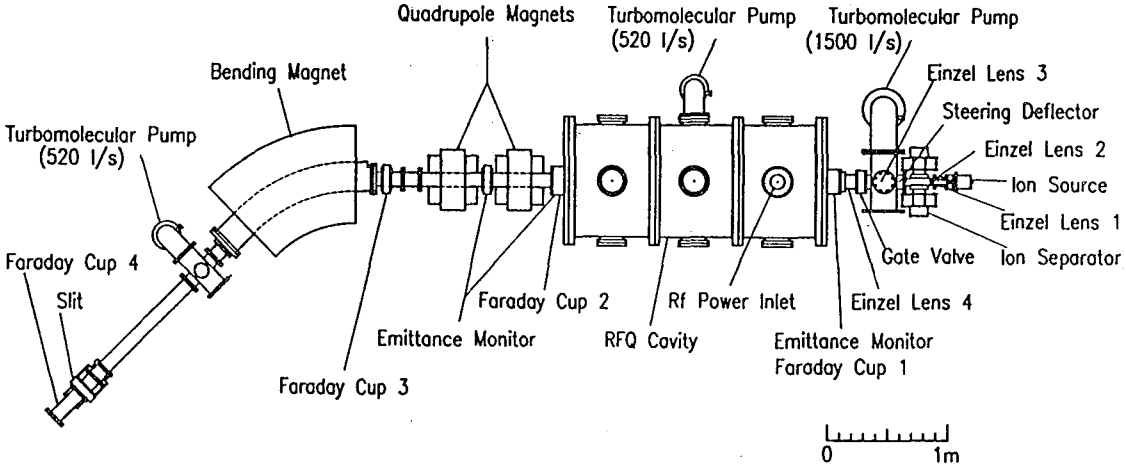

Fig. 10. Layout of the acceleration test stand.

2.4.2. A_{10} coefficient

In the discussion below, we use three versions of the PARMTEQ program: PARMTEQ-2, -M, and -H. In PARMTEQ-2, the electric field is derived from the two-term potential function. In PARMTEQ-M, the A coefficient of the two-term potential function is replaced with A_{10} coefficient calculated by Crandall [11]. In PARMTEQ-H, Crandall's A_{ji} coefficients are used (higher-order multipoles are included).

The two-term potential function, used in PARMTEQ-2, is expressed as:

$$U_2(r,\psi,z) = \frac{V}{2}\left[\left(\frac{r}{r_0}\right)^2 \cos 2\psi + A\, I_0(kr)\cos kz\right], \tag{1}$$

where V is the intervane voltage, $k = \pi/(\text{cell length}) = 2\pi/\beta\lambda$, and I_0 is the modified Bessel function of order zero [15]. The parameters A and r_0 are determined by the boundary conditions:

$$A = \frac{m^2-1}{m^2 I_0(ka) + I_0(mka)}, \quad r_0 = a\,[\,1 - AI_0(ka)\,]^{-1/2}, \tag{2}$$

where a is the minimum distance from the z-axis to the vane tip, and ma is the maximum distance. Equating the right-hand side of Eq. 1 to $\pm V/2$, we have equations representing equipotential surfaces. The ideal vanes would have surfaces same as the equipotential surfaces. For technical reasons, however, the geometry of actual vanes are different from that of the ideal ones, and therefore the actual electric field will be different from that derived from the two-term potential function.

For the actual vanes, the potential function should be expressed in a more general form:

$$U(r,\psi,z) = \frac{V}{2}\left[\sum_{i=1}^{\infty} A_{0i}\left(\frac{r}{r_0}\right)^{2i}\cos 2i\psi + \sum_{i=0}^{\infty}\sum_{j=1}^{\infty} A_{ji}\, I_{2i}(jkr)\cos 2i\psi \cos jkz\right]. \tag{3}$$

From the fourth symmetry condition, if i (j) is even, then j (i) must be odd. Using a program CHARGE 3-D, Crandall calculated eight lowest-order multipole coefficients for differing vane-tip geometries: the transverse radius of curvature ρ_T is variable with respect to z, or constant ($= r_0$ or $0.75\ r_0$); the longitudinal vane profile is standard (derived from the two-term potential function) or sinusoidal [11]. He tabulates resulting A_{ji}'s for an array of the modulation index m and the cell length divided by r_0. At any geometry, the resulting coefficients, except for A_{10}'s, are close to those of the two-term potential function, *i.e.*, A_{01} is almost unity, and higher-order coefficients are small. The A_{10} coefficient is, however, appreciably different from A; particularly at the constant ρ_T vanes, the A_{10}/A ratio is about 0.6 or 0.7 in the low-energy region (short cell length and small m).

At our vanes, ρ_T is constant at $r_0 = 0.946$ cm, and the longitudinal vane tip profile is the standard one. We computed the A_{10}/A ratio for every cell by using an interpolation procedure on the Crandall's table values; a computer program MOD12 was used for the interpolation [16]. The resulting A_{10}/A is shown in Fig. 11, along with the synchronous phase ϕ_s, design values with $A_{10} = A$. The A_{10}/A ratio is smaller than unity in the bunching process, where synchronous phase increases from $-90°$ to $-30°$. According to the PARMTEQ-2 simulation with $A_{10} = A$, many ions lie near the separatrix during the bunching process. If $A_{10} < A$, the separatrix shrinks both in phase width and energy height; as a result, some particles will spill from the rf bucket, and the transmission efficiency will be reduced.

The expected reduction of the transmission efficiency was experimentally verified [14]. Figure 12 shows experimental and simulation results for the transmission efficiency as a function of the normalized intervane voltage V_n. The transmission efficiency is defined by the ratio of the current of accelerated ions to that of the injected ions, and the normalized intervane voltage by the ratio of the measured voltage to the design value. In the range of $V_n \leq 1.3$, the measured transmission efficiencies are much lower than the PARMTEQ-2

values. The result of PARMTEQ-M runs looks better; this program uses A_{10} in place of A, and consequently yields reduced transmission efficiencies.[2] Therefore the A_{10} coefficient of the actual field will be close to the Crandall's value.[3]

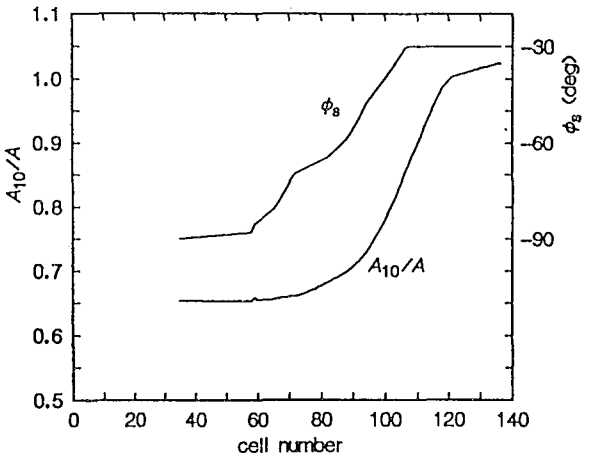

Fig. 11. A_{10}/A ratio and the designed synchronous phase ϕ_s as functions of the cell number.

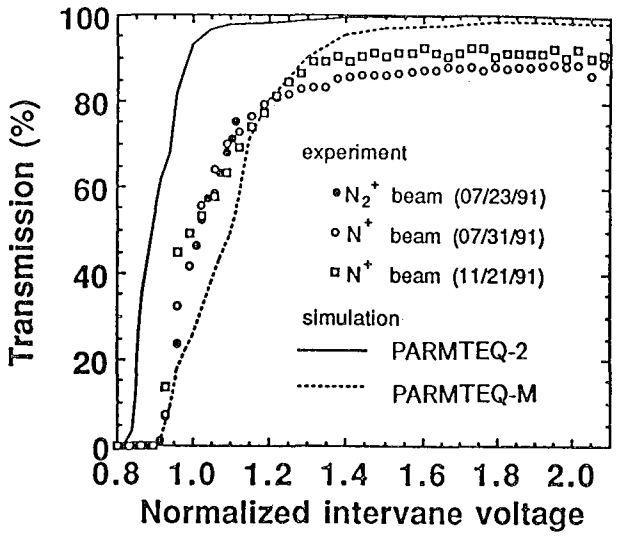

Fig. 12. Transmission efficiencies *vs.* the normalized intervane voltage. Results of experiments and simulations are plotted.

The experiment shows that the A_{10} correction is indispensable to the $\rho_T = r_0$ vane. If $A_{10} < A$, A_{10} should be enhanced by correcting a and m parameters so that the A_{10} after the correction is equal to the A before the correction, and the r_0 value is preserved. This correction is carried out by using MOD12. For the five vane-tip geometries presented by Crandall [11], their performances were compared by running PARMTEQ-H. The results are summarized in Table 2, the run No. 3 ($\rho_T = r_0$, standard modulation) shows that, with the A_{10} correction, we can obtain transmission efficiencies as high as those predicted by PARMTEQ-2. This vane-tip geometry is, however, unacceptable because the minimum longitudinal radius of curvature $\rho_{L,min}$ of the vane tip is too small. At the vane-tip machining by means of the two-dimensional cutting technique with a shaped cutter, $\rho_{L,min}$ must be larger than the cutter radius (= the distance from the axis of rotation to the upper edge of the cutting surface). In our case, the cutter radius is 1.00 cm, which was determined so that the cutter might be strong enough. The $\rho_{L,min}$ before the A_{10} correction is 1.056 cm (Nos. 1 and 2 in Table 2), but after the correction, the radius is no more than 0.66 cm (No. 3). Employing the sinusoidal modulation, we can avoid the $\rho_{L,min}$ problem. Hence the vane-tip geometry of $\rho_T = r_0$, sinusoidal modulation (No. 4) would be the right geometry for the prototype SCRFQ.

[2]Transmission efficiencies provided by PARMTEQ-M are lower than the measured values in the range of $0.9 \leq V_n \leq 1.1$. This would be due to imperfect beam simulation in the radial matching section, as will be discussed later.

[3]Another computer program POT3D [17] yields A_{10}/A ratios nearly same as those by Crandall's CHARGE 3-D; the discrepancy is less than 1%

Table 3

Transmission efficiencies (beam current is 0 or 5 mA, $q/A = 1/30$) and minimum longitudinal radii of curvature $\rho_{L,min}$ for various vane-tip geometries. At PARMTEQ-M, no A_{10} correction is made, and no higher-order multipole is included. At PARMTEQ-H, the correction is made, and all of the Crandall's higher-order multipoles are included.

No.	Program	ρ_T	Modulation	$\rho_{L,min}$	Tr.(0 mA)	Tr.(5 mA)
1	PARMTEQ-2		standard	1.056 cm	92.6%	47.4%
2	PARMTEQ-M	r_0	standard	1.056 cm	25.2%	16.2%
3	PARMTEQ-H	r_0	standard	0.660 cm	92.6%	45.2%
4	PARMTEQ-H	r_0	sinusoidal	1.187 cm	92.6%	47.4%
5	PARMTEQ-H	0.75 r_0	standard	0.572 cm	88.4%	37.8%
6	PARMTEQ-H	0.75 r_0	sinusoidal	1.106 cm	89.6%	40.2%
7	PARMTEQ-H	variable	standard	0.937 cm	92.6%	41.8%

2.4.3. Radial matching section

In the PARMTEQ simulations, we assume that the electric field in the radial matching section (RMS) is derived from the following potential function:

$$U(x,y,z) = \frac{V}{2}\left[1 + \frac{x^2 - y^2}{r_0^2}\right]\frac{z}{L}, \tag{4}$$

where V is the intervane voltage, r_0 the aperture radius at the exit of the RMS (= mean aperture radius), and L the RMS length; at the prototype SCRFQ, r_0 = 0.9458 cm and L = 29.2 cm. Therefore the potential on the beam axis ramps from 0 to $V/2$ in the RMS, or the longitudinal component E_z of the electric field is not zero. Owing to this E_z, the energy and phase modulations that the beam expericences is quite particular: if the input beam is a d.c. beam with the design energy W_{in}, particles move toward $\Delta\phi = \pm\pi$ ($\Delta\phi \equiv$ rf phase ϕ − synchronous phase ϕ_s). Consequently, the beam is bunched, and at the exit of the RMS the particle density is minimum at $\Delta\phi = 0$, and maximum at $\Delta\phi = \pm\pi$. Particles in the peaks around $\Delta\phi = \pm\pi$ will spill from the rf bucket in the bunching process, resulting in a lower transmission efficiency. When the input energy differs slightly from W_{in}, the beam bunching takes place also. The peak position is, however, apart from $\Delta\phi = \pm\pi$, and therefore the particles in the peak will be captured well, leading to a higher transmission efficiency.

The transmission efficiency as a function of the injection energy is shown in Fig. 13, where PARMTEQ-M results and experimental data are plotted [12]. The simulation results are remarkable for holes around $\Delta W_{in}/W_{in} = 0$; the holes are due to the beam bunching in the RMS. The experiment, however, denies apparently the simulation results. This implies that the beam may not be bunched in the RMS, or the actual electric field in the RMS may be different from the potential function of Eq. 4.

In our simulation E_z (here defined as $-\partial U/\partial z$) has a rectangular variation with respect to z. The abruptly ramping E_z causes the beam bunching. According to simulations, the beam bunching is very sensitive to the functional shape of E_z at the RMS entrance; if E_z varies smoothly in the RMS, no beam bunching occurs [18]. It is quite possible that the

actual E_z may not have a step-like shape at the RMS entrance for the following reasons. (1) The vanes are not shaped to the the equipotential surfaces. They will be obtained by equating the right-hand-side of Eq. 4 to 0 or V. The resulting transverse radii of curvature at the vane tips are:

$$\rho_T = r_0 \ (U = 0 \text{ vanes}) , \quad r_0 \left(\frac{2L}{z} - 1\right)^{1/2} \ (U = V \text{ vanes}) . \tag{5}$$

At the actual vanes, however, the vane tips are shaped to a circular arc with $\rho_T = r_0$, in the same manner for the modulated vanes. This shaping would be good for the $U = 0$ vanes, but worse for the $U = V$ vanes. (2) The $U = V$ vanes are truncated at $z = 1.72$ cm, since the equipotential sufaces for these vanes flare out, approaching infinitely the end wall, as shown in Fig. 14. (3) The RMS entrance includes the beam hole. From the above considerations, the actual E_z may vary gently in the RMS entrance, but not ramp on abruptly. For a precise beam simulation, it is necessary to examine the field distribution in the RMS by using a three-dimensional field solver.

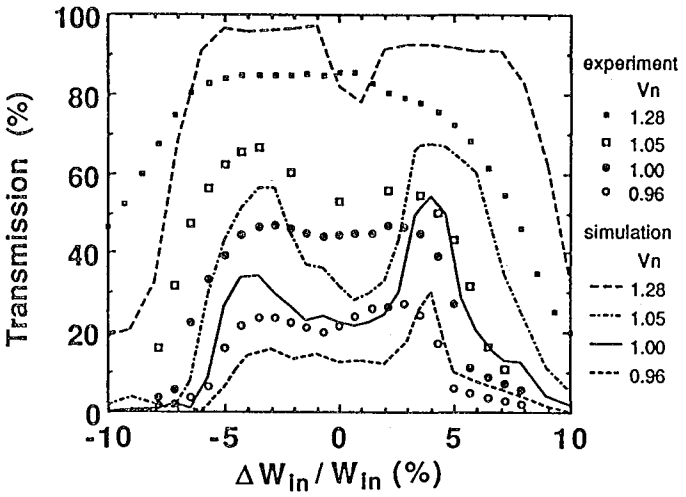

Fig. 13. Transmission efficiency *vs.* injection energy for some values of the normalized intervane voltage V_n. The ions used in the experiments are N_2^+ (V_n = 0.96, 1.00, 1.05) and N^+ (V_n = 1.28).

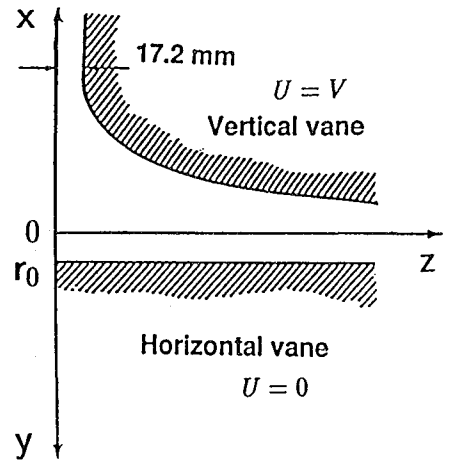

Fig. 14. Longitudinal vane profiles in the radial matching section. At the prototype SCRFQ, r_0 = 0.9458 cm and the section length is 29.2 cm.

3. Long SCRFQ

3.1 Radioactive Beam Facility

A prototype facility for the Exotic-Nuclei Arena (E-Arena) in the Japanese Hadron Project is now under constructione at INS [19]. In the facility, radioactive nuclei will be accelerated by linacs and used for nuclear physics experiments. The primary beam will be a 40-MeV, 10-μA proton beam from the existing sector focusing cyclotron. Radioactive nuclei will be mass-analyzed through an isotope separator on-line (ISOL) with a mass resolution of $\Delta m/m = 1/9000$, and transported to a linac chain, whose layout is shown in Fig. 15 [3 $\sim$ 7].

The front-end linac is a 25.5-MHz, 8.6-m SCRFQ, accelerating ions with $q/A \geq 1/30$ from 2 to 172 keV/u. A carbon-foil stripper is located at the exit of the SCRFQ; through a foil of 10 μg/cm^2 thick or less, the charge-to-mass ratio will be enhanced to $q/A \geq 1/10$. Two doublets of quadrupole magnets will be used for the transverse matching. For the longitudinal matching, a 25.5-MHz rebuncher will be used; a folded $\lambda/4$-resonator with four or six gaps is now being studied. An interdigital-H (IH) linac, consisting of four tanks and three quadrupole-magnet triplets between them, accelerates ions further. The output energy is continuously variable in a range of 172 $\sim$ 1046 keV/u. The variable energy is obtained by adjusting the rf power and phase in the last tank of operating ones.

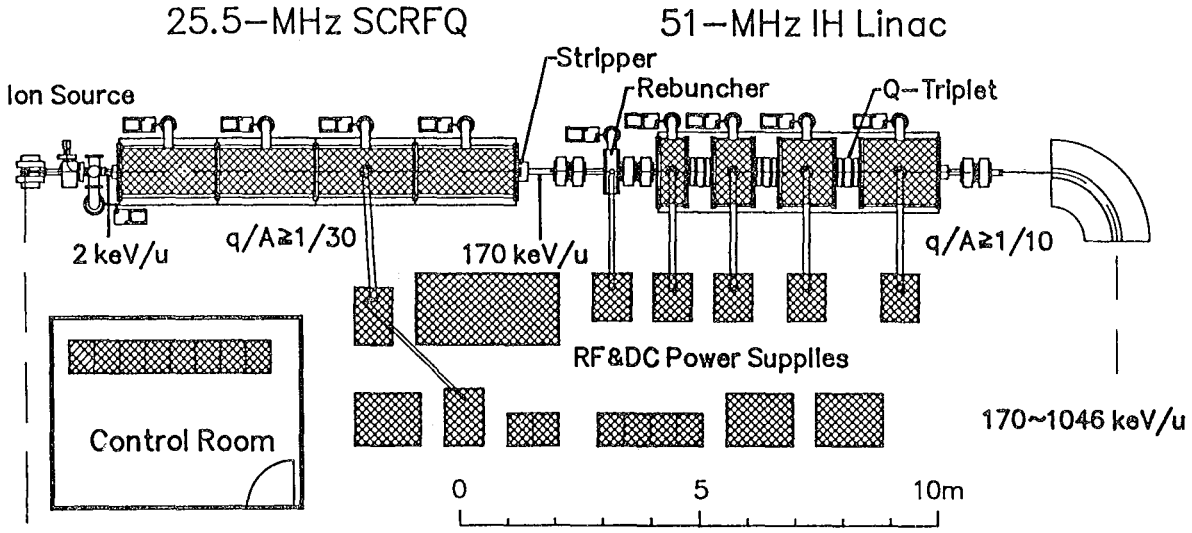

Fig. 15. Layout of the linac chain in the E-Arena Test Facility, now under construction.

Table 3
Main parameters of the long SCRFQ.

Frequency (f)	25.5 MHz	λ = 11.76 m
Charge-to-mass ratio (q/A)	$\geq 1/30$	
Input energy ($T_{\rm in}$)	2 keV/u	β = 0.00206
Output energy ($T_{\rm out}$)	172 keV/u	β = 0.01916
Normalized emittance ($\epsilon_{\rm n}$)	0.06 π cm·mrad	ϵ = 29.1 π cm·mrad (input)
Vane length ($L_{\rm v}$)	858.5 cm	
Number of cells ($N_{\rm c}$)	172	20 cells in radial matcher
Intervane voltage ($V_{\rm vv}$)	108.6 kV	q/A = 1/30 ions
Maximum surface electric field ($E_{\rm s}$)	178.2 kV/cm	2.49 Kilpatrick ($\kappa_{\rm max}$ = 1.615)
Mean bore radius (r_0)	0.9846 cm	
Minimum bore radius ($a_{\rm min}$)	0.5388 cm	
Margin of bore radius ($a_{\rm min}/a_{\rm beam}$)	1.2	zero-current beam
Maximum modulation index ($m_{\rm max}$)	2.53	
Final synchronous phase ($\phi_{\rm f}$)	$-30°$	
Focusing strength (B)	5.5	
Maximum defocusing strength ($\Delta_{\rm b}$)	-0.17	

3.2 Design of the Long SCRFQ

The long SCRFQ is now under construction, to be completed in the spring of 1994. It is an extend version of the prototype: the number of module cavities has been increased to 12, and the overall length is 8.6 m. Main parameters of the long SCRFQ are listed in Table 3. At the construction, the whole cavity is divided into four units (the prototype is a 1-unit cavity). Three of them are newly constructed, and the other one is the prototype with replaced vanes. The units are assembled separately and connected into the whole cavity.

For the new SCRFQ, the following improvements were made. The coupling rings have been removed, since they are harmful to high-power, high-duty operations. The flow rate of the cooling water is to be increased so that the cavity might stand a full-power operation with a duty factor of 30%. The A_{10} correction is applied to the vanes.

The vane-tip geometry is as follows: ρ_T is variable in the low-energy part (up to the center of the 76th cell, 1.1 m down from the RFQ entrance), in the remaining high-energy part, $\rho_T = r_0$ (0.985 cm); the modulation is the standard one at both of the vane-tip geometries. As shown in Fig. 16, the A_{10}/A curves cross at the 76th cell. Therefore, the amount of corrections for a and m are same at this cell, and the two vanes connect smoothly. The vanes in the first unit are machined by using a ball-end mill (three-dimensional cutting), and those in the other units by using a shaped cutter (two-dimensional cutting).

The connection of the two vane-tip geometries may have an advantage that the A_{12} coefficient is minimized. The pseudo-octapole field from the A_{12} term affects the beam performance more than the other higher-oder multipoles do. Without the octapole field, the shape of the beam cross section is nearly circular. The octapole field deforms the beam shape to a square, and as a result, the transmission efficiency will be decreased. We evaluate the strength of the A_{12} multipole by the following ratio:

$$R(r) = \frac{A_{12} I_4'(kr)}{A_{10} I_1(kr)} \ , \qquad (6)$$

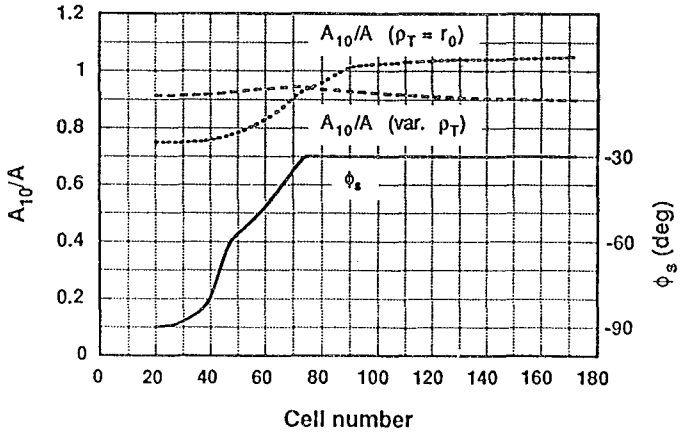

Fig. 16. A_{10}/A ratios for the variable ρ_T vane and the $\rho_T = r_0$ one as functions of the cell number. The synchronous phase ϕ_s is also plotted.

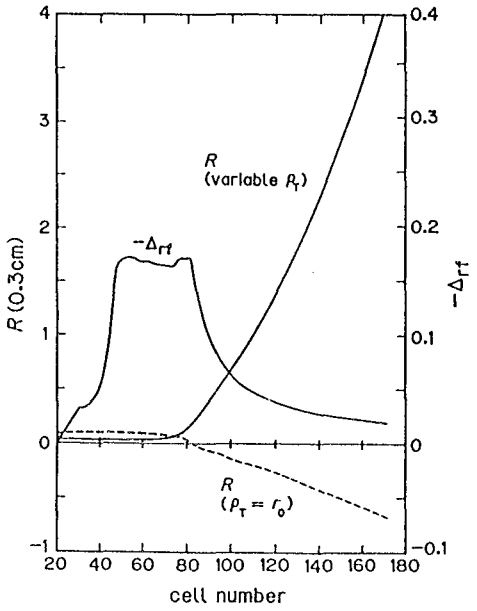

Fig. 17. Ratios $R(r = 0.3$ cm) for the variable ρ_T vane and the $\rho_T = r_0$ one as functions of the cell number. The rf defocusing parameter Δ_{rf} is also plotted.

the numerator and the denominator come from A_{12}- and A_{10}-terms in the E_r derived from the potential function of Eq. 3. The R-ratios at $r = 0.3$ cm for the two vane-tip geometries are plotted in Fig. 17, along with the rf defocusing parameter Δ_{rf}, which is proportional to A_{10}. In terms of smaller A_{12} coefficient, the variable ρ_T vane is better in a low-energy part, and in a high-energy part the $\rho_T = r_0$ vane is better.

Table 4 summarizes transmission efficiencies obtained through PARMTEQ-2 runs and PARMTEQ-H ones for three vane-tip geometries: (1) variable $\rho_T + \rho_T = r_0$ vane (the geometry in our SCRFQ), (2) $\rho_T = r_0$ vane throughout, and (3) variable ρ_T vane throughout. For a zero-current beam, the three vane-tip geometries yield transmission efficiencies almost same as that by PARMTEQ-2. However, as the beam current increases, the difference becomes larger: the variable $\rho_T + \rho_T = r_0$ vane is best, and the variable ρ_T vane is worst. The effect of the A_{12} multipole becomes remarkable at high beam currents, because the beam radius is enlarged by the space charge force, and the A_{12} term in E_r is proportinal to $I_4'(kr)$, approximately $\propto r^3$. It might be overdone to connect together the two vane-tip geometries, because the SCRFQ is for a low-current beam of radioactive nuclei. The vane connection, however, will make sense, considering possible emittance growth brought about by imperfections in the vane alignment or mismatching between the input beam and the RFQ.

Table 4

Transmission efficiencies (beam current is 0, 5, or 10 mA, $q/A = 1/30$) provided by PARMTEQ-2 and those by PARMTEQ-H for various vane-tip geometries with the standard modulation. At PARMTEQ-H, the A_{10} correction is made, and all of the Crandall's higher-order multipoles are included. No beam bunching in the radial matching section is assumed.

No.	Program	Vane-tip geometry	Tr.(0 mA)	Tr.(5 mA)	Tr.(10 mA)
1	PARMTEQ-2		91.4%	87.6%	68.4%
2	PARMTEQ-H	var. $\rho_T + \rho_T = r_0$	91.4%	86.0%	65.2%
3	PARMTEQ-H	$\rho_T = r_0$	90.8%	81.8%	60.2%
4	PARMTEQ-H	variable ρ_T	90.0%	80.0%	55.0%

5. Concluding Remarks

Through the operation of the prototype SCRFQ, we verified that the SCRFQ with the multi-module structure works well and found some items to be improved for better performance. The long SCRFQ is now under construction and will be set up in INS in 1994. The rf power source with an Eimac 4CW150000E tube is ready. Its maximum peak power is 350 kW with a duty factor of 30%. The IH linac and its power sources are being constructed, to be finished in the spring of 1995. The design study on the beam transport lines and model tests on components are in process. The first beam acceleration, probably using a beam of stable nuclei, is scheduled in the fiscal year of 1995.

6. Acknowledgments

The development of the two SCRFQ's has been conducted by S. Arai, A. Imanishi, T. Morimoto, S. Shibuya, T. Takeda, E. Tojyo, and N. Tokuda. I wish to thank J. Staples and S. Yamada for their help in compilation of computer programs and discussion on beam dynamics. In addition, the supports provided by M. Kihara, the Accelerator Research Division, High Energy Physics Division, and Nuclear Physics Division of INS, and by the Grant for Scientific Research of the Ministry Education, Science and Culture are gratefully acknowledged. The computer works were done on FACOM M780 in the INS Computer Room.

6. References

[1] S. Shibuya, "Study of an SCRFQ Linac for Very Slow Heavy-Ion Beams", thesis for Ph.D. (in Japanese), National Laboratory for High Energy Physics, KEK Internal 92-10, 1992.

[2] S. Arai, "Split Coaxial RFQ Structure with Modulated Vanes", Gesellschaft für Schwerionenforschung, GSI-83-11, 1983.

[3] S. Arai *et al.*, "A Heavy-Ion Linac Complex for Unstable Nuclei", IEEE 1993 Particle Accelerator Conference, Washington, D.C., USA, May 1993.

[4] S. Arai *et al.*, "Construction of a Heavy-Ion Linac for Short-Lived Nuclei", 9th Symposium on Accelerator Science and Technology, Tsukuba, Japan, August 1993.

[5] M. Tomizawa *et al.*, "Interdigital-H Linac for Unstable Nuclei at INS", IEEE 1993 Particle Accelerator Conference, Washington, D.C., USA, May 1993.

[6] M. Tomizawa *et al.*, "Development of an Interdigital-H Linac for Unstable Nuclei at INS", 5th Japan-China Joint Symposium on Accelerators for Nuclear Science and Their Applications, Osaka, Japan, October 1993.

[7] K. Niki *et al.*, "Beam Matching Section in the INS Heavy Ion Linac Complex", IEEE 1993 Particle Accelerator Conference, Washington, D.C., USA, May 1993.

[8] N. Tokuda *et al.*, "Structure and RF Characteristics of the INS 25.5-MHz Split Coaxial RFQ", 7th Symposium on Accelerator Science and Technology, Ibaraki, Osaka, Japan, December 1989.

[9] S. Shibuya *et al.*, "RF Tests on the INS 25.5-MHz Split Coaxial RFQ", 1990 Linear Accelerator Conference, Albuquerque, NM, USA, September 1990.

[10] S. Arai *et al.*, "A Split Coaxial RFQ for an ISOL Post-Accelerator", 4th China-Japan Joint Symposium on Accelerators for Nuclear Science and Their Applications, Beijin, China, October 1990.

[11] K.R. Crandall, "Effects of Vane-Tip Geometry on the Electric Fields in Radio-Frequency Quadrupole Linacs", Los Alamos National Laboratory, USA, LA-9695-MS, 1983.

[12] N. Tokuda *et al.*, "Performance Characteristics of the INS 25.5-MHz Split Coaxial RFQ", 3rd European Particle Accelerator Conference, Berlin, Germany, March 1992.

[13] S. Arai *et al.*, "Acceleration Tests of the INS 25.5-MHz Split Coaxial RFQ", IEEE 1991 Particle Accelerator Conference, San Francisco, CA, USA, May 1991.

[14] N. Tokuda *et al.*, "Acceleration Performance of the INS 25.5-MHz Split Coaxial RFQ", 8th Symposium on Accelerator Science and Technology, Wako, Saitama, Japan, November 1991.

[15] K.R. Crandall *et al.*, "RF Quadrupole Beam Dynamics Design Studies", 1979 Linear Accelerator Conference, Montauk, NY, USA, September 1979.

[16] J. Staples, private communication, May 1989.

[17] S. Yamada, "3D Electric Field Caculation with Surface Charge Method", 8th Symposium on Accelerator Science and Technology, Wako, Saitama, Japan, November 1991.

[18] J. Staples, private communication, September 1993.

[19] I. Katayama *et al.*, "Radioactive Ion Beam Facility at INS", 3rd International Conference on Radioactive Nuclear Beams, East Lansing, MI, USA, May 1993.

Reducing RFQ Output Emittance by External Bunching*

John Staples
Lawrence Berkeley Laboratory
One Cyclotron Road
Berkeley, California 94720

Abstract

RFQ accelerators normally incorporate adiabatic bunchers in the accelerator proper. This produces high accelerator acceptance but less-than-optimum longitudinal emittance as a result of severe filamentation of the longitudinal phase space. The use of discrete bunchers both internal and external to the RFQ, along with new approaches in accelerator-only (no adiabatic buncher) RFQ beam dynamics designs produces significantly lower longitudinal output emittance with high acceptance.

Adiabatic Bunching within the RFQ

RFQ accelerators have offered the designer considerable flexibility in beam dynamics design. This unique accelerator type incorporates strong focusing as the primary mechanism, with longitudinal accelerating fields introduced as a perturbation of the structure. This freedom to vary $E_z(z)$ arbitrarily has resulted in several design approaches, all of which incorporate some sort of adiabatic bunching within the RFQ itself.

Several advantages follow: discrete bunchers are eliminated from the LEBT. Adiabatic bunching allows nearly 100% of the beam to be accepted into the r.f. bucket. Adiabatic bunching copes well with space charge forces, which help control the bunching process itself to control the rate of bunch formation.

However, the quasi-adiabatic bunching process is highly nonlinear, resulting in a filamented longitudinal phase space with a relatively large area. The phase space resulting from a more precisely adiabatic bunching process would require an unrealistically long RFQ to accommodate the several phase oscillations needed.

In high-mass, low-current RFQs, a different beam dynamics prescription may be used[1]. Space charge is no longer significant, and the bunching process can be carried on more rapidly, with some attention given to preventing too rapid a bunch collapse. The separatrix area is kept approximately constant in the buncher sections, and grows in the accelerator section so the phase oscillations become more linear. The rapid bunching results in a shorter accelerator but still with a relatively high longitudinal emittance.

The RFQ buncher sections usually dominate the length of the accelerator. Usually significantly less than half the length of an RFQ is devoted to accelerating the beam at full longitudinal gradient. In addition, the introduction of an unbunched beam to the RFQ entrance requires an adiabatic transverse matching section that transforms the time-independent envelope to a time-varying envelope matching the strong r.f. quadrupole focusing inside the RFQ structure.

* This work was supported by the U.S. Department of Energy under contract number DE-AC03-76SF00098.

Discrete Bunchers

Discrete bunchers may be applied to RFQs as they have been to other linear accelerators such as d.c. preinjector - DTL combinations. Fundamental frequency bunchers may be incorporated in the LEBT or the RFQ itself: harmonic bunchers will be restricted to the LEBT. Several types of buncher configurations are described in a comprehensive treatise by Blasche and Friehmelt[2]. We will consider three of these below.

SCR Non-zero Axial Potential Problem

One structure type appropriate for very low velocity, high mass ions is the split coaxial resonator (SCR), a heavily loaded cavity that operates efficiently in the 25–50 MHz region[3]. The SCR uses RFQ-like vanes, allowing the same flexibility in tailoring $E_z(z)$ as in conventional RFQs. However, the potential on the axis of the SCR rises from zero to $V/2$ in the space between the endwall and the vanes, where V is the intervane potential. The beam entering the accelerator must climb this time-varying potential hill without being accelerated or bunched. One scheme is to treat the entrance gap as a long accelerating gap with a negligible transit time factor for particles of all phases. One potential function in the entrance gap region is $V(z)=3a^2-2a^3$, where $a=z/L_{matcher}$ and $L_{matcher}$ is approximately 20 $\beta\lambda$ long. This is accomplished by arranging the grounded vanes to have constant displacement from the axis, and the hot vanes to have a long and gentle departure from the axis as they approach the entrance endwall.

RFQ Accelerator Beam Dynamics Choices

Four design algorithms for the design of a low-β accelerator-only RFQ have been investigated. No adiabatic bunching was used, although a radial matcher was employed in all cases to allow a round beam to be introduced into the RFQ.

The four algorithms differ by requiring two different parameters to be kept constant from cell to cell. For a given set of initial conditions, (frequency, input and output velocity, surface field, q/A and stable phase), the specification of two more parameters fixes all the cell parameters. The four design algorithms are:

(1). Constant $E_{acc}/E_{surface}$ and B in each cell. This results in the lowest required intervane voltage and power dissipation, and allows a moderate growth of the height (energy) of the bucket toward the high-

energy end.

(2). Constant Δ_{gap} and B in each cell. This requires a higher intervane voltage than (1), but has a higher transverse acceptance. The separatrix height grows more slowly, and slightly higher values of m are found at the exit. The accelerator is slightly longer than in (1).

(3). "Conventional" accelerating section, the same as the usual prescription used in GENRFQ for the acceleration section, with B, A_{init} and A_{final} specified. At reasonable values of the focusing parameter B the accelerator is substantially longer than in (1), and the separatrix height grows more than is necessary, throwing away needed acceleration rate. This algorithm works well when started at a higher energy, but not at very low β_{init}.

(4). Constant $E_{acc}/E_{surface}$ and m in each cell. Very heavy tilts of V, a and B occur along the structure. This is not seen as a practical design algorithm and will not be investigated further.

Algorithms 1–3 were tested, optimizing the selected parameters until the best design for that algorithm was found. The best design was defined as an accelerator with the modulation parameter m not significantly more than 2 so the vanetip geometry could be easily implemented; a length less than 3 meters; the lowest longitudinal emittance and the highest particle transmission. The common parameters for all cases were:

Freq	70	MHz
T_{in}	2.5	keV/n
T_{out}	100	keV/n
$E_{surface}$	22	MV/m
ϕ_s	-30	degrees
Input $\Delta\phi$	±30	degrees
Input ΔT	±4	%

The additional parameters for each specific case were:

Case (1): $E_{acc}/E_{surface} = 0.04$, $B = 4$

Case (2): $\Delta_{gap} = -0.065$, $B = 2.5$

Case (3): $B = 3.5$, $A_i = 0.1$, $A_f = 0.6$

The results of PARMTEQ simulations of these best accelerators in each class gave the following results:

Case	V_v (kV)	Length (cm)	m_{max}	Transm %	ε_l (MeV-°)
1	56.2	258	2.12	100	0.104
2	89.9	276	2.24	84	0.084
3	64.2	271	2.06	35	poor

Case (1), with constant $E_{acc}/E_{surface}$ and B is the clear winner. It is the shortest, uses the lowest vane voltage, and has the highest transmission, and the output emittance is satisfactory. We will use this accelerator to test various buncher configurations upon.

Choice of Buncher Configuration

Kick bunchers can be placed in the LEBT or in the RFQ itself. As $E_z(z)$ can be arbitrarily varied in the RFQ, h=1 bunchers can be realized, interposed by drifts in the structure itself. As the r.f. defocusing forces are significant at the low injection velocity, the strong focusing inherent in the RFQ which keep the beam size down may be preferable to bunchers in an external LEBT.

Four buncher configurations were considered:

(A) Single fundamental buncher. This is the easiest, and serves as a basis of comparison for more elaborate configurations.

(B) Single fundamental buncher in or near the RFQ, with a second harmonic buncher upstream in the LEBT.

(C) A fundamental and a second harmonic buncher at the same location in the LEBT.

(D) A sequence of three fundamental bunchers. These may be located in the LEBT or the RFQ itself.

Figures 1 through 4 show the longitudinal phase space for each of these buncher configurations, optimized to place as much of the beam as possible to within a ±50% phase spread, which matches accurately the actual phase acceptance of the test RFQ. A new beam generator was written for PARMTEQ which includes up to 10 spaced bunchers operating at arbitrary voltages and harmonics. The RFQ case (1), the constant $E_{acc}/E_{surface}$ and B case, was used to test each of these buncher combinations.

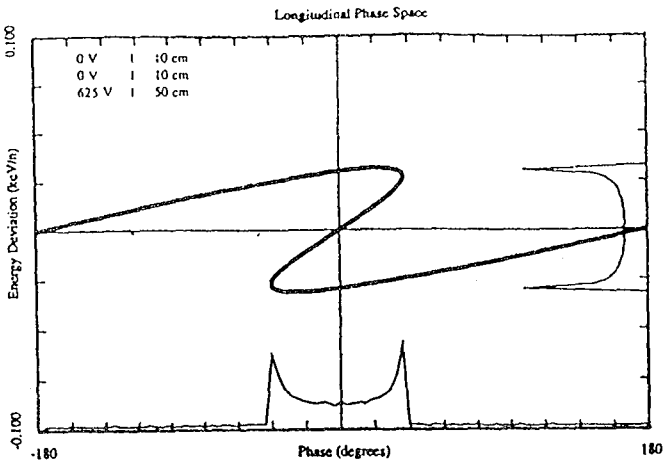

Figure 1. Single Fundamental Buncher

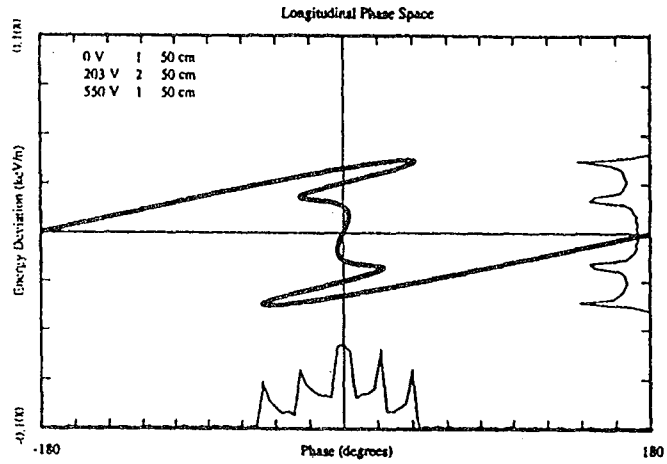

Figure 2. h=2 followed by h=1 Buncher

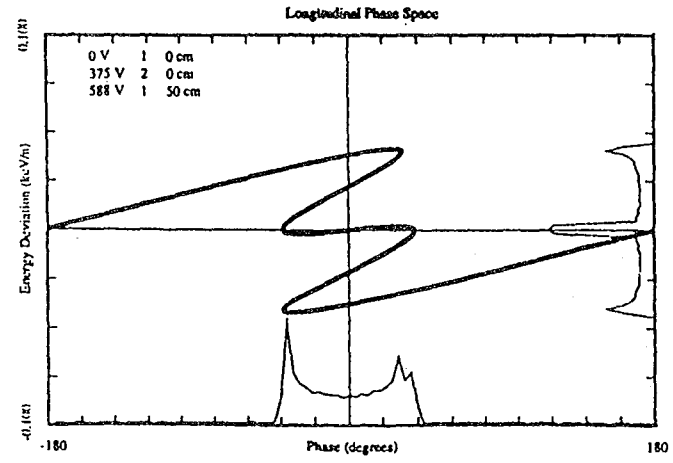

Figure 3. Coincident h=1 and h=2 Bunchers

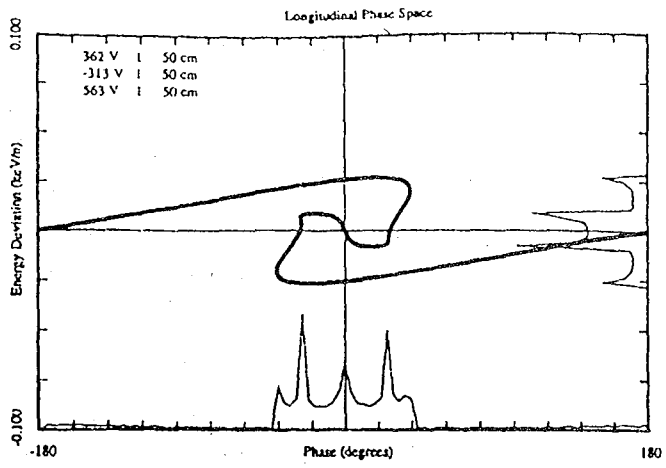

Figure 4. Three consecutive h=1 Bunchers

Results of Simulation Runs

In addition to the four buncher configurations described above, two other classes of tests were added which include: (2) accelerating-only RFQ with an ideally bunched beam and (3) a conventional RFQ with adiabatic buncher. The parameters of each run are:

(1). Beams produced with above-described bunchers, corresponding to cases (A) through (D).

(2). Ideal bunched beam into accelerating RFQ. The two subcases are (A): $\Delta\phi = \pm 30°$ and $\Delta T = \pm 4\%$. (B): zero initial phase space with $\Delta\phi = \Delta T = 0$. These give the lower limit of longitudinal emittance possible with perfect bunching.

(3). Conventional RFQ with adiabatic buncher with two values of surface field: (A) 18 and (B) 22 MV/m, corresponding to 1.8 and 2.2 Kilpatrick. This machine was designed using the design scheme of Yamada[1]. Machines (3A) and (3B) have length of 320 and 210 cm, and intervane voltages of 50 and 75 kV, respectively. (The accelerate-only RFQ in classes (1) and (2) is 258 cm long with a 56 kV intervane voltage.)

In all cases, the initial normalized beam transverse emittance is 0.01π cm-mrad, at the 100% contour of a water-bag distribution, matched into the RFQ transverse phase space.

In each case, the buncher voltages and drift distances to the RFQ were adjusted to give the best match of the longitudinal axis ratio, that is, the best fit of the bucket shape. The most significant differences were in the beam survival fraction and the longitudinal output emittance. In all cases, the transverse emittance of the input beam was not increased appreciably.

The following table summarizes the survival and the contour that contains 95% of the longitudinal output emittance for all the methods of longitudinal beam preparation,

and for two traditional RFQs with adiabatic bunching incorporated in the structure.

Case	% Survival	e_l (MeV-deg)
1A	74	0.289
1B	89	0.202
1C	85	0.230
1D	85	0.180
2A	100	0.104
2B	100	0.025
3A	85	0.466
3B	87	0.447

As can be seen, for the accelerator-only RFQ, all but the simple h=1 buncher (1A) gives acceptable acceptance. The idealized case (2B) with no initial energy or phase spread indicates the lower limit of longitudinal output emittance, 0.025 MeV-degree. The two cases illustrating a conventional RFQ design with integrated adiabatic bunching, (3A) and (3B) show a longitudinal emittance more than twice that of the RFQ with external bunching.

Figures 5 and 6 show the input and output phase space for a representative accelerate-only RFQ, case (1B). Figures 7 and 8 show the output phase space for cases (3A) and (3B), the conventional RFQ, for comparison. The graph scales are ±30° and ±0.05 MeV, or ±2.5 keV/n.

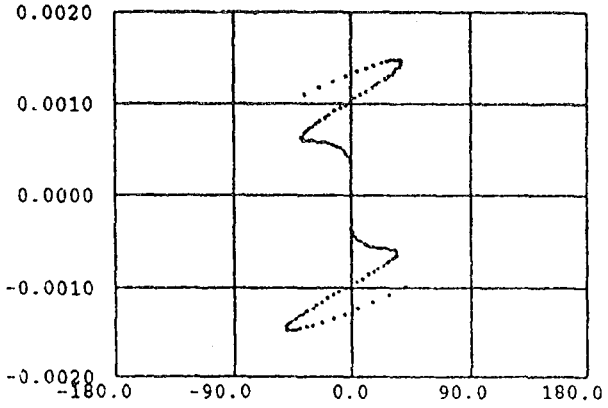

Figure 5. Case (1B) Input Phase Space

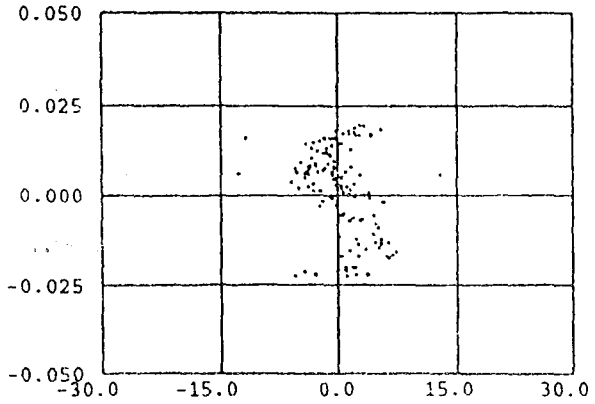

Figure 6. Case (1B) Output Phase Space

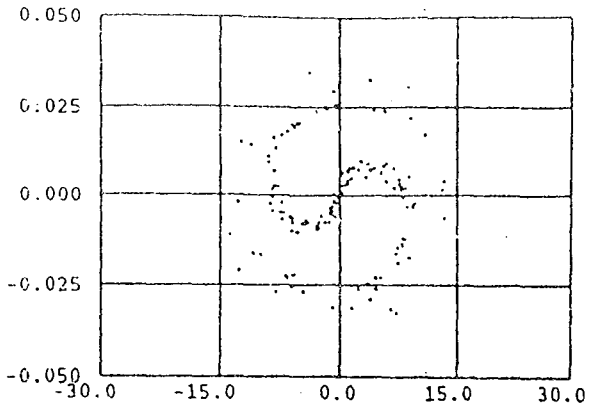

Figure 7. Case (3A) Output Phase Space

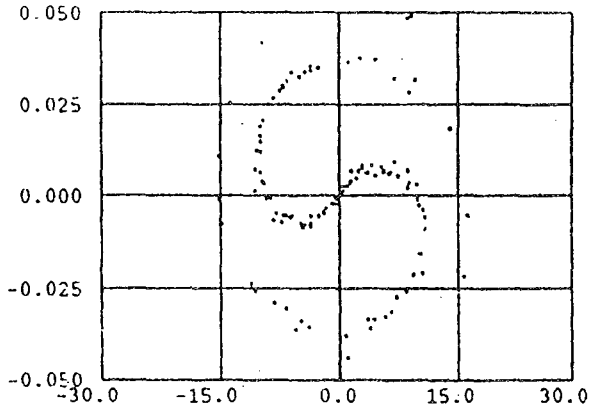

Figure 8. Case (3B) Output Phase Space

Discussion

The longitudinal output emittance of an RFQ can be improved by replacing the adiabatic buncher with external discrete bunchers. The transmission of the RFQ is equal to that of a conventional RFQ with adiabatic bunching, and the RFQ length is reduced.

However, this does not come for free. The stability requirement of the preinjector voltage increases by about an order of magnitude, and the r.f. defocusing of the beam in the discrete buncher may be significant and may require either gridded cavities or small beam size in the bunchers.

The preinjector voltage stability required is

$$\frac{\Delta V}{V} = \frac{\Delta\phi}{\pi}\frac{\beta\lambda}{hL_{drift}}.$$

For a ±5° tolerance and a buncher-RFQ spacing of 25 wavelengths, the preinjector voltage regulation is about $\pm 0.1\%/h$, where h is the harmonic number.

The r.f. defocusing in the buncher cavity causes an angular deflection $\Delta\theta$ given to a particle a distance r from the axis of

$$\Delta\theta = \frac{\pi}{2}\frac{V_{cav}}{V_{prainj}}\frac{r}{\beta\lambda}\cos\phi$$

or, for the case of a q/A=1/20 beam with a 50 kV preaccelerator potential and a 1 kV peak buncher voltage, $\Delta\theta = 30$ r mrad, r in cm, which is significant for a 4π cm-mrad beam

focused to a 0.5 cm spot radius in the buncher. Grids may be required.

If the beam is tightly bunched as it enters the SCR RFQ structure, the effect of the residual bunching while entering the non-zero axial field zone will become less important, and the longitudinal matcher section may be simplified. In addition, the conventional radial matcher may not be necessary.

References

[1]. S. Yamada, *Buncher Section Optimization of Heavy Ion RFQ Linacs,* Proceedings of the 1981 Linear Accelerator Conference, Santa Fe

[2]. K. Blasche and R. Friehmelt, UNILAC Bericht Nr. 1-69, IAP Heidelberg, 1969

[3]. N. Tokuda et al., *Performance Characteristics of the INS 25.5-MHz Split Coaxial RFQ,* Third European Accelerator Conference, Berlin, March 1992

Status of the ISAC Post-Accelerator Design Study

H.R. Schneider, P. Bricault, L. Root
TRIUMF, 4004 Wesbrook Mall
Vancouver, B.C.

Abstract:
Preparation of a proposal for the installation of a radioactive beam ISOL facility (ISAC) with a post-accelerator is in progress at TRIUMF. The accelerator specifications call for acceleration of ions with charge to mass ratios greater than 1/60, to energies up to 1.5 MeV/u, in one beamline, and up to 10 MeV/u in a second beamline. The current accelerator concept is a three stage linac with strippers to increase the ion q/A, between stages. The first stage is a RFQ, while the second and third stages are a series of independently driven superconducting quarter-wave resonators, similar to those used for the ATLAS accelerator at ANL, and the post tandem booster at JAERI. Preliminary results of beam dynamics calculations for this accelerator configuration are given.

1. Introduction:

A radioactive beam ISOL facility with a post accelerator was first proposed at TRIUMF in 1985[1]. The specifications dictated primarily by the astrophysics interests, required a maximum energy of only 1 MeV/u for ion beams with $A \leq 60$. Although the project was not funded at that time, some accelerator studies were continued, in particular to investigate suitability of superconducting accelerator structures for acceleration of the very low charge to mass ratio particles in this application[2]. Now a new proposal is being prepared for submission to our funding agency in early 1994. In support of this new proposal we are in the process of carrying out some post-accelerator design studies, and present here an interim report on the status of our investigations. The results presented are preliminary, and subject to change as the study proceeds. The beam specifications for the present proposal, differing in some respects from those of 1985, and are summarized in Table 1.

Table 1
ISAC Post - Accelerator Basic Specifications

Input Beam:	
Energy	60 keV
Ion Mass	$A \leq 60$
Ion Charge	1^+, or 1^-
Beam Current	< 1 μA dc
Beam Emittance (normalized)	1 π mm mr
Accelerated Beam:	
Output Energy: (beamline 1)	.2 MeV/u ≤ E ≤ 1.5 MeV/u
(beamline 2)	~1.5 MeV/u ≤ E ≤ 10 MeV/u
ΔE/E	10^{-3}
Duty Factor	100 %

The main changes from the earlier proposal is the inclusion of two beamlines and an order of magnitude increase in the maximum output energy specification. To account for a worst case beam emittance (from an ECR source), the input beam emittance specification here is double our 1985 value.

To give some historical perspective, a block diagram of the post - accelerator proposed in 1985, is shown in Fig. 1. It consisted of a 9 metre long RFQ to capture, bunch and accelerate the 60 keV singly charged ISOL beam to 60 keV/u. This is followed by a stripper to increase the ion q/A to ≥ 1/20, before further acceleration in eight short tanks of an inter-digital drift-tube linac, similar to those used for the RILAC heavy ion linac[3], but without the variable frequency capability. As a consequence of the low ion velocities and low q/A, a low operating frequency especially for the RFQ is dictated. In this case 23 MHz was chosen as the operating frequency for both the RFQ and DTL. To preserve as many particles as possible of a desired ion species produced in the ISOL, cw rather than pulsed operation was specified. This then leads to a major drawback of this accelerator concept, namely the large cw rf power requirement for the DTL, which for even the modest output energy of 1 MeV/u, was estimated to be about 1 MW. Overall length of the accelerator was 24 metres, with an additional 9 metre drift required for debunching to reduce energy spread.

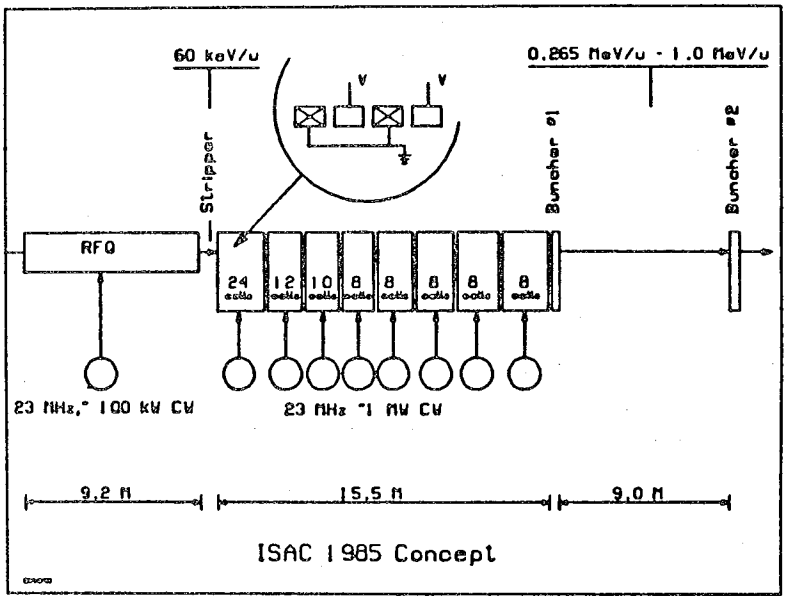

Fig. 1

2. Current Concept:

2.1 General Description

In the mid 1980's Shepard et al at ANL reported on development work of low frequency, low β superconducting accelerator structures, for a proposed positive ion injector for the ATLAS accelerator[4]. Subsequent studies at TRIUMF showed that the ATLAS linac concept, which was developed for ion beams with a charge to mass ratios greater than ~ .08, could be extended to a linear accelerator capable of accelerating ions with even lower charge to mass ratios, as required for ISAC. In our latest conceptual design therefore we base the first section of post RFQ accelerator on the ATLAS structures illustrated in Fig. 2. These are basically quarter wave resonators, capacitvely loaded with a bifurcated drift-tube and counter drift-tube forming four accelerating gaps. The structure, made of niobium and niobium clad copper, is cooled with pool boiling liquid helium in the centre conductor. Three models for mean particle velocities of $\beta = .009$, .016, and .025 were developed at ANL for operation at 48.5 MHz. A fourth model, for $\beta = .037$, was designed to operate at 72.75 MHz. For the ISAC conceptual design, nominal operating frequencies of 50 MHz and 75 MHz have been chosen for acceleration from 60 keV/u to 1.5 MeV/u, ($0.011 \leq \beta \leq 0.057$). For acceleration to higher energies we base our conceptual design on the JAERI superconducting post tandem accelerator structure[5], illustrated in Fig. 3.

This is also a capacitively loaded quarter wave resonator, but with only two accelerating gaps. Its operating frequency is 129.8 MHz, and is designed for a particle velocity, $\beta = 0.1$. For ISAC the nominal operating frequency would be 125 MHz with a design particle velocity range, $.057 \leq \beta \leq .146$, corresponding to the energy range 1.5 MeV/u to 10 MeV/u.

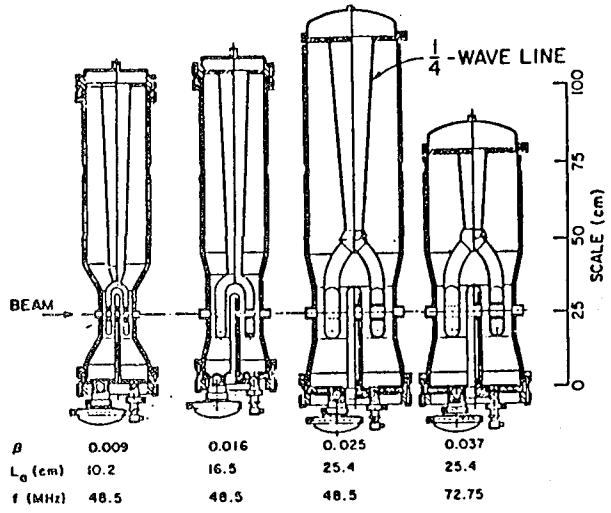

Fig. 2 Cross sections of the 4 gap superconducting resonators for the ATLAS injector linac.

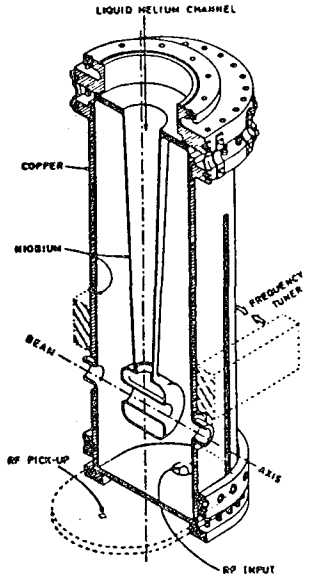

Fig. 3 Two gap superconducting quarter-wave resonator used for the JAERI post-tandem booster.

Fig. 4 is a block diagram of the current (October 1993) concept of ISAC post accelerator, incorporating the superconducting structures discussed above. It is a three stage accelerator with strippers between stages to increase the ion q/A. The first stage is a RFQ to capture, bunch, and accelerate the singly charged dc beam from the ISOL to 60 keV/u. Because the beam delivered from the ISOL is at a fixed energy of 60 keV irrespective of ion mass, the RFQ is mounted on a high voltage deck and operated with a dc bias so the RFQ input energy is at the design 1 keV/u. The second stage accelerates ions with $q/A \geq 1/20$ to 1.5 MeV/u, where the beam is either deflected to a nuclear astrophysics experimental area, or passed through a second stripper before being accelerated to 10 MeV/u in stage 3.

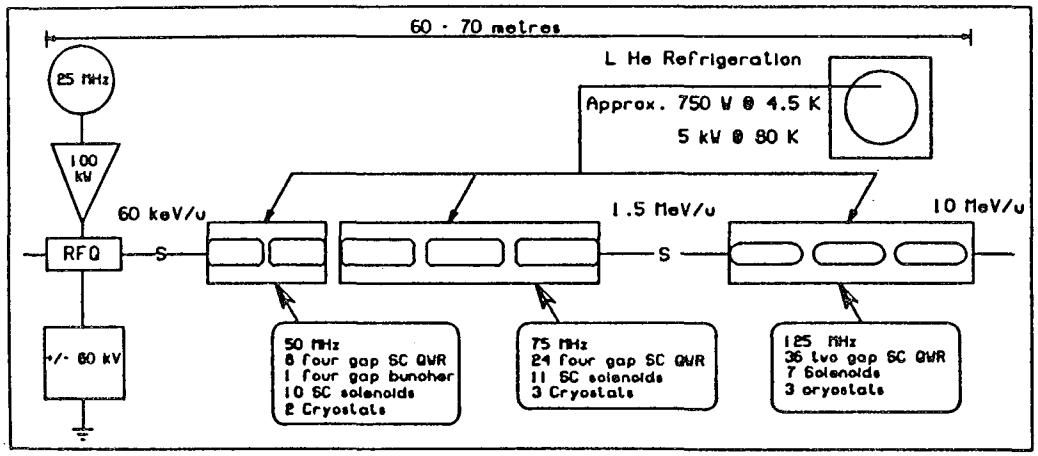

Fig. 4 The ISAC post accelerator concept, October 1993

Based on experience at the ANL ATLAS accelerator and the JAERI booster, the static heat load at 4.5 K would be about 250 watts for both superconducting stages. With rf drive on dissipation in each resonator is about 4 watts, adding another 270 watts to the load. Allowing about 230 watts reserve capacity means that a refrigerator providing at least 750 watts of refrigeration at 4.5 K would be required.

2.2 RFQ

Design parameters for the RFQ in our current conceptual design were determined with the aid of the Los Alamos codes RFQUIK, and PARMTEQ. A relatively high vane voltage must be used to achieve adequate transverse focusing and an acceptance compatible with the specified input beam emittance. We use a design value for the maximum vane surface field of 18 MV/m, about 1.8 times the Kilpatrick sparking criterion corresponding to a 1 cm gap, as given in the plot in Fig. 5 [6]. Table 2 summarizes the RFQ parameters.

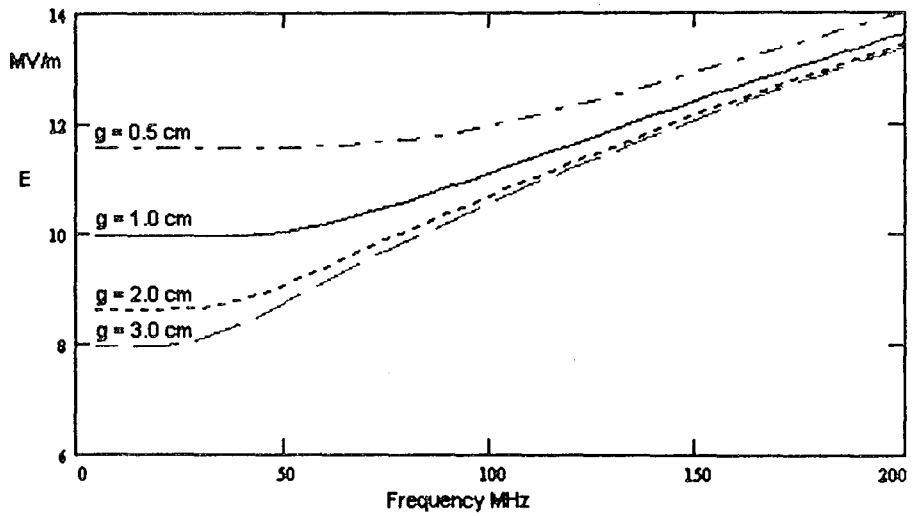

Fig. 5 Kilpatrick sparking limit for various gap sizes.

Table 2
RFQ Parameters

Ion q/A	≥ 1/60
Input Energy	1 keV/u
Output Energy	60 keV/u
Operating Frequency	25 MHz
Vane Voltage	96 kV
E_s	18 MV/m (1.8 x E_{Kil})
RF Power	~ 100 kW
Beam Aperture (min)	0.5 cm (radius)
Ave. Aperture (r_0)	.75 cm
Focusing Parameter (B)	4.72
Synchronous Phase	- 90° (initial) - 30° (final)
No. Cells	289
Length	6.92 m

Phase space plots of the RFQ output beam as calculated with PARMTEQ for an input beam emittance of 0.5 π mm mrad are shown in Fig. 6. The calculated transmission is 97%. No attempt was made in this design to minimize the energy spread of the output beam which is in this case about ± 2%.

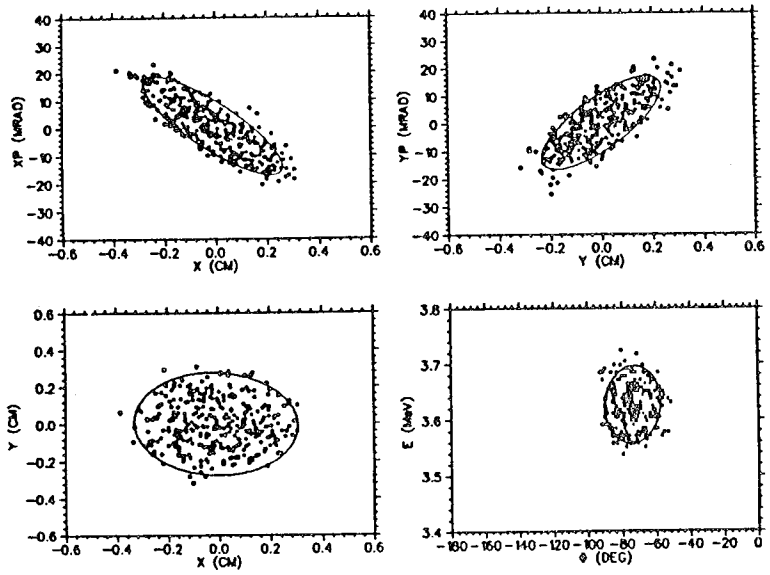

Fig. 6 Phase space and beam size scatter plots for beam at output of the RFQ

2.3 First Stripper and Matching Section

Following the RFQ the beam is passed through a stripper before further acceleration. At the relatively low RFQ output energy, the required stripper thickness to reach an equilibrium charge state distribution is between 0.1 μg/cm² and 0.5 μg/cm². This is about an order of magnitude thinner than can be realized with a foil, so a gas stripper is necessary here. The stripper is accommodated in a 1 metre a space provided in the matching section between the RFQ and DTL as illustrated in Fig.7. Because of the energy spread and low energy of the RFQ beam, debunching distances are short. Therefore, to maintain the bunch structure, provide space for the stripper, and match the beam to the DTL, a rather complex beam transport line including four quadrupole triplets and two rebunchers, is required. Even so this matching section does not meet all of the design objectives, in particular, the 1 π mm mrad transverse acceptance. In this case the matching section will accommodate a beam with half that emittance. Phase space plots of the beam at the stripper and DTL entrance are shown in Fig. 8. There are two stripper options, a gas canal or a gas jet. With the assumed beam emittance at the RFQ input the beam transverse dimension at the stripper location would require rather large aperture gas canal and probably impractical differential pumping requirements. For this reason then, a gas jet is envisioned as the first stripper in the present conceptual design.

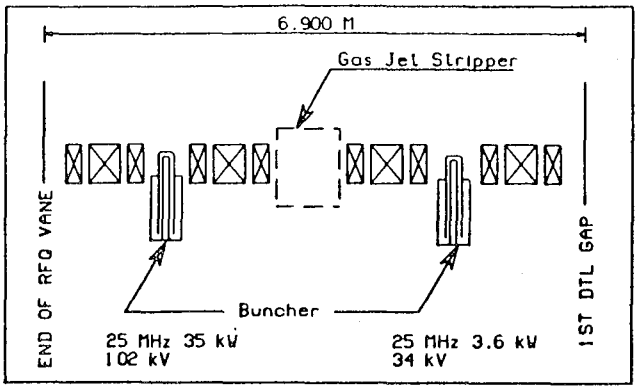

Fig. 7 ISAC RFQ - DTL beam matching section

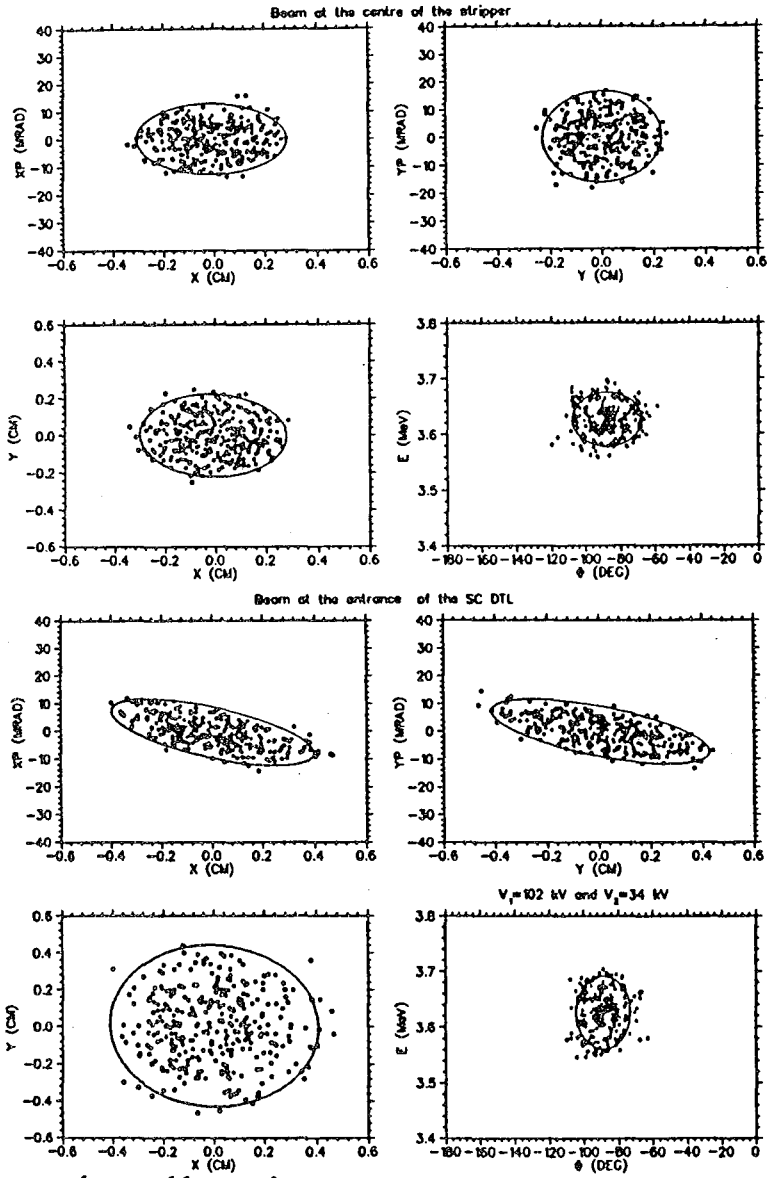

Fig. 8 Phase space plots and beam size scatter plots for beam at stripper and at DTL entrance.

2.4 Superconducting Drift Tube Linac

2.4.1 Elementary Design Considerations

The basic configuration of the superconducting drift tube linac is a series of accelerating gaps separated periodically by superconducting solenoids for transverse focusing of the beam. To gain some insight into the required focal strength and focusing periodicity, two simple calculations were carried out assuming, for the longitudinal motion, an impulse approximation for the energy gain in a multigap module with a drift space between modules, and for the transverse motion, a thin lens approximation for rf defocusing in the multigap modules together with a drift space and solenoid focusing.

For longitudinal motion studies the impulse approximation was applied to a linac consisting of eight independently phased 4 gap accelerator modules operating at 50 MHz, with an accelerating gradient of 5 MV/m, and a synchronous phase of -30°. Such a linac could accelerate ions with q/A = 1/20 from 60 keV/u to 380 keV/u. To determine the longitudinal acceptance of this linac we flood the input with a large longitudinal emittance beam and plot in E - ϕ space the coordinates of the particles successfully accelerated. Three plots are shown in Fig. 9, for cases in which the inter-module drift distances are 20 cm, 50 cm, and 80 cm. An attempt has been made in each of the cases to fit an ellipse that approximates the RFQ longitudinal emittance into the acceptance region. As can be seen this becomes increasingly difficult as the inter-module distances are increased, and it appears that we should avoid drift distances greater than about 50 cm. Since we require a space of about 10 cm between the accelerator module and solenoid, this means that the maximum solenoid length at this energy should be no greater than 30 cm.

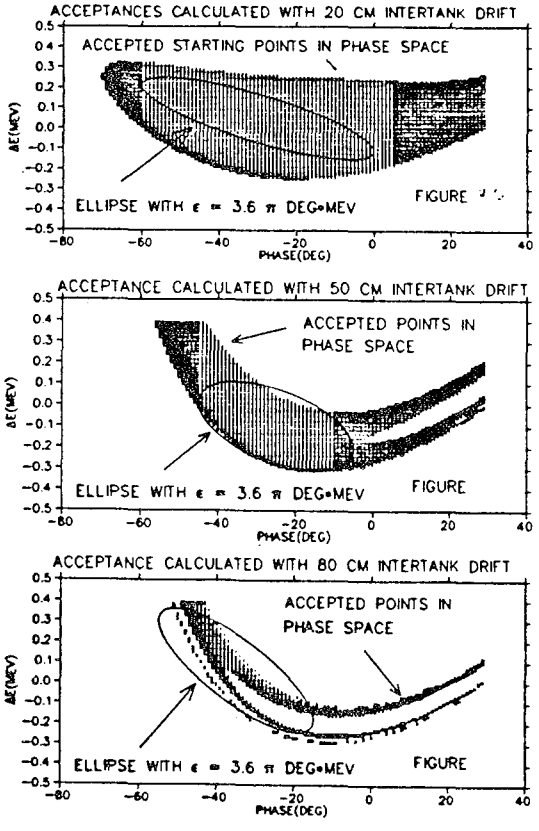

Fig. 9 Longitudinal acceptances in 50 MHz DTL for three inter-module spacings.

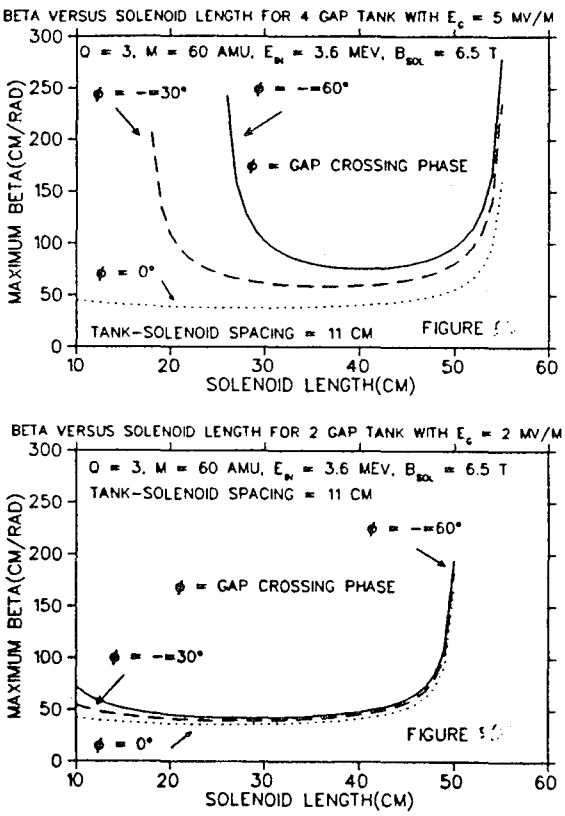

Fig. 10 β_{max} as a function of solenoid length for a 4 gap, 5 MV/m, and a 2 gap, 2 MV/m, DTL configuration

For the transverse motion investigation we assume a magnetic induction of 6.5 T in the solenoid, and calculate, as a function of solenoid length, the maximum beta function (the beam envelope is given by $\sqrt{(\beta \cdot \varepsilon)}$) for a periodic structure in which one cell consists of an accelerator module, a drift space, and a solenoid. The high transverse acceptance objective, along with the limitation on solenoid length noted above, places a constraint on the choice of accelerating gradient. In general, as the accelerating gradient is decreased, the transverse acceptance increases, and the length of solenoid required to produce adequate focusing decreases. Beta function calculations were done for two cases, one assuming an accelerating gradient of 5 MV/m in a 4 gap accelerator module, and the second assuming a gradient of 2 MV/m in a 2 gap module. The results for three gap crossing phases, are plotted in Fig. 10 as a function of solenoid length, (assuming a drift distance of 11 cm between accelerator module and the solenoid). It is apparent from these plots that for 5 MV/m accelerating gradient, 40 cm solenoids, or inter-module drift spaces of 62 cm, $(40 + 2 \cdot 11)$ would be necessary to minimize beta. With a 2 MV/m accelerating gradient, on the other hand, a 20 cm solenoid (42 cm drift space) is adequate. The beta functions in the low gradient case are smaller, and have much less phase dependence.

Although these results have been obtained for the 50 MHz section of the ISAC accelerator, the conclusions are generally true for the higher energy sections as well. At all stages we must be careful not to use too high an accelerating gradient, if large transverse and longitudinal acceptances are to be realized.

2.4.2 Design Description

As illustrated in Fig. 4, the superconducting DTL following the RFQ is divided into three sections with operating frequencies of 50 MHz, 75 MHz, and 125 MHz respectively. In view of the discussion above, the first section begins with short 2 gap quarter wave resonators (QWR) with a relatively low accelerating gradient of 2 MV/m initially, but rising to 5 MV/m at the sixth 2 gap QWR. A second part of the 50 MHz section employs seven 4 gap QWRs and accelerating gradients ranging from 3 to 5 MV/m, to accelerate the beam to 405 keV/u. At this point a structure frequency change is made and the beam is then accelerated in the second DTL section, to 1.5 MeV/u in twenty four 4 gap QWRs Solenoid focusing is used between each QWR. The main parameters of the first and second DTL sections are summarized in Table 3.

Table 3
ISAC Post Accelerator

DTL Sections 1 & 2: Ion q/A ≥3/60

	Section 1 A	Section 1 B	Section 2
Structure	2 gap QWR	4 gap QWR	4 gap QWR
Frequency MHz	50	50	75
Number of Resonators	6	7	24
E_{acc} MV/m	2 - 5	3 - 5	3 - 5
ϕ_s	-30°	-30°	-30°
E_{out} MeV/u	0.118	0.405	1.50
βout	0.0156	0.0292	0.0565
Focusing	Superconducting Solenoid		
Solenoid Length	17.5 cm - 55 cm		45 cm - 105 cm
B_{sol}	6.5 T		6.5 T
Focusing Periodicity	Res - Sol - Res		

On reaching 1.5 MeV/u the beam is either sent to the astrophysics experimental area, or passed through a foil stripper to raise the ion q/A ≥ 18/60, before being accelerated to 10 MeV/u in the thirty six quarter wave resonators of the 125 MHz DTL section. The main parameters of this section are summarized in Table 4.

Table 4
ISAC Post Accelerator

DTL Section 3: Ion q/A ≥ 18/60

Structure	2 gap QWR
Frequency MHz	125
E_{acc} MV/m	3 - 5
ϕ_s	-30°
β_{out}	0.145
E_{out} MeV/u	10
Focusing	Superconducting Solenoid
Solenoid Length	13 cm - 23 cm
B_{sol}	6.5 T
Periodicity	6 Res - Sol - 6 Res

Only preliminary beam dynamics calculations have so far been done. Because design of the matching section between the second and third DTL sections has not yet been done, calculations for the third section assume an input beam transverse emittance of 1 π mm mrad, and a longitudinal emittance as calculated at the output of the second DTL section, and shown in Fig. 11. The calculated phase space plots at the output of the linac are shown in Fig. 12.

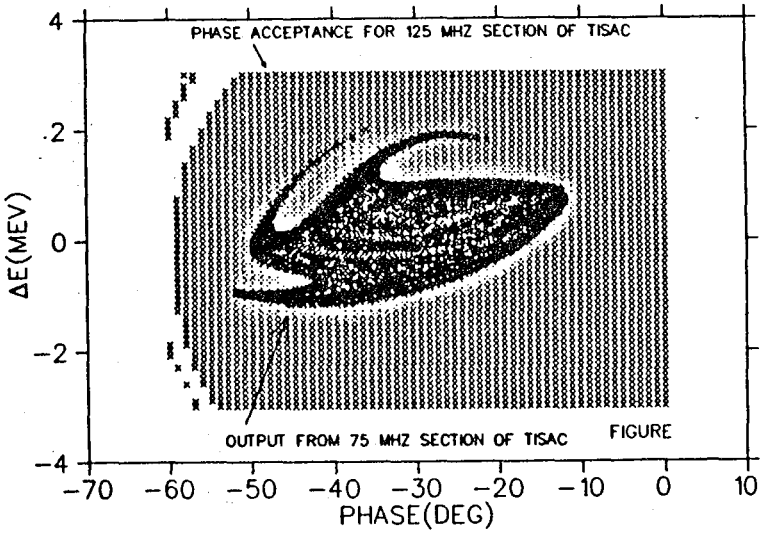

Fig. 11 Acceptance in longitudinal phase space of the 125 MHz linac section.

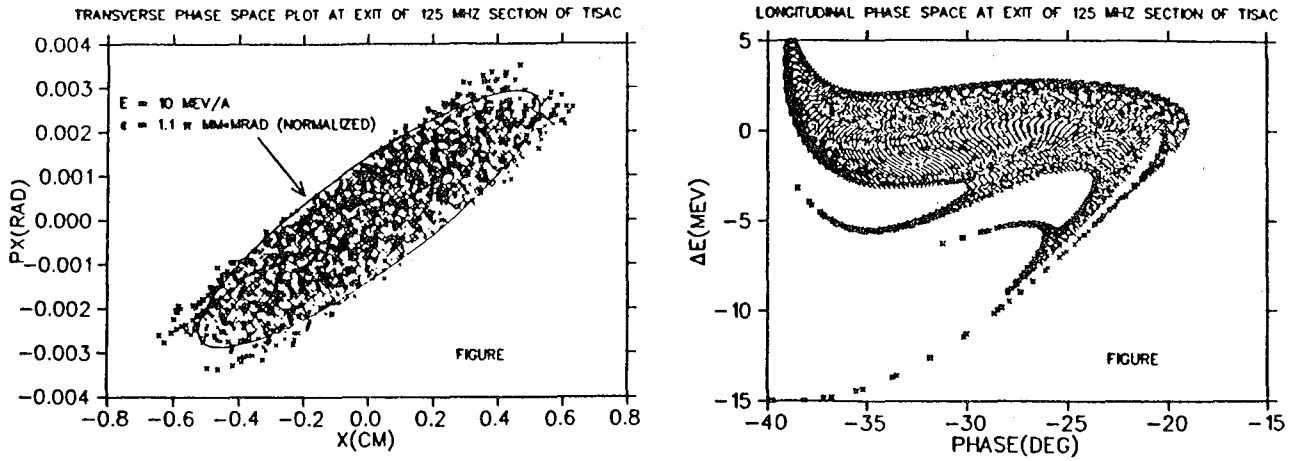

Fig. 12 Transverse and longitudinal phase space plots for beam at exit of the 125 MHz section

Both the longitudinal and transverse emittances of the accelerated beam are large. The longitudinal emittance in this case is approximately 530 keV-ns, or about an order of magnitude larger than the that currently specified for ISL. In part this large longitudinal emittance arises from the energy spread introduced in the RFQ as a consequence of designing it to accommodate the large transverse emittance of the input beam.

3. RFQ Prototype

Design experience for low frequency RFQs is much more limited than for the higher frequency versions appropriate for acceleration of protons or fully stripped light ions. Even for these, few have been designed for cw operation. To gain engineering design and fabrication experience therefore, construction of a prototype RFQ is planned. To keep the project a reasonable size, and match the rf power requirement to an available rf power source, the RFQ will be limited to about two metres in length. Most of the design parameters for the prototype will be the same as for the full size ISAC RFQ. The main difference is in the ion q/A specification, which for the prototype RFQ will be ≥ 1/20. Tentative parameters for the RFQ are summarized in Table 5.

Table 5
RFQ Prototype Parameters

Ion q/A	1/20
Input Energy	2 keV/u
Output Energy	60 keV/u
Operating Frequency	25 MHz
Vane Voltage	81 kV
RF Power	< 30 kW
Modulation Factor (m)	1.95
Focusing Factor (B)	11.07
Beam Aperture (min)	0.5 cm
Ave. Aperture (r_0)	0.75 cm
Bunching	Double Drift Buncher
No. Cells	59
Length	2.05 cm

By using the conventional RFQ design approach, with adiabatic bunching in a gentle buncher section, one gets a RFQ design that is slightly more than 3 metres long. More than half of this length is accounted for by the gentle buncher. To keep within a 2 metre maximum length objective, and still achieve the 60 keV/u output energy, we propose to replace the gentle buncher by a simple double drift buncher incorporated into the vane modulation. Because space charge forces are unimportant, beam capture of over 80% should be achievable in this case. An overall reduction in RFQ design length of about 1 metre is possible with this change. A similar design was employed by Schempp et al in the Cryring injector[7].

In addition to testing of the RFQ at full rf power, we also intend to test it with radioactive beams from the existing TISOL facility at TRIUMF [8]. This will require operation of the RFQ with a dc bias adjustable between ± 20 kV.

4. Discussion

The objective in this study has been to develop a credible, self consistent post-accelerator concept for the ISAC proposal. Although the calculations are still incomplete, it is clear that the RFQ - superconducting DTL concept can probably satisfy the ISAC specifications. Details concerning energy variability, and reduction of energy spread by debunching remain to be investigated. Some problems have however been revealed by this study. The major one is related to the large transverse emittance specification for the input beam. As noted above, because of beam dynamic limitations in the RFQ - DTL matching section, it has not been possible to accommodate the large emittance through the whole accelerator. Moreover the large emittance is at least in part the cause of the large energy spread in the RFQ output. This in turn then leads to undesirable design choices and compromises in the first part of the drift tube linac. In the next design iteration a reduction in both the input beam emittance specification and the linac acceptance should be tried. In addition the RFQ design needs reexamination to see if the output energy spread can be reduced.

5. References

(1) G.E. McMichael, B.G. Chidley, and R.M. Hutcheon, "Conceptual design study for the proposed ISOL post-accelerator at TRIUMF", AECL - 8960 (TRI-DN-85-33), Nov. 1985.

(2) L. Root, H.R. Schneider, and J.S. Fraser, "Post-accelerator studies for the ISOL facility at TRIUMF", Proc. Conference on Cyclotrons and their Applications, Vancouver, 1992, p. 749.

(3) M. Kase et al., "Variable Frequency linac RILAC as an injector of a separated sector cyclotron", Proc. 1984 Cyclotron Conference, 241.

(4) K.W. Shepard, "Development of a very low velocity superconducting linac", Proc. 1987 Particle Accelerator Conf., IEEE Tans. Nucl. Sci. NS-34, 1812.

(5) S. Takeuchi, T. Ishii, H. Ikezoe, and Y. Tomita, "Development of the JAERI tandem superconducting booster", Nuc. Inst. Meth. A287(1990), 257.

(6) K. Mittag, "On parameter optimization for a linear accelerator", KfK 2555, Jan. 1978, p. 54.

(7) A. Schempp, H. Deitinghoff, H. Klein, A. Kallberg, A. Soltan, and C.J. Herrlander, "RFQ injector for Cryring", Proc. 1988 European Accelerator Conf., 590 .

(8) L. Buchmann, J.S. Fraser, H. Schneider, H. Sprenger, J. Vincent, J. D'Auria, M. Dombsky, P. McNeely, and G. Roy, Proc. 2nd Int'l Conf. on Radioactive Nuclear Beams, Louvain-la-Neuve, 1991, p. 109.

Modifications to Baseline ISL Design due to Small (q/A)

John Edighoffer
Center for Beam Physics
Lawrence Berkeley Laboratory
Berkeley, California

Abstract: *The ISL baseline post-accelerator design as described in the ISL concept document[1] can not match the velocity profile of RFQ1 and RFQ2 over the full charge to mass ratios required without some modification. The minimum modification needed is to add an rf accelerating module between RFQ1 and RFQ2. At this workshop for the purpose of minimizing the longitudinal phase space growth, a prebuncher/chopper system was added in front of RFQ1. This allows the added rf acceleration module to be placed in front of RFQ1, allowing RFQ1 to be at ground potential. This is a nice solution if the buncher/chopper system can handle the width range of energy per nucleon. This solution provides for a constant velocity profile past the rf acceleration module for all species of ions.*

Figure 1 shows the ISL baseline post accelerator and Table 1 shows the operational parameters as a function of charge to mass. First, RFQ1 would have to have a variable velocity profile, impossible over the range required. Second, for q/A between 1/6 and 1/8, the ions exiting RFQ1 would have to have a negative energy in order the have the right energy by the time they reach RFQ2; of course they would simply be lost.

Figure 2 shows the first possible modification to the ISL baseline, that of adding a accelerating module after the DC accelerating between RFQ1 and RFQ2. This is also shown in the updated ISL document.[2] Table 2 shows the resulting operating parameters as a function of q/A. The output energy per nucleon has been optimized so as to minimize the acceleration required by the rf acceleration module. RFQ1 can now have a fixed velocity profile. There is no longer a problem of particles going through zero energy for an ion. The rf acceleration is low enough that a single rf cavity would be sufficient.

Figure 3 shows the second possible modification, allowed by the decision to add a prebuncher/chopper in front of RFQ1. That is the adding of the rf acceleration module in front of RFQ1 instead of after it. This allows the removal of the HV DC acceleration into and out of RFQ1. Table 3 shows the operating parameters for this case. This modification also provides a constant velocity profile after the rf acceleration module. This is a very nice solution if the buncher/chopper proves practical over the full charge to mass ratio. The rf acceleration module requires more acceleration capability (380 KeV .vs. 95 KeV) and is therefore probably more than a single cell. The actual design acceleration may well be higher due to the need to help with the bunching/debunching as part of the total buncher/chopper system.

Conclusion: Either modification will over come the problem of matching the energy into and out of the first two RFQ's. The second solution is highly preferred, but contingent on developing a buncher/chopper design that can be flexible enough to handle the full range of ions. The rf acceleration module is part of the buncher/chopper system design, that is the buncher/chopper system design must include the rf acceleration module.

References:

1 "The IsoSpin Laboratory (ISL) Research Opportunities with Radioactive Nuclear Beams", LALP 91-51, 1991.

2 Nitschke,"Future Propects for Radioactive Nuclear Beams in North America", LBL-34239, Proc. of the International School Seminar on Heavy Ion Physics, May 1993, Dubna, Russia.

Table 1 Baseline ISL Concept

q/A	Voltage at Output of High Resolution Separator (KeV/u)	DC Voltage Applied to RFQ1 Housing to get 2 Kev/u at the Entrance (KeV)	Voltage at Output of RFQ1 so that the Input to RFQ2 is 10 KeV/u (KeV/u)	Acceleration due to RFQ1 (KeV)	Acceleration due to RFQ1 (KeV/u)	Voltage at Input of RFQ2 (KeV/u)	Voltage at Output of RFQ2 (KeV/u)
1/6	16.67	88	-4.67	-40	-6.67	10	100
1/7	14.29	86	-2.29	-30	-4.29	10	100
1/8	12.50	84	-0.50	-20	-2.50	10	100
1/9	11.11	82	0.89	-10	-1.11	10	100
1/12	8.33	76	3.67	20	1.67	10	100
1/18	5.56	64	6.44	80	4.44	10	100
1/24	4.17	52	7.83	140	5.83	10	100
1/32	3.13	36	8.88	220	6.88	10	100
1/48	2.08	4	9.92	380	7.92	10	100
1/72	1.39	-44	10.61	620	8.61	10	100
1/96	1.04	-92	10.96	860	8.96	10	100
1/120	0.83	-140	11.17	1100	9.17	10	100
1/180	0.56	-260	11.44	1700	9.44	10	100
1/240	0.42	-380	11.58	2300	9.58	10	100

Table 2 Modified ISL Concept with Rf Acceleration After RFQ1

q/A	Voltage at Output of High Resolution Separator (KeV/u)	DC Voltage Applied to RFQ1 to get 2 Kev/u at the Entrance (KeV)	Voltage at Output of RFQ1 so that the Input to RFQ2 is 10 KeV/u (KeV/u)	Acceleration due to RFQ1 (KeV)	Acceleration due to RFQ1 (set to 9.19) (KeV/u)	Voltage at Entrance to Single Cell (KeV)	Acceleration due to Rf Module (KeV)	Voltage at Input of RFQ2 (KeV/u)	Voltage at Output of RFQ2 (KeV/u)
1/6	16.67	88	11.19	55.14	9.19	155.14	-95.14	10	100
1/7	14.29	86	11.19	64.33	9.19	164.33	-94.33	10	100
1/8	12.50	84	11.19	73.52	9.19	173.52	-93.52	10	100
1/9	11.11	82	11.19	82.71	9.19	182.71	-92.71	10	100
1/12	8.33	76	11.19	110.28	9.19	210.28	-90.28	10	100
1/18	5.56	64	11.19	165.42	9.19	265.42	-85.42	10	100
1/24	4.17	52	11.19	220.56	9.19	320.56	-80.56	10	100
1/32	3.13	36	11.19	294.08	9.19	394.08	-74.08	10	100
1/48	2.08	4	11.19	441.12	9.19	541.12	-61.12	10	100
1/72	1.39	-44	11.19	661.68	9.19	761.68	-41.68	10	100
1/96	1.04	-92	11.19	882.24	9.19	982.24	-22.24	10	100
1/120	0.83	-140	11.19	1102.8	9.19	1202.80	-2.80	10	100
1/180	0.56	-260	11.19	1654.2	9.19	1754.20	45.80	10	100
1/240	0.42	-380	11.19	2205.6	9.19	2305.60	94.40	10	100

Table 3 Modified ISL Concept with Rf Acceleration before RFQ1

RFQ1 is at Ground

q/A	Energy at Output of High Resolution Separator (KeV/u) (100 KeV)	Energy at Output of Buncher (KeV/u)	RF Acceleration Before RFQ1 So that the energy is 2 Kev/u at Entrance (KeV)	Energy at Input of RFQ1 (KeV/u)	Energy at Output of RFQ1 (KeV/u)	Acceleration due to RFQ1 (KeV)	Energy at Input of RFQ2 (KeV/u)
1/6	16.67	16.67	-88	**2.00**	**10.00**	48	10
1/7	14.29	14.29	-86	**2.00**	**10.00**	56	10
1/8	12.50	12.50	-84	**2.00**	**10.00**	64	10
1/9	11.11	11.11	-82	**2.00**	**10.00**	72	10
1/12	8.33	8.33	-76	**2.00**	**10.00**	96	10
1/18	5.56	5.56	-64	**2.00**	**10.00**	144	10
1/24	4.17	4.17	-52	**2.00**	**10.00**	192	10
1/32	3.13	3.13	-36	**2.00**	**10.00**	256	10
1/48	2.08	2.08	-4	**2.00**	**10.00**	384	10
1/72	1.39	1.39	44	**2.00**	**10.00**	576	10
1/96	1.04	1.04	92	**2.00**	**10.00**	768	10
1/120	0.83	0.83	140	**2.00**	**10.00**	960	10
1/180	0.56	0.56	260	**2.00**	**10.00**	1440	10
1/240	0.42	0.42	380	**2.00**	**10.00**	1920	10

Baseline ISL Post Accelerator Concept

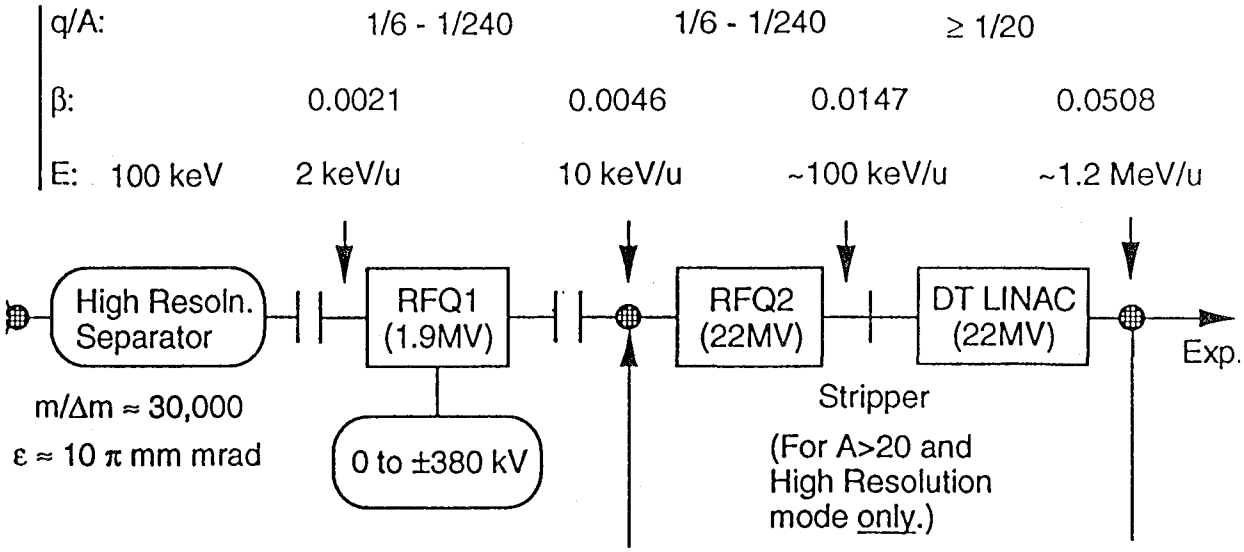

Figure 1

Modified ISL Post Accelerator Concept with RF Module After RFQ1

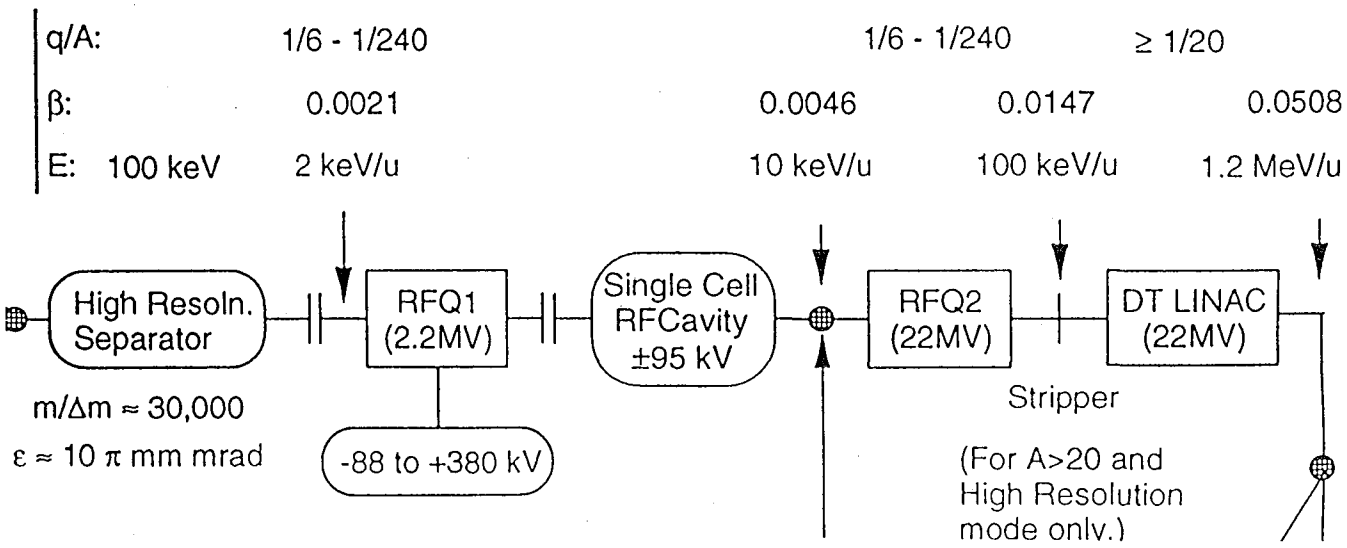

Figure 2

Modified ISL Post Accelerator Concept with RF Module before RFQ1 and RFQ1 Grounded

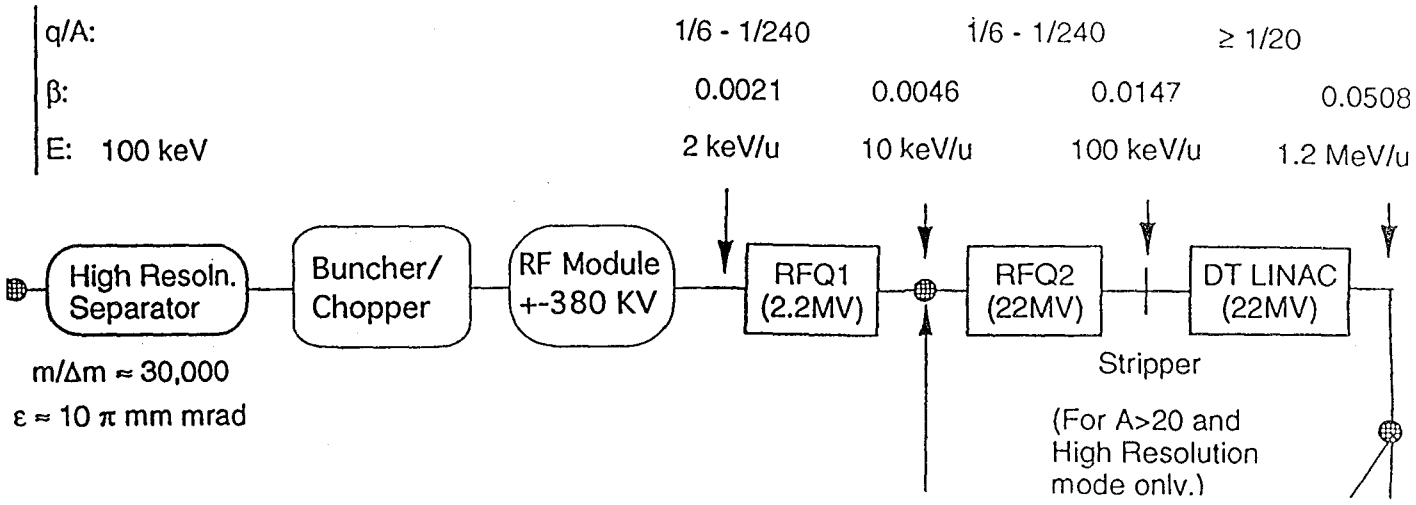

Figure 3

STUDY OF THE STRIPPING SCHEME FOR THE ISL FACILITY

Pierre Bricault
TRIUMF, Vancouver, Canada.

ABSTRACT: To achieve the acceleration of very low charged ions with good efficiency and low cost the charge to mass ratio must be increased by using stripper. In the ISL conceptual design two or more strippers are considered. The total voltage needed to reach the final energy depends on the stripping energy. Using the charge distributions, one can estimate the residual intensity at the end of the LINAC.

INTRODUCTION

The basic principle of the ISL facility is shown in fig. 1. The accelerator is composed in four sections. In this scheme there are strippers placed between the radio frequency quadrupole RFQ and the drift tube linear accelerator DTL, between the DTL and LINAC1, and finally between LINAC1 and LINAC2. The initial charge state of the ions coming from the ion source is assume to be 1^+ or 1^-. The charge to mass ratio must be greater than 1/20 after the first stripper, 1/6 after the second and 1/4 after the third one. In this paper the third stripper is not considered since the efficiency will be very high. Most of the light ions will be fully stripped.

CHARGE STATE DISTRIBUTION

The charge state distribution of an ion after passage through matter depends on the velocity and the atomic number Z. We assume that the initial charge state is much lower than the equilibrium charge state. There are many empirical formulae describing the charge state distribution after stripping. Betz et al. [Betz66] has used the experimental data on many ions

stripped in air and formvar foils at energies between 5 and 80 MeV to derive a semi-empirical relation for average charge state

$$\bar{q}/Z = 1 - C\exp\left[-v/\left(v_0 Z^{\gamma}\right)\right], \qquad 1)$$

where Z is the projectile atomic number, v its velocity, v_0 the Bohr velocity = c/137. C is a constant close to 1 and γ between .5 and .6.

This formula was modified by Baron et al. [Bar88]

$$\bar{q}/Z = 1 - C\exp\left[-83.275\beta/Z^{\gamma}\right], \qquad 2)$$

where β is the projectile velocity and light velocity ratio, C is a function of energy for energy. C = 0.9 + 0.0769*W for energy lower than 1.3 MeV/u, and C = 1 for energy higher than 1.3 MeV/U, and γ is fixed at 0.477

Supposing that no significant shell effects are present and $\bar{q}$ is not too close to Z, the distributions are assumed to be Gaussian with standard deviation d as proposed by Nikolaiev and Dmitriev [Niko68]

$$d = 1/2\sqrt{\bar{q}\left(1-(\bar{q}/Z)^{1.67}\right)} \qquad 3)$$

Small modifications where reported recently by Baron et al. [Bar92] in order to take into account deviations observed for masses greater then Krypton.

For a gas stripper the relation is different. Using the data contains in [Betz72] we can express the average charge state to atomic number ratio for energy lower than 1.5 MeV/u by using a relation similar to Nikolaiev and Dmitriev [Niko68] relation for foil stripper

$$\bar{q}/Z = \left[1 + \left(Z^{-.55} v/v'\right)^{-1/.76}\right]^{-1.12} \qquad 4)$$

where v'=3.6 X 10^8 cm/s. In the case of a gas stripper the charge state distribution is not symmetric. It can be written in the following form

$$F(q) = \left(d\sqrt{2\pi}\right)^{-1} \exp\left(-\left|q-\bar{q}\right|^{u} \Big/ \left(2d^{2}\right)\right), \qquad 5)$$

where d is the width and u the shape parameter of the distribution.

$$\begin{aligned} u &= 2.24 \text{ if } (q-\bar{q}) \le 0, \\ u &= 1.83 \text{ if } (q-\bar{q}) > 0. \end{aligned} \qquad 6)$$

The distribution width in a wide range of both Z and particle velocity show great regularity. The distribution width can be approximate using the simple relation,

$$d = d_1 Z^{w} \qquad 7)$$

Where the parameter d_1 and w have been determined empirically via the mean charge state and the amount to 0.32 and 0.45 in N_2 or Ar gas, and to 0.38 and 0.40 in C, respectively.

TOTAL VOLTAGE

Using these empirical relations, we can find the minimum voltage needed to reach a given final energy. The total voltage needed for the acceleration by the drift tube linacs up to the final energy depends on the Q/A from the ion source and on the charge state after stripping

$$E = (Q/A)_{IS} V_{IS} + E_{RFQ} + (Q/A)_{Strip\#1} V_{DTL\#1} + (Q/A)_{Strip\#2} V_{DTL\#2}, \qquad 8)$$

where

$(Q/A)_{IS}$ is the charge to mass ratio of the ion coming from the ion source,

V_{IS} is the high voltage of the ion source,

E_{RFQ} is the energy after the RFQ,

$(Q/A)_{Strip\#1}$ is the charge to mass ratio after the first stripper,

$V_{DTL\#1}$ is the voltage of the first drift tube linac,

$(Q/A)_{Strip\#2}$ is the charge to mass ratio after the first stripper,

$V_{DTL\#2}$ is the voltage of the first drift tube linac.

The minimization of the total voltage for the first stripper is not the only requirement, because if we want to use a carbon foil the energy must be high enough in order to use practical equilibrium thickness. If the energy is too low, a gas stripper must be used, but the charged states are lower.

First Stripper

For the first stripper the final energy of the DTL section is 1.5 MeV/u. This is mainly governed by the astrophysics and applied physics program. Figures 2 and 3 show the total voltage needs to reach 1.5 MeV/u as a function of the stripper energy for mass 60 and 238 respectively. The minimum is found to be around 0.140 MeV/u for mass 60 and 0.06 MeV/u for mass 238.

The used of multi-charged ions can decrease the total voltage needs to reach the final energy. Figure 4 shows the total voltage in the case of $^{238}U^{4+}$.The total voltage is decreased considerably, 26 instead of 42 MV. In this case the minimum is found around 175 keV/u for the first stripper. But in this case good ionization efficiency must be proved.

Second Stripper

For the second stripper the final energy of the LINAC1 section is 10 MeV/u. Figures 5 and 6 show the total voltage necessary to reach this final energy as a function of the energy at the second stripper. The minimum is found to be around 1.2 MeV/u. This is in agreement with the natural break suggested to be around 1.5 MeV/u for astrophysics and applied physics programs.

RESIDUAL INTENSITY

The final intensity at the end of the accelerator will depend on the stripping scheme. Using the charge distributions 5) one can evaluate the residual intensity after stripping. Figure 7 shows the residual intensity as a function of the atomic number Z assuming that the first stripping is done at 100 keV/u and the second at 1.5 MeV/u. The dashed curve shows the relative intensity after the first stripper and the full line shows the relative intensity after the second stripper. The relative intensity after stripping decrease with the atomic number Z in the worst case the final intensity is about 3% of the initial intensity.

REFERENCE

[Baron88]- E. Baron and Ch Ricaud, EPAC88 (Rome), vol. 2, 839.

[Baron92]- E. Baron, M. Bajard, Ch Ricaud, 6th Conf. Electrostatic Accelerator and Associated Boosters, (Padova), p. 16.

[Betz72]- H. D. Betz, Rev. Mod. Phys. 44 no. 3 (1972).

[Niko68]- V. S. Nikolaev and I. S. Dmitriev, Phys. Letters 24A, 277 (1968).

ISL Concept

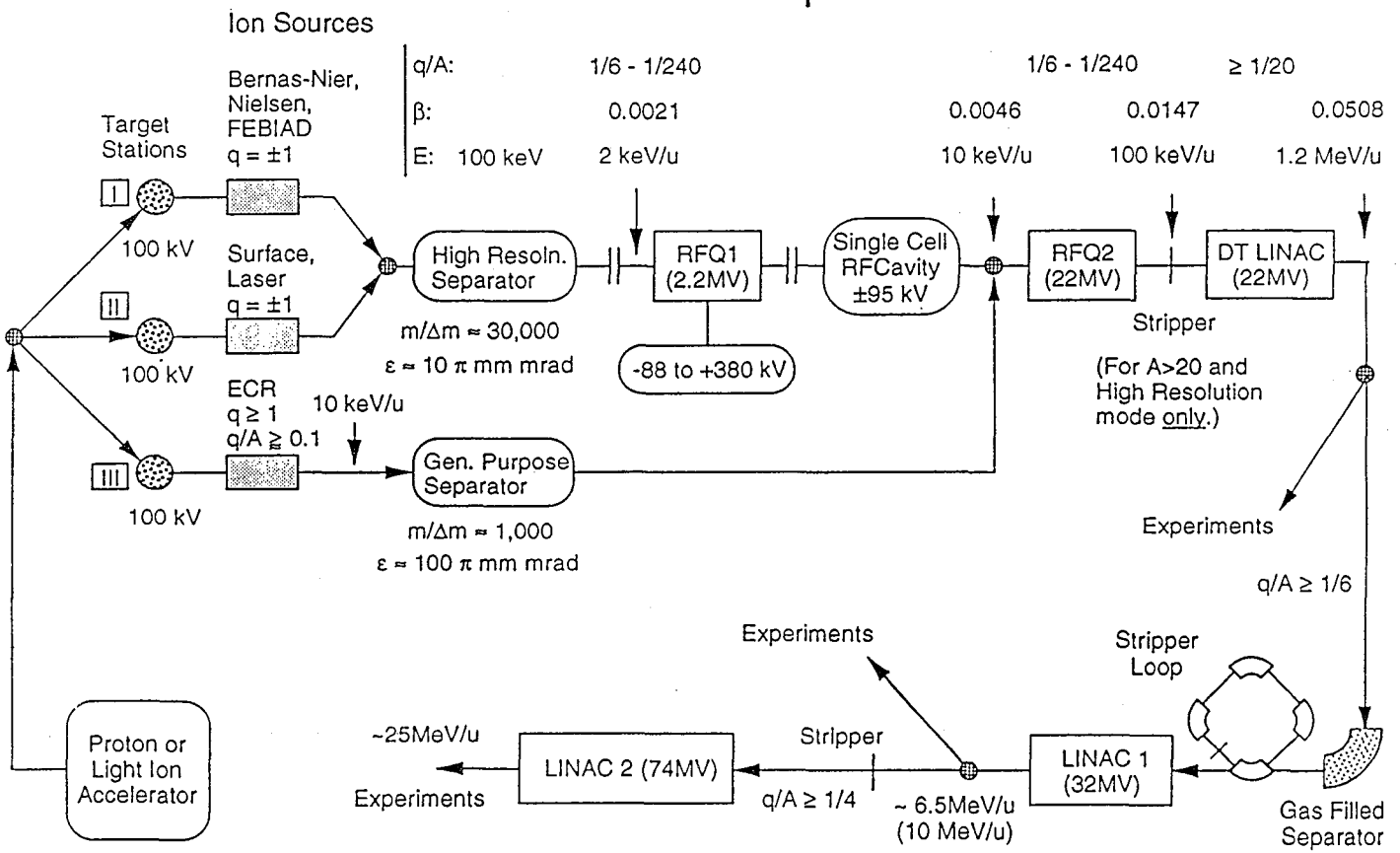
Ion Sources
Target Stations
Bernas-Nier, Nielsen, FEBIAD
q = ±1
Surface, Laser
q = ±1
ECR
q ≥ 1
q/A ≧ 0.1
100 kV
100 kV
100 kV
10 keV/u
q/A:
1/6 - 1/240
1/6 - 1/240
≥ 1/20
β:
0.0021
0.0046
0.0147
0.0508
E: 100 keV
2 keV/u
10 keV/u
100 keV/u
1.2 MeV/u
High Resoln. Separator
m/Δm ≈ 30,000
ε ≈ 10 π mm mrad
RFQ1 (2.2MV)
-88 to +380 kV
Single Cell RFCavity ±95 kV
RFQ2 (22MV)
Stripper
DT LINAC (22MV)
(For A>20 and High Resolution mode only.)
Gen. Purpose Separator
m/Δm ≈ 1,000
ε ≈ 100 π mm mrad
Experiments
q/A ≥ 1/6
Experiments
Stripper Loop
Proton or Light Ion Accelerator
~25MeV/u
Experiments
LINAC 2 (74MV)
Stripper
q/A ≥ 1/4
~ 6.5MeV/u
(10 MeV/u)
LINAC 1 (32MV)
Gas Filled Separator
jmn 8/17/93

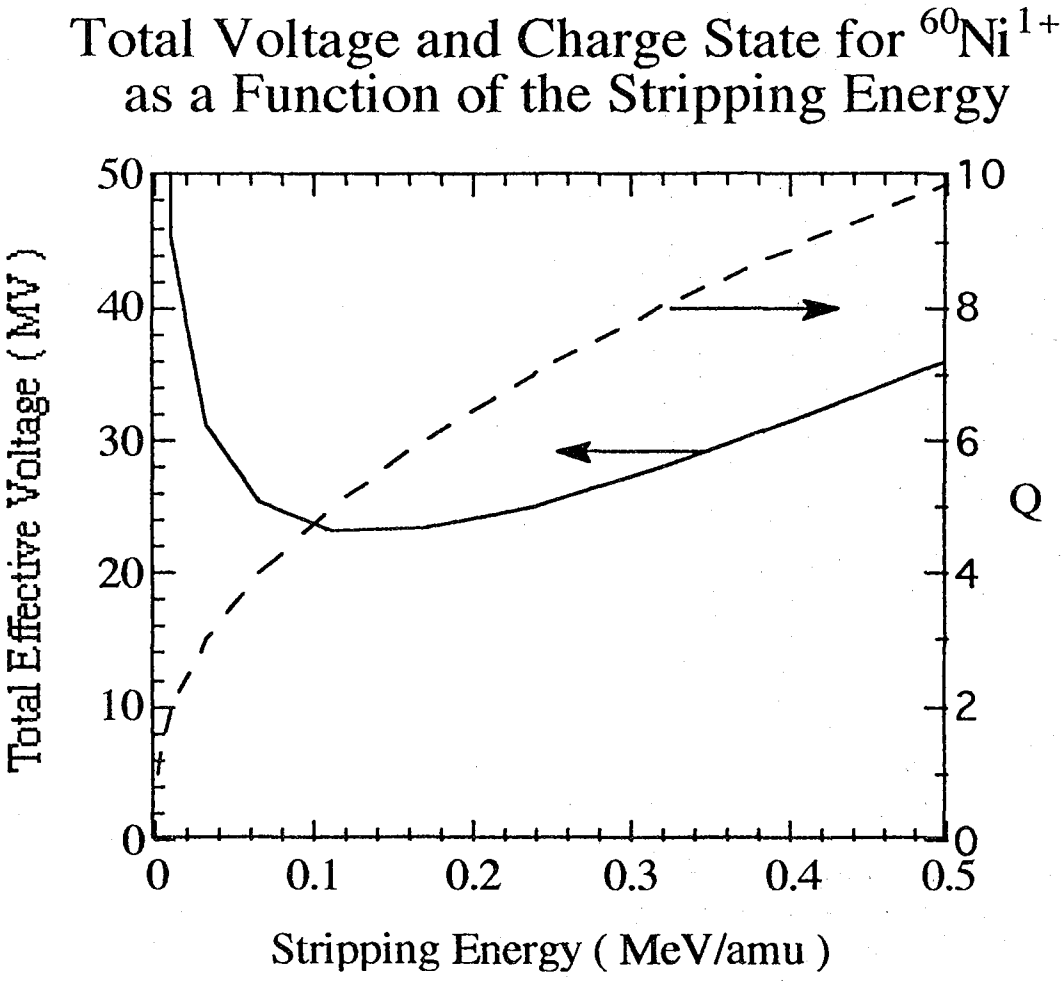

Fig. 2-Total effective voltage needed to reach 1.5 MeV/amu for $^{60}Ni^{1+}$ as a function of the stripping energy using a gas stripper. The dashed curve shows the charge state after stripping.

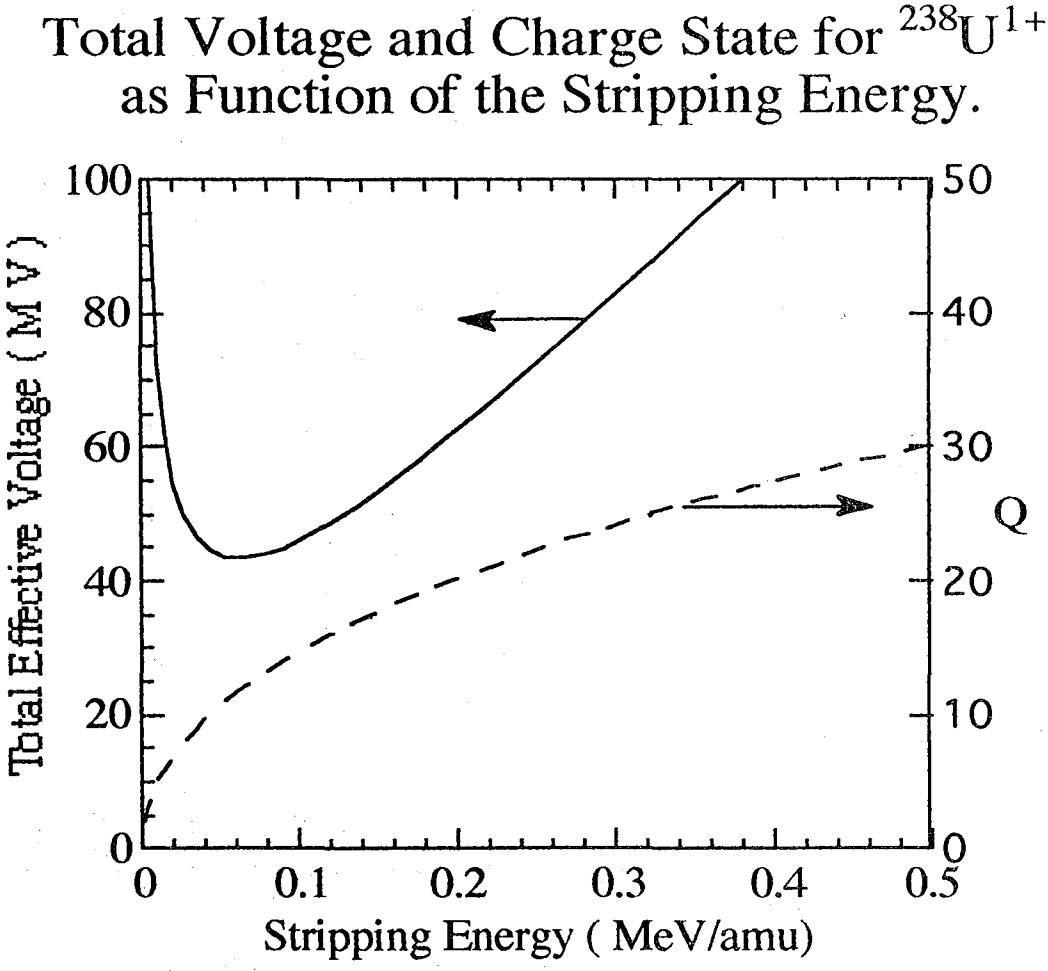

Fig. 3- Total effective voltage needed to reach 1.5 MeV/amu for $^{238}U^{1+}$ as a function of the stripping energy using a carbon foil stripper. The dashed curve shows the charge state after stripping.

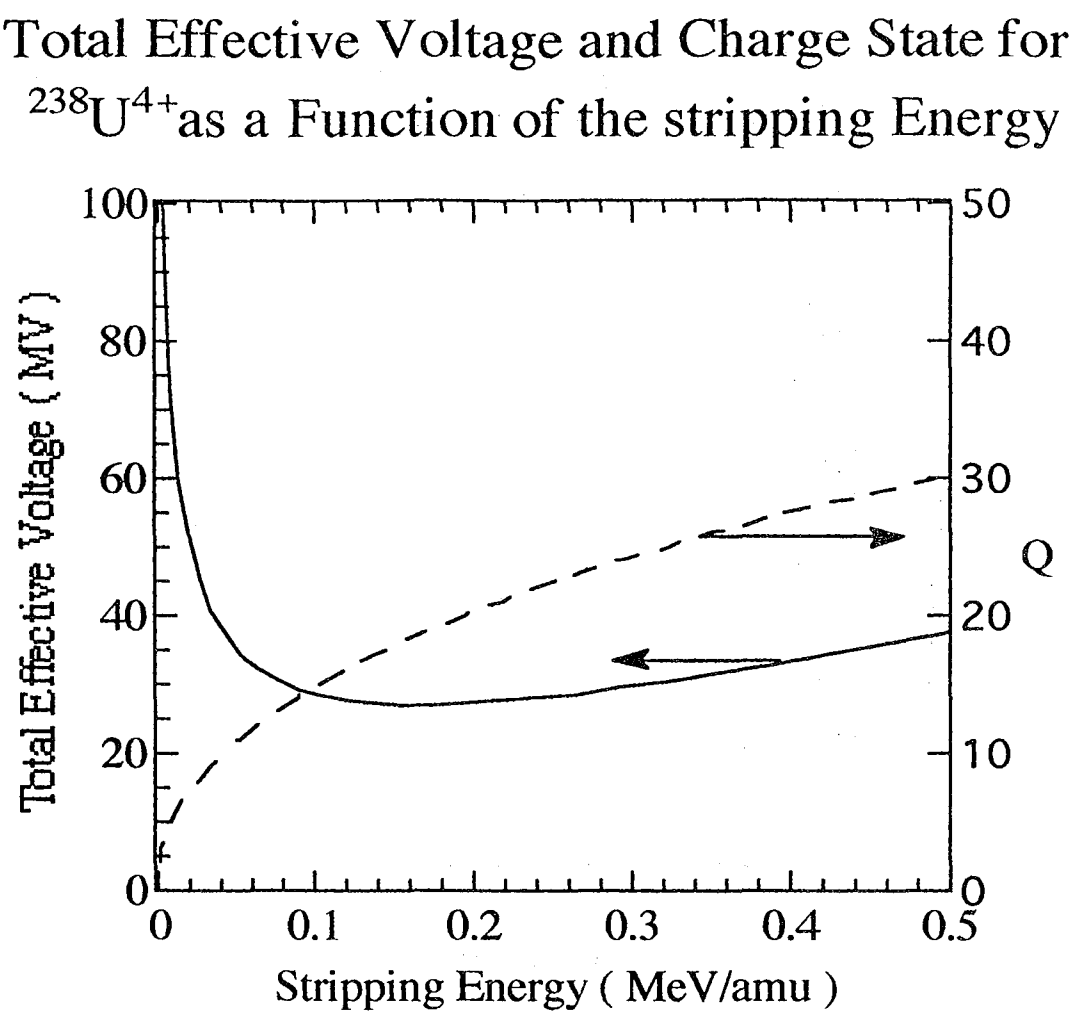

Fig. 4- Total effective voltage needed to reach 1.5 MeV/amu for $^{238}U^{4+}$ as a function of the stripping energy using a carbon foil stripper. The dashed curve shows the charge state after stripping.

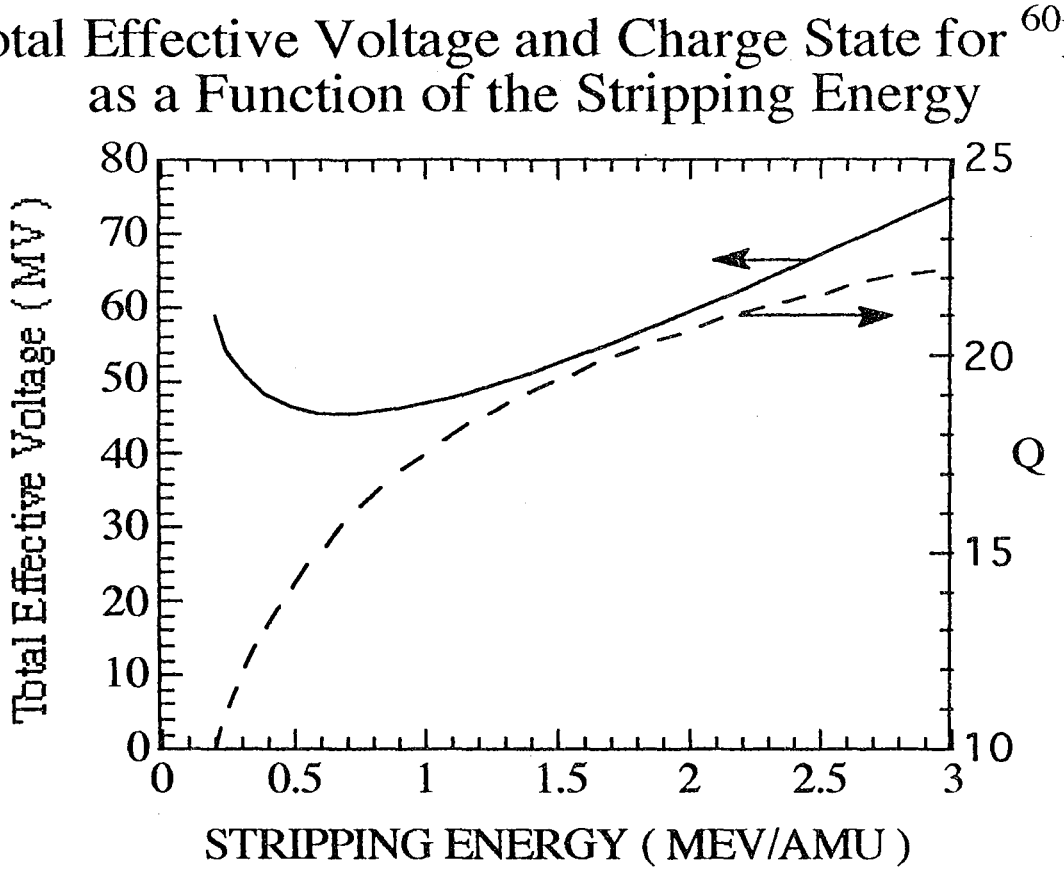

Fig. 5- Total effective voltage needed to reach 10 MeV/amu for $^{60}Ni^{3+}$ as a function of the stripping energy using a carbon foil stripper. The dashed curve shows the charge state after stripping.

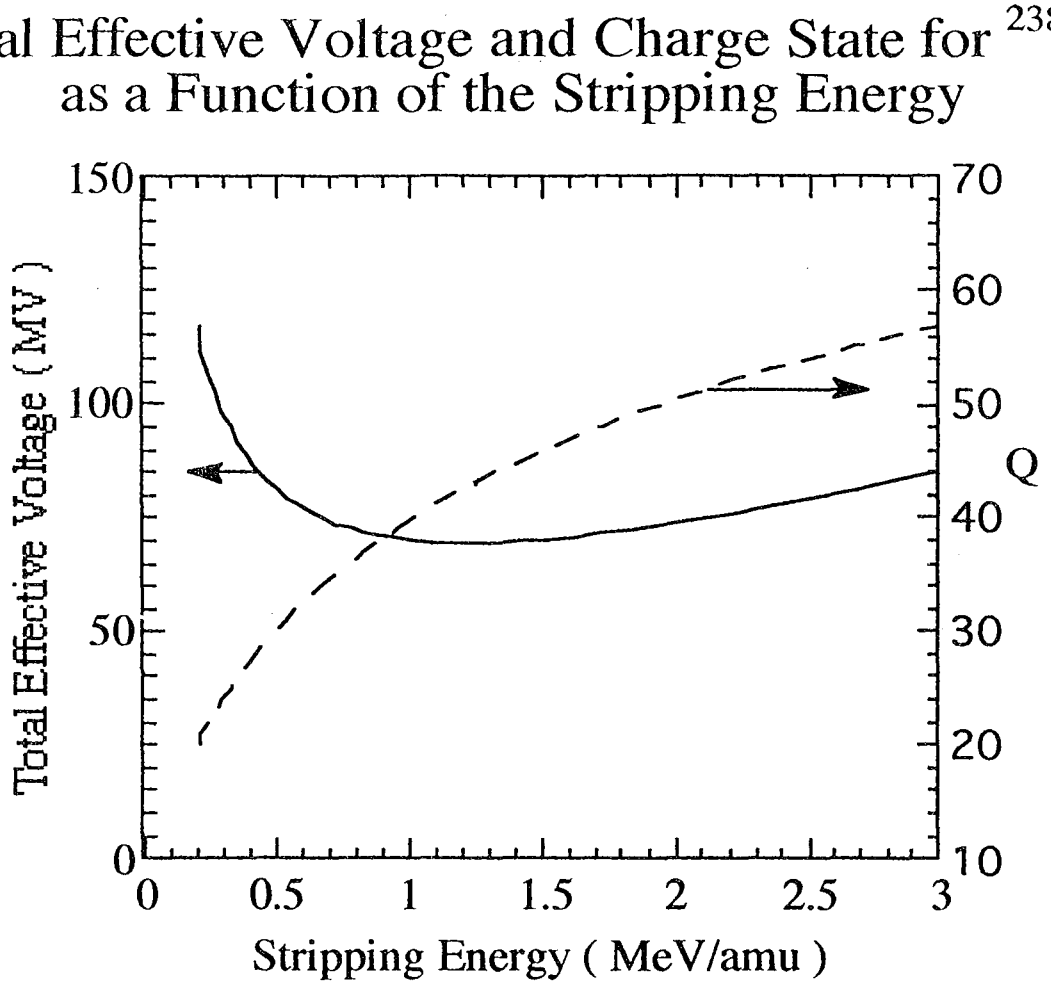

Fig. 6- Total effective voltage needed to reach 10 MeV/amu for ^{238}U as a function of the stripping energy using a carbon foil stripper. The dashed curve shows the charge state after stripping.

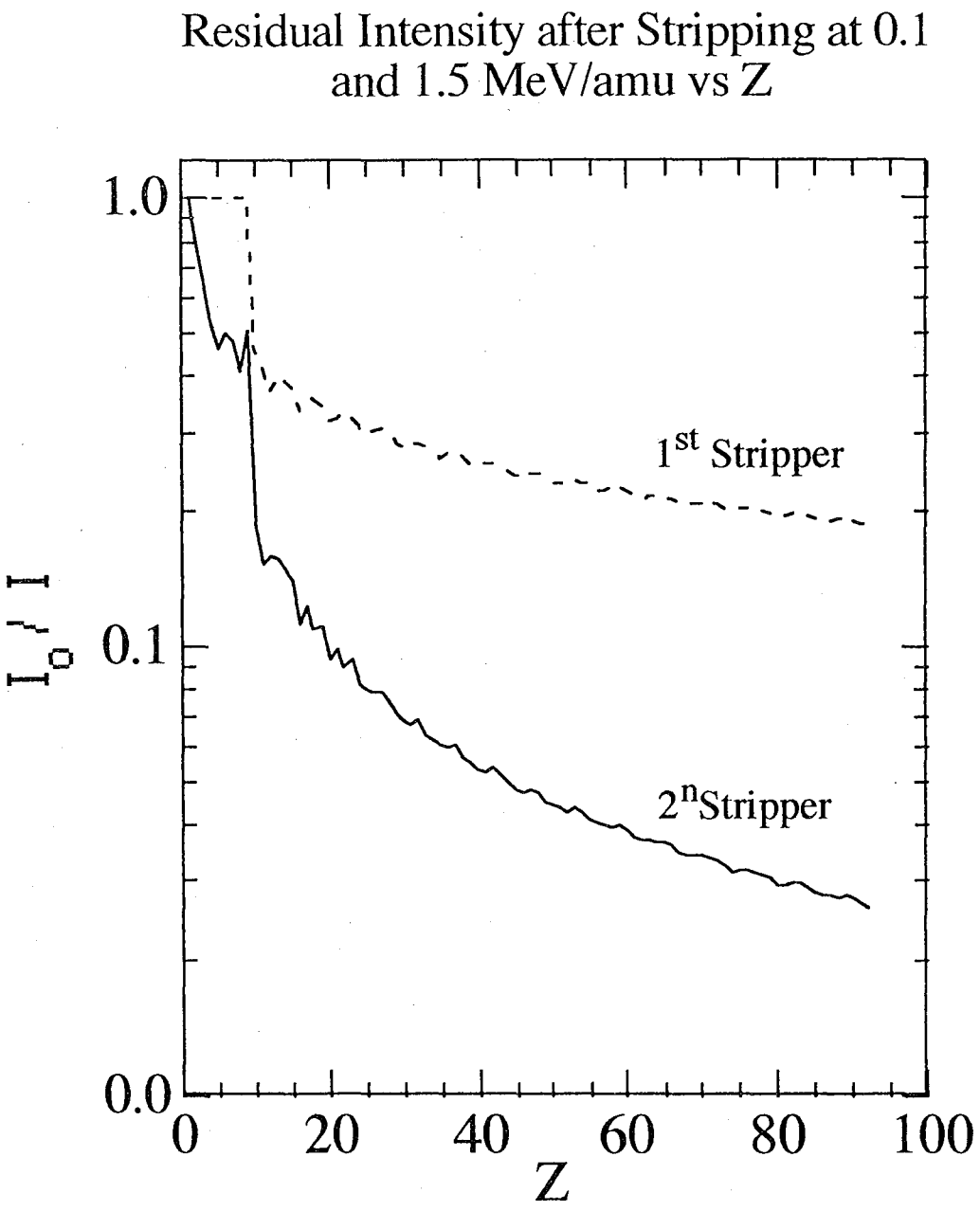

Fig. 7- Residual intensity after the first and second stripper. The first stripper is a carbon foil and the stripping is done at 100 keV/amu. The second stripping is done at 1.5 MeV/amu using a carbon foil.

A Ring to Test Stripping Enforcement*

F. Selph
Lawrence Berkeley Laboratory
1 Cyclotron Road, Berkeley, CA 94720

Introduction

A design of a charge state enforcer ring is shown, which could be used in an ISL facility when ions are stripped, providing 75-90% transmission of the desired charge state. An ISL facility is likely to require stripping at or near 0.2 and 1.5 MeV/u. The ring described here can be used at both energies. This ring could be tested at LBL, using existing equipment for providing ions at both energies.

Design of the ring

The ring comprises 8 dipoles to bend ions through a total of 360 degrees, 20 quadrupoles for transverse focusing, and 8 sextupoles to compensate for higher-order effects. The arrangement is shown in figure 1. The criteria used in the design of these transverse ring elements were described in an earlier paper (1). These require that betatron tunes be integral or half-integral, and that chromaticity be zero. This ring has a horizontal tune of 2.5 and a vertical tune of 0.5. The circumference on the equilibrium orbit is 16.27 m. There are four longer straight sections: one is used for the stripper, one for a buncher cavity, the remaining two are used for extraction of the mean charge state. Two of these (stripper and buncher) are non-dispersive, the other two have dispersion which can be adjusted by quadrupole settings, which would usually be set for separation of adjacent charge states of 10-20 mm.

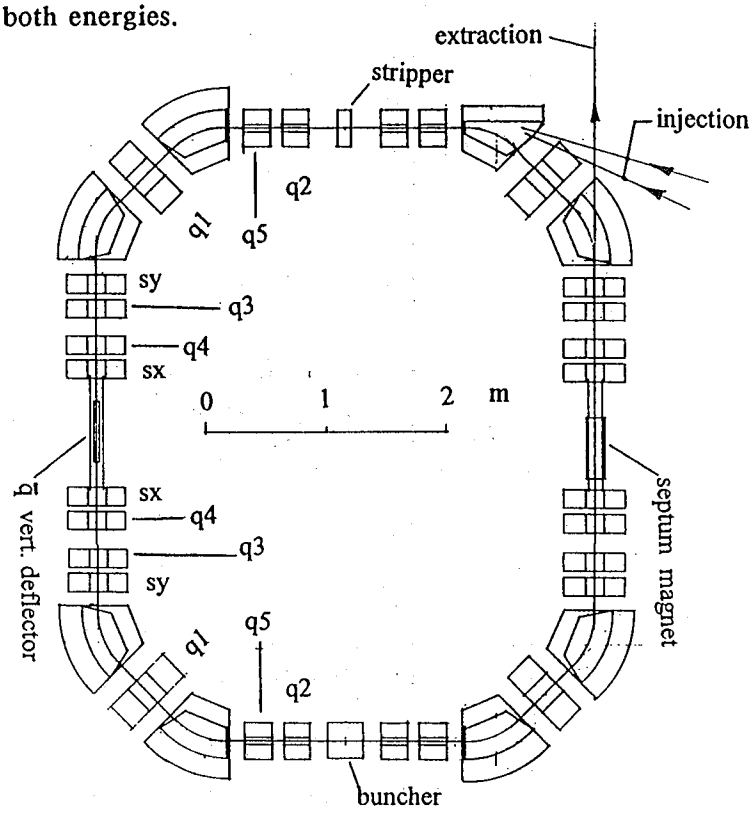

Fig.1. Schematic of the stripper enforcer ring. After, entering from the injection channel, ions are recirculated through the stripping foil, with the mean charge state being extracted on each turn. Energy lost in the stripper is made up in a rf cavity (labeled buncher).

The injection channel goes through one of the dipole gaps. Ions are stripped immediately after injection, which decreases the rigidity and allows them to return again to the stripper. The magnetic field of the dipoles is set so that the mean charge state $\bar{q}$ remains

* This work was supported by the Director, Office of Energy Research, Office of High Energy and Nuclear Physics, of the U.S. Department of Energy under Contract No. DE-AC03765F00098.

on the quadrupole axis. In the straight section following the stripper straight section, these ions enter a narrow channel, and are deflected vertically (the deflecting device can be either electric or magnetic). This causes them to be displaced across the septum of a magnet located on the opposite side of the ring, and to be deflected vertically into the extraction channel.

The buncher cavity serves two purposes: it makes up for energy lost in the stripper, and it acts to minimize energy spread in the emerging $\bar{q}$ beam. The frequency (a harmonic of the revolution frequency), the voltage and phase of the rf must be chosen appropriately in order to accomplish this. They are set so that energy lost in the stripper is restored, and so that ions arriving late are speeded up and ions arriving early lose energy. This produces what is known as a phase-stable rf bucket. The rf voltage determines the size of the bucket and this must be made large enough to encompass all of the ions. Ions with positive Δq will get a greater and those with negative Δq less energy gain for a given voltage than the $\bar{q}$ ions. This leads to a dependence on the rate of rise of the rf (hence the frequency) in order to minimize the energy spread of the extracted beam.

The momentum acceptance of the ring is large, on the order of +/- 25% in $\Delta q/q$, so only a small loss is experienced to the vacuum chamber walls on each turn. After some 12 revolutions for light ions, 14 for the heaviest, essentially all of the injected ions that survive have been extracted.

Expected Performance

To test the expected performance, calculations were done to see, to first order, if the use of this ring would seriously degrade transverse or longitudinal beam emittance. From the results so far, the calculations suggest that the degradation will be acceptable.

Calculations were performed with 5 ions-Ne, Ar, Kr, Xe, U- at two energies- 0.2 and 1.5 MeV/u. Use of a carbon stripping foil was assumed, in preferance to a vapor or gas stripper because the carbon foil yields higher charge states (important particularly for the light ions) and a more precise definition for the stripped beam, important for ring performance. Equilibrium stripping fractions were taken from Ref. 2. For each ion a table of stripping intensities was made- that for Kr at 1.5 MeV/u is shown as Table 1. The first column contains the stripped charge states q, the third column the expected intensity in each charge state (expressed as a percent of the original beam) after one stripping. This is also plotted in the accompanying graph. A small percentage (in this case 0.5%) falls outside the ring acceptance. On each turn, 20% is extracted as q=22. After the second stripping,of the 79.5% reaching the stripping foil, 15.9% were extracted on turn 2 (column 4), 12.64% on turn 3, and so on. The table is terminated after 14 turns, though the 4% remaining can still contribute to the extraction efficiency. The amount each turn adds to $\bar{q}$=22 is used in subsequent analysis of of the contribution of each turn to the transverse and longitudinal emittance spread. Adding up the row for $\bar{q}$=22 shows that we can expect over 93% of the original beam to be extracted. The ring operates continuously, with all turns existing simultaneously. Adding up the row showing recirculating intensities, we see that the total recirculating intensity, plus the original beam, amounts to 472% of the original beam intensity. This is an important consideration in evaluating the expected life of the stripper.

		1.5 MeV/u Kr beam thru Carbon stripper						Brho = 0.6736 T-m									
q	Injected		% distributed to each channel														
17		0.80	0.64	0.51	0.40	0.32	0.25	0.20	0.16	0.13	0.10	0.08	0.06	0.05	0.04	3.75	
18		3.20	2.54	2.02	1.61	1.28	1.02	0.81	0.64	0.51	0.41	0.32	0.26	0.20	0.16	14.98	
19		7.30	5.80	4.61	3.67	2.92	2.32	1.84	1.47	1.16	0.93	0.74	0.59	0.47	0.37	34.18	
20		13.00	10.34	8.22	6.53	5.19	4.13	3.28	2.61	2.07	1.65	1.31	1.04	0.83	0.66	60.86	
21		18.00	14.31	11.38	9.04	7.19	5.72	4.54	3.61	2.87	2.28	1.82	1.44	1.15	0.91	84.27	
22	100.00	20.00	15.90	12.64	10.05	7.99	6.35	5.05	4.01	3.19	2.54	2.02	1.60	1.27	1.01	93.63	<% extracted for
23		17.00	13.52	10.74	8.54	6.79	5.40	4.29	3.41	2.71	2.16	1.71	1.36	1.08	0.86	79.59	100% injected
24		11.00	8.75	6.95	5.53	4.39	3.49	2.78	2.21	1.76	1.40	1.11	0.88	0.70	0.56	51.50	
25		6.00	4.77	3.79	3.01	2.40	1.91	1.51	1.20	0.96	0.76	0.61	0.48	0.38	0.30	28.09	
26		2.40	1.91	1.52	1.21	0.96	0.76	0.61	0.48	0.38	0.30	0.24	0.19	0.15	0.12	11.24	
27		0.80	0.64	0.51	0.40	0.32	0.25	0.20	0.16	0.13	0.10	0.08	0.06	0.05	0.04	3.75	
	n= 0	1	2	3	4	5	6	7	8	9	10	11	12	13	14		
%	recirc.=	79.50	63.20	50.25	39.95	31.76	25.25	20.07	15.96	12.69	10.08	8.02	6.37	5.07	4.03	372.18	< recirculating
																100.00	< injected
																472.18	< intensity on
	total %	99.50															stripper

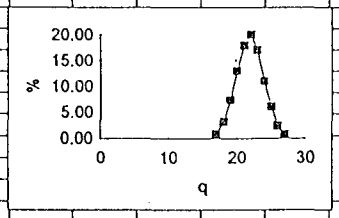

Table 1. Equilibrium stripping fractions for Kr at 1.5 MeV/u, resulting from repeated passes through a carbon stripping foil. Energy lost in the stripper is restored with a buncher rf cavity.

To estimate transverse emittance growth in repeated stripping, a calculation was done in which an angular distribution, initially gaussian, was subjected to repeated transformations simulating a passage through a foil. Emittance growth will be proportional to angular growth because ring properties are such that the spot size on the stripping foil is constant. The intensity distribution before stripping was divided into many narrow slices, and then each slice was converted to a gaussian with the FWHM caused by stripping. Recombining all of these distributions gives an overall (non-gaussian) distribution for the result of the stripping event. This process was repeated a number of times corresponding to the expected number of turns in the ring. For each turn, the integrated intensity was adjusted to correspond to the expected intensity contribution to the extracted beam of that turn. The result of two such calculations are shown in Fig. 2.

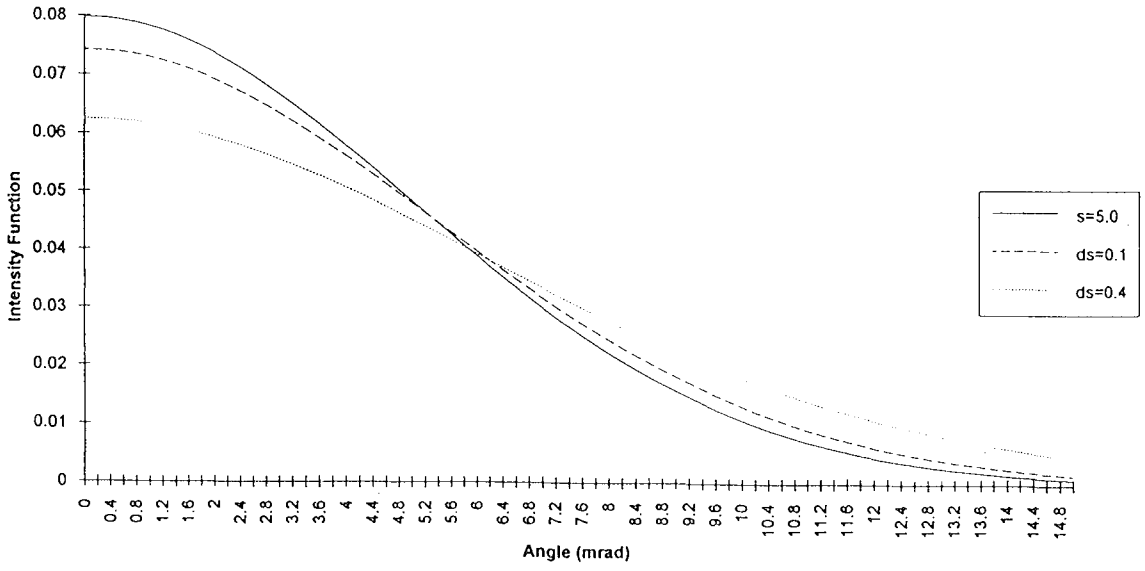

Fig.2. Growth of the transverse emittance, which is proportional to the angular divergence, due to scattering in stripping. Initial divergence FWHM (s) is taken as 5 mrad. Two cases of the resulting spread in the extracted beam are considered, one with half-angle (ds) of 0.1 mrad on each turn, one with ds = 0.4 mrad.

The initial FWHM (s) was taken as 5 mrad. The result with scattering angle FWHM (ds) is shown for ds= 0.1 and 0.4 mrad. Both, as expected, lower the peak intensity and broaden the tail of the distribution. These results suggest that scattering FWHM on the order of 0.1 mrad will have a small effect on emittance growth; the effect of 0.4 mrad scattering will be significantly greater. Scattering in thin carbon foils will depend upon ion species and energy. Calculations show that in scattering of ^{1132}Xe by a 3.0 μgm carbon foil, half-angles should be on the order of 0.1 mrad at 1.0 MeV/u but will be on the order of 1 mrad at 0.1 MeV/u (3). Some experimental data would be helpful in permitting us to be more precise in the estimates of scattering for this ring.

To study longitudinal emittance growth, a calculation was done in which ions are passed through the stripper (energy loss per stripping is taken as 3 keV/u), then through the buncher gap, then again through the stripper, etc. for the specified number of turns. After the first stripping there are n ion beams, where n is the number of stripped states. Each ion beam is assigned an intensity corresponding to its stripping fraction. At the second stripping, each ion beam generates an additional n ion beams, with appropriate q and intensity. During each turn, the mean charge state $\bar{q}$ is assumed extracted. Finally, the superposition of all extracted beams yields a distribution which can be measured in terms of phase spread and energy spread.

ion	A	$\bar{q}$	Δq max.	Δq/$\bar{q}$ max.	h	peak kV	$\sigma_{dT/T}$ %	σ_{rev} rev deg	σ_{prod} (rev deg)* (%dT/T)	Energy increase %	extr. %	stripper intensity %
Ne	20	5	1	0.20	20	120	5.23	2.1	11.02	1.05	75	196
Ar	40	8	2	0.25	10	120	0.46	3.5	1.63	-3.25	77	279
Kr	84	11	3	0.27	10	90	2.42	2.4	5.78	-0.60	86	346
Xe	132	17	4	0.24	10	140	2.52	1.9	4.89	-0.85	72	438
U	238	21	5	0.24	10	160	1.96	2.0	3.98	-1.15	85	506

Table 2. Stripper Ring optimum performance for T=0.2 MeV/u ions. Revolution requency is 0.378803 MHz.

In the calculations, for each ion species and incident energy, the three buncher variables- phase, harmonic number, and peak rf voltage- were found which gave the smallest growth of longitudinal emittance in the extracted beam. These results are shown in Table 2, for 0.2 MeV/u incident energy, and in Table 3, for 1.5 MeV/u incident energy. The extracted mean energy was slightly lower, in most cases. Energy spread FWHM is given as a percent of mean energy; phase spread FWHM is given in terms of revolution frequency (not the rf frequency).

The spreads in energy and phase represent an increase over initial energy and phase spreads, presumably these spreads will combine quadratically. In the case of Ar at 0.2 MeV/u, the low value of ΔT/T suggests that some additional improvement might be found for the other ions.

ion	A	$\bar{q}$	Δq max	$\Delta q/\bar{q}$ max.	h	peak kV	$\sigma_{dT/T}$ %	σ_{rev} rev deg	σ_{prod} (rev deg)* (%dT/T)	Energy increase %	extr. %	stripper intensity %
Ne	20	8	2	0.25	10	70	0.83	0.092	0.0076	-0.09	99	206
Ar	40	13	3	0.23	30	70	0.79	0.110	0.0087	-0.11	98	290
Kr	84	22	5	0.23	30	90	0.84	0.121	0.0101	-0.11	94	472
Xe	132	30	5	0.17	40	90	0.72	0.112	0.0081	-0.11	95	426
U	238	43	5	0.12	40	120	0.48	0.088	0.0042	-0.09	91	509

Table 3. Stripper Ring optimum performance for T=1.5 MeV/u ions. Revolution frequency is 1.043126 MHz.

Studies will continue, with more sophisticated calculations (such as higher order magnetic focusing effects, and coupling of longitudinal and transverse forces) to verify these results and to relate them to realistic beams and experiments forseen for the ISL facility.

Proposed Test Facility

The 88" Cyclotron at LBL can be used as a source of ions to test ring performance. It can deliver a wide range of ion species at suitable energies. A plan showing the proposed installation in an existing cyclotron cave is shown as Fig. 3. One of the existing cyclotron transport lines will be redirected to inject into the ring. Also installed in the cave will be an rfq, originally used as a Bevatron injector, which can be used as an alternate injector to the ring, for 0.2 MeV/u light ions. The rfq will be useful because the cyclotron availabe cyclotron time is limited by commitments to other experiments.

The value of a such a test facility to a future ISL proposal will be great. The stripping enhancement ring is an untried concept, but any ISL facility which proposes to use such a ring to enhance intensity output will have to be sure of its success. The only way to know this is to perform tests with such a ring beforehand. The cost will be modest, and the ring components can be reused in an ISL facility, wherever it may be.

Questions to be studied include stripper foil lifetime, required thickness, resulting charge states, all as a function of ion species. The ease of tuning the magnetic elements and the operation of the buncher will need to be understood. The intensity of the extracted ion beam can be measured, and compared to the intensity of the input beam. The transverse emittance can be measured, and compared to input emittance. After passing through a bending magnet, the energy spread can be measured.

References

1. F. Selph, Proc. of the ORNL Workshop on Prod. and Use of Intense Radioactive Beams at the IsoSpin Laboratory, CONF-92210121, 359-362 (Oct. 1992).

2. K. Shima et. al., Atomic Data and Nuclear Data Tables **51**, 173-241 (1992).\

3. K.E.G. Loebner, Proc. of the ORNL Workshop on Prod. and Use of Intense Radioactive Beams at the IsoSpin Laboratory, CONF-92210121, 353-356 (Oct. 1992).

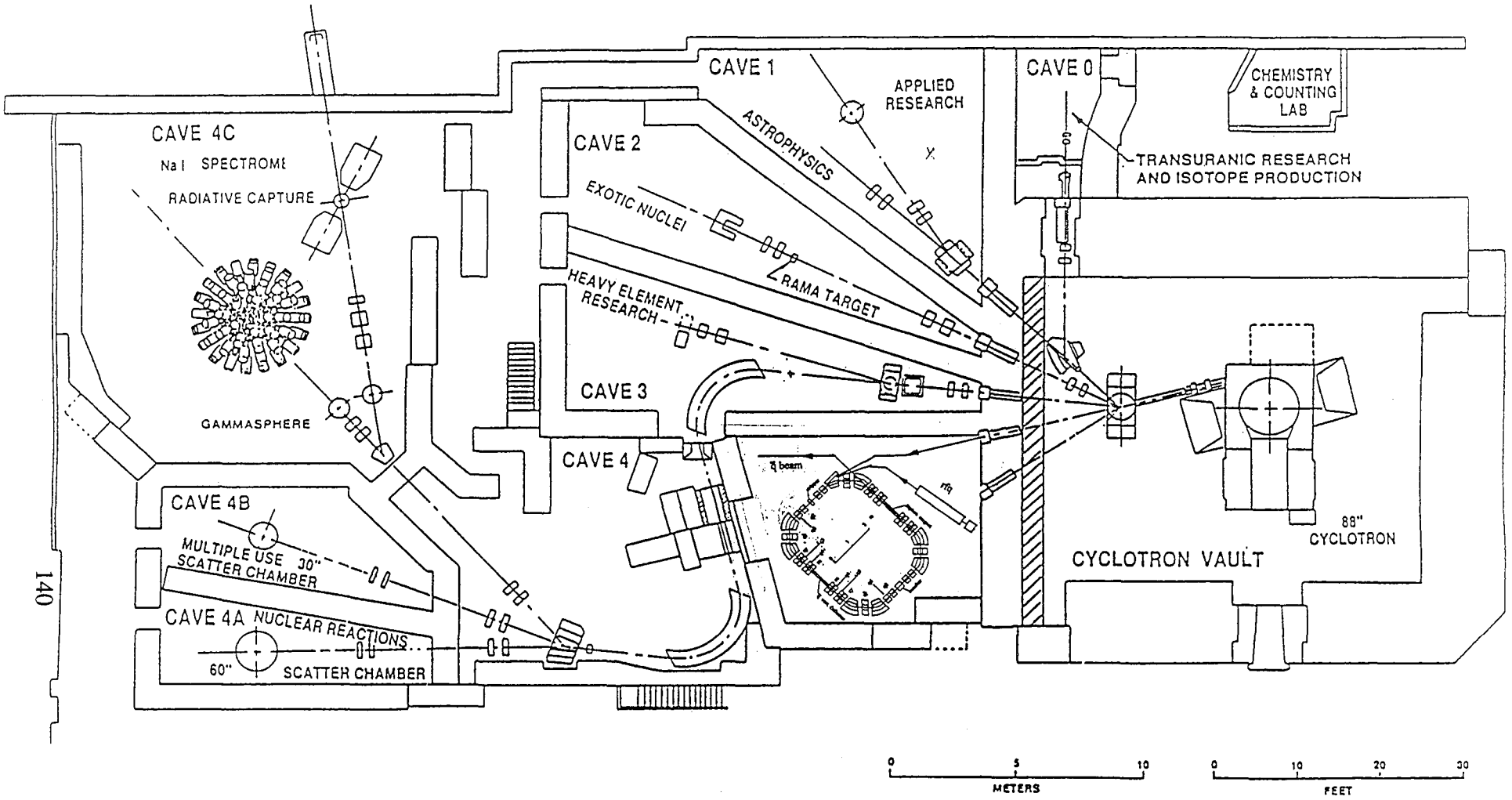

Fig.3. Schematic showing the proposed stripping enforcer ring installed at the 88-inch cyclotron.

Cyclotron Options for an ISL Post-Accelerator

D. J. Clark
Lawrence Berkeley Laboratory
1 Cyclotron Road, Berkeley, CA 94720, U.S.A.

Abstract

A brief review is made of some options for the use of cyclotrons as post-accelerators for an ISL project. Some comparisons with the linac option are made.

Requirements

It is assumed that the post-acelerator is required to accelerate all mass values from A = 1 to 240, from energies of the 100 kV source platform to 25 MeV/u. This can be done by using various combinations of accelerators. This workshop concentrated on the use of linacs for this purpose, particularly at the difficult low energy region. However it is also interesting to see what is possible using cyclotrons.

Options

The options can be classified according to how many stages are used, what starting charge states are used and whether we use only cyclotrons or a combination of cyclotrons and linacs. We will design for the most difficult case, A=240 at full energy of 25 MeV/u. Lower energies can be produced with lower cyclotron magnetic fields, and lower masses have higher Q/A values, giving the same energy with lower magnetic fields or fewer stages. Some options are listed as follows:

1. Use all cyclotrons
   A. Starting charge state Q = 1.
   B. Starting charge state is high.
2. RFQ first stage, Q = 1. Cyclotrons for later stages.

Option 1A

Option 1A uses all cyclotrons. The first question is: how many cyclotrons do we need? To determine this we use the equation for energy of a cyclotron: $E/A = K (Q/A)^2$, where K is the non-relativistic energy constant for the magnet, generally in MeV. This equation tells us, for example, that if we were to try to use only one stage, the K value would be over 10^6 MeV. This would be a Tevatron, entirely too large for a cyclotron. So we need to use the largest practical cyclotron and several stages. A good example is the successful NSCL K1200 at Michigan State University. The energies and charge states at each stage are as follows:

Stage	Q Accel.	Final E/A
1	1	.021
2	6	.75
3	35	25

The first stage would be injected axially by the 100 kV source beam. The second stage would be injected radially, with stripping by a carbon foil located near the cyclotron center so that the beam is centered after stripping. The third stage would be injected radially in a similar way. The injection stripping losses would be up to a factor of 6 in stripping in stage 1 and 2, or a factor of 36 total, for the case of 25 MeV/u, A = 240 shown. For lower energies and masses only 1 or 2 stages may be needed.

There are many questions to be studied in this system, including the problems with carbon foil stripping at only .021 MeV/u, and the various harmonics, rf frequencies and magnetic field levels for variable particle and energy operation.

Option 1B

If an ECR source is used, high charge states can be produced and the energy of one cyclotron is greatly increased. For example, to get 25 MeV/u, A = 240 beams, one K1200 cyclotron would need Q = 35. This is close to the peak of the charge state distribution of present advanced ECR sources. The great advantage of this system is the elimination of stripping foils and the resulting gain in transmission. The beam is stripped in the source. There are questions to answer about the efficiency of the source for converting atoms into high charge state ions, for gases and solids, and about reducing the gas flow from the target to the low value required by the ECR. The GANIL group is planning a system like this. If this idea works the linac post-accelerator would also become much simpler.

Option 2

In looking at Option 1A we see that the large K1200 Stage 1 cyclotron can reach only .021 MeV/u or 5.0 MeV. Using 3 dees, 6 gaps, at 100 kV each, it has about 500 keV/turn giving only 10 turns total. This doesn't make good use of the magnet. The reference design RFQ1 reaches .01 MeV/u and a slightly larger RFQ could probably reach .02 MeV/u. The RFQ is a much simpler and cheaper device than a K1200 cyclotron. So we could think of a first stage RFQ replacing the Stage 1 cyclotron of Option 1A. Its beam could be allowed to debunch and then a buncher would rebunch it to match the variable cyclotron frequency. Replacing Stage 2 of Option 1A with a linac would not have such an obvious advantage. One could also look at using cyclotrons after RFQ2 in the reference design.

Cyclotrons vs. Linacs

Cyclotron transmision is lower than that of linacs. For axial injection, the efficiency from source to extracted beam can be 20-25%. Part of this is the extraction efficiency, the ratio of external to internal beam, which can be 70%. The stripper foil losses are similar for both systems. The above Options 1A or 2 have 2 strippers, while the linac option has 3 strippers, with a the option of a stripper loop to replace some strippers. A stripper loop is not an option for the cyclotron since the stripping is necessary for injection into stages 2 and 3 of options 1A or 2.

Beam quality, transverse and longitudinal, can be excellent for a modern linac. It is worse for many cyclotrons because of multi-turn extraction, in which several turns are extracted at once, adding to both the transverse and longitudinal emittance. However some cylotrons have developed single-turn extraction, giving excellent emittance, at the expense of intensity. Transmission is dependent on good bunching and careful beam control during the injection process. If good beam quality is produced in the first cyclotron, the transmission is high through the later stages. This area needs further study.

One component of the post-accelerator system is the high resolution separator, which is needed to separate the closely spaced isobars. The cyclotron separates closely spaced Q/A values by its basic resonant operation. The resolution is proportional to the number of turns and the harmonic number of the rf. Typical resolution available is 10^3 - 10^4. The resolution can be varied by changing the dee voltage, which changes the number of turns. So the first cyclotron in the system could be used as a mass separator.

Report from Working Group 1 - Ion Sources & Separators

Group Leader: Hermann Wollnik
Oak Ridge National Laboratory
Oak Ridge, TN 37831

Reporter: Jose R. Alonso
Lawrence Berkeley Laboratory
1 Cyclotron Road
Berkeley, CA 94720

Abstract

This Working Group concentrated on issues associated with ion sources and separators, summarizing both the state of the art in these areas as well as needs and requirements for first stages of the ISL post-accelerator. This report is divided into three sections: a summary of presentations made to the Working Group, a comparison of ion source technologies, and a discussion of front-end configuration issues. A concluding section summarizes key design issues novel to the ISL application, and points out areas where technology development is required.

Presentations:

G. Alton (ORNL)

Alton presented work currently underway for the Holifield Radioactive Ion Beam Facility (HRIBF) at the Oak Ridge National Laboratory (ORNL) (cf separate contribution in these proceedings). The central region of the ORIC cyclotron is being modified to optimize the generation, acceleration, and extraction of light ions (^{1}H, ^{2}H, ^{3}He and ^{4}He) from the machine which will be used to produce radioactive species in a thick target, close-coupled to an ISOL target/ion source located on a high-voltage platform. The platform will serve as a second injector for the 25-MV tandem accelerator. For optimum production, primary beam energies of 10 to 70 MeV will be utilized. In order to avoid excessive activation of the cyclotron and beam transport system to the target/ion source, beam intensities and beam power will be limited to $\approx$100 μA and 2 kW, respectively. Because of the low energies available from the ORIC, fusion-type reactions will dominate; therefore, the target materials must be carefully selected to optimally generate the radioactive species of interest. for example, CeS or ThS are candidate target materials for generating $^{32}Cl^{-}$ and $^{33}Cl^{-}$ radioactive beams (RIBs) produced in the respective reactions, $^{32}S(p,n)^{32}Cl$ and $^{32}S(d,n)^{33}Cl$.

A CERN ISOLDE-type, high-temperature, electron-impact ionization source has been designed, fabricated, and is presently being evaluated for initial use for generation of radioactive ion beams of elements with low electron affinities. Because of the necessity of injecting negative ion beams into the 25-MV tandem for post-acceleration, positive-ion beams from this source must be converted to negative-ion beams through charge exchange. A complementary negative-surface ionization source has been designed for direct generation of negative-ion beams from elements with high electron affinities (e.g., the halogens [F, Cl, Br, I and At]); this source will be a direct replacement for the CERN ISOLDE-type electron-impact ionization source; negative ions will be formed by thermal evaporation from a low-work-function LaB_6 surface which will be maintained at 1100°C. A heat sink will be placed between the target and the ionizing surface which will be maintained at a temperature high enough to allow transmission to the ionizing surface, but low enough to condense less volatile components which otherwise would poison the LaB_6 ionizer.

In order to minimize the diffusion release times, it is desirable to heat the target to high temperatures (up to 2000°C, for example); selection of wall materials with low enthalpy values is

also desirable to minimize hold-up times due to surface adsorption between the target and ionization chamber of the source. Attempts will be made to reduce the hold-up times of species during transport from the target to the ionization chamber of the source by coating all surfaces that will be exposed to the vapor with Ir. Experiments are planned which are designed to determine the effectiveness of this concept.

Ion beams will be extracted from the source at energies up to 50 keV and momentum analyzed in a split-pole, homogeneous-sector, magnetic-field isotope separator with a bending angle of 151 degrees and a bending radius of 0.56 m; the isotope separator is expected to have a nominal resolution of 800 and a maximum resolution of 2000. When positive-ion sources are used, the extraction energy is chosen to optimize charge-exchange reactions in Cs or Rb vapor following momentum analysis. After momentum analysis, all ion beams will be post-accelerated to energies up to 300 keV for injection into the 25-MV tandem accelerator.

The overall performance of the system, in terms of ionization efficiencies, beam emittances of the sources considered, and beam transport from ion source to the tandem accelerator, should be as good as or better than state of the art. The HRIBF is scheduled for first testing of ORIC and all equipment located on the high-voltage platform in April 1994; in these tests, low-intensity RIBs will be produced with proton beams in the target ion source, momentum analyzed, and post-accelerated to the 300 keV injection energy. The HRIBF is scheduled for commissioning in April 1995, at which time the experimental program will be initiated.

K-N. Leung (LBL)

Leung presented his ion source design as a possible candidate for radioactive beam production systems. The Multi-Cusp (bucket) source offers many potential advantages in this application: good ionization efficiency, wide range of operating temperatures (>1500°C if needed), good emittance and low noise, flexible geometry, good lifetime and reliability of operation. It operates over a wide range of gas pressures, can be configured for either positive or negative ion production, and can be optimized for high yield of higher charge states (2+ or 3+). Although the source has found wide acceptance in the conventional accelerator community, some questions related to specific needs of the RIB application must be answered: absolute efficiency of conversion of material from the target into a beam of the desired charge state; hold-up times in the source; specific materials and design questions relevant for operation in the high radiation fields (protection of the permanent magnets, wall-liner material, filament material or rf-electrode coating).

M. Nitschke (LBL)

Nitschke presented a concept for a wide-band separator system called BRAMA (Broad Range Atomic Mass Analyzer). (c.f. separate contribution to these proceedings.) This device would considerably improve the overall efficiency of a radioactive beams facility by making use of the diversity of reaction products generated simultaneously from spallation and fission targets. These reaction products are transported to the source and ionized with little selectivity, so the beam produced consists of many atomic and isotopic species. Typical separator systems must be tuned for transmission of a single species, most of the others are lost. The BRAMA concept, based on an Elbek-type spectrometer, would provide an extensive focal plane allowing the separation of different q/A constituents along this focal plane that could then be tapped off for specific applications. Specifically, several experimental ports could be serviced simultaneously. Feasibility studies indicate such a scheme could be employed for bombarding a radioactive target (atoms accumulated at one site of the spectrometer) with a radioactive beam (extracted and accelerated from another site). (E.g. for 10^{10} ions/sec at each channel, beam and target sizes of 1 mm^2, a target lifetime of 1000 seconds and a reaction cross section of 100 mb, the reaction rate will be 1/sec.) Another application could be the dedication of "unused" ports to constantly monitor and provide tuning information for the spectrometer. Such a concept would operate most

efficiently with a "universal" (plasma) source capable of delivering the maximum number of reaction products as ions to the spectrometer entrance.

Ion Source Technologies:

Reference was made to Kirchner's excellent review in these proceedings of the different ion sources available for radioactive beam applications. The Working Group spent considerable time analyzing the performance of several of these sources, with specific reference to beam quality produced, and matching to a high-quality separator. Resolving power for such a device contemplated for RIB research could be as high as 30,000, but to achieve this value requires very high-quality incident beams. The energy spread of the beams (characterized as the ion temperature in the source) should be below about 0.5 eV, if no additional energy-compensating stage is used, i.e. a large electrostatic sector field. The unnormalized emittance of the beam entering the spectrometer should be below 2π mm-mrad. The table below summarizes the consensus of opinion on the achievable performances of different source technologies.

Table I

Ion Source Inter-comparisons (at 30 kV extraction potential)

Source Type	ε π mm-mrad	M amu	ΔE eV	ε_n π mm-mrad
ECR	**100**	**40**	**(5-10)*q**	**.15**
FEBIAD	**<10**	**84**	**<5**	**≈.01**
Hot Cavity Ionizer	**<2**	**40**	**.4**	**<.01**
Surface Ionizer (+)	**<2**	**40**	**.2**	**<.01**
Surface Ionizer (-)	**<2**	**40**	**.2**	**<.01**
Cusp	**1**	**40**	**2-3**	**<.01**
Laser	**?**	**?**	**?**	**?**

Notes:

- All sources have respectably low emittances, though achieved ECR performance is notably inferior. Optimization of this source could improve its usefulness for RIB applications. Such improvements seem feasible since so far ECR ion source developments have focused on maximum output of highly charged ions, optimization for small energy spread has received little attention.

- Performance figures are given for one set of parameters (extraction potential, mass); optimization for other masses and experimental configurations will undoubtedly yield somewhat different values.

- Ion energy spreads are lowest for the cavity and surface ionizers, these would perhaps be the best sources to interface with a very-high resolution separator.

- Not enough is known about laser source performance now to make a meaningful comparison with other technologies.

It should be noted that optimization of source performance for radioactive beams applications will emphasize parameters quite different from other, more conventional applications. While low emittance and energy spread are of course important, overall efficiency of ionization from neutral atom to a single charge state, very short hold-up times and ability to operate at high temperatures in a highly radioactive environment are of critical importance.

Maximizing radioactive beam current requires delivering at the high-energy end of the post-accelerator the highest possible fraction of the selected ions. Highest efficiency is obtained if all the radioactive atoms can be converted in the source into ions of a unique charge state. The best case is expected for ions of charge-state 1. The sources described elsewhere in these proceedings have in fact very high atom-to-ion conversion efficiencies for singly-charged ions. However, this leads to limited ion energies and a complex post-accelerator design because of the extreme rigidity of the ions. Cost optimization usually calls for one or two stripping stages to increase the charge state of the ion during the acceleration process. Each of these stages, if conventional stripping foils are used, is accompanied with a significant dilution of beam purity (hence to beam loss) owing to the distribution of charge states emerging from the foil. The problem is particularly pronounced for the heaviest elements: for masses greater than about 100 one should not expect more than 15% of the beam to emerge in the most-probable charge state. Thus for such ions, each stripping station entails a loss of a factor of 7, or about a net efficiency of 2% transmission through an accelerator system with two strippers. The problem is not so severe for lighter ions with narrower distributions, but it still significantly affects the overall transmission efficiency. Several ways exist for maximizing efficiency: the use of a charge-state "enforcer" ring (cf separate contribution in these proceedings) that keeps passing the beam through the stripper on each pass through the ring, extracting from the ring only those ions in the "right" charge state; design of linac sections that can accelerate more than one charge state (experience at the SuperHILAC has shown this to be difficult because of significant phase-space dilution and emittance growth of the beam); or the use of a high-efficiency, very high-charge-state ion source. An example of the latter would be an ECR source from which ions might emerge with sufficiently high q/A ratios ($q/A \approx\geq 0.2$) that postacceleration could be accomplished without stripping. Achieving suitable efficiency (from incoming atom to ion in a unique, and very high charge state) from such a source is an interesting problem.

Front-end Configuration Issues:

Another difference between a RIB facility and a conventional accelerator configuration is that in the latter the ion source is normally very tightly coupled to the first stage of rf acceleration, to increase the ion velocity as quickly as possible to minimize transport and space-charge problems. However, because of the "universal" nature of the ion sources to be employed in the radioactive ion beam application, efficient isotope separators of high mass resolving power are needed to identify and isolate the specific ion species desired from the many emerging from the source for further acceleration. Such an isotope separator must feature, furthermore, an extremely low mass cross contamination between neighboring isobars and even between neighboring elements within the same isobaric chain since the production rates of such neighboring nuclei often differ by many orders of magnitude. This separation should take place prior to any rf acceleration, to optimize beam quality and separation capability. To achieve the required degree of species-purity it is anticipated that two stages of separation may be required, the first with a resolving power of about one in a thousand (adequate for isotopic analysis), and also a second, to separate elements with the

same A, with a resolving power of around one in twenty-thousand, so that ions can be separated whose Q-beta/A value is larger than perhaps 5 MeV/100 amu.

The configuration of the front-end: the type of separators used (cf separate contribution in these proceedings), the ion source characteristics, experimental stations feeding directly from the separators, and the post-accelerator interface itself, presents a large number of design challenges. Some types of separators require extremely low energy spread from the source and very high stability of accelerating voltages from the source, while others are more forgiving, but have their own limitations. While this Workshop has not addressed the full range of design parameters and options, one parameter that was investigated at some depth was the question of relative high-voltage potentials between the various elements, and more specifically, arguments for holding individual stages at ground potential.

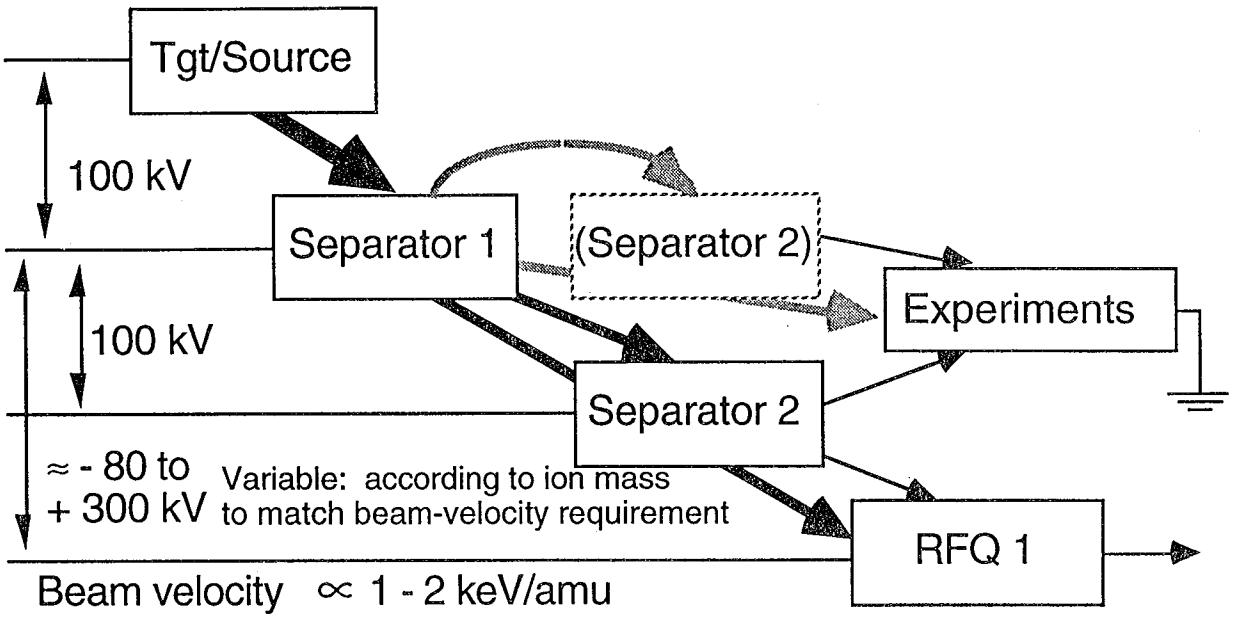

Figure 1: Front-end Configuration Schematic

Figure 1 shows a schematic of the various elements of the front-end of a RIB facility. Arrows represent ions transported between the various elements, vertical height related to the potential of each element. Voltages between the different stages are shown based on generally acceptable values: 100 kV is within the state-of-the-art for this type of application, and appears to be suitable for achieving good beam emittances and species purification. The schematic indicates that beams can be used with or without a second separator, and that this second separator can either be kept at the same potential as the first or ions can be further accelerated between separator stages in order to eliminate ions that were formed initially at slightly wrong energies due to charge-exchange reactions in the initial ion acceleration canal. The configuration is dependent on the specific separator types used, and the particular goals of the experimental program. The voltage between the separator(s) and the first stage of post-acceleration is determined by the particular design of the first stage of post-acceleration, shown here as an RFQ, and the ion species to be accelerated. If an rf accelerator is used, the mechanical dimensions of the accelerator require a fixed velocity profile of the ions traversing the structure. Thus the voltage between separators and

the accelerator must be adjustable to bring the ions into this accelerator always with the proper input velocity. Lighter ions will have to be decelerated for proper matching.

The question of where to establish ground potential for this system of electrostatic voltages is quite complex; strong technical arguments can be made for the advantages of grounding each of the elements of the front-end. For the most part, however, good technical solutions exist for the case where each of these elements is not grounded. The only area in which general agreement was expressed was that any experiments operating off of the separators must be at ground potential. The complications to the experimenters of having to float their apparatus would be prohibitive.

Floating the target-ion-source system presents the problem of compensating for drain on the power supply from the primary beam striking the target. In addition to the anticipated ISL proton current of up to 100 μA steady state on the target (with potentially much higher peak currents), one must also consider the electron backstreaming currents or discharge currents generated when the primary beam strikes the target. For example, at ISOLDE, the PS Booster delivers about 2 amps (instantaneous current) for about 1 μsec at an 0.8 Hz repetition rate (≈ 2 μA average beam current) to the target. In this case the beam traverses a region of air at 1 atm. To prevent the high discharge currents, the target is dropped from its normal 60 kV to ground during the beam pulse, then is restored to its high-voltage setting (to a stability of 1 part in 10^5) in a few milliseconds after the beam pulse. The anticipated higher current at the ISL increases the air-activation problem for any air-path for the primary beam, rendering more attractive the option of maintaining the target in vacuum. Such an option would be important as well should it be desired to keep the target at its high-voltage operating potential throughout, as would be necessary were the primary beam to come (continuously) from a cyclotron. To maintain the operating voltage will require high-power charging and feedback systems; complex, but not outside the state-of-the-art.

The most likely component to be grounded is the separator system. This will eliminate the requirement of having high-voltage columns on all the lines to experiments taking beam directly from the separators. If the separators were to float, and the source be maintained at ground, then the ions reaching the experiments would in fact do so at zero velocity, thus creating experimental complications. In addition, providing power and suitable mechanical support systems for a high-voltage platform add significant cost and complication to the design of separator systems.

Rf accelerators are normally thought of as being at ground potential, although there is no *a priori* reason why this should be so. The RFQ community at the Workshop actually did not feel uncomfortable with the idea of floating the first RFQ to ensure proper velocity matching of the beam. Note that floating the first RFQ (to different levels for different q/A beams) will require an additional rf cavity to adjust the exit velocity from this RFQ to compensate for the velocity gain (or loss) in bringing the beam from the potential of this RFQ to ground (presumably the potential of the remaining rf accelerators).

It was noted, on the other hand, that single-gap cavities placed upstream of the first RFQ accelerator could prove very helpful. Such cavities could bunch the beam, and can in fact accomplish this at least as efficiently as the normal RFQ bunching methods, possibly yielding even smaller logitudinal phase-space distributions. With higher voltage cavities also the beam-velocity could be properly matched to the first RFQ even if this accelerator were maintained at ground potential.

The decision between these two options, whether to float the first RFQ or add single-gap cavities and maintain the first RFQ at ground potential, will depend on a detailed optimization of beam dynamics calculations and economic factors for the specificied range of performance requirements.

Conclusions

Several salient points emerged from the discussions of the Working Group. First, and perhaps most important, there are no technological "show-stoppers" in the current concept of the ISL. It was felt that the parameters and performance sought were within the capabilities of available technologies, as well as being appropriate for the ISL to discharge its stated mission. However, actually achieving this performance is not straightforward. It will require considerable extension in the state of the art in a number of areas. Specific areas for R&D are outlined below.

With regard to ion sources, all the source technologies discussed will deliver beam that is acceptable for all the post-accelerator concepts. However, the most stringent constraints on source requirements will come from matching to the acceptance of the separators. Specifics of maximum transverse emittance and energy spread will have to be closely coupled with the particular separator designs employed.

There are a number of aspects of the ISL that are challenging the accelerator physicist to new areas beyond the normal configuration of accelerator systems: the extremely wide range of beam parameters (q/A, intensity), the complexity of the low-velocity transport and separator systems, and the concept of having to float rf accelerator sections. These challenges should stimulate creativity in addressing new problems, none of them were viewed as insurmountable.

Specific areas where significant R&D efforts should be concentrated are: source performance (high efficiency, low hold-up time, low emittance, low energy spread, good high-charge-state performance, operation in high radiation environment, design for remote handling, decontamination issues); schemes for maintaining high voltage-stability for the target/source in the presence of intense, quite-possibly pulsed primary beam current loads; designs for high performance mass separators for low and high beam currents; as well as the placement of complex, high-power equipment on high-voltage platforms.

Report from Working Group 2 - RFQs & Linacs

Group Leader: Jerry A. Nolen
Argonne National Laboratory
Argonne, IL 60439

This Working Group concentrated on issues associated with low-β, low (q/A) accelerating structures and Radio Frequency Quadrupoles (RFQs). Since a large number of outstanding presentations and contributions were already made, as evidenced by the articles in this proceedings, we will simply present, in their bare form, the questions that were raised and the collective answers to those questions in the following. The issues dealt with in this group included specifications of longitudinal and transverse beam emittances, radioactive contamination issues, tunability over large dynamic range, stripping and separator issues, normal conducting and superconducting RFQs, injectors, high voltage platforms, cyclotron options and general issues of parameters and design.

Questions and Answers

Q. What is the specification for longitudinal emittance?

A. With prebunching before RFQ1, a specification of 20π keV-ns seems possible. With this specification, energy resolutions of 0.1% are easily achievable.

Q. What is the specification for transverse emittance?

A. A variety of ion sources (as discussed here by R. Kirchner) have emittances of 10π mm-mr or less at 60-100 keV energies. The normalized emittances of such sources are about 0.01π mm-mr. ECR ion sources generally have larger emittances due to the axial magnetic fields. There are also low-field ECRs for low charge states and higher field ECRs for higher charge states. ISL beams from the high charge state ECRs would bypass RFQ1. Hence, if RFQ1 had a normalized admittance of at least 0.2π mm-mr it would have a high transmission for most known ion sources.

Q. Are there issues related to contamination or radioactivity in resonators (superconducting or normal) due to beam losses?

A. This should not be a performance issue, but should be quantified. Transmission losses should be minimized, but the main issue is probably related to access for maintenance rather than performance.

Q. What are the issues related to diagnostics for tuning a broad range of intensities (10^2-10^{13} pps)?

A. There is experience with such beams, e.g. at the Bevalac, NSCL, and GANIL.

Q. What are the issues related to stripping?

A. There are many issues here. P. Bricault presented calculations done to choose the optimum energy for the first stripping of Uranium beams. A good choice for the first energy seems to be about 200 keV/A. More detailed optimizations are required, including the cost of MV at various energies and the practicality of foils and gases at various energies. A. Schempp discussed the idea of capturing and accelerating more than one charge state between the first and second strippers to gain a factor of 2 to 3 in beam intensity. This concept needs further investigation.

Q. Is the stripper loop concept likely to be useful at the ISL?

A. F. Selph presented the present status of his studies. It seems that the main remaining question is the beam quality at the output of the ring. Detailed simulations which include realistic foil thickness and the associated multiple scattering and energy loss/straggling effects are now needed. Such a ring has the potential to increase final beam intensities by a factor of 4 to 20, depending on whether one or two rings could be used. However, it is not clear that the beam degradation issue can be solved.

Q. Could a gas-filled separator play an important role in the ISL post accelerator?

A. M. Nitschke made an informal presentation on the features of a gas-filled separator and some previous experience. If used in place of the second stripper, it could provide a "Z" discrimination to remove certain beam impurities left by the high resolution separator. However, transverse emittance would be degraded; quantitative simulations of this device must be done.

Q. What is the present beam parameter list and best guess for the block diagram of the post accelerator?

A. We discussed these issues and with the help of a concept for RFQ1 proposed by A. Schempp have revised parameters.

Q. What are the special issues with the RFQs, especially RFQ1?

A. A preliminary design study by H. Schneider shows that the previous transverse emittance specification of 1π normalized is very hard to deal with. Also the longitudinal emittance after adiabatic bunching is very large. A. Schempp's proposal is to use a 10 MHz RFQ with a prebuncher/chopper to achieve excellent longitudinal emittance and an admittance of at least 0.2π mm-mr (normalized). Such an RFQ could start at 1 keV/A which may eliminate the need for the HV platform.

Q. Does the 100 nsec pulse spacing specification pose special problems?

A. With the present concept for a 10 MHz RFQ1 this is a perfect match. It would still be OK with a higher frequency RFQ as long as a 10 MHz prebuncher/chopper were used.

Q. Are the specifications for RFQ1 achievable? (mass 6 to 240 1 + ions, CW operation, good transverse and longitudinal emittances).

A. A. Schempp says this can all be done over an energy range from 1 to 10 keV/A with about 200 kW of RF power. A detailed design study of this RFQ should now be carried out.

Q. What are the possible roles for superconducting RFQs?
A. K. Shepard's experience is that he expects 50 MHz to be the lowest feasible frequency for superconducting RFQs, at least for now, due to mechanical stabilization requirements. Hence, they are most likely to play a role in the intermediate velocity regime of the post accelerator, and not at the low end.

Q. Is more than one injector for the post accelerator required or desirable?
A. The present concept for RFQ1 solves all of the basic problems for the first acceleration stage over the entire dynamic range of the proposed facility. However, for masses less than 25, RFQ1 is not required to reach 10 keV/A, so a bypass or alternate beamline may be desirable. Also, a high charge state ECR ion source would produce beams which would bypass RFQ1.

Q. What are the special problems associated with the HV platforms?
A. It is desirable to operate the primary production target and ion source at the highest voltage achievable. 60 kV has been used at ISOLDE for years, but at lower intensities than the ISL. It is speculated that 100 kV may be possible at the ISL, but this in not proven, and may require some R&D. With RFQ1 operating at an input energy of 2 keV/A, it would have to be on a HV platform at up to 380 kV. This seems possible, but if the input energy is reduced to 1 keV/A, the voltage requirement is reduced to 140 kV, and the HV platform may possibly be eliminated entirely by using a single cell rf cavity for velocity matching. This deserves further study.

Q. What structures are appropriate for the intermediate energy sections of the post accelerator?
A. There are several options for these sections: IH, RFQ, DT linacs, and superconducting or normal. In the relatively long section after RFQ1 and before the first stripper (1+ beams) transverse focusing is an issue due to the rigidity of these beams. The solutions chosen here are likely to vary from lab to lab.

Q. What are the possible roles for cyclotrons in the ISL post accelerator?
A. D. Clark gave a presentation on some of the options for using cyclotrons for either all or various sections of the post accelerator. In principle, cyclotrons could be used for the entire complex. One advantage the cyclotrons provide is an inherent high mass resolving power. However, a detailed solution based on cyclotrons has not been worked out. More work is required here to make cost, efficiency, and performance capability comparisons.

Appendix

Appendix A

R. Kirchner
(GSI)

Common requirements:

Universal:	suited for all elements
reliable	long lifetime
reproducible:	
stable:	no beam instabilities
compatible:	with beam optics

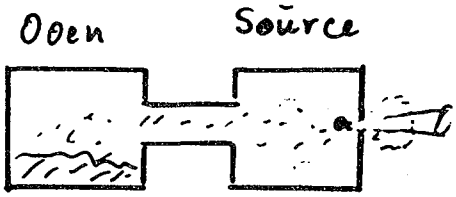

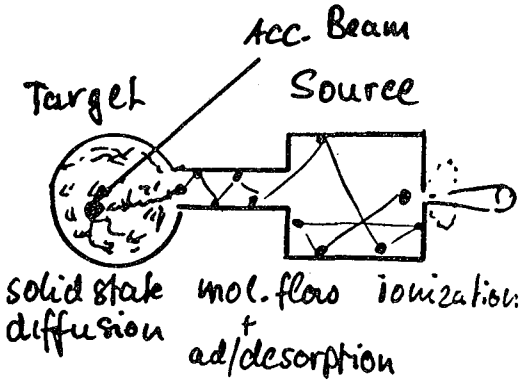

	Accelerator Source	ISOL Source
Input	Charge material: unlimited stable well-defined	Nuclear reaction products limited radioactive (short-lived) many elements (isotopes)
Output	intense ion current	efficient ionization fast release selective

Ion Source Classification

(ionizing mechanisms)

1. Electron impact
   - Low pressure arc discharge sources
   - Space-charge compensated electron-bomb. sources
   - Electron-cyclotron-resonance (ECR) sources

2. Heat
   - Positive surface ionizers
   - Negative surface ionizers
   - High temperature cavity ionizer

3. Light
   - Resonant photoionization (Laser-) sources

4. Penetration of matter
   - Ion guides

5. Electric fields

1.1. Low pressure arc discharge sources

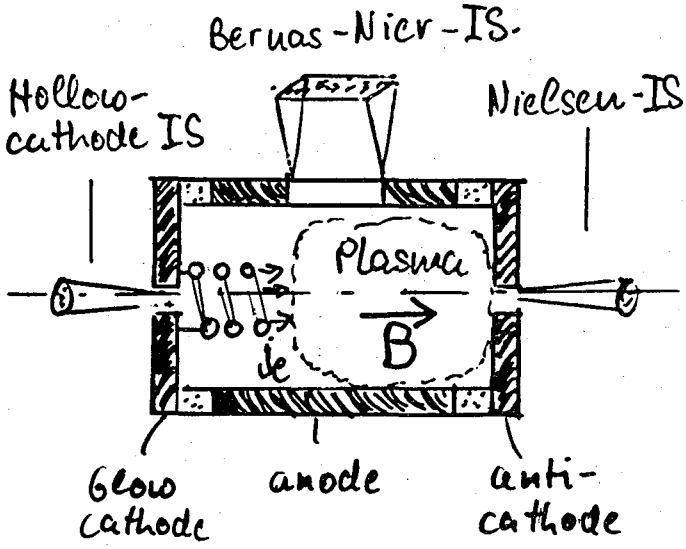

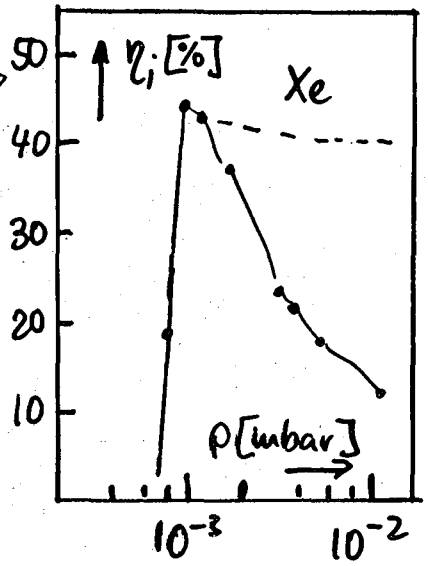

(+) High ionization efficiency (5-50%), $\eta_i \sim \tau \cdot j_e \cdot \sigma_i$

τ high: gastight enclosure; multiple passage radial ion confinement, preferred ion emission at plasma boundary

j_e high: extraction by double-layer, space-charge compensated by plasma, enforced by magnetic field

Universal source for all elements or compounds of sufficient volatility within the hot enclosure (up to 2000°C)

Emittance (95%, 30kV) $\lesssim 20\pi$ mm mrad $\Delta E < 5$eV

j_i high: ($\gtrsim 10$ mA/cm^2); tolerates high vapour load

(−) j_i high: requires medium intensity separator

Discharge Instabilities close to pressure threshold

1.2. Space-charge compensated electron-bomb. I.S.
Extraction of primary electrons by grid instead of cathode double layer

⊕ Primary electron current decoupled from plasma
→ stable discharge
→ high efficiency at very low pressure
→ j_i low, i.e. easily compatible with low intensity separators

⊖ Not suited for coupling of "volatile" targets

1.2.1 FEBIAD ion source (GSI 1975)
(forced electron beam induced arc discharge

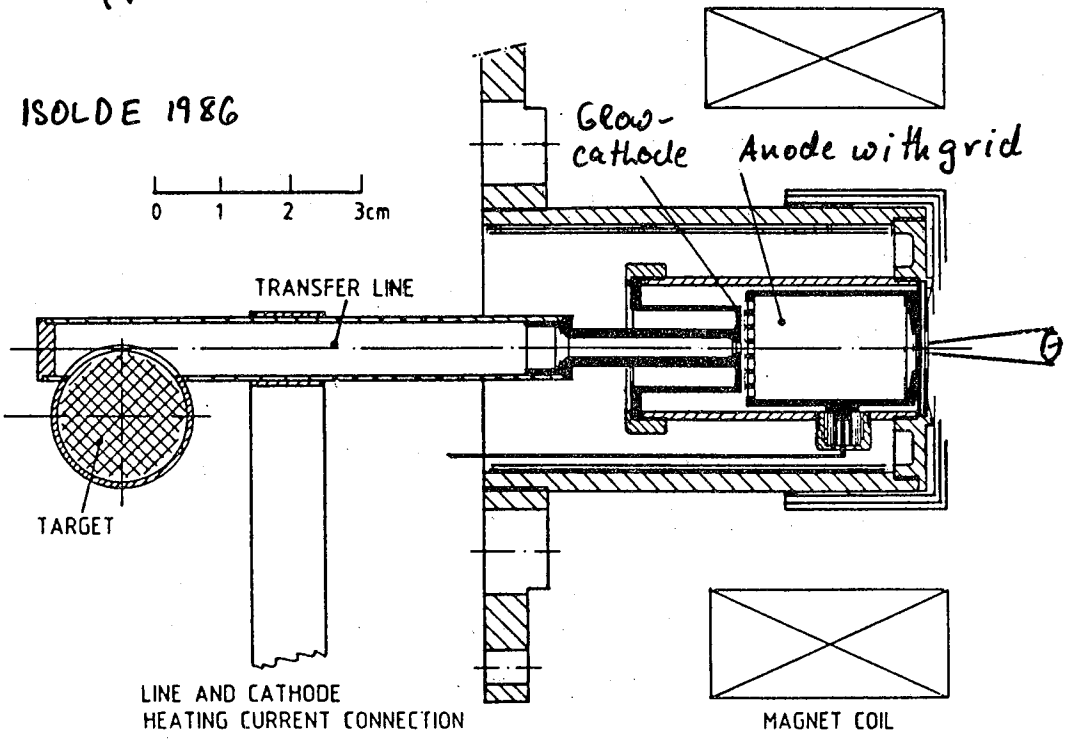

1.2.1. FEBIAD ion source

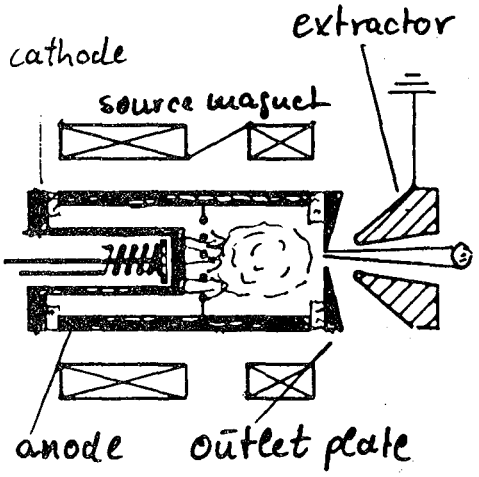

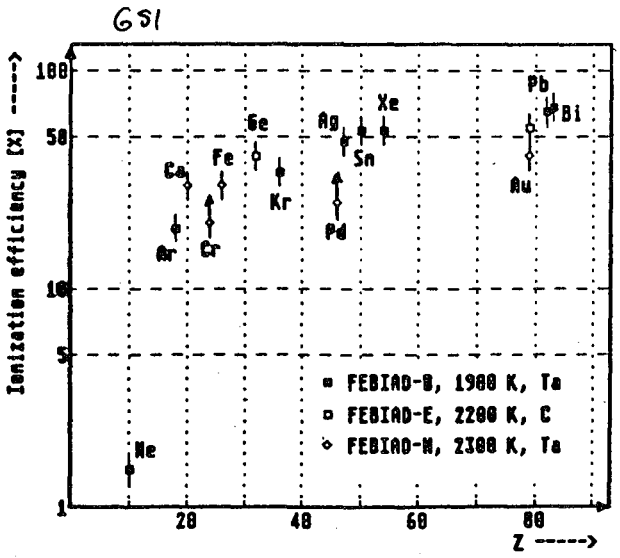

⊕

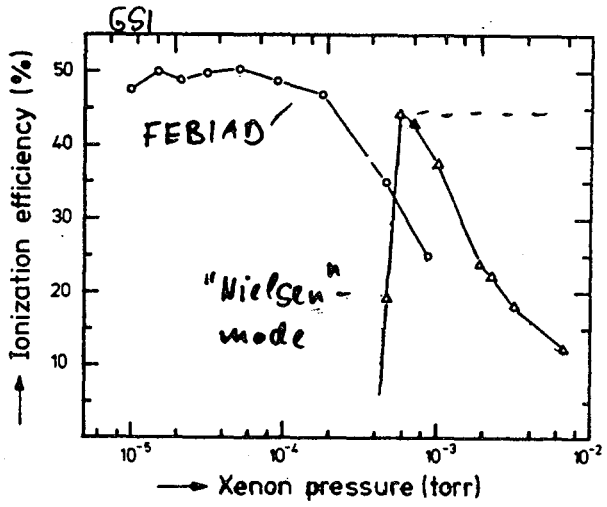

High and widely pressure-independent efficiency
Low j_i ($< 1 mA/cm^2$)
Emittance $< 10\pi$ mm mrad
$\Delta E < 10$ eV
High operation temperature (up to 2400K)

→ Nielsen i.s. for coupling to "oolahic" targets
Axial cathode-grid geometry → rugged + flexible design

⊖ Not suited for elements ≤ Ne, especially not for molecular compounds of C, N, O:
(CO, N_2, O_2 only inert at low temperatures)
(low degree of dissociation to C^+, N^+, O^+)

1.2.2 EBGP - ion source (LBL 1985)

(Electron beam generated plasma)

Radial cathode-grid geometry

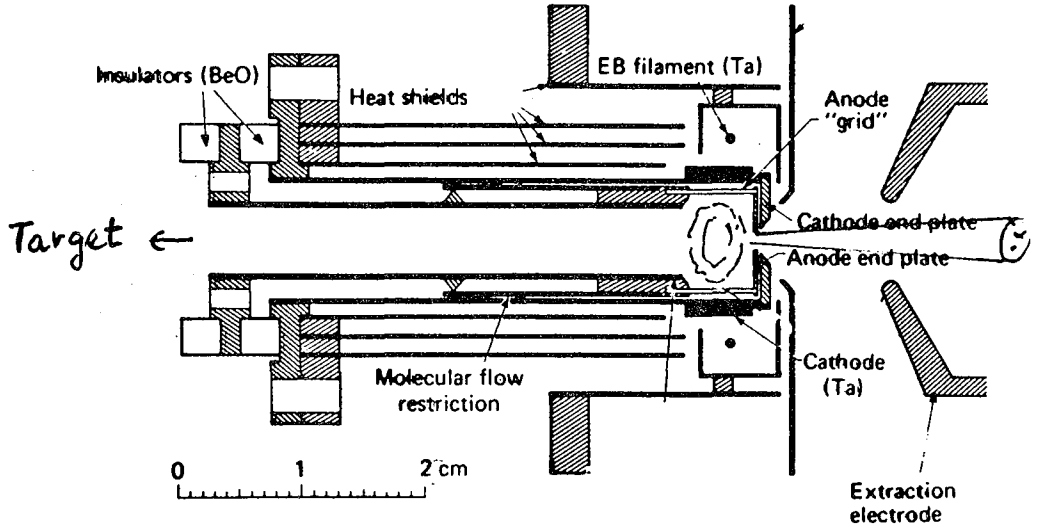

⊕ Similar as for FEBIAD
Higher temperature (≳ 2500K): "No" insulators
Active heat shielding

Primary electrons radially to axis:
→ High j_e → depression of plasma potential (i.e. ion confinement) without magnetic field
Easily convertible to Hot Cavity Thermoionizer

⊖ Delicate design and mounting
Not suited for C, N, O etc and for coupling to volatile targets

1.3. ECR ion source for 1^+ ions (Karlsruhe 1985 Leuven Vancouver)

(Electron-cyclotron-resonance)

Microwave-driven Rf-discharge in a magnetic configuration of axial mirror + radial hexapole field

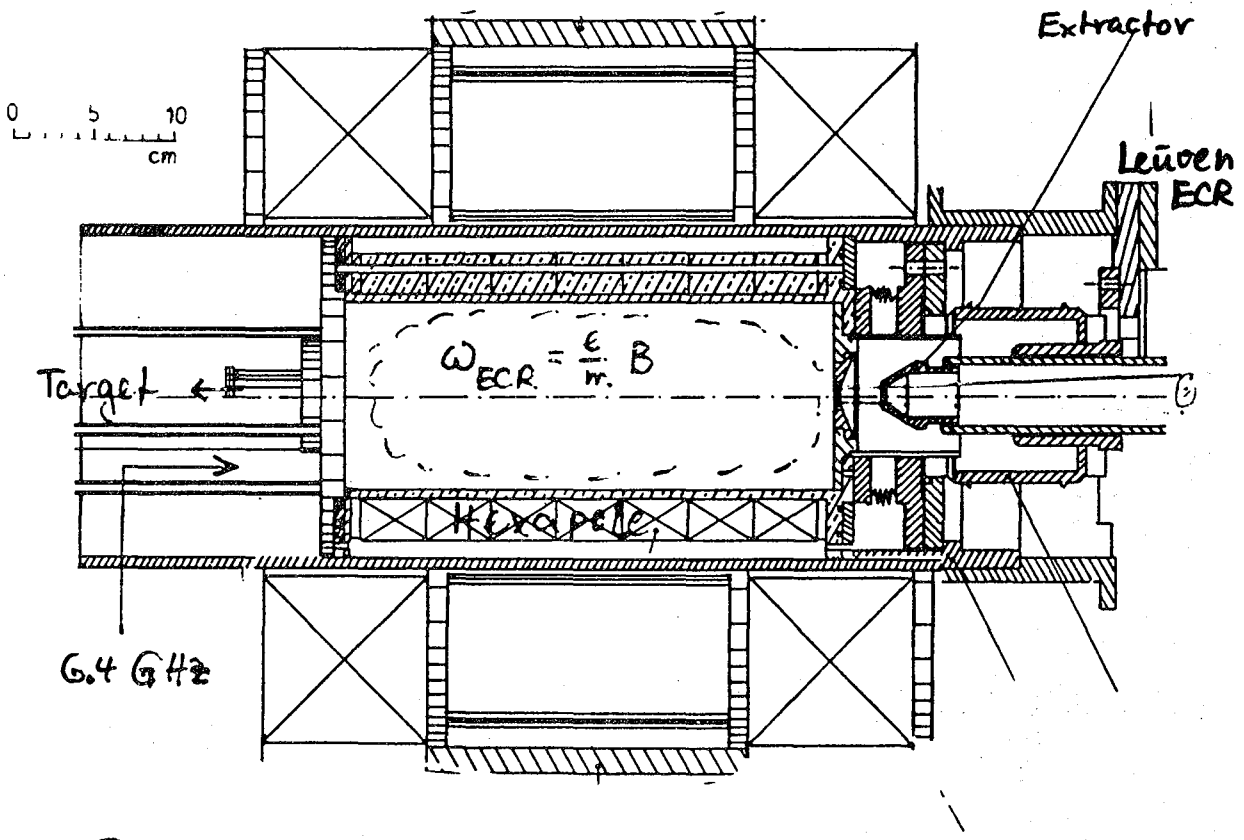

⊕ High density of energetic electrons
- → good ion confinement
- → High 1^+ ionization eff. for gases (upto 90%), especially for C^+, N^+, O^+ (effective dissociation of CO, N_2, O_2; handling possible due to cold enclosure
- → Optional: efficient prod. of multiply-charged ions

No "wearing" parts → Long + stable operation (for gases)

1.3. ECR ion source

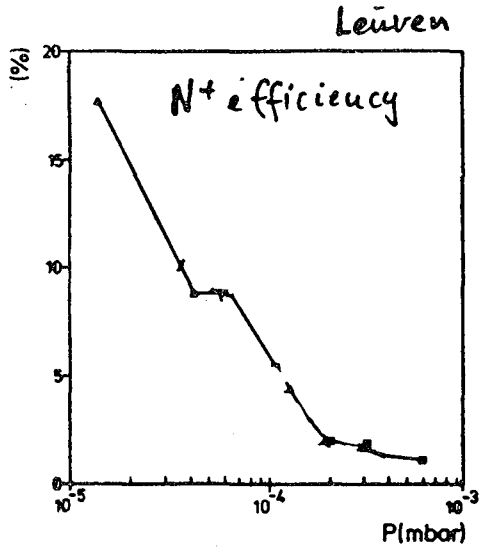

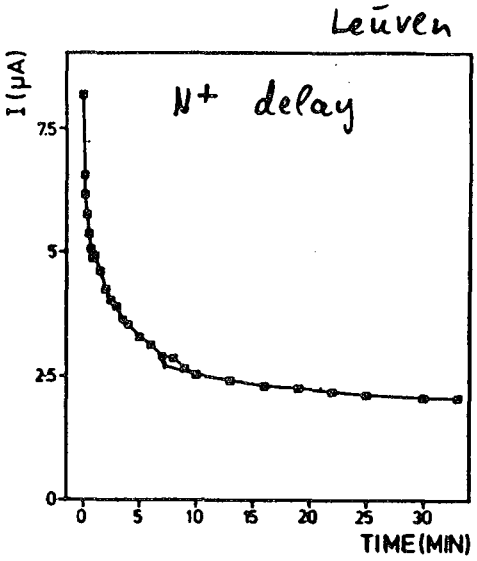

⊖ Efficiency strongly pressure-dependent
→ not compatible with "volatile" targets
Large outlet holes (diam 3-10 mm)
→ mA-currents
→ high emittance 70-150 π mm mrad
Cold enclosure
→ low efficiency for "refractory" elements
Interesting, however, if highly charged ions are required by post-accelerator:
η_i (high charge states of Ca) ≈ 1%
η_i (Ar^{8+}) ≈ 25%

2. Thermionic ion sources

2.1 Positive + negative surface ionizers

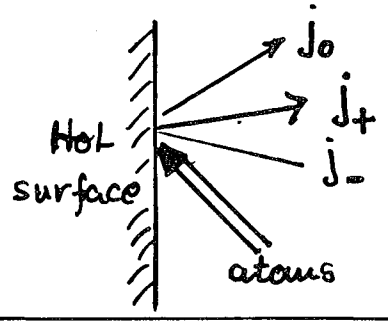

$$\frac{j_+}{j_0} \approx \exp\frac{\varphi - W_i}{kT}$$ Langmuir 1925

$$\frac{j_-}{j_0} \approx \exp\frac{E_A - \varphi}{kT}$$ Sutton 1935

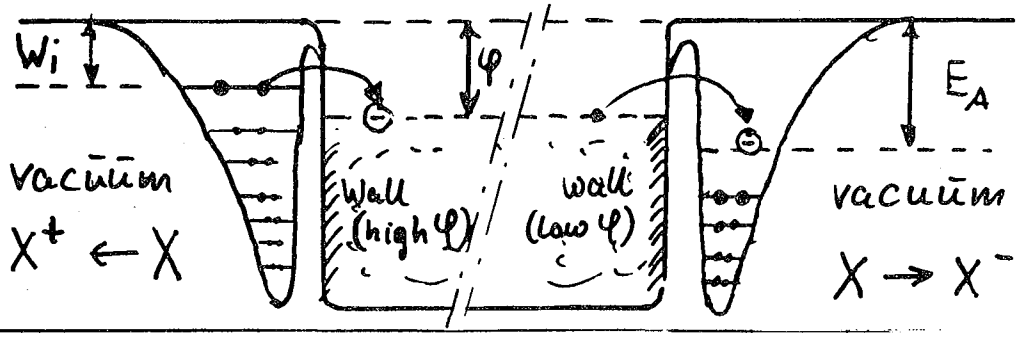

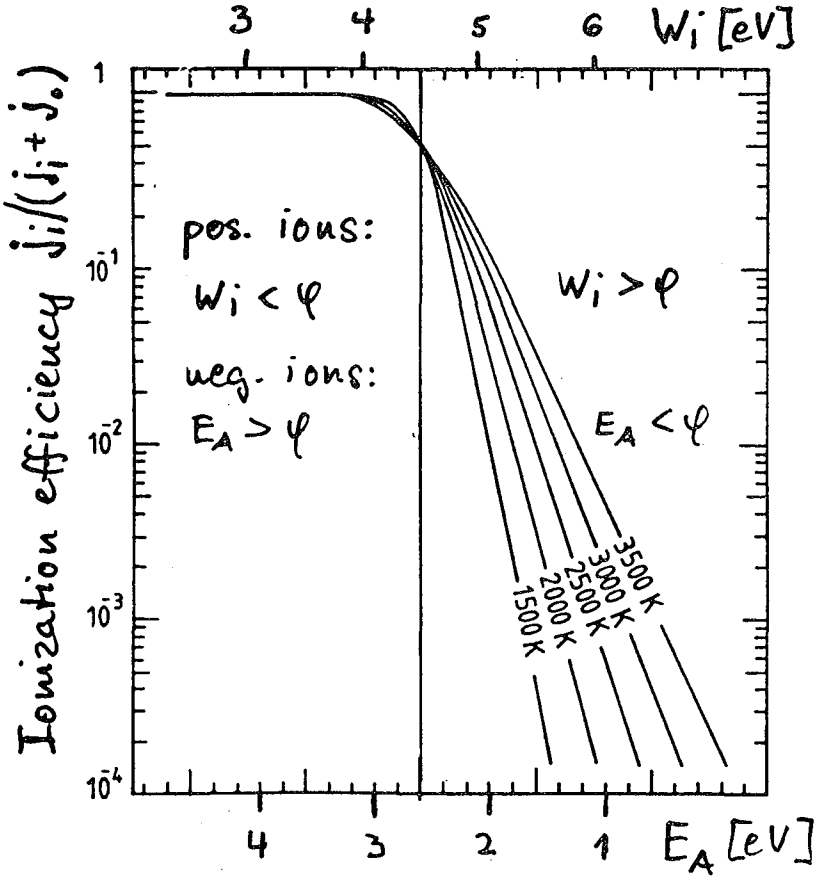

pos. SI on W-surface ($\varphi = 4.5$ eV)

neg. SI on LaB_6-surface ($\varphi = 2.6$ eV)

2.1.2. Negative surface ionizer (Isolde 1980)

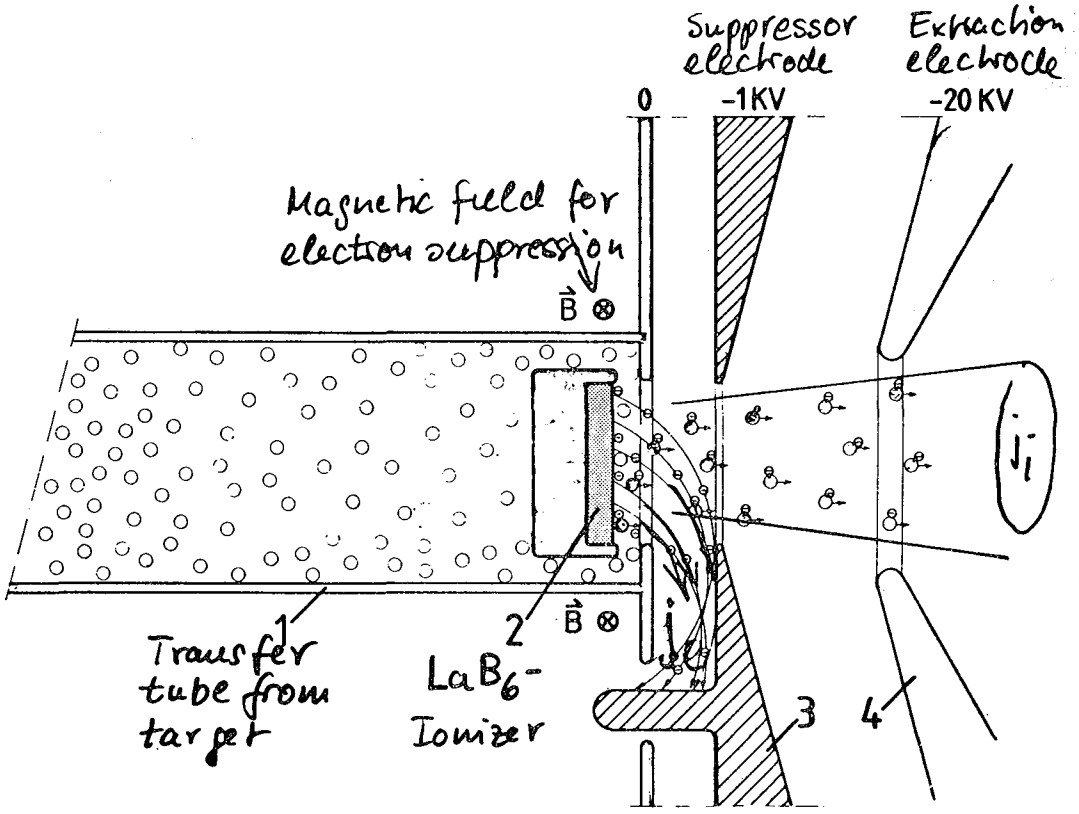

⊕ Highly efficient for halogenes: e.g. $\eta_i^- = 50\%$ for Br, I selective, except for group VIa-elements (e.g. Se, Te)

⊖ Low-Ψ material
→ limited in operation temperature
→ long surface delays for halogenes
→ suppression of large electron currents required

2.2. High temperature cavity source (Dubna 1971

Pos. SI + ion confinement in space-charge well

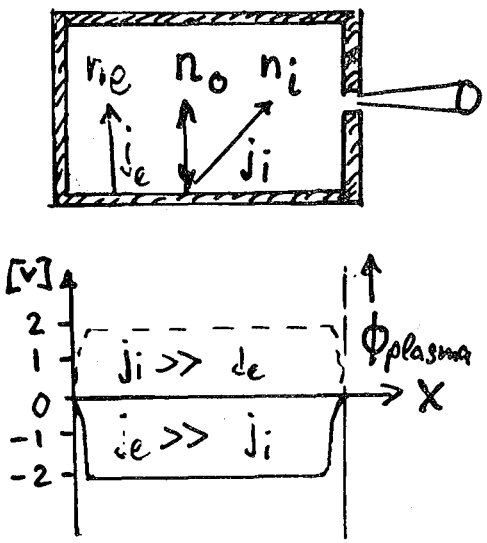

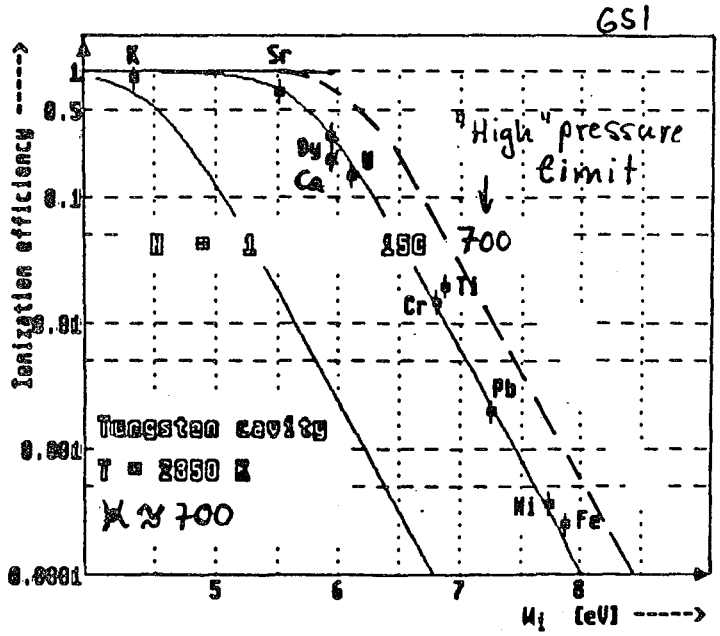

⊕ High ionization eff. $\frac{n_i}{n_o}$ (volume) $\gg \frac{n_i}{n_o}$ (surface)
Intrinsicly selective for elements differing in W_i
Principly simple design (no insulators)
→ Temperatures > 3000K
→ access to refractory elements
Compatible with high neutral densities ("volatile target")
→ $\frac{n_i}{n_o}$ - Amplification N may become as high as the mean number of wall collisions α of atoms
Low emittance + ΔE ($< 2\pi$ mm mrad, < 1eV)
Low current density (down to $1\mu A/cm^2$)

⊖ Restricted to elements with $W_i \leq 7$eV
Strong efficiency reduction for high plasma density
→ not compatible with "volatile" targets, if vapour surface-ionizable

3. Resonant multistep photo-(Laser) ionization source

GSI - Mainz - Troitzk - collab. 1993 Leuven 1993

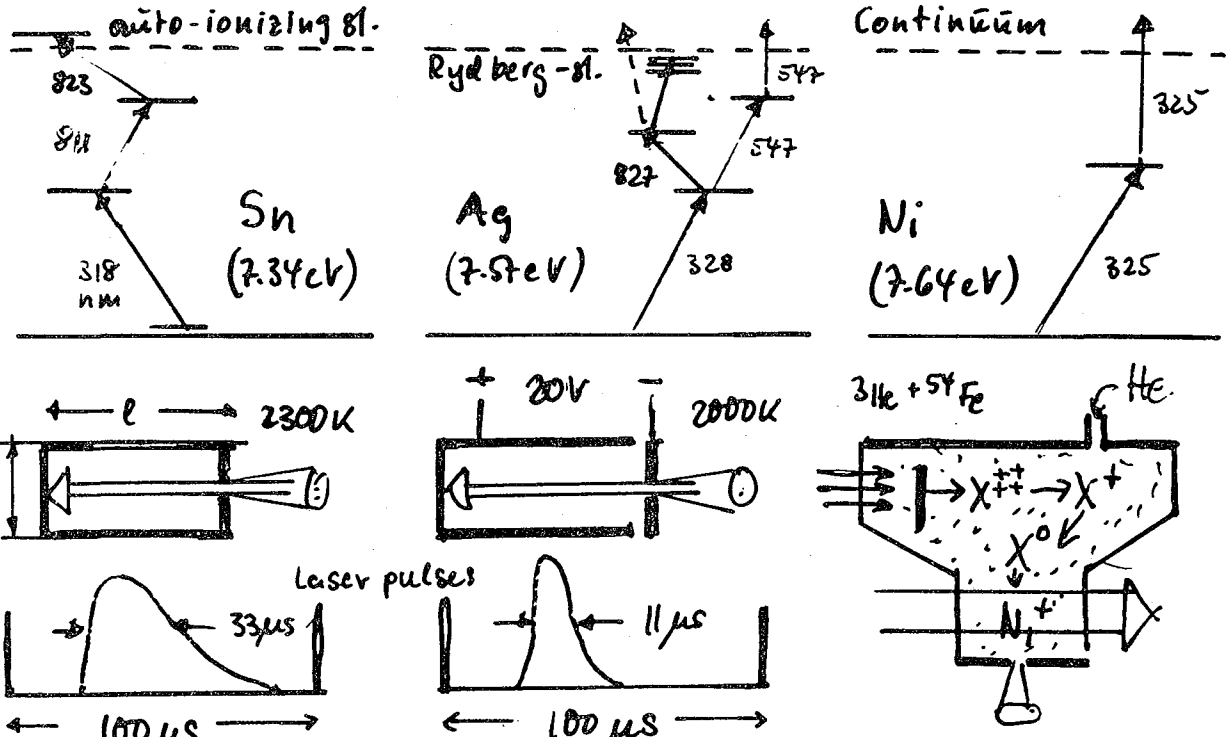

η_i (Sn) = 9 (6%)
Sn/In ≈ 16×
$^{58}Ni\ (^{50}Cr, xpyn)^{101,103}Sn$

η_i (Ag) ≈ 1‰
Perspective:
some %

η_i (Ni) ≈ 1‰
Perspective 30%
$^{3}He\ (^{54}Fe, 2n)^{55}Ni$

⊕ Principly efficient for 80% of the elements
Intrinsicly selective
Emittance low (< 10π mm mrad), ΔE low (or ≤ 20eV)
Pulsed ion beam → enhanced selectivity
→ useful for post-accelerator?

⊖ Selectivity limited by surface-ionized particles
Increased complexity (up to 5 lasers simultaneously)
Lot of R+D

4. Ion guide (Jyväskylä 1986)

Utilizes the high initial charge states of recoils by discharging to 1^+ ions in pure He.

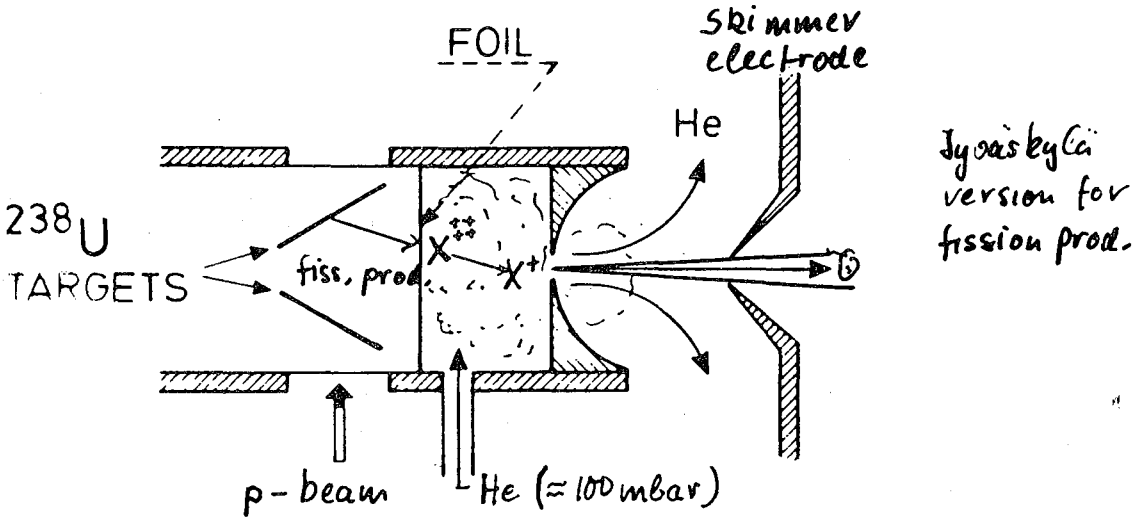

⊕ Universal ion source (all elements)
very fast (for $T_{1/2} \gtrsim 100\,\mu s$)
Simple and long-living

⊖ No selectivity
High energy spread (typical 10 eV)
Separated Rates $\lesssim 10^5$/s ← thin targets
← ion losses (recombination at wall + in gas)
→ suited for RIB-projects ?

5. The target/ionsource-system

5.1. Effect of target material + enclosure

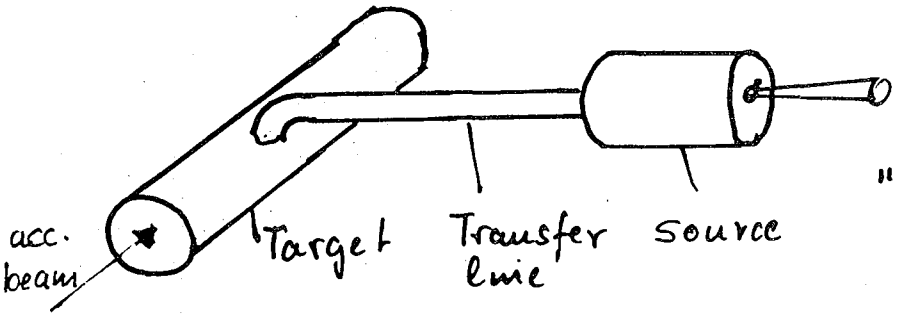

"Isolde-System"
2500K, Ta encl.

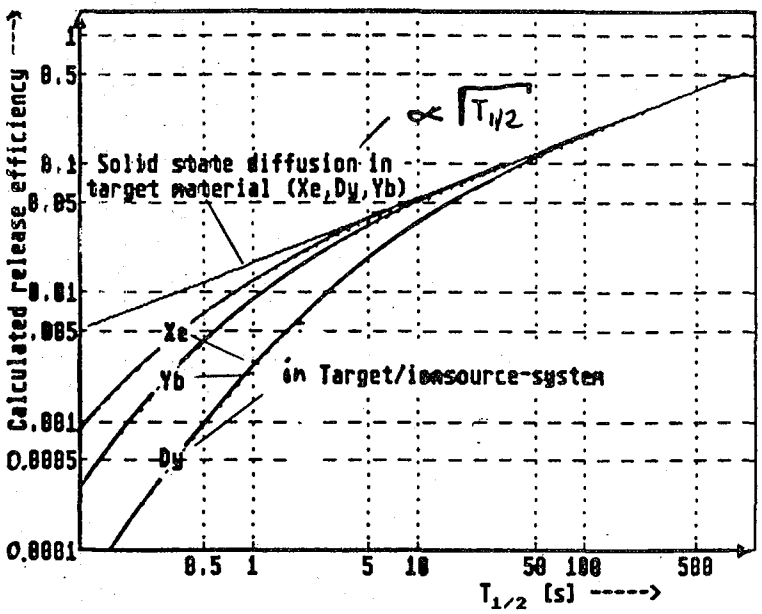

Target:
100 µm Ta foils

→ main loss due to solid state diffusion

→ no selectivity

$D(Xe,Yb,Dy)\,|_{Ta,2500K} \approx 5\times10^{-9}\,\frac{cm^2}{s}$

$T_a(Xe,Yb,Dy)\,|_{Ta,2500K} \approx 0,50\,\mu s,500\,\mu s$

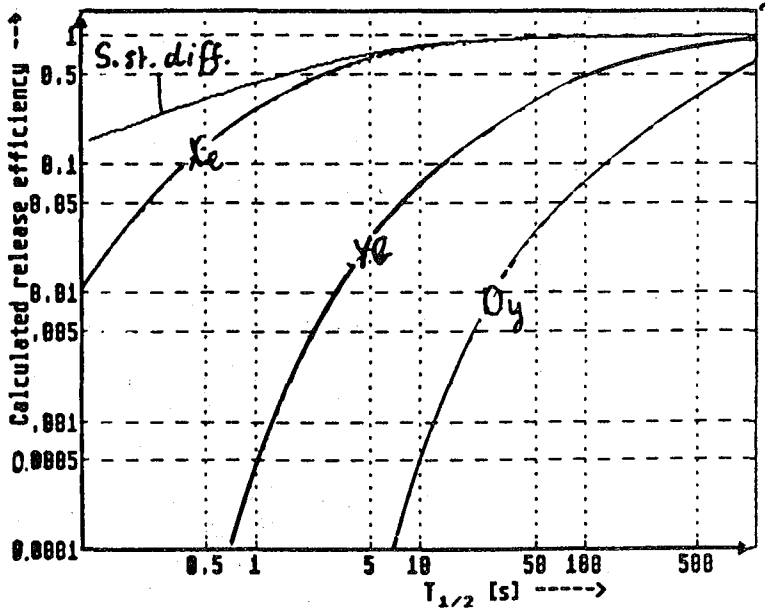

Target:
10 µm Ta powder

→ main loss due to adsorption

→ Xe enhanced

→ Dy (+ other REE) discriminated

→ Yb selective

5.2. Adsorption-based techniques

Cooled transfer lines (ISOLDE)
→ discriminates less-volatile elements

Temperature-variable cold traps (GSI)
→ "bunched beams"
→ selectivity by time gate on bunch
→ selectivity for volatile elements (anti-bunch-gate)

Chemical evaporation techniques (ISOLDE + others)

e.g. $Ba + CF_4 \longrightarrow BaF^+$
→ higher desorption speed
→ higher ionization efficiency (~100%)
→ lower operation temperature
→ 100% selectivity (no CsF^+)

$F + Al$	$\longrightarrow$	AlF^+	
$Cl + Al$	$\longrightarrow$	$AlCl^+$	
$Se + O_2$ (+ graphite)	$\longrightarrow$	$COSe^+$	(CO_2-homologue)
$Hf + CF_4$	$\longrightarrow$	HfF_3^+	(ISOCELLE)
$La + O_2$	$\longrightarrow$	LaO^+	(JAERI)

Appendix B

D. Clark
(LBL)

Cyclotron Options

① Replace all RFQs, linacs with cyclotrons
$E/A = k(Q/A)^2$. 25 MeV/A for A = 240

Ⓐ Start with Q = 1

One stage: $k = 10^6$, too large (TEV)

Multi-stage: Let k = 1200

Stage	Q	E/A	$Q_{str.}$ (foil)	
1	1	.021	12	foil o.k.?
2	12	3.0	50	
3	50	52		

→ Ⓑ Start with Q = 35, k = 1200

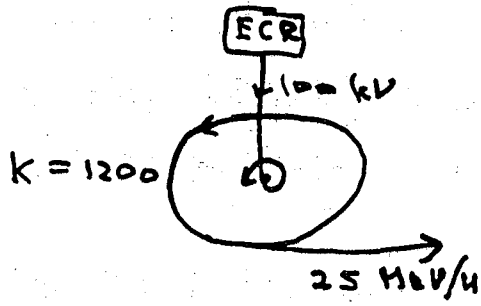

- Stripping in ECR
- No foil strippers
- ECR ionis. pot. ?

Note: 88" AECR peak of chg. dist. = U^{33+}

Cyclotron Options

② RFQ1, 2 inject cyclotrons

Cycl. Stage	Q	K	E/A	$Q_{Str.}$ (foil)
1	12	1200	3.0	50
2	50	"	52	

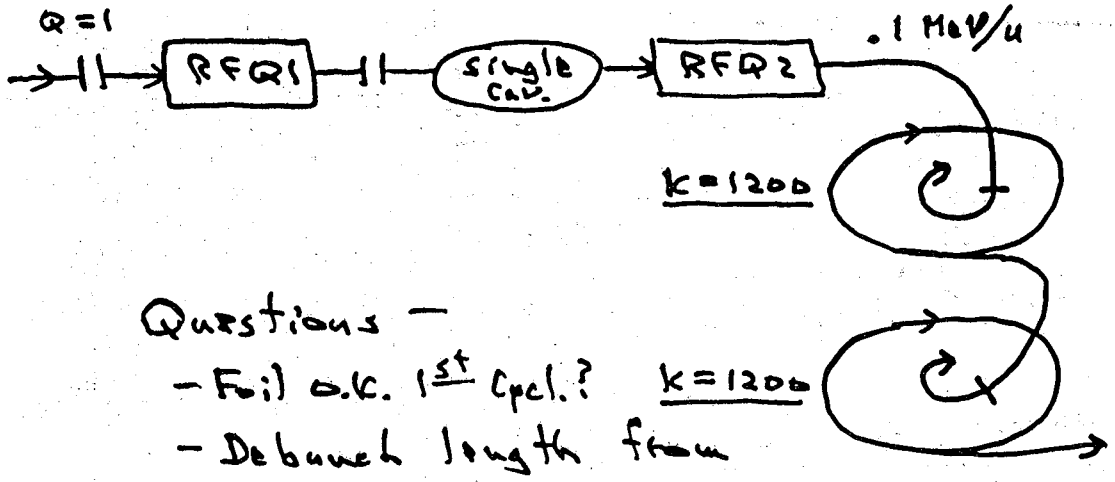

Questions –
- Foil o.k. 1st Cycl.?
- Debunch length from RFQ?
- Var. freq. RFQ feasible?

Cyclotron vs. Linac:

Cycl. – Needs collim. of beam for good quality.
- Can get higher energy light ions at ~ same cost.

Cyclotron Emittance

Multi-turn Extraction

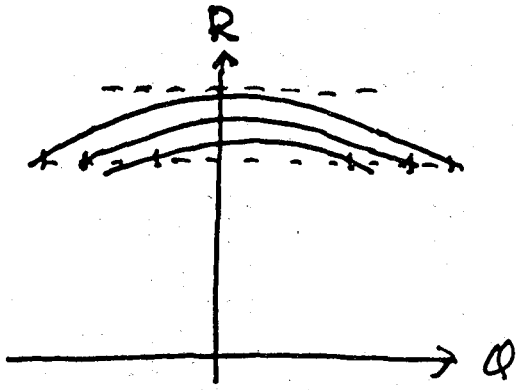

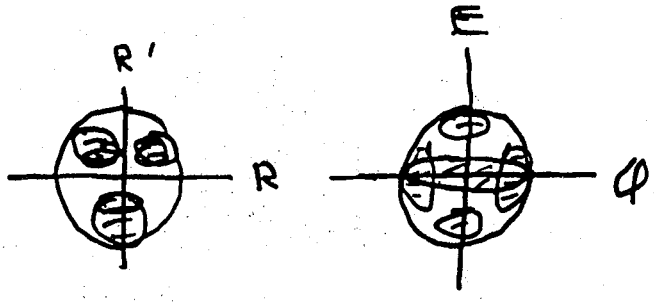

Long: 88": 5 MeV/u, A = 30, E = 150 MeV

$\Delta E = .3\% \times 150$ MeV $= 500$ keV

$\Delta t \simeq 5$ ns

$\Delta E \cdot \Delta t = 500 \times 5 = 2500$ keV-ns

Transverse: ~ 1 π mm-mrad, norm.

Single-turn Extraction

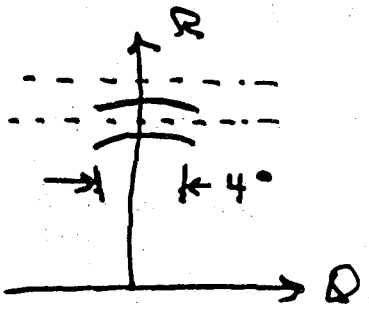

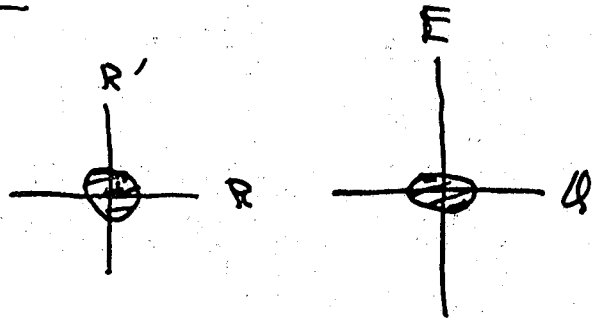

Long.: 5 MeV/u, A = 30, E = 150 MeV

$\Delta t = 1$ ns $\simeq 4°$ RF,

$\Delta E/E = 1 - \cos 2° = 6 \times 10^{-4}$

$\Delta E = 6 \times 10^{-4} \times 150 = 90$ keV

$\Delta E \cdot \Delta t = 90 \times 1 = 90$ keV-ns

Appendix C

K. Shepard
(ANL)

SUPERCONDUCTING STRUCTURES

- CURRENT ANL ISOL FACILITY PLAN
- GENERAL LOW VELOCITY ISSUES
- SUITABILITY OF PRESENT SC SYSTEMS
- CURRENT SC STRUCTURE DEVELOPMENT EFFORTS
- PROSPECTS

NITSCHKE III

ISL Concept

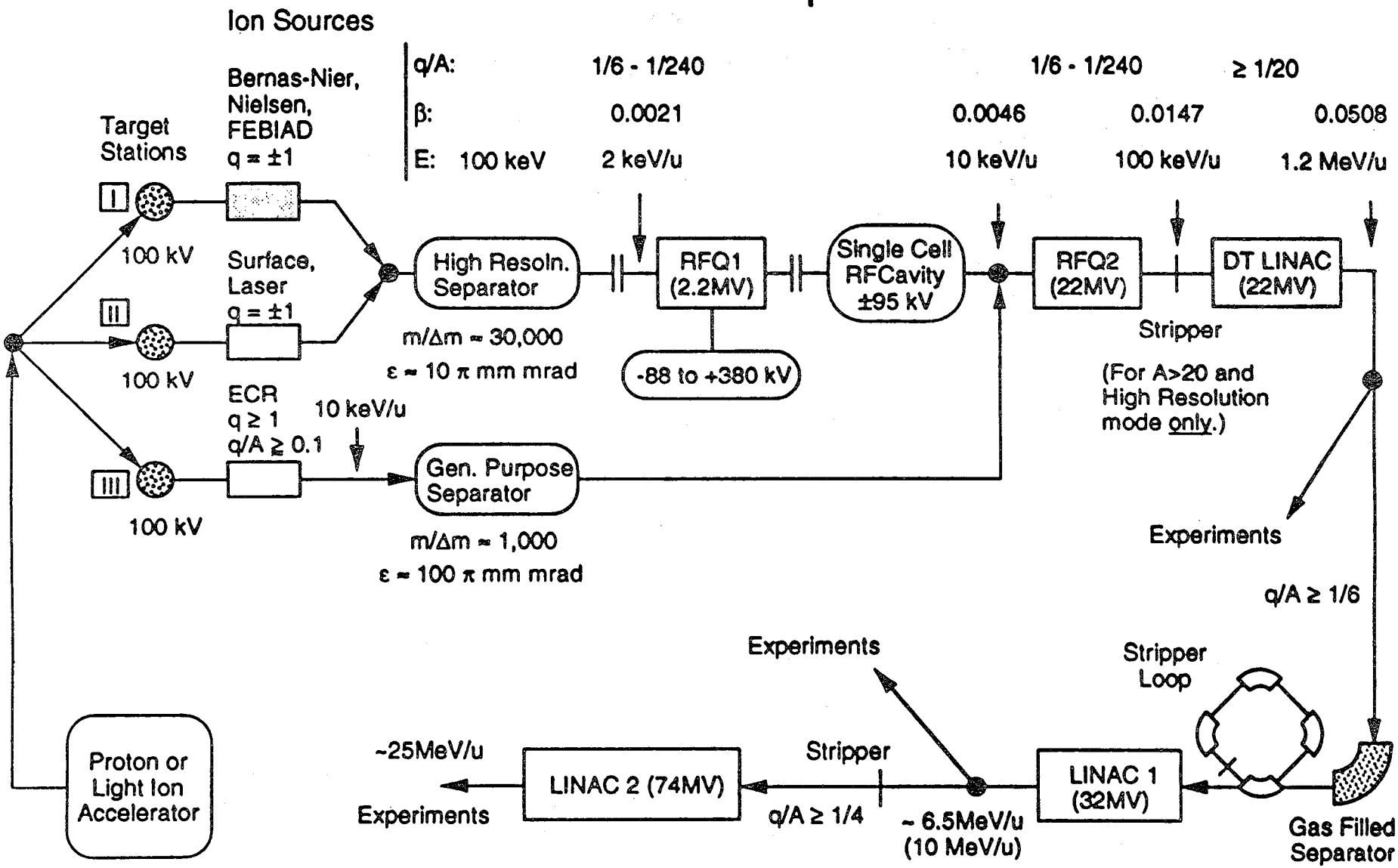

jmn 8/17/93

NOLEN I

Argonne National Laboratory

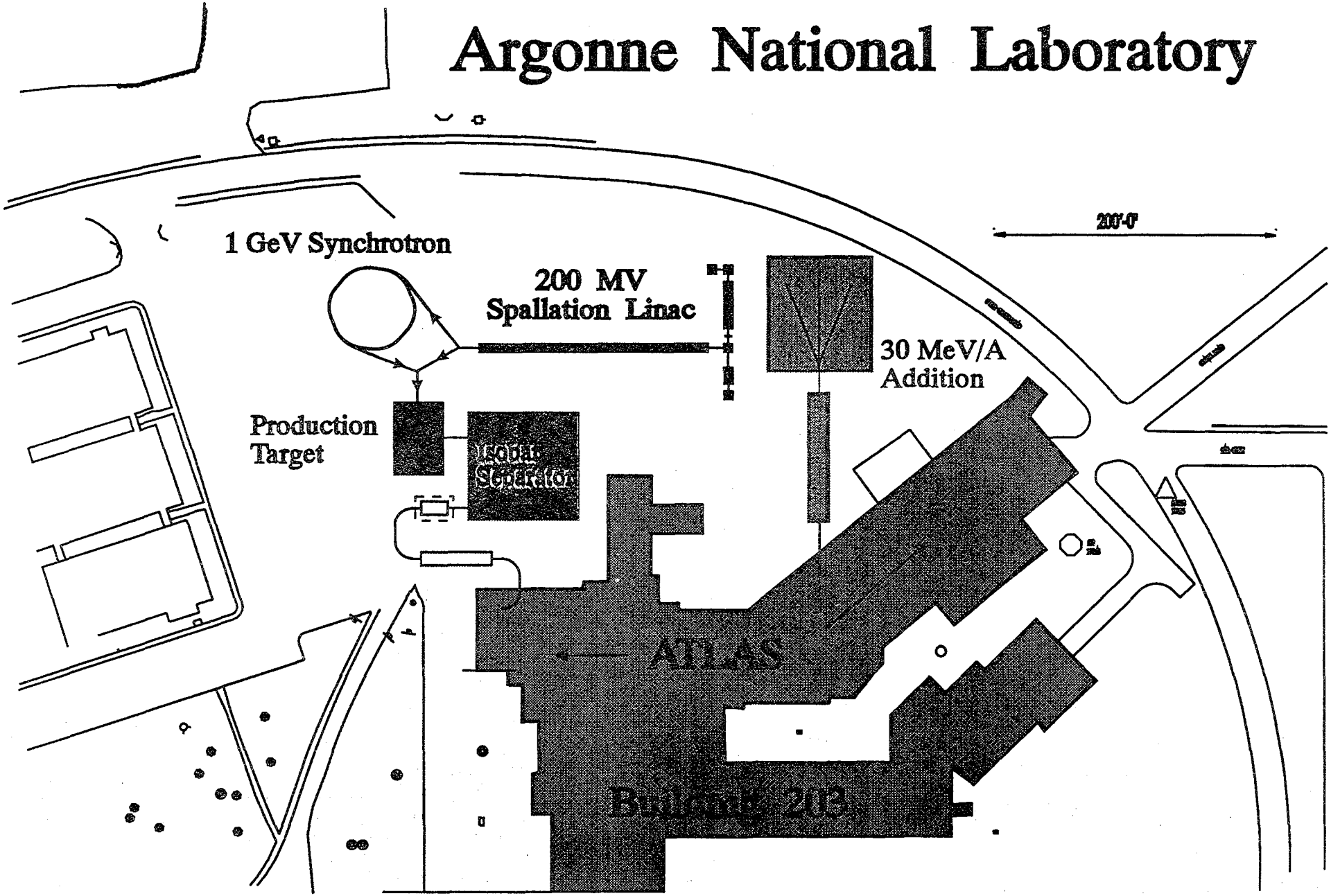

RBFANL2.XLS

Radioactive Beam Facility							
Driver Accelerator:							
	Phase 1:	200 MV Linac, q/m=0.5, 100 kW beam power, 120 Hz (Comm					
	Phase 2:	1 GeV proton rapid cycling synchrotron, 10 Hz, 100 microam					
Radioactive Beam Accelerator:							
	132Sn Example		A=	132			
V gain (MV)	q	T/A (MeV/A)	beta	length (m)	efficiency (this step)	efficiency (cumulat.	Intensity (Ions/sec)
							6.00E+11
0.1	1	0.000758	0.001276		0.3	0.3	1.8E+11
					1	0.3	1.8E+11
					0.7	0.21	1.26E+11
0.3	1	0.00303	0.002551	1	1	0.21	1.26E+11
0.3	1	0.005303	0.003375	1	1	0.21	1.26E+11
-0.3	1	0.00303	0.002551	1	1	0.21	1.26E+11
0	2	0.00303	0.002551	2	0.5	0.105	6.3E+10
0.4	2	0.009091	0.004419	1	1	0.105	6.3E+10
2	2	0.039394	0.009199	2	1	0.105	6.3E+10
30	2	0.493939	0.032561	15	1	0.105	6.3E+10
	20	0.493939		1	0.2	0.021	1.26E+10
	20	0.493939		2	1	0.021	1.26E+10
50	20	8.069697	0.130816	25	1	0.021	1.26E+10
50	40	23.22121	0.219268	25	0.2	0.0042	2.52E+09

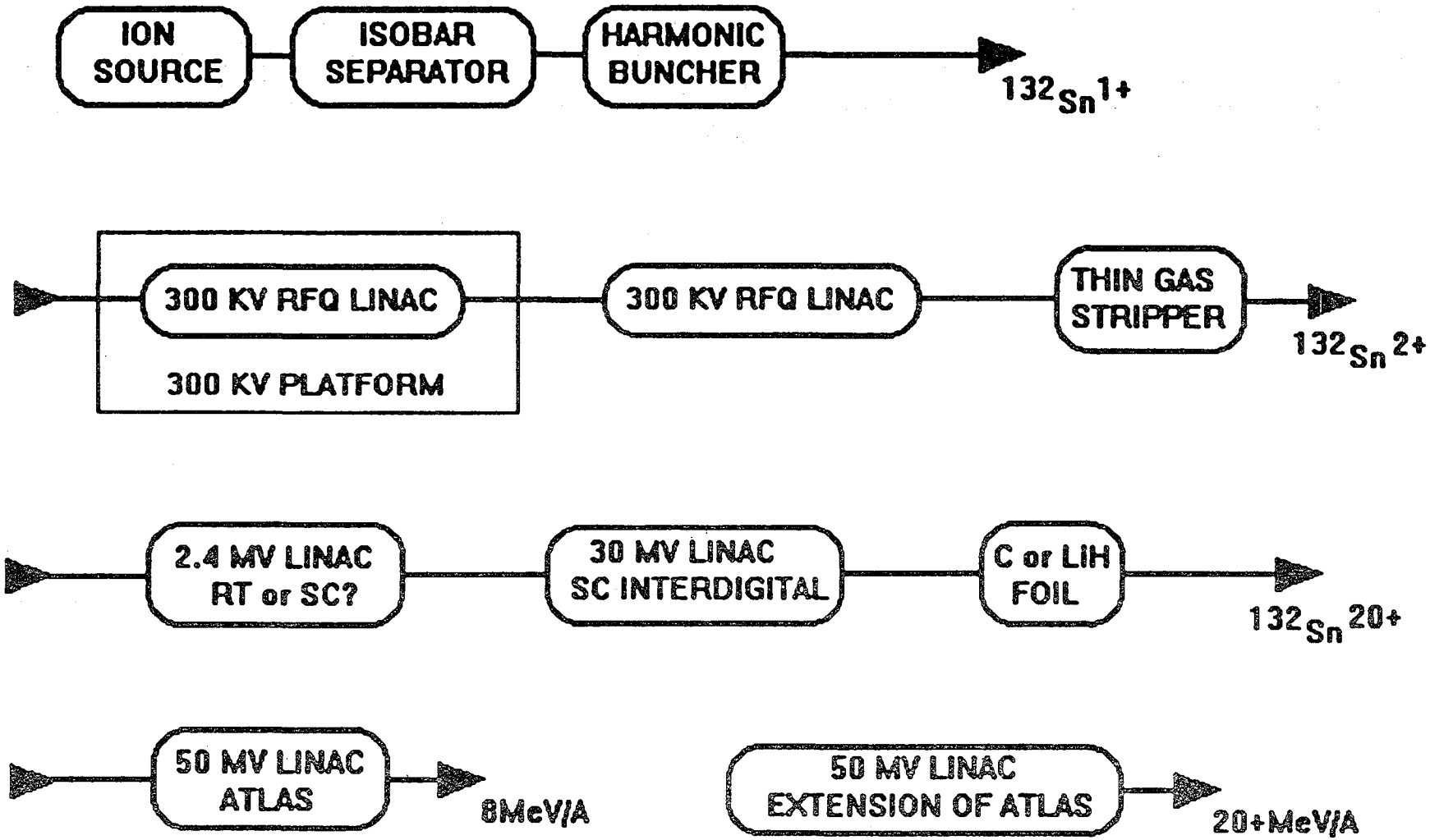
ION SOURCE
ISOBAR SEPARATOR
HARMONIC BUNCHER
$^{132}Sn^{1+}$
300 KV RFQ LINAC
300 KV PLATFORM
300 KV RFQ LINAC
THIN GAS STRIPPER
$^{132}Sn^{2+}$
2.4 MV LINAC RT or SC?
30 MV LINAC SC INTERDIGITAL
C or LIH FOIL
$^{132}Sn^{20+}$
50 MV LINAC ATLAS
8MeV/A
50 MV LINAC EXTENSION OF ATLAS
20+MeV/A

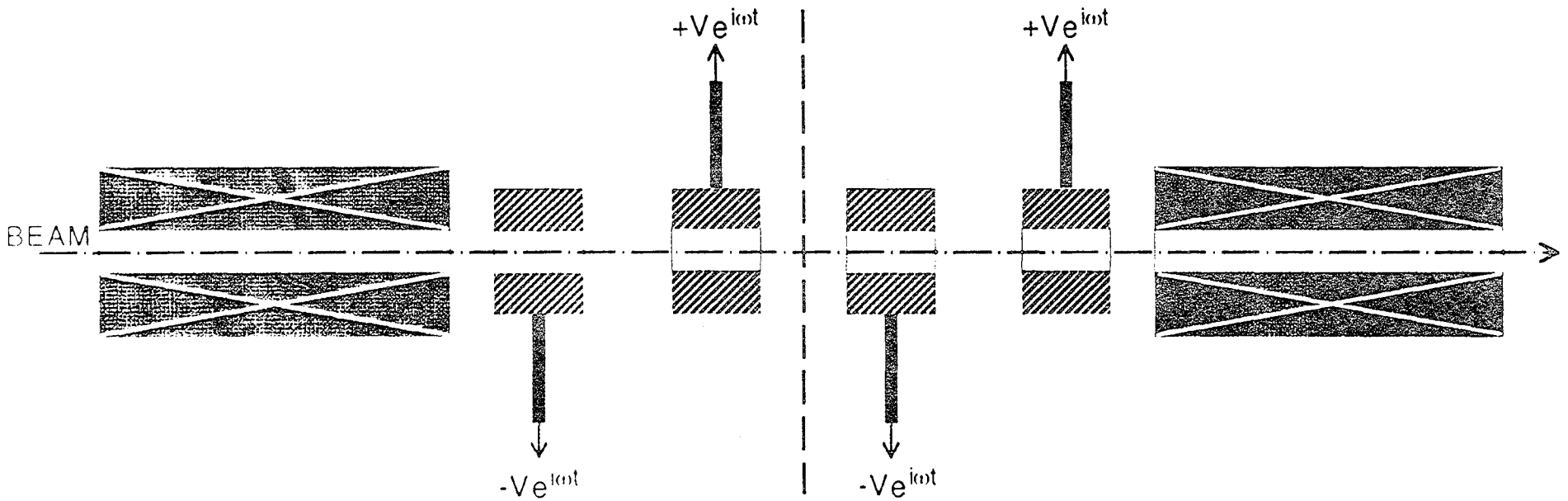
+Ve^iωt
+Ve^iωt
BEAM
-Ve^iωt
-Ve^iωt

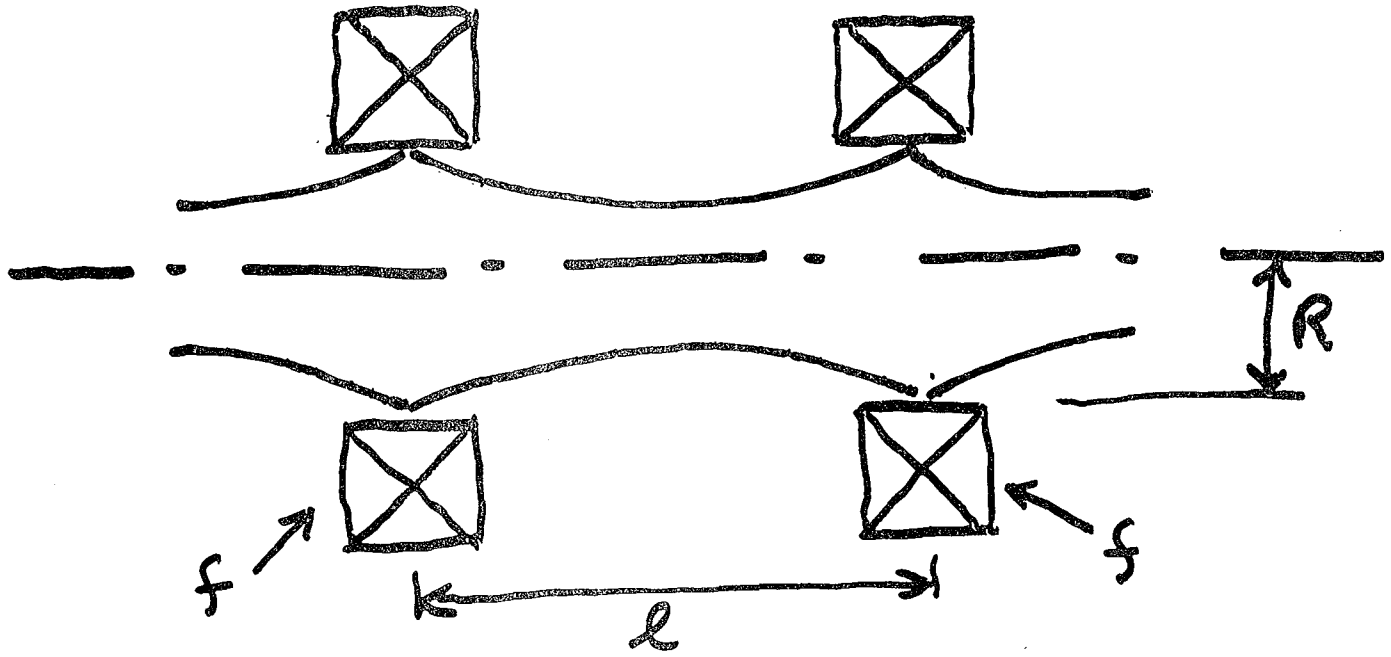

$$\pi R^2 \cong \epsilon \sqrt{Lf} \qquad f \geq L/2$$

For a solenoid axial field B_0 the min. f.l. is $\frac{1}{f_{min}} = \frac{\pi B_0}{8C}\left(\frac{q}{m}\right)\frac{1}{\beta}$

For an optimum solenoid array the beam size is

$$\pi R^2 = 2\epsilon f = \frac{16C}{\pi B_0}\epsilon_N\left(\frac{m}{q}\right)$$

Radial Defocusing

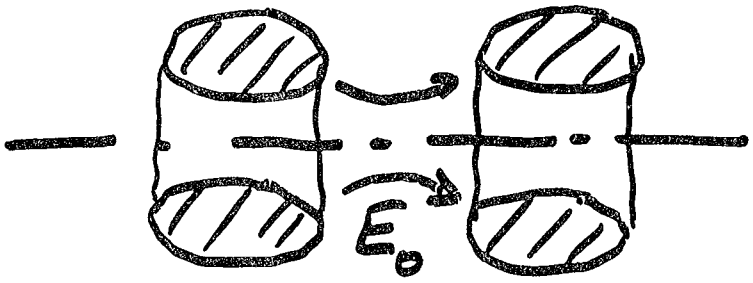

for a ubiquitous matched particle:

$$-1/f_d = \frac{q}{m}\frac{E_0}{\beta^2 c^2}\sin\phi$$

Longitudinal Emittance Growth

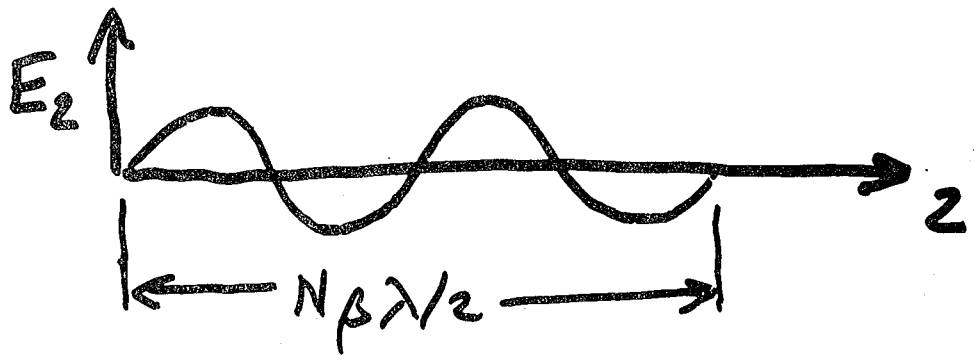

with optimum focusing:

$$\frac{\text{Energy Spread}}{\text{Energy Gain}} \simeq \frac{\delta E_z}{E_z} \simeq \frac{N\pi\, f_{req}\, \epsilon_N}{\beta^2 c}$$

RESONATORS FOR POSITIVE-ION INJECTOR

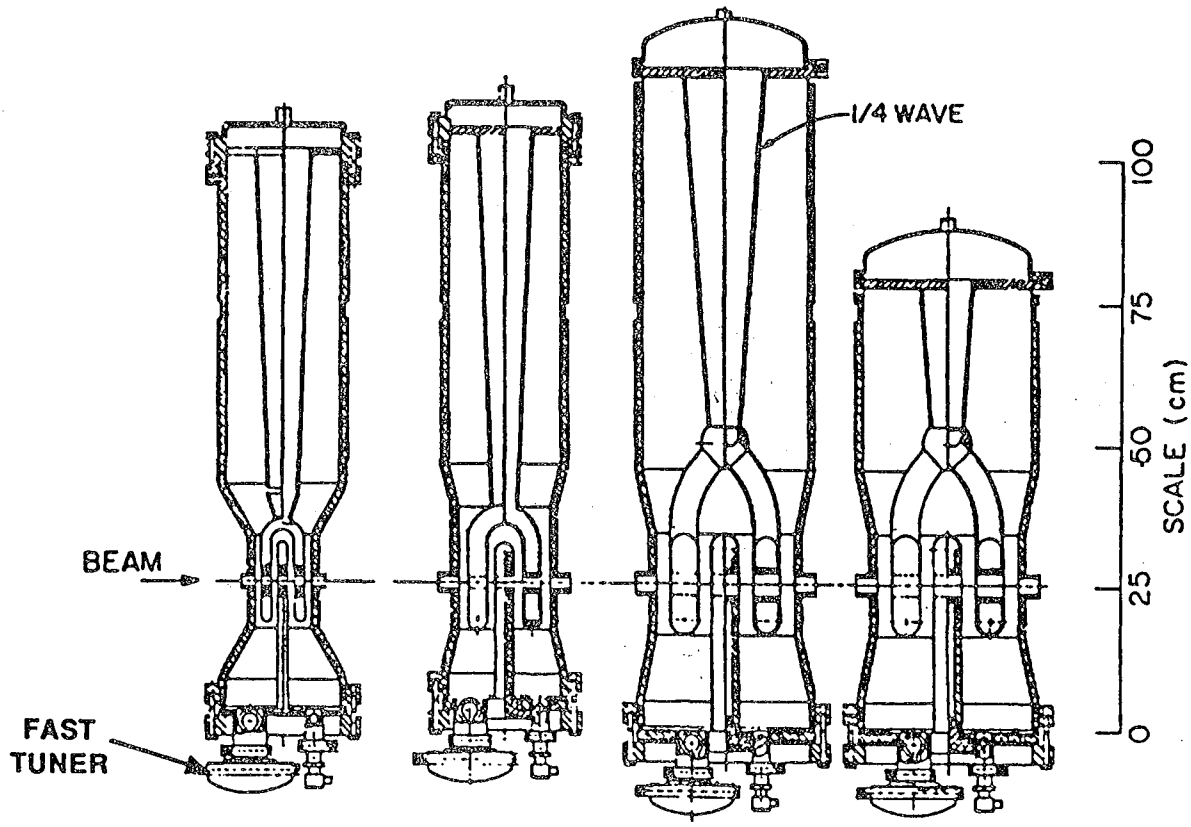

β	0.009	0.016	0.025	0.037
L_s	10.2	16.5	25.4	25.4
f (MHz)	48.5	48.5	48.5	72.75
E_s (MV/m)	4.5	3.0	3.0	3.0

SUPERCONDUCTING OPTION

PRO:

- DEMONSTRATED CW OPERATION
- SUPERB BEAM QUALITY
- GOOD WALL-PLUG POWER EFFICIENCY
- HIGHLY MODULAR:
  A) SYSTEM IS HIGHLY FLEXIBLE
  B) EASY ALIGNMENT & DIAGNOSTICS

CON:

- RELATIVELY HIGH CAPITAL COSTS ESPECIALLY AS $\beta \rightarrow 0$

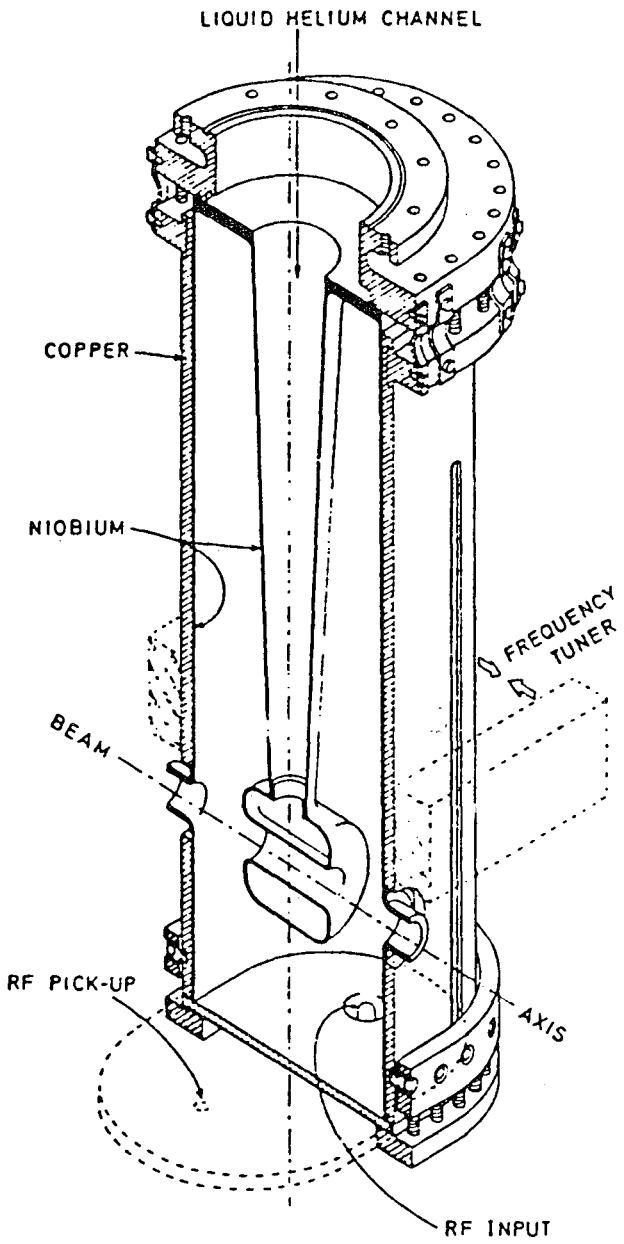
LIQUID HELIUM CHANNEL
COPPER
NIOBIUM
FREQUENCY TUNER
BEAM
RF PICK-UP
AXIS
RF INPUT

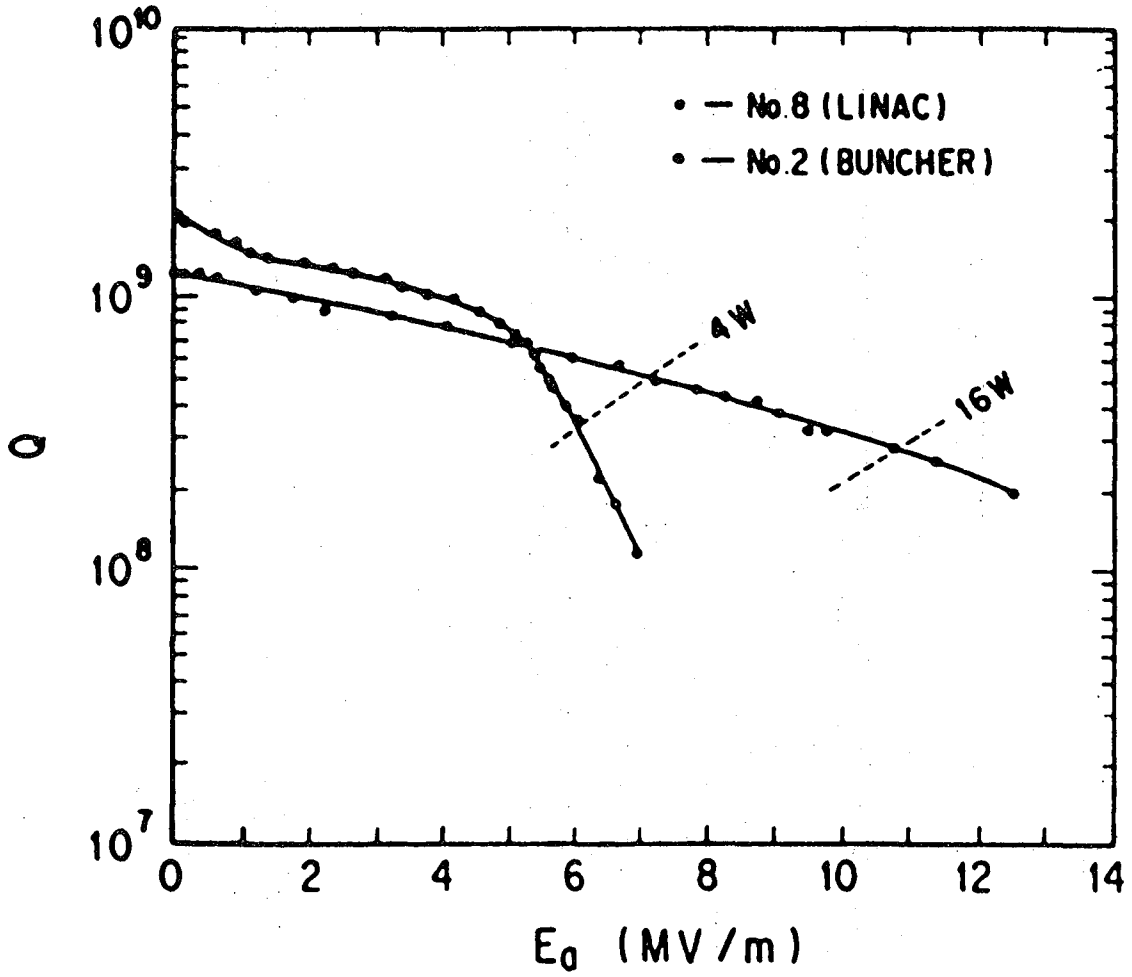

Fig. 2. $Q-E_a$ curves for quarter wave resonators of $f_0 = 129.8$ MHz. Closed circles are for QWR no. 8 for the linac and open circles are for no. 2 for the buncher. The $Q-E_a$ curve for QWR no. 2 was obtained earlier [2].

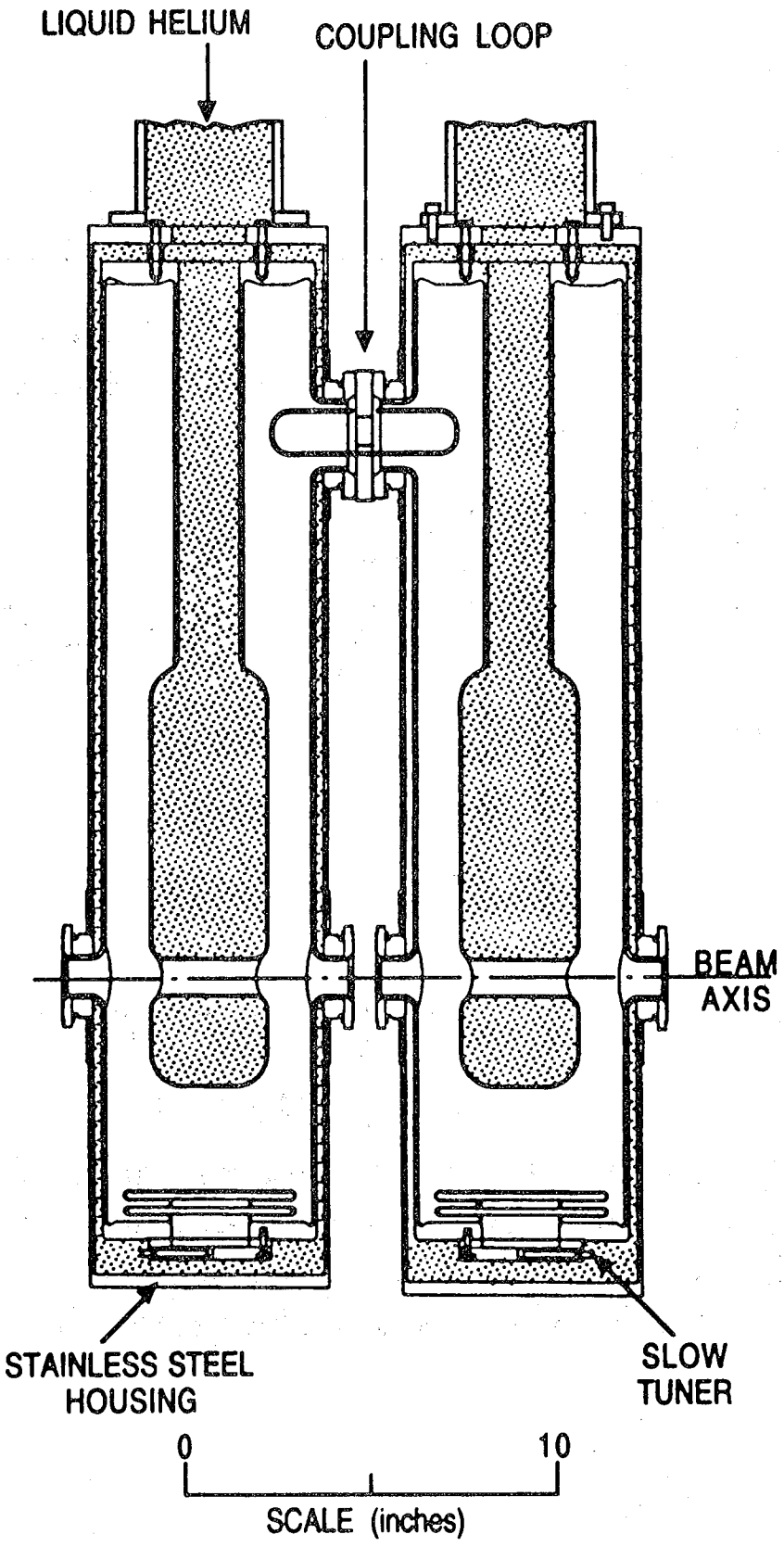
LIQUID HELIUM
COUPLING LOOP
BEAM AXIS
STAINLESS STEEL HOUSING
SLOW TUNER
0
10
SCALE (inches)

Cavity Performance

Type	№ Cavities	$\overline{E_a}$
I1	1	4.5 MV/m
I2	2	3.9
I3	5	3.5
I4	10	3.7
L	12	3.1 (3.5)
H	26	2.9 (3.2)
V	4	1.9

ATLAS LINAC delivers:

$^{238}U^{39+}$ 5-7 pnA at 1535 MeV

(6.45 MeV/A)

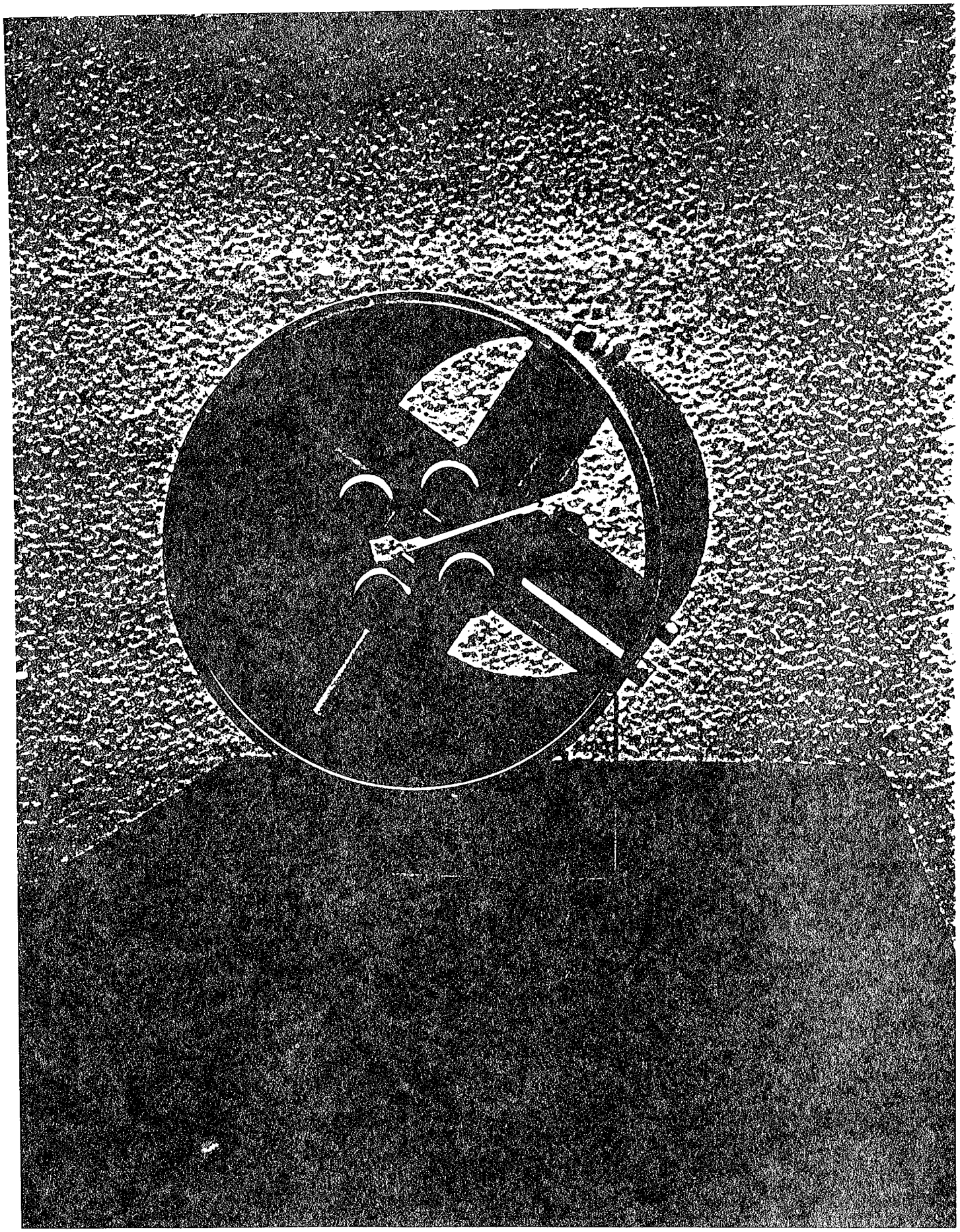

Stony Brook – Legnaro Collaboration

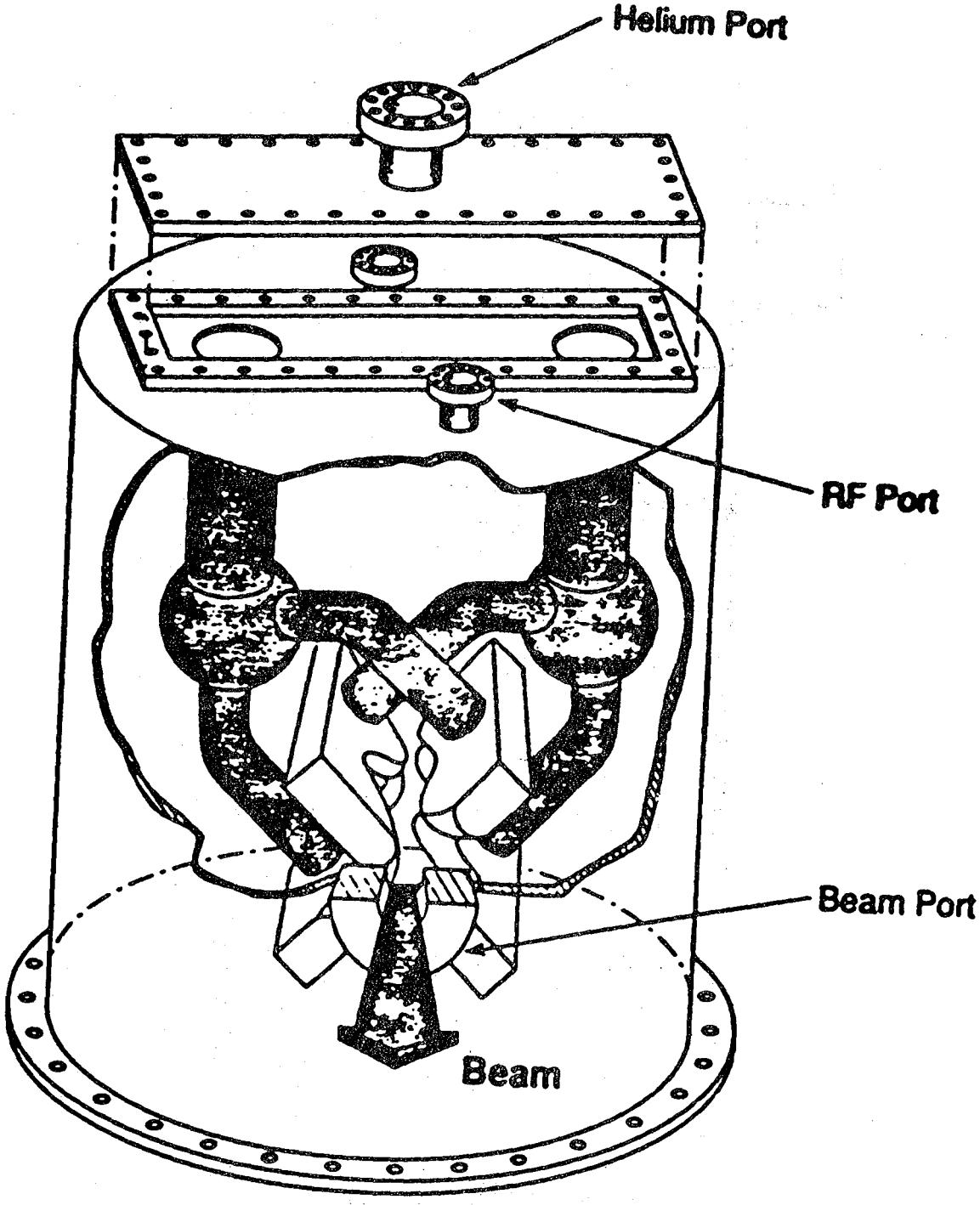

Jain et al

Superconductor: Pb – Sn alloy on copper

$\beta_{IN} \approx 0.03$

$f_{RF} \approx 57$ MHz

length = 0.40 m

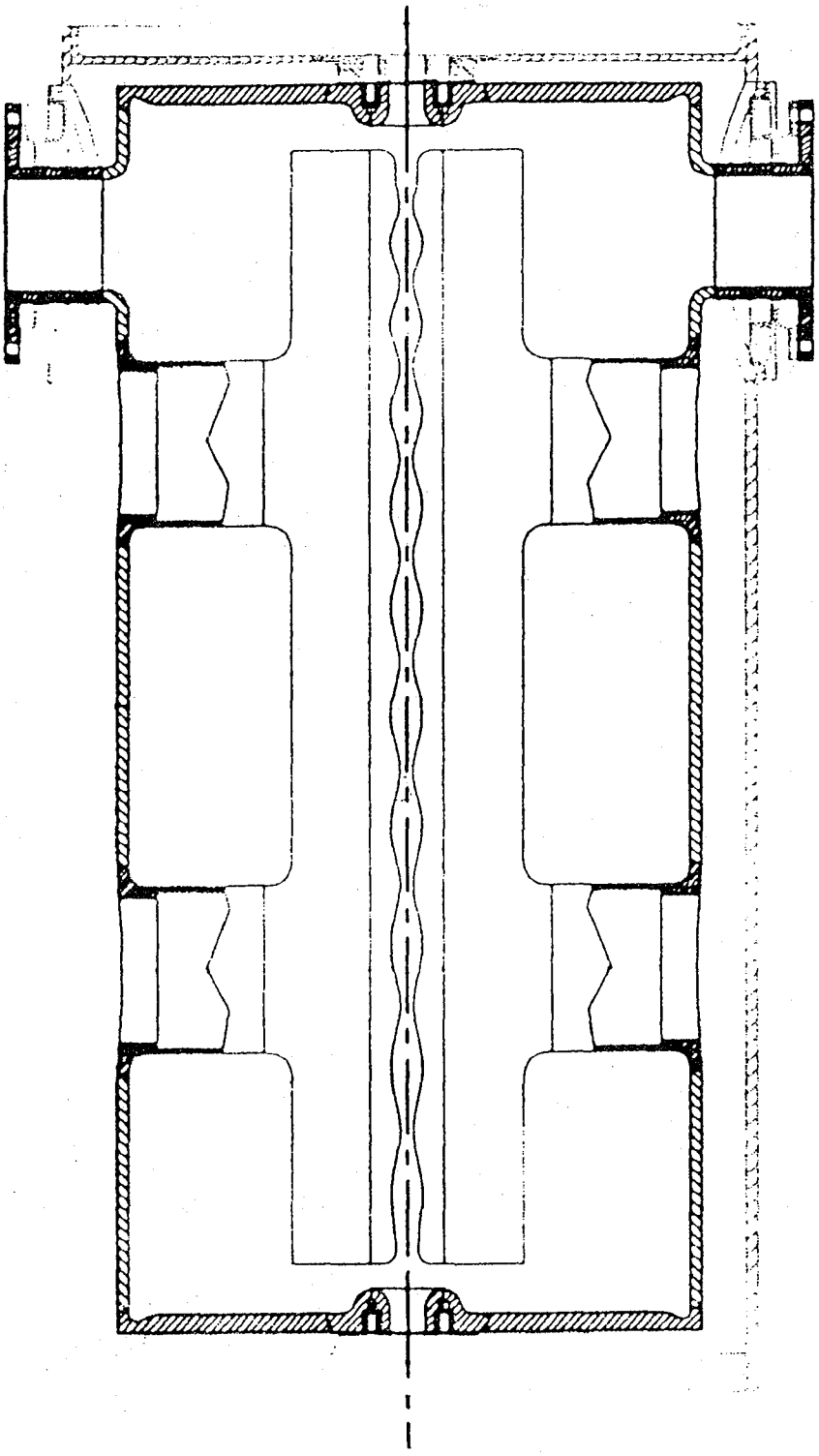

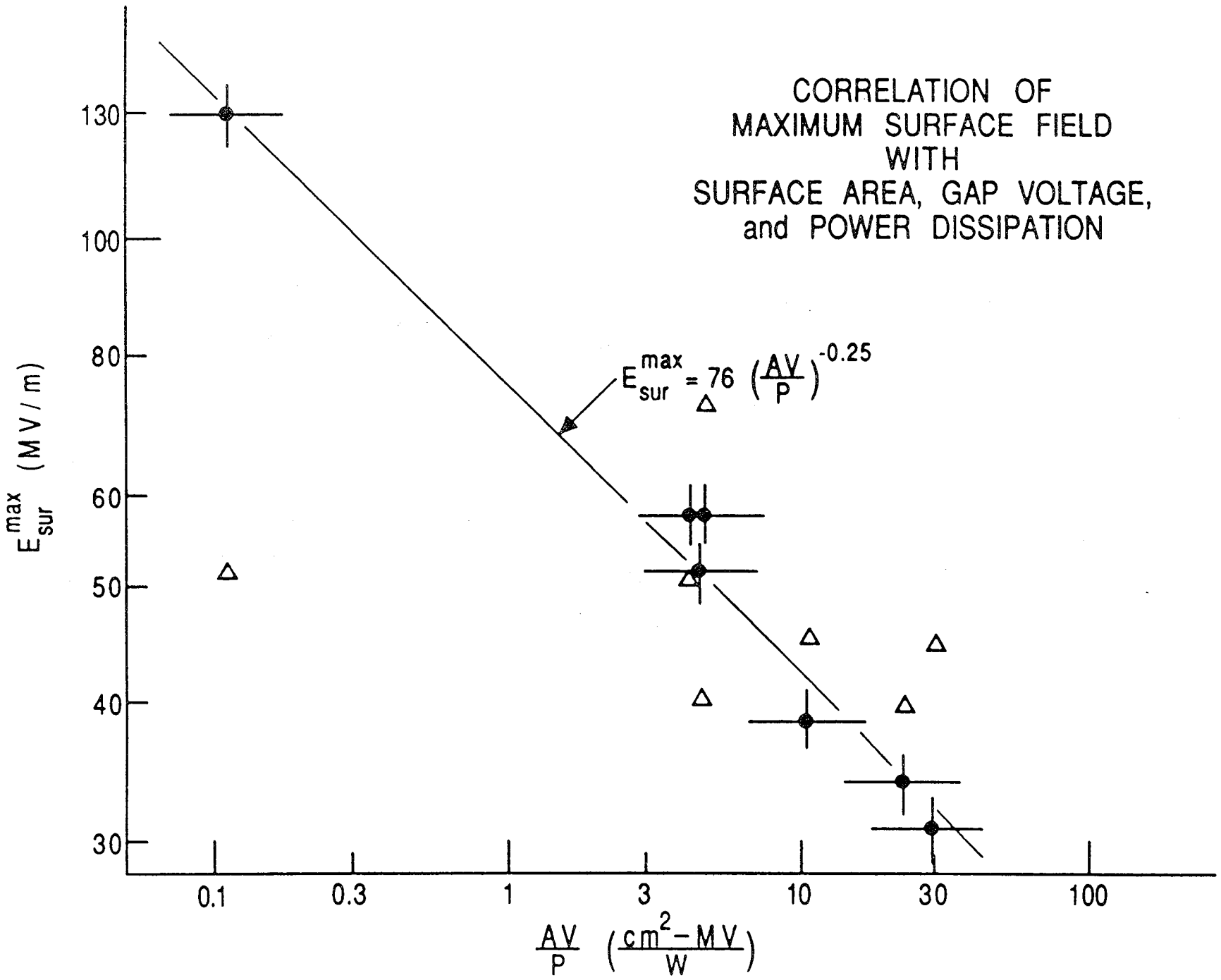
CORRELATION OF
MAXIMUM SURFACE FIELD
WITH
SURFACE AREA, GAP VOLTAGE,
and POWER DISSIPATION
$E_{sur}^{max} = 76 \left(\frac{AV}{P}\right)^{-0.25}$
E_{sur}^{max} (MV/m)
130
100
80
60
50
40
30
0.1
0.3
1
3
10
30
100
$\frac{AV}{P}$ $\left(\frac{cm^2 - MV}{W}\right)$

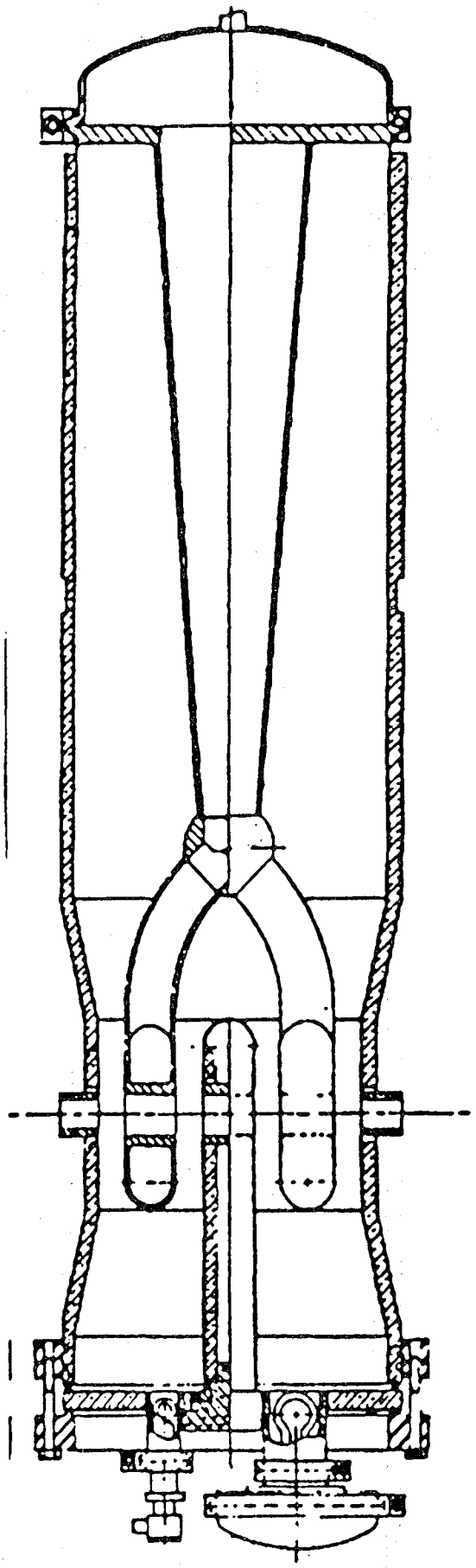

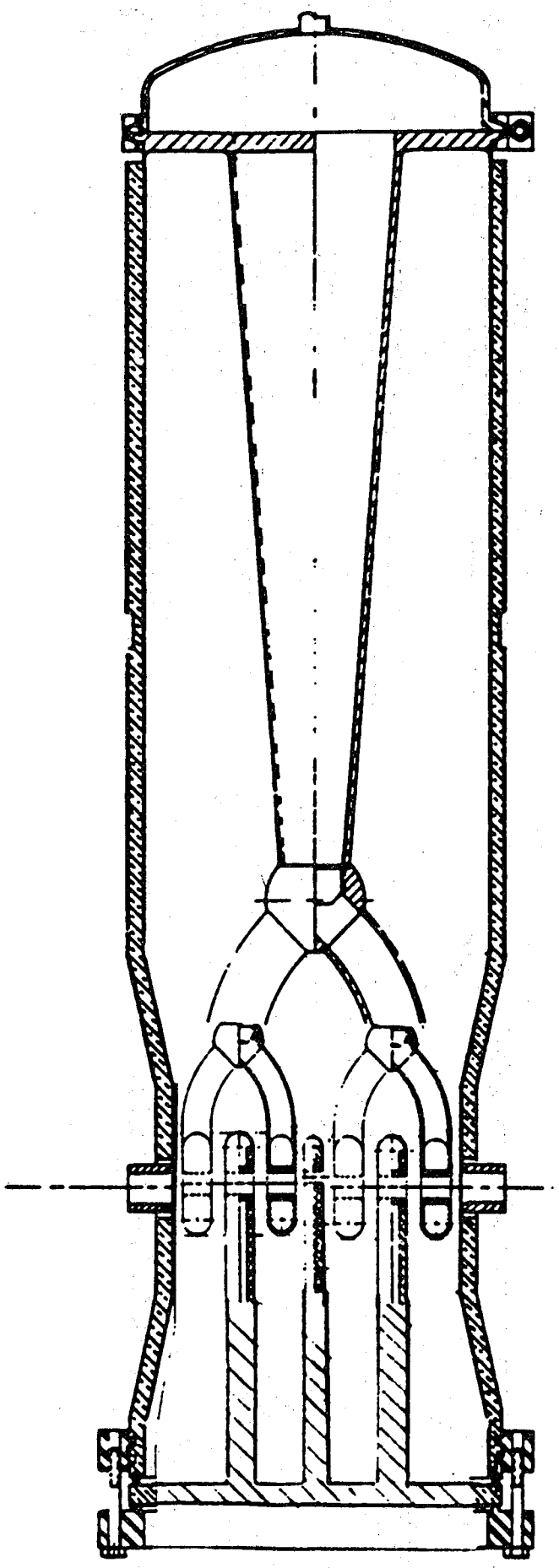

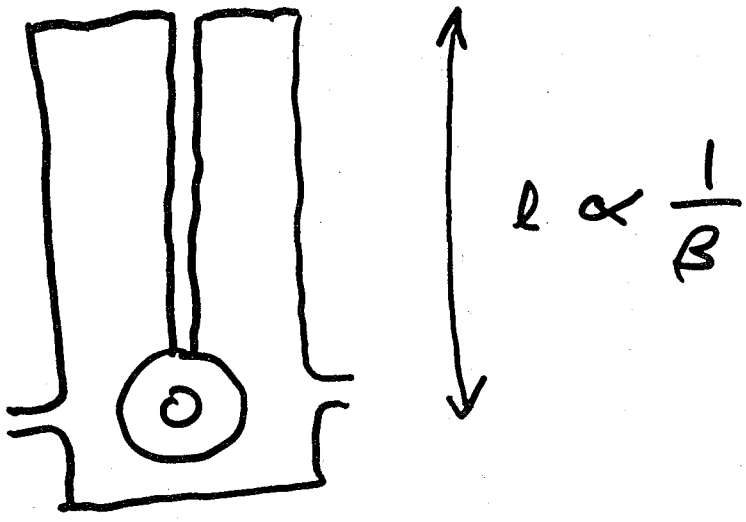

Tuning requires

$$\text{Power} = \delta\omega_{rf} \times (\text{RF Energy})$$

$$= \delta\omega_{rf} \times G \times \mathcal{E}_a^2$$

but $\delta\omega_{rf} \propto \ell^3 - \ell^4$

CONCLUSIONS

- FOR β>0.03, PRESENT SC STRUCTURES WILL WORK VERY WELL IN AN ISOL LINAC
- DEVELOPMENT OF A 1/2 METER LONG SC RFQ WITH E_s>30 MV/M WOULD OPEN MANY OPTIONS
- AN EXTENDED INTERDIGITAL STRUCTURE CAN SUBSTANTIALLY REDUCE SC FRONT-END COSTS
- DIELECTRIC SUPPORT / 25 MHZ CAPABILITY COULD OPEN SIGNIFICANT DESIGN OPTIONS

Appendix D

October 27, 1993

WORKSHOP AGENDA

<u>October 27, '93</u>

8:45 AM	Welcome	W. Barletta (LBL)
9:00 AM	Physics Motivations and Concepts	M. Nitschke (LBL)
9:45 AM	Accelerator Issues and Challenges	S. Chattopadhyay (LBL)
10:30 - 11:00 AM	Coffee	
11:00 AM	Ion Sources for Radioactive Beams	R. Kirchner (GSI)
11:45 AM	Transport, Separation and Matching of Ion Beams between Sources and Accelerators	H. Wollnik (Giessen)
12:30 - 2:00 PM	Lunch	
2:00 PM	Superconducting Low Velocity Accelerating Structures	K. Shepard (ANL)
2:45 PM	Further Progress in normal conducting RFQs in Franfurt	A. Schempp (IAP, Frankfurt)
3:30 - 4:00 PM	Tea	
4:00 PM	Current Status of the ISAC Design Study	H. Schneider (TRIUMF)
4:45 PM	Progress in Low β, Low q/A RFQs in Japan	N. Tokuda (INS, Tokyo)
6:15 PM	Workshop Dinner	

<u>October 28, '93</u>

8:45 AM	Workshop Sessions: Orientation
9:00 - 10:30 AM	Separate sessions of Working Groups I, II & III
10:30 AM	Coffee
10:45 AM - 12:30 PM	Separate session of Working Groups I, II & III
12:30 - 1:30 PM	Lunch
1:30 PM	Developing strategies: joint session with working groups I, II & III

October 28, '93 (cont'd.)

2:00 - 3:30 PM	Separate session I, II & III
3:30 - 3:45 PM	Tea
3:45 - 5:30 PM	Separate session I, II & III

October 29, '93

Summary Talks:

8:45 - 9:30 AM	Working Group I
9:30 - 10:15 AM	Working Group II
10:15 AM	Coffee
10:30 - 11:15 AM	Working Group III
11:15 AM - 12:00 PM	Closing Remarks + Outlook (M. Nitschke & S. Chattopadhyay)

Working Groups:

I	Ion Sources + Separators
II	Low-β DT Structures
III	Radio-Frequency Quadrupoles (RFQs)

GPO 586-405/19231

This report was done with support from the United States Energy Research and Development Administration. Any conclusions or opinions expressed in this report represent solely those of the author(s) and not necessarily those of The Regents of the University of California, the Lawrence Berkeley Laboratory or the United States Energy Research and Development Administration.